UNIVERSITAT DE BARCELONA

Cyclometallated platinum compounds: optical and biological applications

Ariadna Lázaro Palacios

Programa de Doctorat de Química Orgànica

Cyclometallated platinum compounds: optical and biological applications.

Ariadna Lázaro Palacios

Memòria presentada per optar al grau de Doctor per la Universitat de Barcelona

Directores:

Prof. Laura Rodríguez Raurell

Dra. Margarita Crespo Vicente

Tutora:

Dra. Margarita Crespo Vicente

Secció de Química Inorgànica

Departament de Química Inorgànica i Orgànica

Facultat de Química

Universitat de Barcelona

UNIVERSITAT DE BARCELONA

Para Noemí

“It's like in the great stories, Mr. Frodo. The ones that really mattered. Full of darkness and danger they were. And sometimes you didn't want to know the end. Because how could the end be happy? How could the world go back to the way it was when so much bad had happened? But in the end, it’s only a passing thing, this shadow. Even darkness must pass. A new day will come. And when the sun shines it will shine out the clearer. Those were the stories that stayed with you. That meant something, even if you were too small to understand why. But I think, Mr. Frodo, I do understand. I know now. Folk in those stories had lots of chances of turning back, only they didn’t. They kept going because they were holding on to something. That there is some good in this world, and it's worth fighting for.”

The Lord of the Rings: The Two Towers
-J.R.R. Tolkien

AGRAÏMENTS

L'important no és el destí sinó el viatge. I tot i que el destí és escriure una tesi, estic molt més orgullosa del camí que m'ha portat fins a fer-ho. I dono gràcies perquè mai l'he caminat sola. Tinc la sort d'haver-lo recorregut acompanyada i per això, vull agrair a tothom que, per poc o molt que sigui, m'ha ajudat a completar-lo.

Primerament, a les meves codirectores, que han estat la guia que ha fet possible que estigueu llegint aquestes paraules. A Margarita, por aceptar a una estudiante de máster que ni sabía lo que era una ciclometalación, por enseñarme desde cero a trabajar con platino y por tener siempre la respuesta, el articulo o el consejo en cada obstáculo que he encontrado. A la Laura, per venir a dir-me aquell dia el que jo no m'atrevia a preguntar i així confiar en mi per començar tot això. Gràcies per el suport, per totes les oportunitats donades, per la paciència i sobretot, per fer-me veure que valc.

I entre aquestes oportunitats, les dues més importants, de poder treballar en altres països, de les quals m'enduc una infinitat de coses apreses.

To Fernando, for letting me work in his group in Durham and making sure I was feeling comfortable in a new city. To Peter, for the endless hours of help with the equipment and with trying to understand the weirdest compounds ever. But most importantly, for becoming my greatest support there, being always willing to talk and help and for all the great pints and moments. And to Larissa, for the help in our fights with computers, for sharing all the moments either in the gym, in the pub or in Mallorca. And for all the support and conversations about life. To all the people in office 129, for the several coffee breaks and conversations and the learning of each other's languages. To Kleitos for the car rides while listening to Greek and Spanish music. To Héctor for the chats in Spanish and about the geekiest stuff ever (Spain>Mexico). To Ivan for the random vodka shots on a Tuesday and for being always in a good mood. Thank you all along with Ettore, Danos, Suman and Paloma for helping me miss home a little less.

To Sergio, for a great collaboration in Coimbra and all the knowledge in photophysics that you could ever imagine. To João for all the help with the measurements and to Carla for guiding us through everything while speaking portunyol to each other. Y también a João Carlos por la ayuda en este y tantos otros proyectos en los que la fotofísica se nos queda grande, y por los refranes en catalán. Al Team Coimbra, por descubrirme la alheira, el karaoke, el quim dos ossos y la playa de Tocha. A la Fani, xiqueta, per cuidar-nos tant bé i fer-nos sentir una part més del grup. A Roberto, porque tenemos un amigo de treinta años que sale de fiesta con espada y nos parece normal. A Dani, por no estar de acuerdo en nada, pero pasar-lo siempre tan bien. Junto con Dani Acho y Aingeru, mais uma sempre.

A tothom que m'ha fet costat durant aquesta etapa.

A l'Andrea, la clara co-protagonista d'aquest camí. Perquè sense ella si que literalment no existiria aquesta tesi. Per recolzar els meus mental breakdowns, la trama del drama i més. Per compartir amb mi congressos, viatges, estades, cafès, birres, sandwich de la màquina, karaokes, balls al laboratori…podria no acabar la llista. Crec que mai dues persones tant diferents han viscut tantes coses en comú, i les que ens queden.

A la Rosa, perquè no hay dos sin tres, i perquè sense ella els dies de feina haguessin estat molt més avorrits. Per el suport incondicional en les bones i en les dolentes, per tots els pitis que remunten el pitjor dia, per les lliçons fallides de piano i les cançons improvisades, per els millors riures que he tingut en la meva vida i per ser tant crack que fins i tot aconsegueix que s'entengui el magnetisme.

A Guillermo, mi mejicano favorito. Porque, aunque me quiera matar a base de tequila, cosas con tamarindo y bombones que te emborrachan a las 10 de la mañana, no habría sobrevivido sin los cafés del día y las birras de la tarde (o no tan tarde...), aunque espero llegue el día que nos podamos tomar solo una. Por escuchar y apoyar todos mis enfados, la compañía en los momentos finales y la Quinta Estación a pleno pulmón.

Al Fran (Flan), per ser la persona que més tranquil·litat aporta a qualsevol situació quan tu estàs perdent la calma, per saber sempre que dir i com dir-ho, per totes les tonteries i riures al laboratori, i per arreglar tot el que la resta no sabem (quan no està en modo genio del mal).

A la Lídia, que tot i estar acabant la tesi treia el temps per escoltar els meus drames a l'hora de dinar i que em va ensenyar que mai més tornaré a menjar un caqui. Per el bodorrio de la història, els mil vídeos de gats, l'arena més èpic, i perquè si ningú toca el triangle Fardatxo no va enlloc. Ah, i tens gana, ho sé.

A tota la gent amb la que he pogut compartir temps al laboratori.

A l'Araceli, per tenir sempre un moment per ajudar a entendre fotofísica i per ser la persona amb qui estar sempre al dia de tot el salseo. A Anyie, por poco tiempo compartido, pero siempre con una palabra de ánimo. A totes les persones que han vingut d'altres països. To Cami, for all the fun, drinks and parties and the laughs. A Vale, por la paciencia y la comprensión, y por cercar un centro di gravità permanente. I a tots els nens i minions que ens ajuden tant com nosaltres a ells: Júlia, Albert, Ulunay, Raúl, Íngrid, Ona, Eli, Marc, César, Carlota, Xavi, Alba, Raúl i Andrés. I a l'Àlex, per un any del màster més surrealista compartit i per assegurar que sonés l'alarma a l'hora del cancaneo.

A tothom del Departament amb qui he tingut el plaer de compartir lloc de feina.

To Manto, malaka, for the best moussaka ever, the great talks and the best gossip. A la Mariona, per portar sempre un somriure a la cara i contagiar l'alegria allà on va. Al Guillem, per les xerrades compartides al seu laboratori a les 5 i per ser sempre un cavaller. Al David, que sempre té unes paraules de suport i, junt amb la Beltzane, són el teu millor aliat als sopars de nadal. A l'Arnald, senyor cap d'estudis, per tenir sempre una broma per alegrar la rutina. A l'Albert Figuerola, per tots els anys de classes compartides i per confiar en la meva capacitat per impartir-les. I a tota la resta de persones amb les agraeixes creuar-te cada dia pel passadís: Saskia, Júlia, Raúl, Berta, Guti, Jan, Hellen, Laia Ràfols, Dana, Laia Navarro, Mauri, Adriana, Guillem Gabarró...i segur que me'n deixo moltes més.

A totes les persones que ens ajuden a fer la nostra feina més fàcil. Al Francisco, Víctor i Albert per les facilitats i la paciència per programar els dos cents RMN que volem fer. I a la Laura Ortíz per la perseverança en trobar el pic molecular.

I tot i que són analítics, a l'Isaac, Joan, Dídac i Xavi per uns divendres que saps com comencen però mai com acaben, tot i que probablement a Plataforma.

I per suposat, a l'Arnau, per el cafè religiós de cada matí (i migdia) acompanyat de converses plenes de consells mutus i sincers. Perquè és difícil trobar persones amb les que parlar sigui tant fàcil, per estar sempre que el necessites i per tot el suport i comprensió.

A totes les persones que ja m'acompanyaven abans, i que ho continuen fent cada dia.

A les dues extravertides per excel·lència que un dia ja fa 10 anys van decidir adoptar a una introvertida i treure-la a passejar. Les responsables de que vulgui tornar cada dia a començar el grau per poder-lo tornar a compartir amb elles. Perquè no sé si ho saben però gràcies a elles he après, he madurat, he crescut i sobretot he viscut. Per tot el que han aguantat, per escollir tenir-me al seu costat quan no era fàcil, per ser incondicionals, per escoltar-me, per entendrem, per fer-me sentir vàlida i per comptar sempre amb mi. I tenen l'agraïment juntes si, perquè a l'Ana i l'Ainoa no se les pot separar, en cap dels sentits.

A la Nora, per contagiar la seva locura a tothom, per la diversió pura, per ser capaç d'ajudar-te a riure de les desgràcies, per sumar sempre i dir que endavant a tot. Per les vivències que mai oblidarem i per totes les converses profundes dinant al terra d'un passadís. A Judith, por el estrés compartido en los laboratorios, por todo el apoyo en los exámenes y por la paciencia y todos los momentos de la mejor de las etapas.

Al Wan Yu crew, perquè són els reis de muntar-te una festa allà on van, per tots els dijous on t'oblides de la resta del món, les cases rurals, el clínic, el telebar i més. Al Jostan i al Ninil, que van viure l'etapa universitària amb mi i amb els que sé que puc parlar de qualsevol cosa. Sumant-los al Rovira, Husky, Dani, Víctor, Garru, Ana, Ainoa, Carol, Edgar i Arnau, ens queden moltíssimes taules per omplir junts.

A la Pua de Barto 🔌, que són la meva família tot i no tenir la mateixa sang. Portem tota la vida junts, hem viscut i hem crescut però res ens ha separat. No tothom pot tenir l'orgull de dir que manté el primer grup d'amics que va fer. Ells ja saben que son els meus germans, de les millors coses que m'ha donat la vida, i que continuarem estant junts per sempre. Al Xavi, per ser el meu fals marit, la quarantena al pisito, i els millors consells de la història. Al Marc, per les converses birra en mano a la millor terrassa del món i les que teníem de camí al cole, i per estar sempre pendent de mi. Al Guillem, perdonant-li que li agradi Antonia Font, per els riures més contagiosos i per ser l'únic amic de la infància amb qui parlar de vida acadèmica i que t'entengui. A Víctor, a pesar de sus comentarios inapropiados, por estar siempre para lo que necesites. I a la Laura, la persona que més anys porta amb mi, i que per lluny que estigui quan ens veiem és com si no hagués passat el temps. Perquè ningú em coneix i m'entén com ella.

Ho deia un savi:

"Whatever you do in this life, it's not legendary, unless your friends are there to see it."
Barney Stinson

Per últim, però el contrari de menys important, a la meva família. A tots els meus tiets i cosins de Girona. A la meva àvia, que té una mentalitat més oberta que la meva i el millor sentit de l'humor. I als meus tres avis que no hi són. A la família d'Hospitalet, per els millors vermuts i escape rooms. A la Irina i l'Hèctor, amb els que pràcticament m'he criat i els que m'alegren els dinars familiars a base de cotilleos.

A mi padre, que es el perfecto ejemplo de lealtad y compromiso. Por inculcarme los mejores valores cuando aún no los sabía entender. Por saber que siempre estará dispuesto a ayudarte en todo y por los buenos consejos.

A la meva mare, la persona que m'ha ensenyat el que és la fortalesa, la resiliència i la independència. Que dedica la seva vida a les persones que estima i sacrificaria el que fos per elles. Per ensenyar-me la definició d'amor incondicional i per donar-me el seu suport en tot el que faig. I per fer-me sentir orgullosa del que faig, del que sento i del que soc.

I a Noemí, porque por mucho que digan soy yo la que tendría que ser más como tú. Porque, aunque todo sea más difícil, nunca te falta una gota de felicidad. Y porque todo el mundo es más feliz a tu alrededor. No lo sabes, pero estas en mi corazón en todo lo que hago.

Gràcies a tots, ni aquesta tesi ni res en la meva vida seria possible sense vosaltres.

Us estimo.

Ari

CONTENTS

RESUM

Aquesta Tesi Doctoral està centrada en la síntesi de compostos ciclometal·lats de platí amb diferents modificacions estructurals dissenyades racionalment per dur a terme aplicacions biològiques o òptiques. Específicament, s'han sintetitzat compostos ciclometal·lats tridentats [C,N,N'] i [N,C,N] que es diferencien en el seu estat d'oxidació, naturalesa del lligand ciclometal·lat, amb variacions en la rigidesa i l'aromaticitat, i amb una varietat de lligands auxiliars. S'han utilitzat diferents metodologies sintètiques i s'ha comprovat la correcta formació dels compostos amb una gran varietat de tècniques com l'espectroscòpia RMN i infraroja, l'espectrometria de masses, l'anàlisi elemental i la difracció de raigs-X de monocristall.

Quant a les aplicacions biològiques, s'han sintetitzat amb èxit diversos compostos amb propietats anticancerígenes, obtenint algunes espècies amb eficàcia elevada i amb toxicitat mínima que han estat estudiades a través d'assajos de viabilitat en cèl·lules. A més, diversos compostos dels que s'han sintetitzat van presentar una absència completa de resistència entrecreuada i gràcies a proves addicionals com la voltametria cíclica, estudis de la interacció amb l'ADN i experiments de distribució a les fases del cicle cel·lular, s'ha observat que presenten mecanismes no anàlegs als dels fàrmacs clínicament aprovats.

Quant a les aplicacions òptiques, l'afinació de l'estructura dels compostos, especialment en el lligand ciclometal·lat, ha estat clau per aconseguir compostos de platí(II) amb una fosforescència eficient i amb diversos estats emissius. S'han determinat els rendiments quàntics i temps de vida d'emissió i els càlculs DFT han permès un coneixement més detallat dels estats excitats de les molècules. A més, la modificació dels lligands auxiliars, el dissolvent, la concentració o la presència d'un catió metàl·lic addicional, s'han utilitzat com a estratègia per promoure un desplaçament cap al vermell en l'emissió a través de la formació d'agregats o compostos heterometàl·lics. Finalment, s'ha seleccionat un compost per la preparació de cel·les electroquímiques emissores de llum (LEECs) obtenint nous resultats per un dispositiu dopat amb platí que són competitius amb els resultats descrits a la bibliografia per altres metalls i, dins del nostre coneixement, el sistema de platí més eficient utilitzat per la seva aplicació en LEECs.

ABSTRACT

This Doctoral Thesis is focused on the synthesis of cyclometallated platinum compounds with different structural modifications rationally designed specifically for biological or optical applications. Specifically, tridentate [C,N,N'] and [N,C,N] cyclometallated compounds have been synthesised, differing in their oxidation state, the nature of the cyclometallated ligand, with variations in the rigidity and aromaticity, and with a variety of ancillary ligands. Several synthetic methodologies have been employed and the correct formation of the compounds has been checked by a great variety of techniques such as NMR and infrared spectroscopy, mass spectrometry elemental analysis and single crystal X-ray diffraction.

Concerning biological applications, several compounds with anticancer properties have been successfully synthesised, obtaining some species with a high efficacy and minimal toxicity studied through cell viability assays. Additionally, several of the designed compounds presented a complete absence of cross-resistance and thanks to additional testing such as cyclic voltammetry, DNA interaction studies and cell-cycle phase distribution experiments, it has been observed that they present mechanisms of action not analogous to those of the clinically approved drugs.

Concerning optical applications, the tuning of the structure of the compounds, especially in the cyclometallating ligands, has been key to achieve efficient phosphorescent platinum(II) compounds with various emissive states. Both emission quantum yields and lifetimes have been determined and DFT calculations have allowed a further understanding of the molecules excited states. Additionally, modification of the ancillary ligands, the solvent, the concentration or the presence of an additional metallic cation have been used as a strategy to promote a red-shift in the emission through the formation of aggregates or heterometallic compounds. Finally, one compound has been selected and tested for the preparation of a Light-Emitting Electrochemical Cell (LEEC) obtaining novel results for a platinum-doped device which are competitive with those reported in the literature for other metals and, to the best of our knowledge, the most efficient platinum system used for LEEC applications.

PREFACE

The research reported in this Thesis was developed in the Supra and Nanostructured Systems (SuNS) and the Synthesis and Applications of Cyclometallated Compounds (CM) groups at the Inorganic Chemistry Section from the Department of Inorganic and Organic Chemistry in the Universitat de Barcelona. This work was financially supported by a PhD fellowship from Generalitat de Catalunya (Ajuts per la contractació de personal investigador novel (FI-SGR)) and by Ministerio de Ciencia e Innovación de España (AEI/FEDER, UE Projects CTQ2015-65040, CTQ2016-76120-P and PID2019-104121GB-I00).

The photophysical characterisation depicted in *Chapter 5* was performed during a short stay (one month) in the Photochemistry group at the Faculty of Sciences and Technology from Universidade de Coimbra under the supervision of Prof. J. Sérgio Seixas de Melo, which was funded by Laserlab-Europe (grant agreement no. 284464, EC's Seventh Framework Programme). In *Chapter 7*, the device fabrication and photophysical characterisation was performed during a three months stay in the Organic Electroactive Materials group at the Faculty of Physics from Durham University under the supervision of Dr. Fernando Dias and Dr. Piotr Pander, which was funded by the mobility program from a PhD fellowship from Generalitat de Catalunya (Ajuts per la contractació de personal investigador novel (FI-SGR)).

Cell viability assays were performed by Dr. Cristina Balcells (*Chapter 3*) and Alba Calvet and Dra. Sílvia Marin (*Chapter 4*) under the supervision of Prof. Marta Cascante at the Faculty of Biology from Universitat de Barcelona. DNA migration studies (*Chapters 3* and *4*) were performed by Prof. Josefa Badia and Prof. Laura Baldomà, and NMR stability studies (*Chapter 3*) were performed by Dr. Josefina Quirante, all of them at the Faculty of Pharmacy of the Universitat de Barcelona.

Crystal structures were solved by Dr. Mercè Font-Bardia from the Centres Científics i Tecnològics from Universitat de Barcelona (*Chapters 2* and *3*) or by Dr. Jas S. Ward or Khai-Nghi Truong (*Chapters 3*, *5* and *6*) under the supervision of Prof. Kari Rissanen from the University of Jyväskylä.

Computational calculations from *Chapters 5* and *6* were performed by Dr. Ramón Bosque from the Universitat de Barcelona.

The results of this research have been disseminated in several national and international conferences:

- Lázaro, A.; Crespo, M.; Rodríguez, L. XXXVII Reunión Bienal de la Real Sociedad Española de Química (San Sebastián, Spain, **May 2019**). Poster communication entitled "*Luminescence studies of new [C^N^N'] cyclometallated platinum(II) and platinum(IV) compounds*".
- Lázaro, A.; Crespo, M.; Rodríguez, L. Reunión del Grupo Especializado de Química Organometálica (Alcalá de Henares, Spain, **September 2019**). Poster communication entitled "*Synthesis of cyclometallated platinum(II) and platinum(IV) compounds. Cytotoxic and photophysical properties*".
- Lázaro, A.; Crespo, M.; Rodríguez, L. III International Workshop on Chemistry of Group 11 Elements (Lisbon, Portugal, **January 2020**). Flash and poster communication entitled "*Exploring metallophilic interactions in cyclometallated platinum(II) and gold(III) compounds*".
- Lázaro, A.; Crespo, M.; Rodríguez, L. AEBIN Photochemistry School 2020 (Online, **September 2020**). Oral communication entitled "*Room-temperature phosphorescence and efficient singlet oxygen production by cyclometallated Pt(II) complexes with aromatic alkynyl ligands*".
- Lázaro, A.; Crespo, M.; Rodríguez, L. 1st Supramat Meeting (Online, **February 2021**). Poster communication entitled "*Promoting excimer formation in [N^C^N] cyclometallated platinum(II) compounds with aromatic alkynyl ligand*".
- Lázaro, A.; Crespo, M.; Rodríguez, L. Simposio de Jóvenes del Grupo Especializado en Química Organometálica (Online, **March 2021**). Poster communication entitled "*Anticancer activity of luminescent PtII and PtIV platinacycles against multiplatinum-resistant metastatic CRC and CRPC cell models*".
- Lázaro, A.; Crespo, M.; Rodríguez, L. 24th Virtual Conference on Organometallic Chemistry (EuCOMC XXIV Virtual Conference) (Online, **September 2021**). Poster communication entitled "*Influence of the structure, ancillary ligands and oxidation state in the photophysical properties of cyclometallated platinum compounds*".

- Lázaro, A.; Crespo, M.; Rodríguez, L. 1st Women in Supramolecular Chemistry workshop: (Cagliari, Italy, **September 2021**). Oral communication entitled "*Promoting excimer formation in [N^C^N] cyclometallated platinum(II) compounds with aromatic alkynyl ligands*".
- Lázaro, A.; Crespo, M.; Rodríguez, L. 4th GDRI-HC3A Meeting (Barcelona, Spain, **January 2022**). Oral communication entitled "*Antitumoral activity of luminescent cyclometallated Pt(II) and Pt(IV) compounds against multiplatinum-resistant cell models*".
- Lázaro, A.; Crespo, M.; Rodríguez, L. Dotzena Trobada de Joves Investigadors dels Països Catalans (Girona, Spain, **January 2022**). Oral communication entitled "*Síntesi de compostos ciclometal·lats de platí(II) amb lligands alquinil-aromàtics per l'estudi de les seves propietats luminescents i la formació d'excímers*".
- Lázaro, A.; Crespo, M.; Rodríguez, L. 2nd Supramat Meeting (Mallorca, Spain, **March 2022**). Oral communication entitled "*Red-emissive cyclometallated [N^C^N] Pt(II) and Pt(II)/Ag(I) compounds*".
- Lázaro, A.; Crespo, M.; Rodríguez, L. XL Reunión del Grupo Especializado de Química Organometálica (Barcelona, Spain, **September 2022**). Oral communication entitled "*Cyclometallated Pt(II)/Ag(I) luminescent compounds for the fabrication of optical devices*".

Additionally, the research reported in *Chapters 2*, *3*, *5* and *6* has already been published in:

Chapter 2:

- Lázaro, A.; Serra, O.; Rodríguez, L.; Crespo, M.; Font-Bardia, M. *New J. Chem.* **2019**, *43*, 1247-1256.

Chapter 3:

- Lázaro, A.; Balcells, C.; Quirante, J.; Badia, J.; Baldomà, L.; Ward, J. S., Rissanen, K.; Font-Bardia, M.; Rodríguez, L.; Crespo, M.; Cascante, M. *Chem. Eur. J.*, **2020**, *26*, 1947-1952.

Chapter 5:

- Lázaro, A.; Cunha, C.; Bosque, R.; Pina, J.; Ward, J.S.; Truong, K.N.; Rissanen, K.; Lima, J.C.; Seixas de Melo, J. S.; Crespo, M.; Rodríguez, L. *Inorg. Chem.* **2020**, *59*, 8220-8230.

Chapter 6:

- Lázaro, A.; Bosque, R.; Ward, J.S.; Rissanen, K.; Crespo, M.; Rodríguez, L. *Inorg. Chem.* **2023**, *62*, 2000-2012.

ABBREVIATIONS

AIE	Aggregation induced emission
ATR	Attenuated total reflectance
CT	Charge transfer
CPCM	Conductor-like Polarizable Continuum Model
CRC	Colorectal cancer
CRPC	Castration-resistant prostate cancer
CV	Cyclic voltammetry
d	doublet
DCA	Dichloroacetate
DCFH-DA	Dichlorodihydrofluorescein diacetate
DFT	Density functional theory
DMEM	Dulbecco's modified eagle medium
DMF	N,N-dimethyl formamide
DMSO	Dimethyl sulfoxide
EDTA	Ethylenediaminetetraacetic acid
EQE	External quantum efficiency
ES	Electrospray
ESA	Excited state absorption
ET	Energy transfer
FBS	Fetal bovine serum
FT	Fourier transform
HEPES	4-(2-hydroxyethyl)-1-piperazineethanesulphonic acid
HOMO	Highest occupied molecular orbital
IC	Internal conversion
IC_{50}	Half-maximal inhibitory concentration
ILCT	Intraligand charge transfer
IR	Infrared

ISC	Intersystem crossing
ITO	Indium tin oxide
LC	Ligand-centred
LC/MSD-TOF	Liquid Chromatography/Mass Selective Detector-Time of Flight
LEECs	Light-emitting electrochemical cells
LL	Ligand-to-ligand
LM	Ligand-to-metal
LUMO	Lowest unoccupied molecular orbital
m	multiplet
MLCT	Metal-to-ligand charge transfer
MMLCT	Metal-to-metal-to-ligand charge transfer
MPR	Multiplatinum resistance
MS-ESI$^+$	Mass Spectrometry-Positive Electrospray Ionization
MTT	3-(4,5-dimethylthiazol-2-yl)-2,5-diphenyltetrazolium bromide
NIR	Near infrared
NMR	Nuclear Magnetic Resonance
OLEDs	Organic Light Emitting Diodes
OXD7	1,3-bis[2-(4-tert-butylphenyl)-1,3,4-oxadiazo-5-yl]benzene
PBS	Phosphate Buffer Saline
PEDOT:PSS	Poly(3,4-ethylenedioxythiophene) polystyrene sulfonate
PI	Propidium iodide
PVK	Poly(9-vinylcarbazole)
QY	Quantum yield
RI	Resistance index
ROS	Reactive oxygen species
RPM	Revolutions per minute
s	singlet
SHE	Standard hydrogen electrode
t	triplet

TA	Transient absorption
TADF	Thermally activated delayed fluorescence
TAE	Tris-acetate-EDTA
TCSPC	Time-correlated single photon counting
TD	Time-dependant
TE	Tris-EDTA
TFA	Trifluoroacetate
$THABF_4$	Tetrahexylammonium tetrafluoroborate
TMS	Tetramethyl silane
UV-Vis	Ultraviolet-visible

CHAPTER 1

Introduction

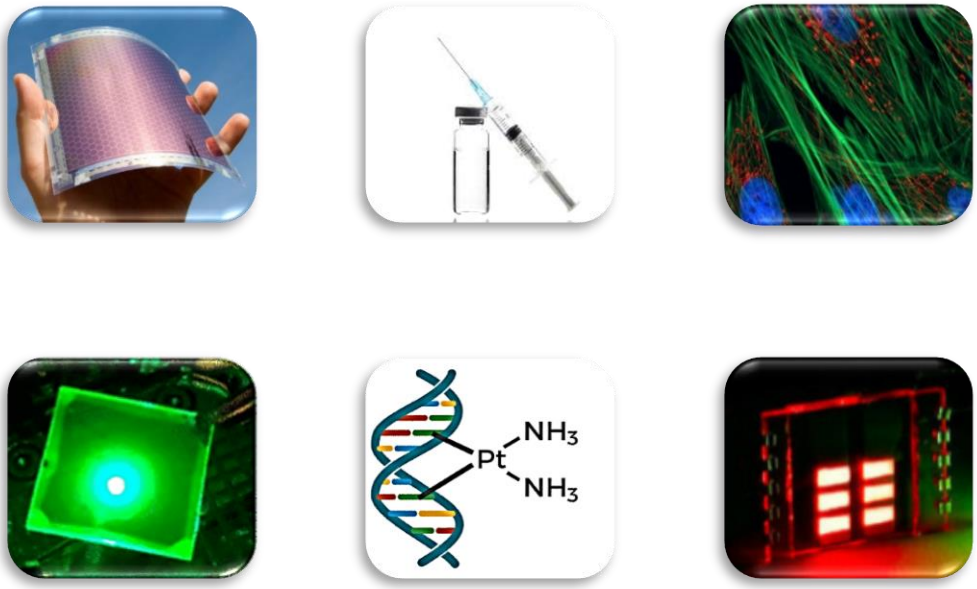

1. Introduction

Platinum compounds have had a great impact in several areas of inorganic chemistry such as coordination and organometallic chemistry, and in the establishment of reaction mechanisms. Upon the discovery by Werner of the existence of *cis* and *trans* isomers of $[PtCl_2(PPh_3)_2]$, the square-planar geometry of platinum(II) compounds was elucidated and lead to several mechanistic studies on substitution reactions and the *trans* effect.[1] Regarding organometallic chemistry, the first compound containing an unsaturated hydrocarbon attached to a metal was $K[PtCl_3(C_2H_4)]\cdot H_2O$, known as Zeise's salt. Afterwards, the first σ-bonded compounds containing a trimethylplatinum(IV) group were reported by Pope and Peachey in 1907.[2] Moreover, since the work from Shilov in the early 1970s, platinum has played an important role in the study of C-H bond activation.[3]

1.1. Cyclometallated platinum compounds

Cyclometallated compounds are one specific kind of organometallic compound that present a platinum-carbon bond intramolecularly stabilized by one or several neutral donor atoms. Both the carbon and the neutral donor atom or atoms are located in the same ligand, which acts as polydentate thus forming a platinacycle where the metal is bound to carbon through a covalent bond while the donor atoms present coordinate bonds. These donor atoms can be either a sulphur, phosphorus, or oxygen but this work, as they are the more commonly studied, is focused on compounds containing one or more nitrogen atoms.[4,5] As platinum compounds can present either a square-planar (platinum(II)) or octahedral (platinum(IV)) geometry, the remaining positions are occupied by ancillary ligands which can be of various natures.[6] Depending on the number and nature of the ligands, cyclometallated platinum compounds can either be neutral or ionic.

The first reported examples of cyclometallated platinum compounds were obtained by Cope and Friedrich in the 1960s.[7,8] In 1988 Zelewsky and co-workers synthesised the first bis-cyclometallated [C,N,C] platinum(II) compounds.[9,10] It was not until 1999 when Rourke and co-workers reported a versatile synthetic route to prepare this class of compounds in a high yield.[11,12] Since then, a large amount of cyclometallated compounds has been reported in the literature with a great range of different structures.[13–16]

Generally, they have resulted of interest in two main fields, in biochemistry as anticancer agents but also for other bioorganometallic applications,[17] and in the field of optical materials as photophysical devices in organometallic light emitting diodes,[18,19] for light harvesting and energy transfer such as in photovoltaic cells[20] or as active units in sensors.[21]Additionally, some have been used as gelators[22], birefringents in liquid crystalline materials[23,24] or molecular or crystalline switches.[25]

1.1.1. Types of cyclometallated compounds

In general, there are five coordination patterns for platinum(II) cyclometallated compounds which differ in the type of cyclometallating ligand (bidentate, tridentate or tetradentate) and the presence or absence of ancillary ligands which can be monodentate or bidentate (*Figure 1.1*).[26]

The first type is the bidentate-monodentate-monodentate compounds (**1**) containing a bidentate cyclometallating ligand and two monodentate ancillary ligands. Type **2** (bidentate-bidentate) contains two bidentate ligands with at least one cyclometallating ligand. Although most of these compounds present a non-cyclometallating second ligand, both homoleptic and heteroleptic bis-cyclometallated complexes are known.

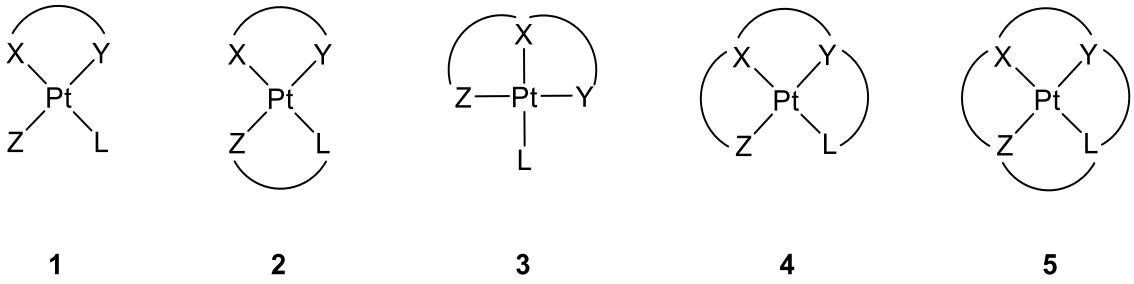

Figure 1.1. Types of cyclometallated platinum(II) compounds. X, Y, Z, L = structural units containing a donating atom, with at least one of them being the carbon donor in the cyclometallating ligand.

Tridentate-monodentate compounds (**3**) present a tridentate cyclometallating ligand and an ancillary monodentate ligand. Finally, types **4** and **5** are based on a single tetradentate cyclometallating ligand, that can be either acyclic (tetradentate-open, **4**) or cyclic (tetradentate-closed, **5**).

The work carried out along this Thesis is mainly based on tridentate cyclometallated platinum(II) compounds with nitrogen donor atoms and one monodentate ancillary

ligand, therefore type **3** compounds. These compounds can display different structures depending on the number and arrangement of the carbon and nitrogen atoms in the cyclometallating ligands. The larger number of reported compounds contain one platinum-carbon bond and two coordinative bonds with nitrogen atoms.[13,27,28] This results in neutral compounds with an anionic monodentate ancillary ligand, which is the usual, and in ionic compounds with neutral ancillary ligands. The position of the carbon atom can give rise to [C,N,N] or [N,C,N] compounds (*Figure 1.2*).

In the case of [N,C,N] compounds, the cyclometallating ligand gives rise to the formation of two metallacycles. This is in contrast with [C,N,N] compounds were a metallacycle and a chelate ring are formed. Depending on the nature of the ligand, this chelate can be more or less rigid and give rise to more or less planar compounds.

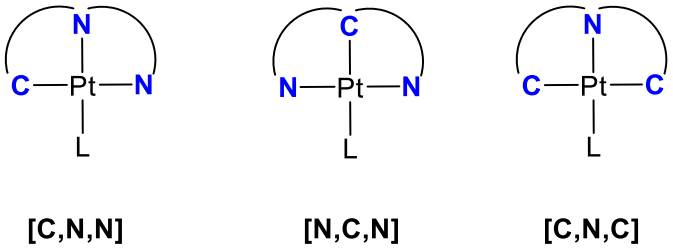

Figure 1.2. Types of cyclometallated tridentate platinum(II) compounds with N as donor atoms.

Additionally, some [C,N,C] cyclometallated compounds have been reported although they have been less studied and they usually present a neutral monodentate ancillary ligand for the obtention of neutral compounds. Finally, [C,C,N] cyclometallated compounds are extremely rare.[29,30]

Cyclometallated platinum(IV) compounds, which usually arise from the oxidative addition of halogens, hydrogen peroxide or alkyl halides that occurs in *trans*, present the same equatorial plane as the starting platinum(II) compounds with two ancillary ligands in axial positions giving rise to an octahedral geometry.[31] However, in some cases, upon similar sizes between the axial and the equatorial ancillary ligand, isomerisation can occur.[32]

1.1.2. Cyclometallation reactions

Cyclometallation refers to the transition metal-mediated activation of a C-R bond to form a metallacycle comprising a new metal-carbon σ bond. Among the literature, it is the preferred method to obtain cyclometallated platinum compounds, although alternative methods such as oxidative addition involving a C-X bond activation (X = F, Cl, Br, I, OTf) have been reported. Less common preparation methods include transmetallation, elimination, cycloaddition or hydrometallation reactions.[5]

This reaction consists of two consecutive steps. First, the metal centre is coordinated to the cyclometallating ligand through one or more donor groups. Secondly, the C-R bond is activated followed by the closing of the metallacycle, which needs to be assisted by the donor heteroatom coordination (*Scheme 1.1*).[33] By far, the largest portion of cyclometallation reactions occurs through C-H bond activation, which can mainly proceed through electrophilic activation or oxidative addition. This is highly depending on the metal compound used as a metalating substrate.[34]

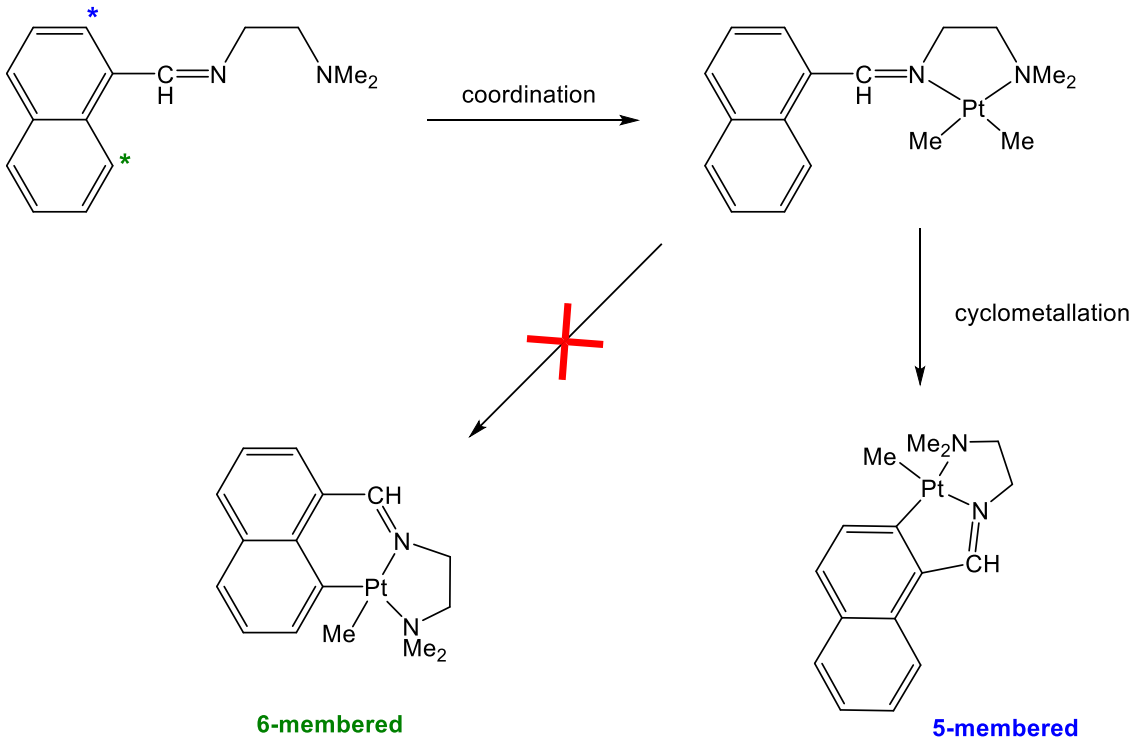

Scheme 1.1. Cyclometallation by C-H bond activation and formation of five-membered metallacycles.[35]

This is why, metallacycles have been successfully applied in traditional domains of organic transformations and catalysis,[36] such as the catalytic activation of C-H bonds in unreactive alkanes[37] or the stabilization of reactive intermediates.[38,39]

Commonly, these reactions result in the formation of the more stable five-membered metallacycles, usually by the activation of a C-H bond in the *ortho* position of an aromatic ring (*Scheme 1.1*). It is known that if all the elements of a ring are carbon, the equilateral pentagon easily forms in an almost planar stable structure without strain because the bond angles of the tetrahedral structure are almost the same as the interior angles of the equilateral pentagon. If the metal and coordination atom have similar bond angles to that of carbon, the compound tends to easily form an almost planar structure, which is the case for the square planar platinum(II).[33] However, some examples of six-membered platinacycles are also reported, but more uncommon.[40]

Additionally, if a C=N bond is present in the ligand, two different five-membered metallacycles could in principle be obtained, one which contains the C=N bond (endo) and one that does not (exo). It was observed that there is a strong tendency to form endocyclic compounds, as the C=N bond can provide extra stability to the platinacycle. However, this is considering that imines usually exist in the more stable E form, from which both endo- and exo-cycles can be formed, while if the imine displays a Z conformation only the obtention of exo-cycles is possible (*Scheme 1.2*). [41,42]

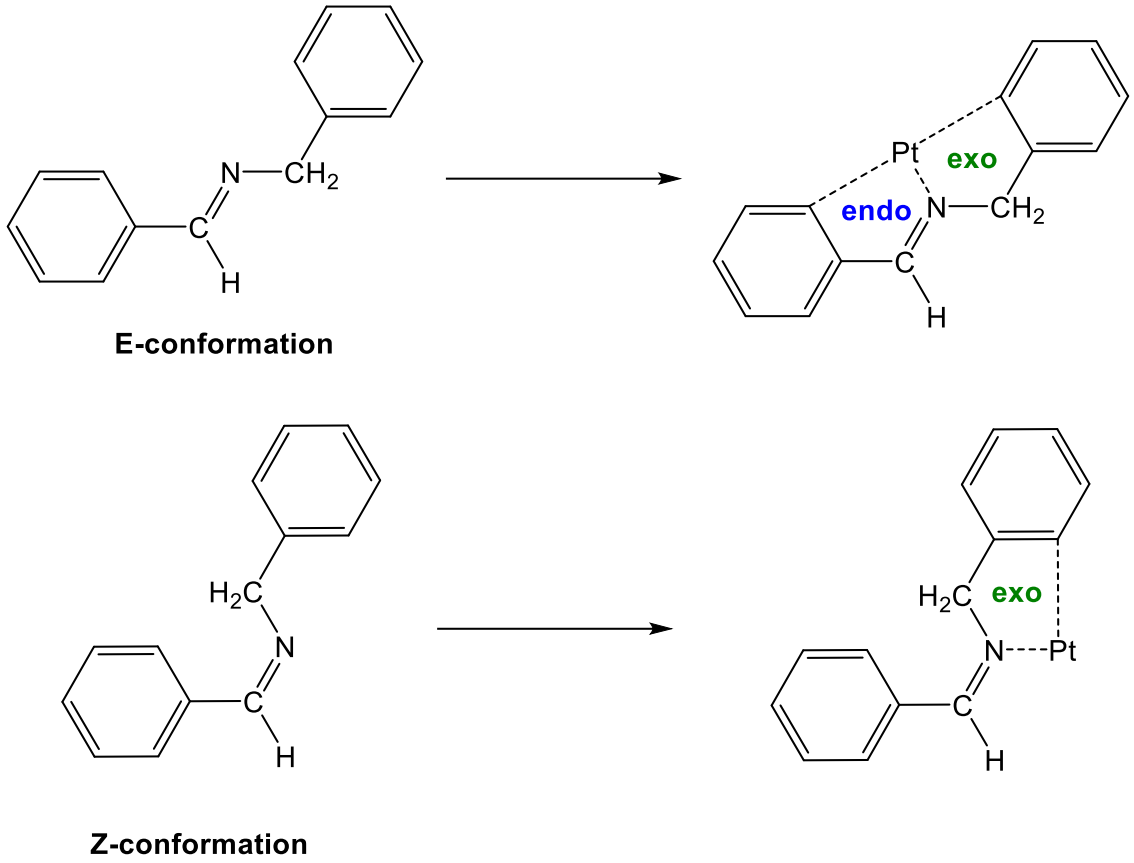

Scheme 1.2. Possible conformations of the iminic ligands and resulting cyclometallated products.[41]

1.2 Biological activity

One of the main applications for cyclometallated platinum compounds is their use as potential anticancer drugs. These compounds arise as an alternative to the conventional platinum drugs whose development and properties are described below.

1.2.1. Platinum compounds as anticancer agents

Upon the demonstration in the 1960s that cisplatin was able to inhibit cellular division of Escherichia coli bacteria,[43] it was discovered subsequently that it was able to act as an efficient antitumor agent in mouse models despite its simple structure.[44] Afterwards, it was validated as an efficient anticancer drug in humans as well.[45–48] Therefore, in 1978 it was approved by FDA for the treatment of metastatic ovarian and testicular cancer.[49] With its introduction, the survival outlook was significantly improved from a 10% cure rate for testicular cancer up to a 90% with the use of this modern platinum chemotherapy.[50]

The mechanism of action of cisplatin depicted in *Figure 1.3* was later elucidated and was found to be based in the crosslinking of DNA and the inhibition of transcription.[51] This starts with the entrance of cisplatin in the cell where it undergoes aquation which results in the loss of one or both chlorido ligands, giving rise to the formation of a platinum(II) aqua complex, a potent electrophile. Then, the resulting compound can readily react with many biological molecules found in cell media with loss of the bound water molecules. Specifically, the purine bases of nucleic acids that form DNA are strongly nucleophilic at the N7 position. Therefore, the electrophilic aqua complex derived from cisplatin binds easily to DNA, forming mainly bifunctional adducts, being the intrastrand 1,2-d(GpG) the major one, accounting for a 60-65% of the bound platinum.[52,53] The resulting Pt-DNA adducts can inhibit transcription as they bend and distort the DNA structure, which ultimately leads to cell death.[54–57]

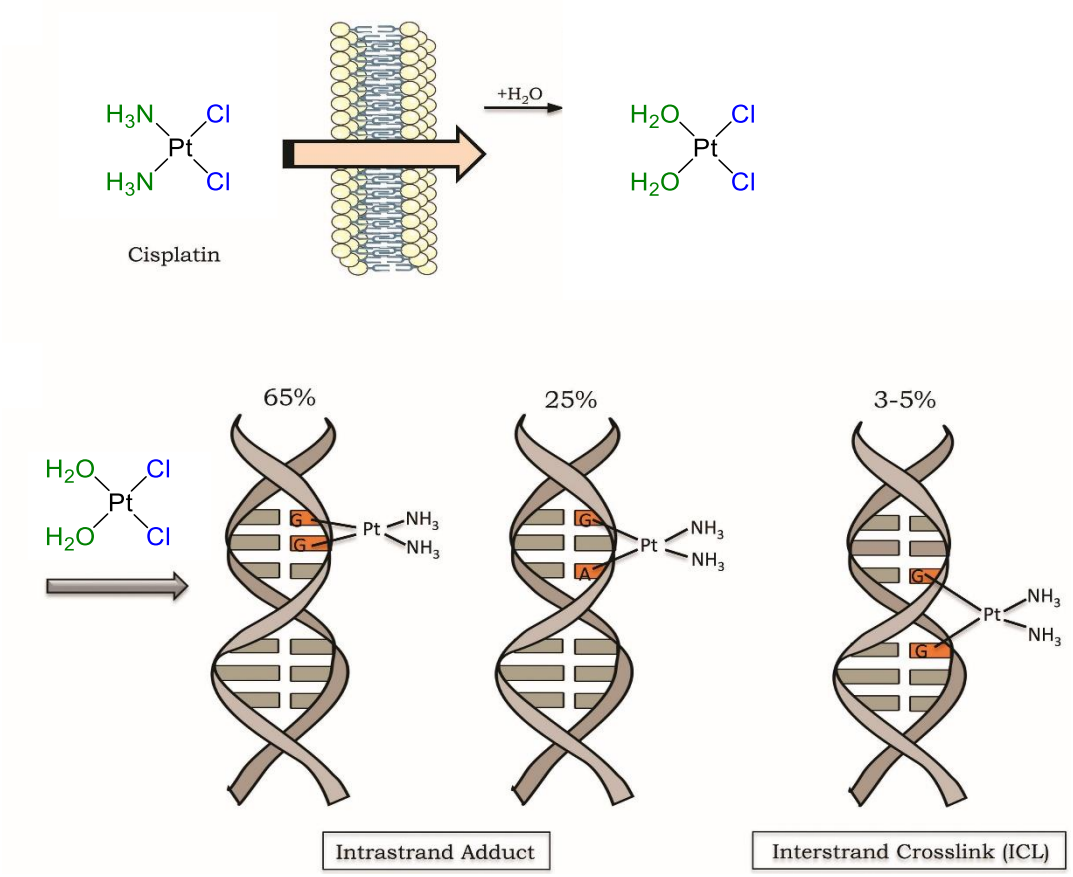

Figure 1.3. Cisplatin activation and DNA damage induction. The percentages represent the frequency of each type of DNA damage induced by cisplatin. Adapted figure.[53]

However, despite its great success in the treatment of testicular cancer, it was found to be not as effective for other cancer types and to induce toxicity and thus a large number of side effects.[58–60] Additionally, it was observed that some cancers could be resistant to its action, whose resistance could be intrinsic or acquired during prolonged treatment.[61,62] This is why, for years, wide research has been devoted to find new platinum complexes with antitumour activity to avoid these problems. Even though several thousands of compounds have been prepared and tested, only two have been approved for clinical use worldwide, with three additional ones approved for regional use in Asia. All these compounds, displayed in *Figure 1.4* operate with a similar mechanism of action than cisplatin.[63–66]

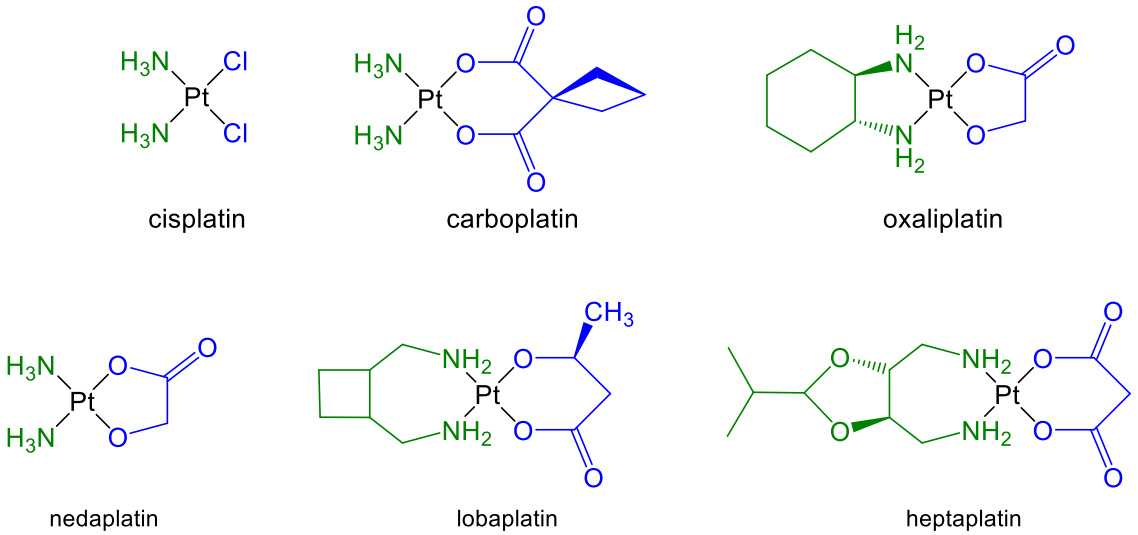

Figure 1.4. Chemical structures of the clinically used platinum anticancer drugs. Cisplatin, carboplatin and oxaliplatin are approved for use worldwide. Nedaplatin, lobaplatin and heptaplatin are approved for use in Japan, China, and Korea respectively.

These compounds generally present three types of ligands that can be strategically modified to tune the final anticancer properties of the platinum complexes (*Figure 1.5*). First, ligands L, referred as non-leaving groups, are typically nitrogen donors and are retained in the final platinum-DNA adduct as they form thermodynamically stable bonds with platinum. Therefore, the nature of these ligands will affect how the cellular repair pathways respond to those adducts.[67,68] This has been evidenced with oxaliplatin, which contains a chelating 1,2-diaminocyclohexane ligand instead of the ammonia ligands from cisplatin. This allows oxaliplatin to display a different spectrum of activity in cancer cell lines and avoid the cisplatin cross-resistance.

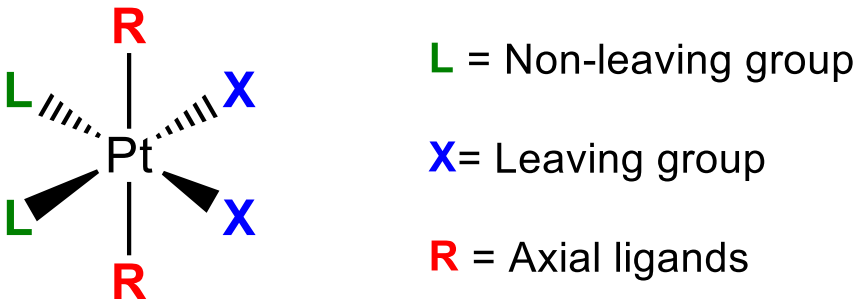

Figure 1.5. Different ligands in platinum anticancer complexes.

Leaving group ligands (X), named as they are lost upon binding to DNA, can be modified to alter the aquation dynamics and overall reaction stoichiometry of the platinum

complexes. With the use of highly labile ligands, such as nitrate, complexes can react very quickly which causes a greater toxicity as they can indiscriminately bind to off-target biological nucleophiles.[69,70] Carboplatin, on the other hand, contains a relatively stable chelating 1,1-cyclobutanedicarboxylato leaving group and upon comparison with cisplatin, containing a much more labile chlorido, it can be administered at higher doses as it displays a lower toxicity profile. However, they both present a similar spectrum of activity because of the same ammino ligand as a non-leaving group and therefore, they form the same kind of Pt-DNA adduct. Consequently, carboplatin is not able to display cross-resistance to cisplatin.[45,71,72]

Finally, the axial ligands (R), which are only present in platinum(IV) compounds, can be dissociated upon the reduction of the complex to a platinum(II) species under cellular media. It has been proved that their nature is the responsible for the rate of reduction of the final complexes and they additionally provide a point of installation for tumour targeting moieties.[73,74] Overall, the modification of any of the ligand types can alter the water solubility and the lipophilicity of the final platinum complex, which can significantly affect its ability to interact with or penetrate the cell.[75]

Specifically, platinum(IV) compounds have been given less attention, as they were not studied in depth before due to their less effectiveness than cisplatin. However, recently they have received a renewed interest based in the assumption that they can overcome some of the problems associated with acquired resistance and severe side effects.[76–78] This is because these octahedral complexes with a low spin t_2g^6 configuration are considered inert towards substitution reactions and therefore are believed to be stable outside the cell and activated by a two-electron reduction only when they reach the inside.[79] The hypoxic environments of cancer cells, with a high concentration of reducing agents, allow the intracellular reduction of these complexes to give the cytotoxic platinum(II) active compound.[80,81] However, although some platinum(IV) compounds have undergone clinical trials, none of them have been approved for clinical use yet.[1]

1.2.2. Anticancer properties of cyclometallated platinum compounds

After years of research devoted to finding new platinum compounds with improved anticancer properties regarding cisplatin, organometallic platinum compounds became interesting candidates. Recent studies indicate that organometallic compounds are promising anticancer agents despite the initial assumption that they would be unstable

under physiological conditions.[82–84] These compounds present the combined properties of a metal centre and the organic ligands, with the presence of strong M-C bonds which improve their stability and greatly influence the lability of the other present bonds. In addition, they can be easily modified, and a wide range of C-donor ligands provides the opportunity to perform a rational design and establish structure-activity relationships.[85]

Among them, cyclometallated platinum compounds have attracted a greater interest as they are generally more stable than acyclic compounds, thus increasing their probability to reach the cell unaltered avoiding the appearance of side effects. [1,86] Furthermore, the presence of aromatic planar groups might favour intercalative binding to DNA through non-covalent π-π stacking interactions, while the labile positions in the coordination sphere of the metal favour covalent interaction to DNA as for cisplatin. The latter is largely favoured by the higher lability of the ligands in *trans* to a σ(Pt-C) bond.[87]

A large number of cyclometallated platinum(II) compounds containing bidentate [C,N] or tridentate [C,N,N'] ligands have been screened against tumour cells and their properties can be easily modulated by modifications in the substituents of the aromatic rings of the cyclometallating moieties or by the use of different ancillary ligands. Some examples are shown in *Figure 1.6*. Compound **1** is the most potent anticancer agent among the [C,N,N'] reported compounds, exhibiting cytotoxic activity higher than cisplatin both *in vitro* and *in vivo* assays and [C,N] compound **2** exhibits high cytotoxicity toward cells that have acquired cisplatin resistance.[84,88] Fewer reports exist on the anticancer properties of [N,C,N] cyclometallated platinum(II) compounds although some examples, such as compound **3** shown in *Figure 1.6*, have displayed interesting antitumoral properties.[89] Moreover, several of these compounds present luminescent properties, making them potential luminescent probes for DNA in living cells and allowing the tracking of their cellular uptake and distribution in the cell by fluorescence microscopy.[90–92]

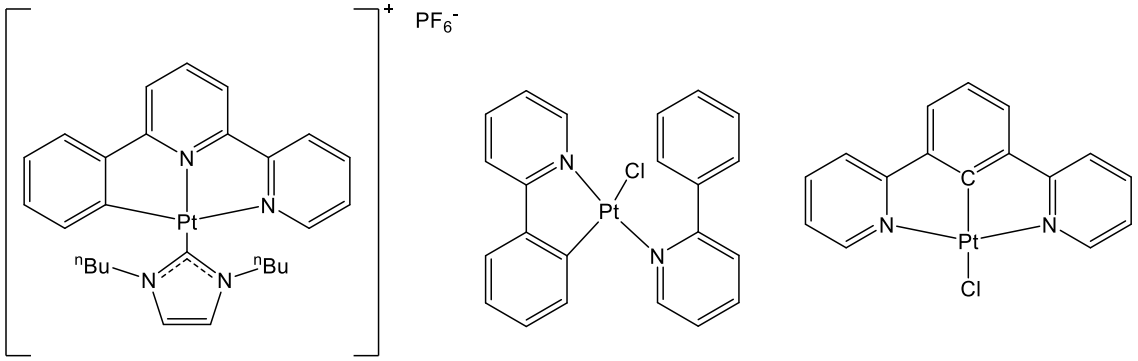

1 2 3

Figure 1.6. Relevant examples of cyclometallated platinum(II) compounds with anticancer activity.

However, less attention has been focused in cyclometallated platinum(IV) compounds, that present the combined properties of the platinum(IV) centre and a cyclometallated ligand. The few [C,N,N'] platinum(IV) compounds that have been reported recently presented remarkable anticancer properties, with lower activity for bidentate [C,N] derivatives. Thus, it could be a starting point in the research to find new alternatives as anticancer drugs.[93–96]

1.3. Optical properties

The other main application of cyclometallated platinum compounds is in the fabrication of optical materials due to their interesting photophysical properties which are described below.

1.3.1. Luminescent properties of platinum compounds

To understand the different photophysical properties of platinum compounds, it is necessary to clarify some fundamental bases on this topic. Specifically, photophysics researches the several electronic internal processes that occur after the absorption of light by a molecule without leading to changes in its chemical structure. All these processes are described in the Jablonski diagram, which illustrates the possible electronic and vibrational transitions between the ground and excited states of any molecule (*Figure 1.7*).

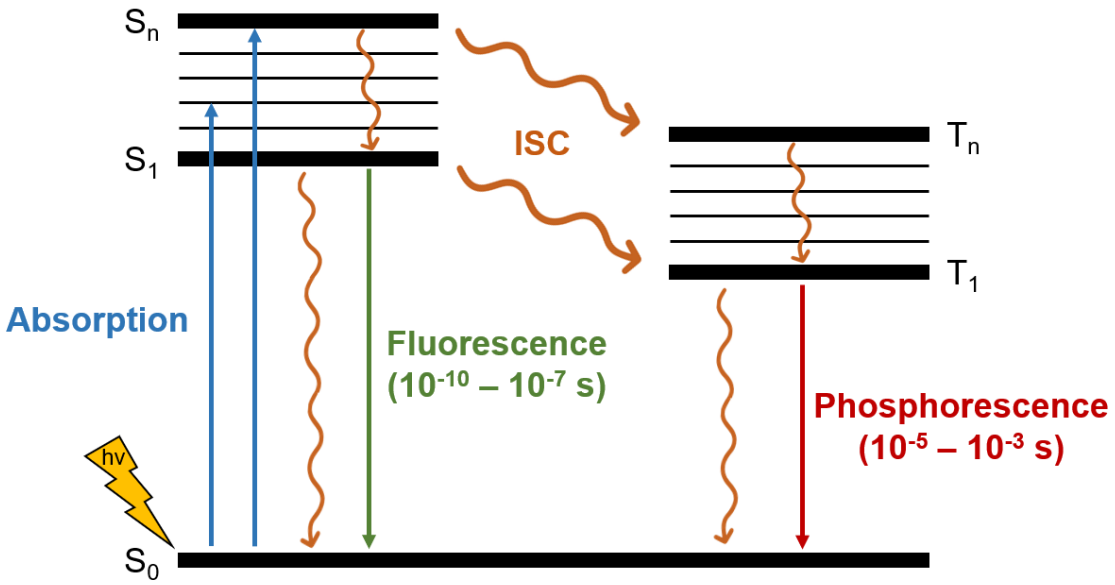

Figure 1.7. Simplified Jablonski diagram illustrating the main photophysical processes. Non-radiative transitions are drawn in orange.

For any molecule, absorption occurs when it receives a photon of light promoting the excitation of one electron from the ground state (S_0) to a higher energy excited state (S_n). This electron then relaxes through internal conversion (IC), which is a vibrational non-radiative process, to the lowest excited state (S_1). From there, this electron can undergo several pathways to return to the ground state. The first one consists in the emission of a

photon from the first singlet excited state (S_1) to the ground state (S_0), which corresponds to a radiative pathway called fluorescence. Since this transition is between two states with a singlet multiplicity, it is spin allowed and therefore is a fast process that occurs in the picoseconds to nanoseconds time scale. On the other hand, the electron can undergo intersystem crossing to a triplet excited state (T_n), relax through internal conversion to the first triplet excited state (T_1) and then be followed by the emission of a photon to the ground state (S_0). Since this transition is spin forbidden, this decay occurs at a much lower time scale, from microseconds to seconds, and it is named phosphorescence. Finally, a non-radiative vibronic relaxation mediated by the collisions of the molecules in the surrounding environment can occur from either the singlet or the triplet excited states resulting in the molecule not displaying any luminescence. Therefore, it is evidenced that the challenges in the obtention of luminescent compounds rely in the favouring of the radiative versus the non-radiative pathways.

Additionally, one of the areas of interest in the preparation of luminescent compounds is the obtention of phosphorescence emission, which is more challenging as it requires an intersystem crossing transition which is spin forbidden. One strategy to favour this transition is by the introduction of a heavy atom in the chemical structure, which presents a high spin orbit coupling constant due to relativistic effects allowing the $S_1 \rightarrow T_1$ transition. However, the emission from the singlet might compete with ISC, which can result in one molecule displaying either fluorescence, phosphorescence, or both at the same time (dual emission).

Therefore, the use of platinum, which is a heavy atom, results in a fast intersystem crossing promoting this phosphorescent emission. Particularly, cyclometallated platinum compounds have been widely studied for their application as phosphorescent materials as they display more efficient emission regarding other platinum complexes.[97,98] This is because they present a strong Pt-C bond, whose strong ligand field nature can induce a large d-orbital splitting, raising the non-radiative d-d transition to a higher energy to avoid competition with the emissive states which are usually identified as metal-to-ligand charge transfer (^{3}MLCT), or a ligand centred (^{3}LC) mixed state.[99] The energy gap for these transitions is between the d_z^2 orbital of the platinum and the π^* orbital of the ligand (^{3}MLCT) or between the π and π^* orbitals of the ligand (^{3}LC).[100] Additionally, they are geometrically rigid because of the nature of chelation, which is a major factor as geometric distortion in the excited state would accelerate the non-radiative decay through

vibrational transitions. The combination of both factors contributes to a high quantum efficiency of the emission in these compounds, therefore making them excellent candidates for the fabrication of efficient optical devices.[19,101,102]

1.3.2. Tuning of the luminescence

Research in the obtention of phosphorescent materials is mainly focused in improving the emission quantum efficiency and tuning the colour of the emission. This is necessary for the fabrication of efficient devices such as solar cells or OLEDs; or their use in other applications such as photocatalysis or chemosensing among others.[103]

Cyclometallated platinum compounds, which can accommodate bidentate, tridentate or tetradentate chelating ligands and complementary ancillary ligands when required that can be easily modified, allow a considerable flexibility in the design of a compound with specific properties. The HOMO and LUMO levels of the ligands must be managed to allow the participation of the platinum heavy atom in the emissive transition state, which is crucial for promoting phosphorescence emission.[26]

For this, the photophysical properties of a large number of cyclometallated platinum(II) compounds have been reported allowing to establish some correlations between their structure and their emissive character.[104,105] Generally, it has been observed that upon increase in the rigidity of the cyclometallating ligand (from bidentate, to tridentate or tetradentate), an increase in the quantum efficiency of the emission is generally observed, due to a reduction of the vibrational transitions. As expected, this is also seen upon increasing aromaticity of the ligand.

Additionally, upon decrease of the emission energy, the quantum yield of the emission is expected to decrease according to the energy gap law that favours the non-radiative deactivation pathways. Therefore, one of the major challenges is to develop highly efficient materials emitting in the red and near-infrared (NIR) region. This is of interest for the fabrication of optical devices that emit in this region, but it is particularly meaningful in in vivo biological sensing and imaging because the near-infrared region is the optical window for biological systems in which their absorption is minimum compared with the other areas of the visible region.[106,107]

Some changes in the energy gap, and thus in the emission colour, can be induced by the use of either electron donating or electron withdrawing substituents in both the

cyclometallating ligand or in the ancillary positions. However, this is not straight forward as the change in the emission energy might not be accompanied with an increase in the emission quantum yield.[97]

For example, a series [N,C,N] cyclometallated platinum(II) compounds were reported which differ in the substituent in the 4- position (R) of the central phenyl ring. It was observed that the introduction of electron-releasing aryl groups shifts the emission increasingly to the red according to their electron-donating ability (*Figure 1.8*). DFT calculations confirmed that the influence of the substituent is primarily on the HOMO, and that the observed red shift with increasing electron-donating ability reflects an increase in the HOMO level and a LUMO that remains essentially unchanged, as it is localised predominantly on the pyridyl rings.[108]

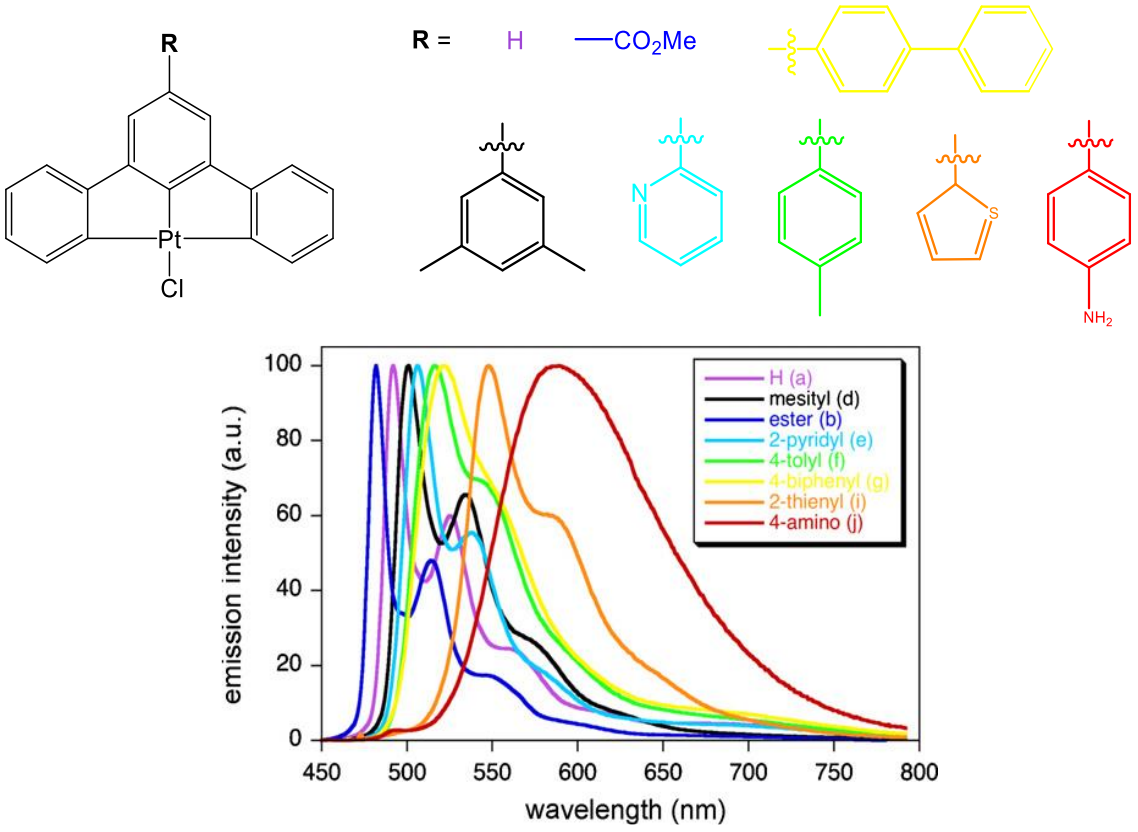

Figure 1.8. Normalised emission spectra for [N,C,N] compounds at room temperature in CH_2Cl_2 (λ_{exc} = 400 nm).Adapted figure.[97]

The planar geometry of cyclometallated platinum(II) compounds facilitates their aggregation through the presence of intermolecular interactions, including π-π stacking between the aromatic parts of the molecule.[109] Metallophilic interactions can also be

observed if the platinum atoms are at a distance no longer than the sum of their van der Waals radii (3.5 Å), specifically called platinophilic interactions. All these are sensitive to both the solvent composition and the compound concentration, as well as the steric hindrance and nature of both the cyclometallating and the ancillary ligands.[110,111]

According to Miskowski and co-workers, upon the presence of platinophilic interactions, the axial $5d_z^2$ orbitals of two platinum(II) atoms overlap to give bonding (dσ) and antibonding (dσ*) orbitals. This also happens with the π and π* orbitals localized in the aromatic ligand upon the presence of π-π stacking interactions, which produce bonding (σ(π) and σ(π*)) and antibonding (σ*(π) and σ*(π*)) orbitals. Consequently, dσ* → σ(π*) metal-to-metal-to-ligand charge transfer (^{3}MMLCT) transitions occur with a reduced energy gap, giving rise to a red-shifted absorption and emission maxima (*Figure 7.9*).[112–114] Even if no metallophilic interactions are present, σ*(π) → σ(π*) transitions because of intermolecular π-π interactions also lead to electronic excited states of lower energy.[100,115,116]

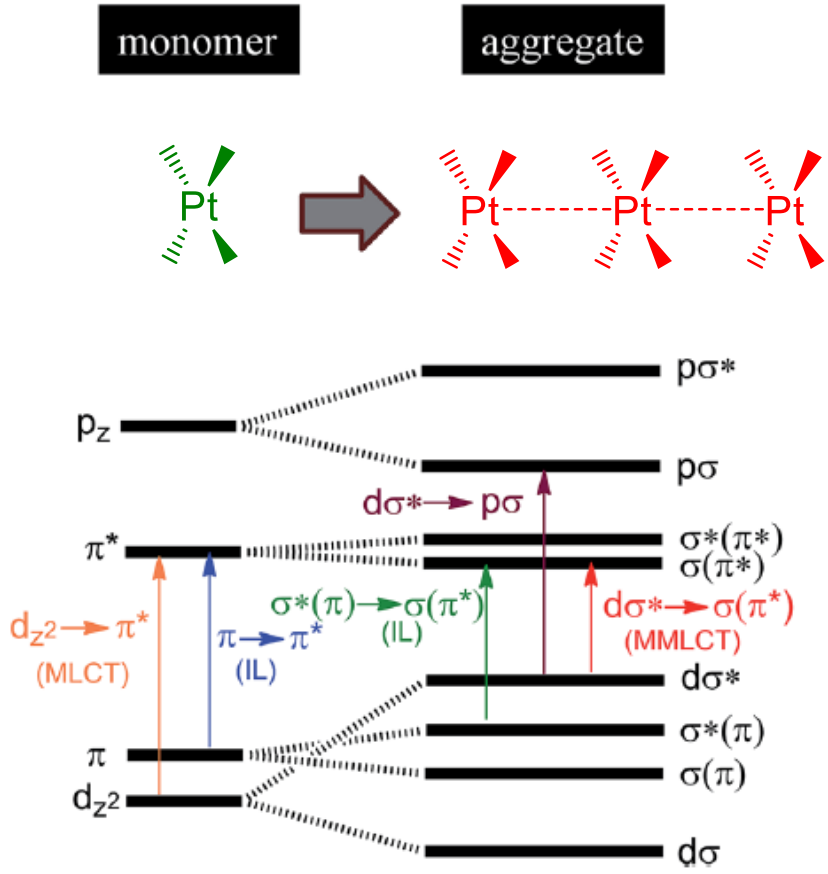

Figure 1.9. Proposed molecular orbital diagram illustrating d^8-d^8 and π- π interactions in platinum(II) compounds. Adapted figure.[109]

As a summary, the presence of these platinophilic or π-π contacts implies a raise in energy in the ground state compared to that of the isolated molecules, therefore shifting the emission to lower energies. However, it has to be considered that these interactions can also be present in the excited state, resulting in lower-energy emissive excimeric ^{3}MMLCT or $^3\pi\rightarrow\pi^*$ excited states.[117,118] Furthermore, the packing of the monomers in fixed assemblies contributes to the decrease of non-radiative processes by reducing vibration which can lead to aggregation induced emission (AIE) enhancement behaviours.[119]

1.4. Objectives of the present work

For several years, the Synthesis and Applications of Cyclometallated Compounds (CM) group from Universitat de Barcelona has been devoted to the synthesis and mechanistic studies of cyclometallated platinum(II) and platinum(IV) compounds.[120–122] More recently, the group has successfully designed and evaluated the anticancer properties of several of these compounds setting a base on the correlation between their biological activity and their structural modifications.[1,93,95,96,123] Moreover, the Supra and Nanostructured Systems (SuNS) from Universitat de Barcelona has developed an extensive research in luminescent compounds and their application in optical devices, specifically studying the photophysical properties of some cyclometallated platinum(II) compounds in collaboration with the CM group.[124]

Therefore, this Thesis follows up with this prior knowledge as a collaboration between the two groups, with the aim to synthesise several cyclometallated platinum compounds with different structural modifications rationally designed specifically for biological or optical applications. This requires the use of different synthetic strategies to achieve the final products and a wide use of characterisation techniques (^{1}H and ^{19}F NMR, mass spectrometry, IR spectroscopy, elemental analysis, and X-ray diffraction), to evidence the correct formation of the desired compounds.

For the biological applications, the specific objectives are to obtain efficient alternatives to the clinically approved platinum anticancer drugs, minimizing their side effects and attempting to overcome platinum resistance. On the other hand, for the optical applications this research aims towards the obtention of luminescent compounds with an optimized, red-shifted phosphorescence emission with the possibility to be applied in the fabrication of optical devices.

The particular objectives of this Thesis are summarized below.

In *Chapter 2*, a large family of [C,N,N’] cyclometallated platinum(II) and platinum(IV) compounds will be prepared with the use of different synthetic methods from ligand 4-$FC_6H_4CH=N(CH_2)_3N(CH_3)_2$, previously known to give rise to luminescent compounds. It will be aimed to establish a correlation between the nature of the ancillary ligands (methyl or halido) and the oxidation state of the platinum with the resulting optical properties of the final compounds.

In *Chapter 3*, an analogous family of [C,N,N'] cyclometallated compounds will be synthesised from ligand 4-$FC_6H_4CH=N(CH_2)_2N(CH_3)_2$ with a more rigid ethylene chain. Following up on previous studies, these compounds along with some selected from *Chapter 2* will be studied to establish the effect of their nature (oxidation state, ancillary ligands, and length of the aliphatic chain) in their anticancer activity, as well as their differences in their luminescence properties and their ability to overcome platinum resistance in different cancer cell lines.

In *Chapter 4*, the structure of compound $[PtCl_3\{(CH_3)_2N(CH_2)_3N=CH(4\text{-}FC_6H_3)\}]$ (**5a**), which gave the more promising results in *Chapter 3*, has been selected to introduce hydroxido or carboxylato groups as axial ancillary ligands to prepare cyclometallated platinum(IV) compounds and attempt to enhance their anticancer activity through the introduction of these groups. The biological properties of the new compounds will be studied and compared with compound **5a** and their reduction potentials will be determined to establish their ability to reduce under cellular media and perform as pro-drugs, all as a direct relation with the nature of the axial ligands (chlorido, hydroxido or carboxylato).

In *Chapter 5*, upon selection of the structure $[PtCl\{(CH_3)_2N(CH_2)_2N=CH(4\text{-}FC_6H_3)\}]$ (**4a**) from *Chapter 3* that gave rise to the most efficient luminescent properties, the substitution of the chlorido for different alkynyl aromatic ligands will be performed to evaluate their effect in the optical properties of the new compounds. An exhaustive photophysical characterisation will be performed to understand the different radiative and non-radiative pathways that govern the emission of these molecules along with testing their ability to produce singlet oxygen ($^1O_2$).

In *Chapter 6*, two series of planar [N,C,N] cyclometallated platinum(II) compounds derived from 1,3-di(2-pyridinyl)benzene (**L3**) or 2,2'-(5-fluoro-1,3-phenylene)dipyridine (**L4**) will be synthesised with an alkynyl chromophore moiety as an ancillary ligand. The effect of both the cyclometallated moiety as well as the nature of the chromophore in the photophysical properties and the ability of the compounds to establish intermolecular interactions will be evaluated, aiming to achieve a red-shifted emission due to excimeric excited states or aggregation.

In *Chapter 7*, the effect of the addition of silver(I) in the photophysical properties of the compounds synthesised in *Chapter 6* will be evaluated with the aim to induce a red-

shifted emission without modifications in the environment. Upon selection of the best results, two families of heterometallic platinum(II)/silver(I) compounds will be synthesised to evaluate the difference in their luminescent properties in comparison with their precursors. Compound [{2,6-(2-$C_5H_4N)_2$-4-FC_6H_2}Pt(μ-C≡CPhen)Ag(μ-C≡CPhen)Pt[{2,6-(2-$C_5H_4N)_2$-4-FC_6H_2}] **(12e**) will be used for the preparation of Light-emitting electrochemical cells (LEECs) and therefore to evaluate its possible application in optical devices.

1.5. References

1. Crespo, M. *J. Organomet. Chem.* **2019**, *879*, 15–26.
2. Klein, A. *Inorganics* **2015**, *3*, 155–159.
3. Labinger, J.A. *Chem. Rev.* **2017**, *117*, 8483–8496.
4. Jain, V.K. *Coord. Chem. Rev.* **2021**, *427*, 213546.
5. Albrecht, M. *Chem. Rev.* **2010**, *110*, 576–623.
6. Rendina, L.M.; Puddephatt, R.J. *Chem. Rev.* **1997**, *97*, 1735–1754.
7. Cope, A.C.; Siekman, R.W. *J. Am. Chem. Soc.* **1965**, *87*, 3272–3273.
8. Cope, A.C.; Friedrich, E.C. *J. Am. Chem. Soc.* **1968**, *90*, 909–913.
9. Cornioley-Deuschel, C.; Ward, T.; Zelewsky, A. V. *Helv. Chim. Acta* **1988**, *71*, 130–133.
10. Maestri, M.; Deuschel-Cornioley, C.; von Zelewsky, A. *Coord. Chem. Rev.* **1991**, *111*, 117–123.
11. Cave, G.W.V.; Alcock, N.W.; Rourke, J.P. *Organometallics* **1999**, *18*, 1801–1803.
12. Cave, G.W.V.; Fanizzi, F.P.; Deeth, R.J.; Errington, W.; Rourke, J.P. *Organometallics* **2000**, *19*, 1355–1364.
13. Yam, V.W.W.; Au, V.K.M.; Leung, S.Y.L. *Chem. Rev.* **2015**, *115*, 7589–7728.
14. Yam, V.W.W.; Law, A.S.Y. *Coord. Chem. Rev.* **2020**, *414*, 213298.
15. Puttock, E. V.; Walden, M.T.; Williams, J.A.G. *Coord. Chem. Rev.* **2018**, *367*, 127–162.
16. Haque, A.; Xu, L.; Al-Balushi, R.A.; Al-Suti, M.K.; Ilmi, R.; Guo, Z.; Khan, M.S.; Wong, W.Y.; Raithby, P.R. *Chem. Soc. Rev.* **2019**, *48*, 5547–5563.
17. Kurzeev, S.A.; Vilesov, A.S.; Fedorova, T. V.; Stepanova, E. V.; Koroleva, O. V.; Bukh, C.; Bjerrum, M.J.; Kurnikov, I. V.; Ryabov, A.D. *Biochemistry* **2009**, *48*, 4519–4527.
18. Hong, G.; Gan, X.; Leonhardt, C.; Zhang, Z.; Seibert, J.; Busch, J.M.; Bräse, S.

Adv. Mater. **2021**, *33*, 2005630.

19. Fleetham, T.; Li, G.; Li, J. *Adv. Mater.* **2017**, *29*, 1–16.
20. Gao, H.; Yu, R.; Ma, Z.; Gong, Y.; Zhao, B.; Lv, Q.; Tan, Z. *J. Polym. Sci.* **2022**, *60*, 865–916.
21. Zhao, Q.; Cao, T.; Li, F.; Li, X.; Jing, H.; Yi, T.; Huang, C. *Organometallics* **2007**, *26*, 2077–2081.
22. Isozaki, K.; Takaya, H.; Naota, T. *Angew. Chem. Int. Ed.* **2007**, *46*, 2855–2857.
23. Hudson, S.A.; Maitlis, P.M. *Chem. Rev.* **1993**, *93*, 861–885.
24. Zhang, Y.P.; Zheng, Y.X. *Dalton Trans.* **2022**, *51*, 9966–9970.
25. Albrecht, M.; Lutz, M.; Spek, A.L.; Van Koten, G. *Nature* **2000**, *406*, 970–974.
26. Huo, S.; Carroll, J.; Vezzu, D.A.K. *Asian J. Org. Chem.* **2015**, *4*, 1210–1245.
27. Manar, K.K.; Ren, P. *Adv. Organomet. Chem.* **2021**, *76*, 185-259. Chapter 4: Recent Progress on Group 10 Metal Complexes of Pincer Ligands: From Synthesis to Activities and Catalysis. *Academic Press.* Ed: Pérez, P.J..
28. Hruzd, M.; Gauthier, S.; Boixel, J.; Kahlal, S.; le Poul, N.; Saillard, J.Y.; Achelle, S.; Guen, F.R. le *Dyes Pigm.* **2021**, *194*, 109622.
29. Zhao, S.; Yang, Z.; Jiang, G.; Huang, S.; Bian, M.; Lu, Y.; Liu, W. *Coord. Chem. Rev.* **2021**, *449*, 214217.
30. Yam, V.W.; Tang, R.P.; Wong, K.M.; Lu, X. *Chem. Eur. J.* **2002**, *8*, 4066–4076.
31. Nabavizadeh, S.M.; Amini, H.; Rashidi, M.; Pellarin, K.R.; McCready, M.S.; Cooper, B.F.T.; Puddephatt, R.J. *J. Organomet. Chem.* **2012**, *713*, 60–67.
32. Juliá, F.; García-Legaz, M.D.; Bautista, D.; González-Herrero, P. *Inorg. Chem.* **2016**, *55*, 7647–7660.
33. Omae, I. *Coord. Chem. Rev.* **2014**, *280*, 84–95.
34. Crespo, M. *Inorganics* **2014**, *2*, 115–131.
35. Crespo, M.; Font-Bardía, M.; Pérez, S.; Solans, X. *J. Organomet. Chem.* **2002**, *642*, 171–178.

36. Selander, N.; Szabó, K.J. *Dalton Trans.* **2009**, 6267–6279.

37. Goldman, A. S.; Roy, A. H.; Huang, Z.; Ahuja, R.; Schinski, W.; Brookhart, M. *Science* **2006**, *312*, 257–261.

38. Li, J.; Luo, Y.; Hu, L.; Liu, L.; Lai, Y.L.; Xiong, W. *Eur. J. Org. Chem.* **2023**, *26*, e202201387.

39. Powers, D.C.; Ritter, T. *Nat. Chem.* **2009**, *1*, 302–309.

40. Omae, I. *J. Organomet. Chem.* **2017**, *848*, 184–195.

41. Crespo, M.; Martinez, M.; Sales, J.; Solans, X.; Font-Bardía, M. *Organometallics* **1992**, *11*, 1288–1295.

42. Sahoo, S.R.; Dutta, S.; Al-Thabaiti, S.A.; Mokhtar, M.; Maiti, D. *Chem. Commun.* **2021**, *57*, 11885–11903.

43. Topps, J.; Elliott, R.C. *Nature* **1965**, *205*, 498–499.

44. Traub, W.; Yonath, A. *Nature* **1969**, *224*, 177–178.

45. DeConti, R.C.; Toftness, B.R.; Lange, R.C.; Creasey, W.A. *Cancer Res.* **1973**, *33*, 1310–1315.

46. Talley, R.W.; O'Bryan, R.M.; Gutterman, J.U.; Brownlee, R.W.; McCredie, K.B. *Cancer Chemother. Rep.* **1973**, *57*, 465–471.

47. Higby, D.J.; Wallace, H.J.; Albert, D.; Holland, J.F. *J. Urol.* **1974**, *112*, 100–104.

48. Higby, D.J.; Higby, D.J.; Wallace, H.J.; Albert, D.J.; Holland, J.F. *Cancer* **1974**, *33*, 1219–1225.

49. Rozencweig, M.; Von Hoff, D.D.; Slavik, M.; Muggia, F.M. *Ann. Inter. Med* **1977**, *86*, 803–812.

50. Bosl, G.J.; Motzer, R.J. *New Engl. J. Med.* **1997**, *337*, 242–253.

51. Todd, R.C.; Lippard, S.J. *Metallomics* **2009**, *1*, 280–291.

52. Fichtinger-Schepman, A.M.J.; Lohman, P.H.M.; van der Veer, J.L.; den Hartog, J.H.J.; Reedijk, J. *Biochemistry* **1985**, *24*, 707–713.

53. Rocha, C.R.R.; Silva, M.M.; Quinet, A.; Cabral-Neto, J.B.; Menck, C.F.M. *Clinics*

2018, *73*, 1–10.

54. Takahara, P.M.; Rosenzweig, A.C.; Frederick, C.A.; Lippard, S.J. *Nature* **1995**, *377*, 649–652.

55. Takahara, P.M.; Frederick, C.A.; Lippard, S.J. *J. Am. Chem. Soc.* **1996**, *118*, 12309–12321.

56. Todd, R.C.; Lippard, S.J. *J. Inorg. Biochem.* **2010**, *104*, 902–908.

57. Ang, W.H.; Myint, M.; Lippard, S.J. *J. Am. Chem. Soc.* **2010**, *132*, 7429–7435.

58. Daugaard, G.; Abildgaard, U. *Cancer Chemother. Pharmacol.* **1989**, *25*, 1–9.

59. Cvitkovic, E. *Cancer Treat. Rev.* **1998**, *24*, 265–281.

60. Screnci, D.; McKeage, M.J. *J. Inorg. Biochem.* **1999**, *77*, 105–110.

61. Galluzzi, L.; Senovilla, L.; Vitale, I.; Michels, J.; Martins, I.; Kepp, O.; Castedo, M.; Kroemer, G. *Oncogene* **2012**, *31*, 1869–1883.

62. Shen, D.W.; Pouliot, L.M.; Hall, M.D.; Gottesman, M.M. *Pharmacol. Rev.* **2012**, *64*, 706–721.

63. Jamieson, E.R.; Lippard, S.J. *Chem. Rev.* **1999**, *99*, 2467–2498.

64. Wheate, N.J.; Walker, S.; Craig, G.E.; Oun, R. *Dalton Trans.* **2010**, *39*, 8113–8127.

65. Peña, Q.; Wang, A.; Zaremba, O.; Shi, Y.; Scheeren, H.W.; Metselaar, J.M.; Kiessling, F.; Pallares, R.M.; Wuttke, S.; Lammers, T. *Chem. Soc. Rev.* **2022**, *51*, 2544–2582.

66. Alassadi, S.; Pisani, M.J.; Wheate, N.J. *Dalton Trans.* **2022**, *51*, 10835–10846.

67. Lovejoy, K.S.; Todd, R.C.; Zhang, S.; McCormick, M.S.; D'Aquino, J.A.; Reardon, J.T.; Sancar, A.; Giacomini, K.M.; Lippard, S.J. *Proc. Natl. Acad. Sci. U. S. A.* **2008**, *105*, 8902–8907.

68. Spingler, B.; Whittington, D.A.; Lippard, S.J. *Inorg. Chem.* **2001**, *40*, 5596–5602.

69. Cleare, M.J.; Hoeschele, J.D. *Platin. Met. Rev.* **1973**, *17*, 2–13.

70. Silverman, A.P.; Bu, W.; Cohen, S.M.; Lippard, S.J. *J. Biol. Chem.* **2002**, *277*,

49743–49749.

71. van der Vijgh, W.J.F. *Clin. Pharmacokinet.* **1991**, *21*, 242–2261.

72. Aziz, M.H.; Ahmad, A. *Cancer Drug Resist.* **2020**, *3*, 113–116.

73. Zhang, S.; Wang, X.; Guo, Z. *Rational Design of Anticancer Platinum(IV) Prodrugs* **2020**, *75*.

74. Wilson, J.J.; Lippard, S.J. *Chem. Rev.* **2014**, *114*, 4470–4495.

75. Gibson, D. *Dalton Trans.* **2016**, *45*, 12983–12991.

76. Johnstone, T.C.; Suntharalingam, K.; Lippard, S.J. *Chem. Rev.* **2016**, *116*, 3436–3486.

77. Kenny, R.G.; Chuah, S.W.; Crawford, A.; Marmion, C.J. *Eur. J. Inorg. Chem.* **2017**, *2017*, 1596–1612.

78. Su, S.; Chen, Y.; Zhang, P.; Ma, R.; Zhang, W.; Liu, J.; Li, T.; Niu, H.; Cao, Y.; Hu, B.; Gao, J.; Sun, H.; Fang, D.; Wang, J.; Wang, P. G.; Xie, S.; Wang, C.; Ma, J. *Eur. J. Med. Chem.* **2022**, *243*, 114680.

79. Wexselblatt, E.; Gibson, D. *J. Inorg. Biochem.* **2012**, *117*, 220–229.

80. Hall, M.D.; Hambley, T.W. *Coord. Chem. Rev.* **2002**, *232*, 49–67.

81. Johnstone, T.C.; Wilson, J.J.; Lippard, S.J. *Inorg. Chem.* **2013**, *52*, 12234–12249.

82. Zhang, P.; Sadler, P.J. *J. Organomet. Chem.* **2017**, *839*, 5–14.

83. Gasser, G.; Ott, I.; Metzler-Nolte, N. *J. Med. Chem.* **2011**, *54*, 3–25.

84. Hartinger, C.G.; Metzler-Nolte, N.; Dyson, P.J. *Organometallics* **2012**, *31*, 5677–5685.

85. Cutillas, N.; Yellol, G.S.; De Haro, C.; Vicente, C.; Rodríguez, V.; Ruiz, J. *Coord. Chem. Rev.* **2013**, *257*, 2784–2797.

86. Khoury, A.; Deo, K.M.; Aldrich-Wright, J.R. *J. Inorg. Biochem.* **2020**, *207*, 111070.

87. Jurgens, S.; Kuhn, F.E.; Casini, A. *Curr. Med. Chem.* **2017**, *25*, 437–461.

88. Liu, W.; Gust, R. *Chem. Soc. Rev.* **2013**, *42*, 755–773.

89. El-Mehasseb, I.M.; Kodaka, M.; Okada, T.; Tomohiro, T.; Okamoto, K.; Okuno, H. *J. Inorg. Biochem.* **2001**, *84*, 157–158.

90. Pang, Y.; Li, C.; Deng, H.; Sun, Y. *Dalton Trans.* **2022**, *51*, 16428–16438.

91. Tsai, J.L.L.; Zou, T.; Liu, J.; Chen, T.; Chan, A.O.Y.; Yang, C.; Lok, C.N.; Che, C.M. *Chem. Sci.* **2015**, *6*, 3823–3830.

92. Mauro, M.; Aliprandi, A.; Septiadi, D.; Kehr, N.S.; De Cola, L. *Chem. Soc. Rev.* **2014**, *43*, 4144–4166.

93. Bauer, E.; Domingo, X.; Balcells, C.; Polat, I.H.; Crespo, M.; Quirante, J.; Badía, J.; Baldomà, L.; Font-Bardia, M.; Cascante, M. *Dalton Trans.* **2017**, *46*, 14973–14987.

94. Escolà, A.; Crespo, M.; Quirante, J.; Cortés, R.; Jayaraman, A.; Badia, J.; Baldomà, L.; Calvet, T.; Font-Bardía, M.; Cascante, M. *Organometallics* **2014**, *33*, 1740–1750.

95. Escolà, A.; Crespo, M.; López, C.; Quirante, J.; Jayaraman, A.; Polat, I.H.; Badía, J.; Baldomà, L.; Cascante, M. *Bioorg. Med. Chem.* **2016**, *24*, 5804–5815.

96. Solé, M.; Balcells, C.; Crespo, M.; Quirante, J.; Badia, J.; Baldomà, L.; Font-Bardia, M.; Cascante, M. *Dalton Trans.* **2018**, *47*, 8956–8971.

97. Gareth Williams, J.A.; Develay, S.; Rochester, D.L.; Murphy, L. *Coord. Chem. Rev.* **2008**, *252*, 2596–2611.

98. Zhang, Q.C.; Xiao, H.; Zhang, X.; Xu, L.J.; Chen, Z.N. *Coord. Chem. Rev.* **2019**, *378*, 121–133.

99. Berenguer, J.R.; Lalinde, E.; Moreno, M.T. *Coord. Chem. Rev.* **2018**, *366*, 69–90.

100. Ravotto, L.; Ceroni, P. *Coord. Chem. Rev.* **2017**, *346*, 62–76.

101. Williams, J. A. G. *Top Curr. Chem.* **2007**, *281*, 205-268.

102. Cebrián, C.; Mauro, M. *Beilstein J. Org. Chem.* **2018**, *14*, 1459–1481.

103. Chaaban, M.; Zhou, C.; Lin, H.; Chyi, B.; Ma, B. *J. Mater. Chem. C* **2019**, *7*, 5910–5924.

104. Feng, Z.; Sun, Y.; Yang, X.; Zhou, G. *Chem. Rec.* **2019**, *19*, 1710–1728.

105. Hamidizadeh, P.; Babadi Aghakhanpour, R.; Chamyani, S.; Paziresh, S.; Shahsavari, H.R.; Nabavizadeh, S.M. *Organometallics* **2022**, *41*, 1325–1333.

106. Liu, Y.; Li, Z.; Chen, L.; Xie, Z. *Dyes Pigm.* **2017**, *141*, 5–12.

107. Li, J.; Ma, Y.; Liu, S.; Mao, Z.; Chi, Z.; Qian, P.C.; Wong, W.Y. *Chem. Commun.* **2020**, *56*, 11681–11684.

108. Farley, S.J.; Rochester, D.L.; Thompson, A.L.; Howard, J.A.K.; Williams, J.A.G. *Inorg. Chem.* **2005**, *44*, 9690–9703.

109. Li, K.; Ming Tong, G.S.; Wan, Q.; Cheng, G.; Tong, W.Y.; Ang, W.H.; Kwong, W.L.; Che, C.M. *Chem. Sci.* **2016**, *7*, 1653–1673.

110. Sathish, V.; Ramdass, A.; Thanasekaran, P.; Lu, K.L.; Rajagopal, S. *J. Photochem. Photobiol. C Photochem. Rev.* **2015**, *23*, 25–44.

111. Aliprandi, A.; Mauro, M.; De Cola, L. *Nature Chem.* **2016**, *8*, 10–15.

112. Miskowski, V.M.; Houlding, V.H. *Inorg. Chem.* **1991**, *30*, 4446–4452.

113. Zheng, Q.; Borsley, S.; Nichol, G.S.; Duarte, F.; Cockroft, S.L. *Angew. Chem.* **2019**, *131*, 12747–12753.

114. Xie, M.; Lu, W. *Dalton Trans.* **2019**, *48*, 1275–1283.

115. Miskowski, V.M.; Houlding, V.H. *Inorg. Chem.* **1989**, *28*, 1529–1533.

116. Martínez-Junquera, M.; Lara, R.; Lalinde, E.; Moreno, M.T. *J. Mater. Chem. C* **2020**, *8*, 7221–7233.

117. Lai, S.W.; Chan, M.C.W.; Cheung, T.C.; Peng, S.M.; Che, C.M. *Inorg. Chem.* **1999**, *38*, 4046–4055.

118. Young, R.M.; Wasielewski, M.R. *Acc. Chem. Res.* **2020**, *53*, 1957–1968.

119. Zhao, Z.; Zhang, H.; Lam, J.W.Y.; Tang, B.Z. *Angew. Chem. Int. Ed.* **2020**, *59*, 9888–9907.

120. Bernhardt, P. V.; Calvet, T.; Crespo, M.; Font-Bardía, M.; Jansat, S.; Martínez, M. *Inorg. Chem.* **2013**, *52*, 474–484.

121. Crespo, M.; Font-Bardia, M.; Hamidizadeh, P.; Martínez, M.; Nabavizadeh, S.M.

Inorg. Chim. Acta **2019**, *486*, 8–16.

122. Anderson, C.M.; Crespo, M.; Kfoury, N.; Weinstein, M.A.; Tanski, J.M. *Organometallics* **2013**, *32*, 4199–4207.

123. Escolà, A.; Crespo, M.; Quirante, J.; Cortés, R.; Jayaraman, A.; Badia, J.; Baldomà, L.; Calvet, T.; Font-Bardía, M.; Cascante, M. *Organometallics* **2014**, *33*, 1740–1750.

124. Gandioso, A.; Valle-Sistac, J.; Rodríguez, L.; Crespo, M.; Font-Bardía, M. *Organometallics* **2014**, *33*, 561–570.

CHAPTER 2

Influence of the ancillary ligand and oxidation state in the photophysical properties of cyclometallated [C,N,N'] platinum compounds

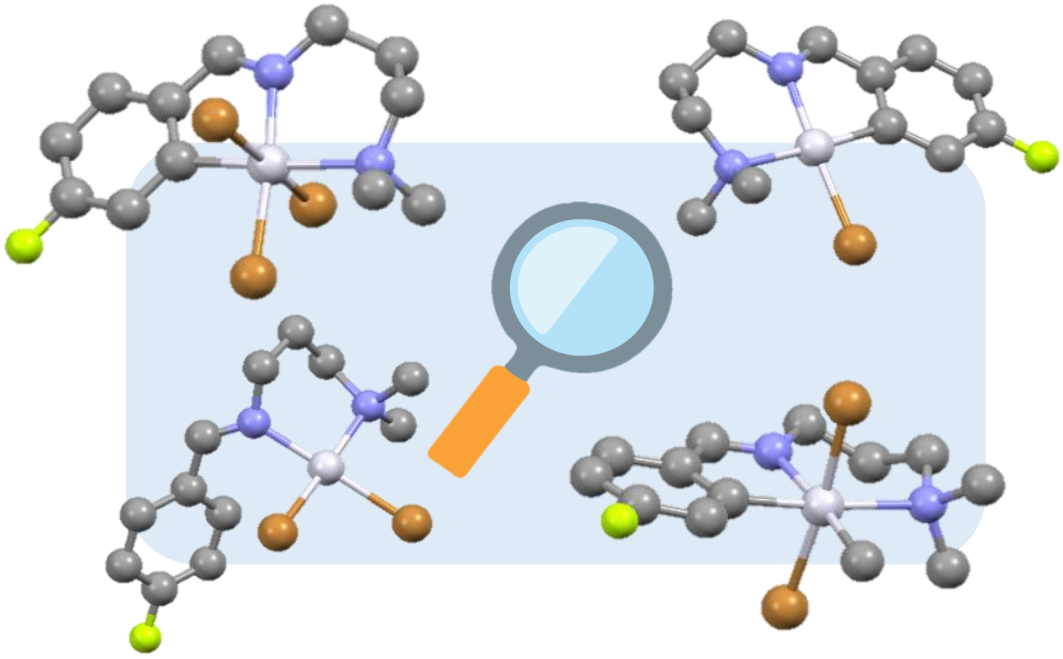

Part of this chapter has been published in: Lázaro, A.; Serra, O.; Rodríguez, L.; Crespo, M.; Font-Bardia, M. *New J. Chem.* **2019**, *43*, 1247-1256.

2. Influence of the ancillary ligand and oxidation state in the photophysical properties of cyclometallated [C,N,N'] platinum compounds

2.1. Introduction

Cyclometallated platinum(II) compounds containing a tridentate [C,N,N'] ligand have attracted a great interest thanks to their photophysical properties. These properties are enhanced compared to [C,N] cyclometallated compounds, due to their higher rigidity which favours luminescence over other non-radiative decay pathways. Additionally, they benefit from a second N-donor atom that gives them higher stability.[1–4] Moreover, several studies carried out in different families of compounds reveal that their emission can be tuned by structural modifications, such as the functionalization of the tridentate ligand as well as the nature of the ancillary ligand.[5–7]

However, in spite of the great number of cycloplatinated compounds for which the luminescence properties have been studied so far, those containing aldimide or ketamide ligands have been less explored.[8–10] The synthesis of these compounds can be carried out through different methods although cyclometallation, which can undergo different mechanisms, is the most commonly used. For all of them, the first step is the coordination of the ligand as a bidentate [N,N'] ligand, for which is required to use a platinum(II) metallating agent that contains two labile ligands that could be replaced. Once the [N,N'] coordination compound is formed, in order to form the Pt-C bond, a C-H activation has to take place.[11,12]

This activation proceeds through different mechanisms depending on the type of platinum(II) complex used as a metallating agent. The first mechanism, shown in *Scheme 2.1*, is the oxidative addition of the C-H bond at the platinum(II) centre, which implies its oxidation to platinum(IV) and immediate reductive elimination to the initial oxidation state.[13–15]

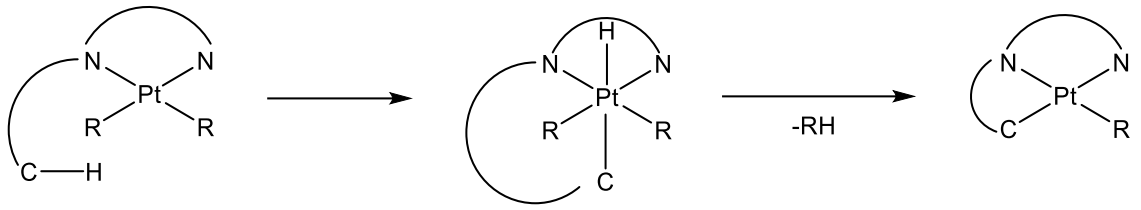

Scheme 2.1. Oxidative addition mechanism for C-H activation.

The second mechanism is an electrophilic activation (*Scheme 2.2*), where the aromatic carbon undergoes an electrophilic aromatic substitution of the H for the metal, giving rise to the formation of the Pt-C bond. The presence of a base in this reaction is essential for the removal of the protons that are generated.[16,17]

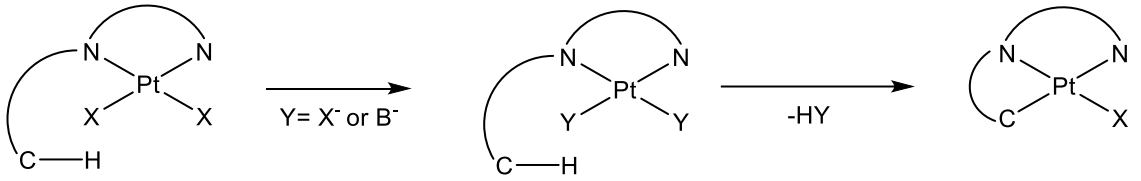

Scheme 2.2. Electrophilic substitution mechanism for C-H activation, X: Halogen, B: Base.

Another less common method to prepare these compounds is by a metathesis reaction, widely used for other square planar complexes, which consists in the exchange of the ancillary ligand of a cyclometallated platinum (II) compound.

On the other hand, the photophysical properties of analogous cyclometallated platinum(IV) compounds have attracted less attention.[18–20] For their preparation, the oxidative addition of molecules like methyl iodide to a cyclometallated platinum(II) compounds has been extensively studied; which takes place through an S_{N2} mechanism. However, oxidative halogenation, which follows the same mechanism as for conventional square planar complexes, is not as widely studied for these compounds.[21]

In the first step, a halogen molecule coordinates in an axial position. Depending on the solvent used, a halide anion may be released, and a molecule of solvent can coordinate in the free axial position to give a cationic complex. This is usually an intermediate to the final compound, where the solvent molecule is substituted by the halide anion giving the expected compound (*Scheme 2.3*).[22,23]

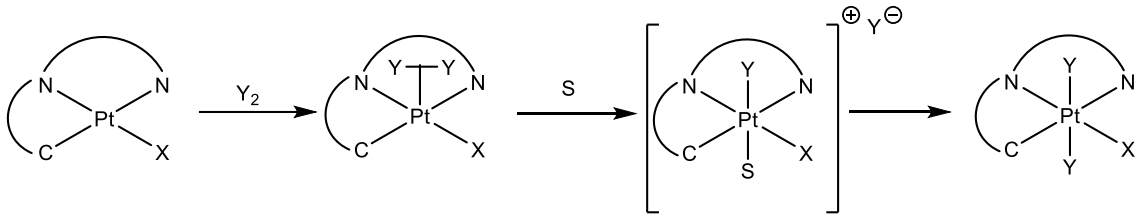

Scheme 2.3. Oxidative halogenation mechanism in platinum (II) cyclometallated compounds (Y: halogen, X: halogen or R).

In this chapter, a large family of [C,N,N'] cyclometallated platinum(II) and platinum(IV) compounds derived from ligand 4-$FC_6H_4CH=N(CH_2)_3N(CH_3)_2$ was synthesized through the different processes mentioned above. The resulting compounds differ in the nature of the ancillary ligand (methyl or halido) and the platinum oxidation state. This study should allow us to evaluate the effect of these variables in the resulting luminescent properties of the platinacycles. This ligand was selected for this chapter since, according to previous results, it allows the formation of luminescent tridentate [C,N,N'] platinum(II) compounds. It contains a fluoro substituent in *para* which has proven to lead to higher quantum yields compared to it being in other positions.[24] The presence of this fluorine atom not only favours their photophysical properties, but also provides these compounds with a higher stability, due to the strength of the C-F bond, and it results useful to complete their characterisation by ^{19}F NMR spectroscopy.[25]

2.2. Results and Discussion

2.2.1. Synthesis and characterisation

Ligand 4-$FC_6H_4CH=N(CH_2)_3N(CH_3)_2$ (**L**) was prepared as reported in the literature *via* the condensation of 4-fluorobenzaldehyde and 3-dimethyl-1-propylamine in toluene, with the consequent removal of the water released (*Scheme 2.4*). Characterisation by ^{1}H and ^{19}F NMR spectroscopy matched with the literature and showed the formation of only one isomer. It is attributed to the more stable *E* configuration around the C=N bond.[24]

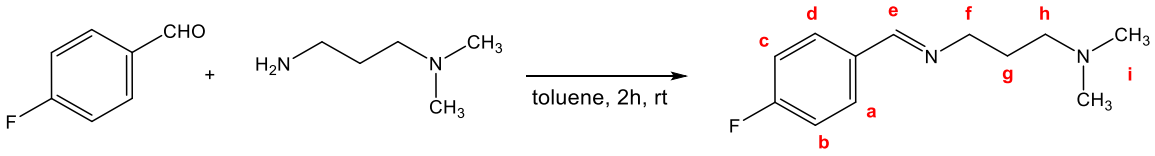

Scheme 2.4. Synthesis of ligand **L1**.

A series of tridentate [C,N,N'] cyclometallated platinum(II) compounds that differ in the ancillary ligand were synthesized with this imine as a cyclometallating ligand. The synthesis of compound $[PtCl\{(CH_3)_2N(CH_2)_3N=CH(4\text{-}FC_6H_3)\}]$ (**1a**) was carried out as reported in the literature by using *cis*-$[PtCl_2(DMSO)_2]$ as a metallating agent (*Scheme 2.5*). In this reaction, after the coordination of the imine as a bidentate [N,N'] ligand substituting both DMSO molecules, the C-H bond activation occurs due to an electrophilic substitution on the aromatic carbon with the consequent release of HCl.[17] Therefore, the use of sodium acetate (CH_3COONa) as a base is essential to achieve the final product, not only for the neutralization of the formed hydrochloric acid, but because it can substitute one of the chloride ligands *cis* to the iminic nitrogen. The presence of the acetate allows a $CH^{(+)}\text{-}N^{(-)}\text{-}CH_2$ intramolecular interaction that stabilises the iminic positive carbon, which favours the intramolecular reaction for the C-H activation, minimizing charge separation. To facilitate this charge transfer a donor solvent such as methanol is more adequate to perform the cyclometallation.[26]

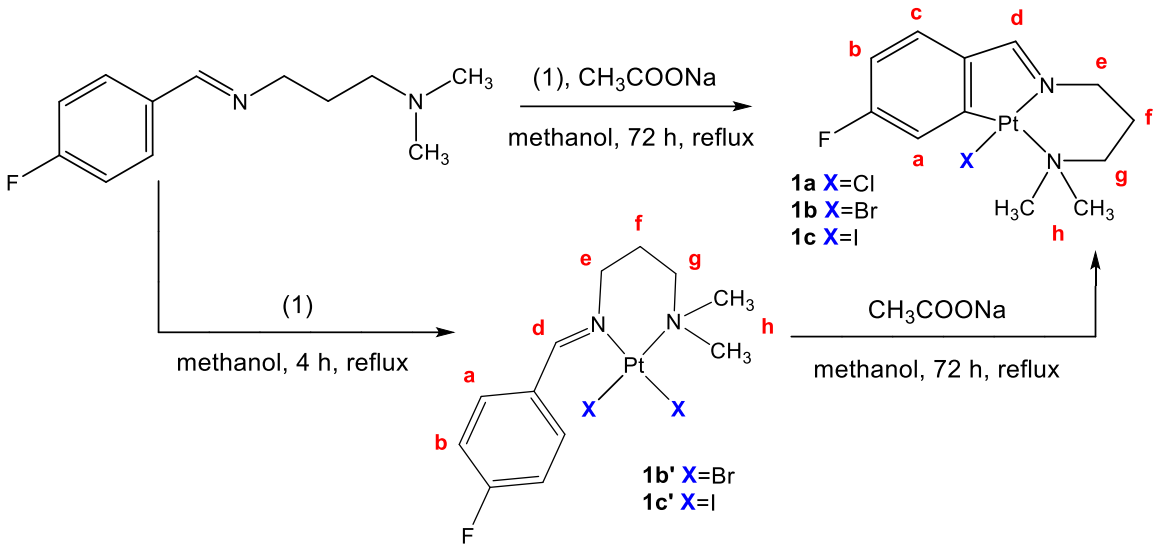

Scheme 2.5. Synthesis of compounds **1a**, **1b** and **1c**. (1) *cis*-[$PtCl_2(DMSO)_2$] (**1a**); *cis*-[$PtBr_2(DMSO)_2$] (**1b**); *cis*-[$PtI_2(DMSO)_2$] (**1c**).

The synthesis of compounds [$PtBr\{(CH_3)_2N(CH_2)_3N{=}CH(4\text{-}FC_6H_3)\}$] (**1b**) and [$PtI\{(CH_3)_2N(CH_2)_3N{=}CH(4\text{-}FC_6H_3)\}$] (**1c**) by the same method with the corresponding *cis*-[$PtX_2(DMSO)_2$] precursors was only successful in the obtention of compound **1c**. For compound **1b**, it resulted in a mixture of the final compound and the non-cyclometallated coordination compound [$PtBr_2\{(CH_3)_2N(CH_2)_3N{=}CH(4\text{-}FC_6H_4)\}$] (**1b'**). Both this compound and compound [$PtI_2\{(CH_3)_2N(CH_2)_3N{=}CH(4\text{-}FC_6H_4)\}$] (**1c'**) can be isolated from the reaction in the absence of sodium acetate, which prevents the C-H activation from taking place (*Scheme 2.5*). Compound **1b** was finally obtained in a pure form by ligand exchange with KBr from compound **1a** (*Scheme 2.6*).

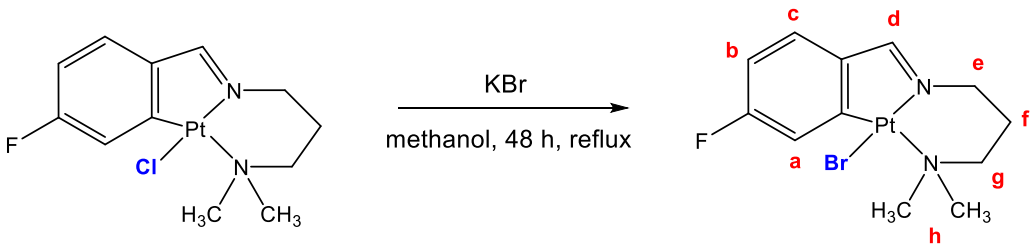

Scheme 2.6. Synthesis of compound **1b**.

Compound [$Pt(CH_3)\{(CH_3)_2N(CH_2)_3N{=}CH(4\text{-}FC_6H_3)\}$] (**1d**) was prepared following the reference method by direct cyclometallation of [$Pt_2(CH_3)_4\{\mu\text{-}S(CH_3)_2\}$] with imine **L1** in refluxing toluene (*Scheme 2.7*).[24] In this case, the C-H bond activation takes place through

oxidative addition. Firstly, the imine substitutes the dimethyl sulphide bridge groups acting as a bidentate [N, N'] ligand, obtaining both *E* and *Z* configurations around the C=N bond. In the second step of the synthesis, this compound isomerizes into the configuration where the C-H bond is closer to the aromatic ring, which is activated by the oxidative addition to the metal. Then, a platinum(IV) intermediate is formed with the immediate reductive elimination of methane to give the cyclometallated platinum(II) compound.[27]

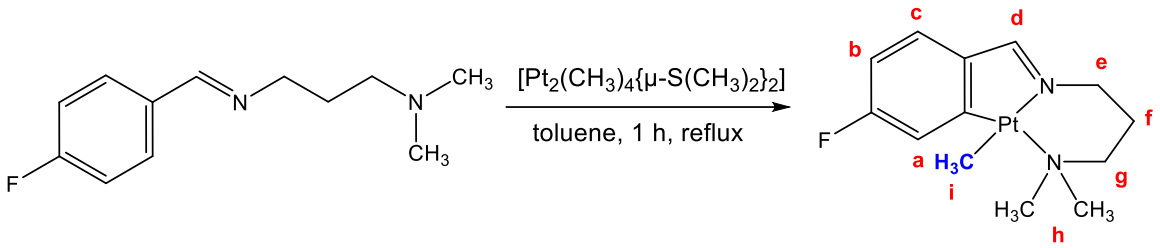

Scheme 2.7. Synthesis of compound **1d**.

All platinum(II) compounds were characterised by ^{1}H and ^{19}F NMR spectroscopy, mass spectrometry and elemental analysis, matching the desired structures. For both [N,N'] chelate compounds (**1b'** and **1c'**) the iminic proton was coupled to platinum with the expected coupling constant (^{3}J(Pt-H) = 115.6 Hz). This value agrees with the imine ligand having an *E* configuration, where the iminic proton (H^{d}) is in *trans* to the platinum atom. This later favours the intramolecular C-H bond activation pathway since it brings the aryl close to the halido ligand.[24]

Cyclometallated platinum(II) compounds gave the expected fused [6,5,6-tricyclic] systems. The aromatic region of the ^{1}H NMR spectra for these compounds is depicted in *Figure 2.1* The coupling constant of the iminic proton (H^{d}) with the platinum atom in compounds **1a**, **1b** and **1c** (^{3}J(Pt-H) = 135.8-143.7 Hz) matches those reported in the literature for similar compounds. However, in compound **1d** where the ancillary ligand is a methyl instead of a halido, this coupling constant is significantly reduced to 62.8 Hz, due to the higher *trans* influence of this group. The higher the *trans* influence of the ancillary ligand, the stronger is its bond with platinum. Therefore, the Pt-N bond in *trans* is weakened which lowers the coupling constant of the adjacent iminic proton (H^{d}) with platinum.[28,29]

The proton adjacent to the metalated carbon (H^{a}) is also coupled with platinum with values around 40 Hz and its chemical shift is significantly dependant on the nature of the

ancillary ligand. For compounds **1a**, **1b** and **1c** containing a halido as an ancillary ligand, it shifts downfield following the sequence Cl (7.72 ppm) < Br (8.00 ppm) < I (8.45 ppm). Although a decrease in the chemical shift of a nucleus with increasing atomic number of the vicinal halogen is frequently observed, inverse halogen dependence can also be observed, and it suggests a relationship with spin-orbit coupling.[30]

In compound **1d**, the chemical shift of H^a is lower than those of the halido ligands and, additionally, the CH_3 ancillary ligand (δ = 0.81 ppm) is also coupled to platinum with a coupling constant of 81.7 Hz.

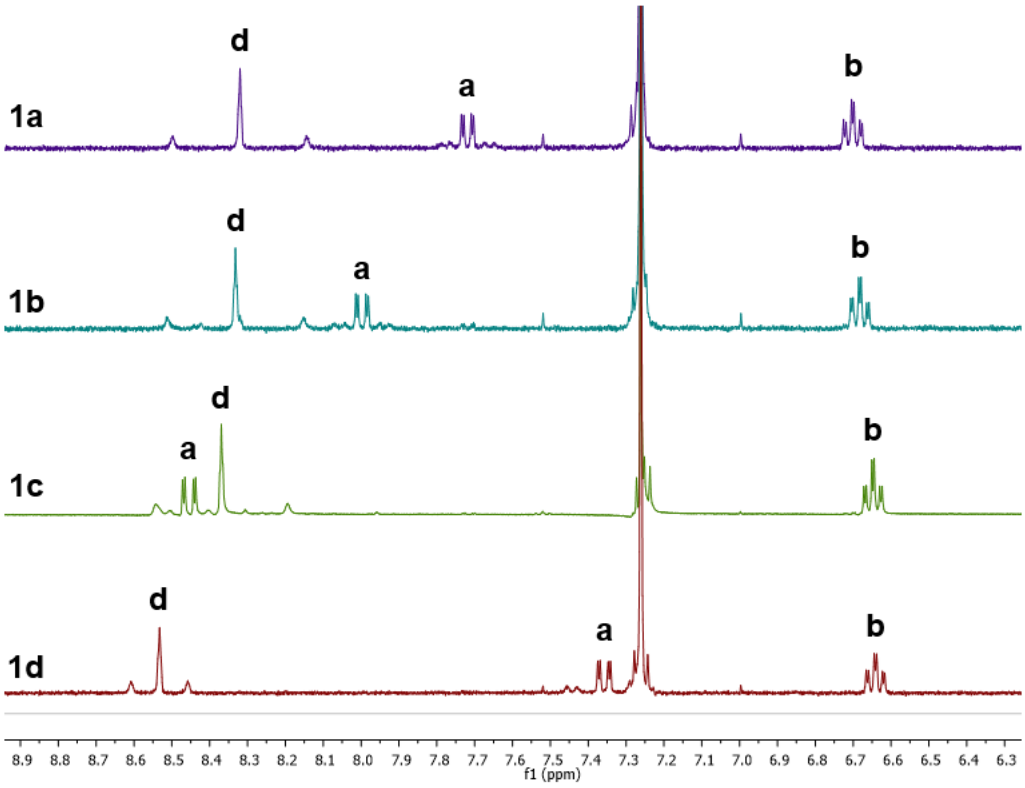

Figure 2.1. Aromatic region of the ^1H NMR spectra for compounds **1** in $CDCl_3$.

Cyclometallated platinum(IV) compounds [$Pt(CH_3)X_2\{(CH_3)_2N(CH_2)_3N{=}CH(4\text{-}FC_6H_3)\}$] (**2a**, X = Cl; **2b**, X = Br; **2c** X = I) were synthesized by oxidative addition of Cl_2 (**2a**), Br_2 (**2b**) and I_2 (**2c**) to the platinum(II) compound **1d** in acetone at room temperature. For the addition of Cl_2, iodobenzene dichloride ($PhICl_2$) was used as an oxidant to avoid the use of chlorine gas. The proposed mechanism for the oxidative addition of halogens in this type of compounds points to the formation of an octahedral

platinum(IV) compound where the new ligands are added in *trans* to each other (*Scheme 2.8*).[21–23,31]

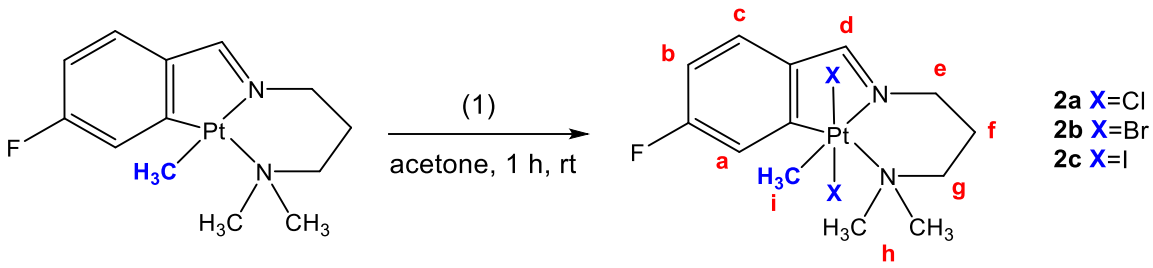

Scheme 2.8. Synthesis of compounds **2a**, **2b** and **2c**. (1) $PhICl_2$ (**2a**); Br_2 (**2b**); I_2 (**2c**).

However, further isomerization can take place after the reaction depending on the size similarity of the ancillary ligands. For all compounds, only one isomer was observed by ^1H NMR spectra. Compounds **2b** and **2c**, containing bromido and iodido ligands, significantly bigger in size than the methyl group, stay in a *trans* configuration after the reaction.[32] However, compound **2a** undergoes isomerization to finally give the *cis* isomer. This is evidenced by the doubled signals of the $N(CH_3)_2$ and the $(CH_2)_3$ protons in the ^1H NMR spectra, meaning that they become diastereotopic due to the formation of a new chiral centre in the platinum(IV) atom.

This isomerization could arise from the exchange of a chlorido for a methyl ligand, as depicted in path 1 from *Scheme 2.9.* Nevertheless, the higher strength of the Pt-C bond suggests a more likely path in which the exchange takes place between a chlorido and the dimethyl amino moiety (path 2, *Scheme 2.9*). This is in agreement with the *mer* to *fac*-[C,N,N'] isomerization previously reported for similar cyclometallated platinum(IV) compounds.[13,33]

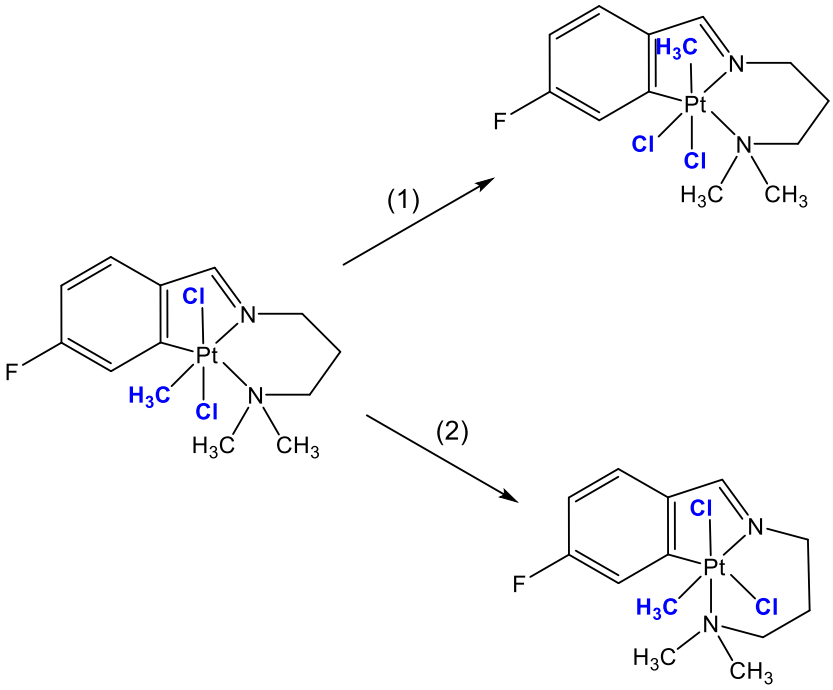

Scheme 2.9. Possible isomerization paths for compound **2a**. (1) CH_3/Cl exchange; (2) $N(CH_3)_2$/Cl exchange.

Cyclometallated platinum(IV) compounds [PtX_3{$(CH_3)_2N(CH_2)_3N=CH(4\text{-}FC_6H_3)$}] (**3a**, X = Cl; **3b**, X = Br; **3c** X = I) were synthesized following the same procedure from compounds **2**. In this case, the possibility of having different isomers is avoided by having three identical ancillary ligands in all compounds. Therefore, they were all obtained as the only single possible isomer (*Scheme 2.10*).

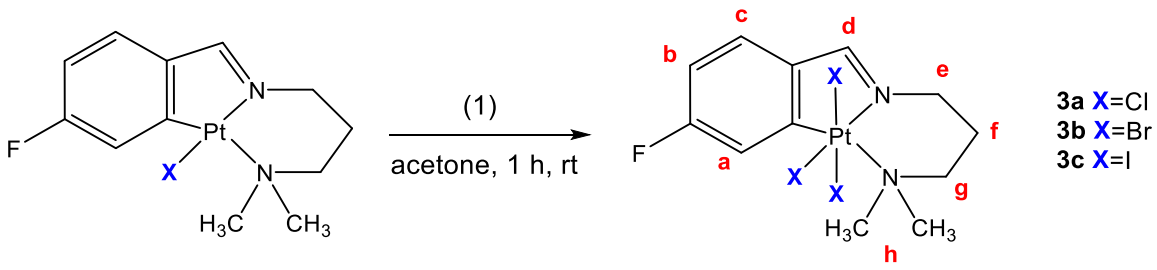

Scheme 2.10. Synthesis of compounds **3a**, **3b** and **3c**. (1) $PhICl_2$ (**3a**); Br_2 (**3b**); I_2 (**3c**).

Platinum(IV) compounds **2** and **3** were characterised by ^1H and ^{19}F NMR spectroscopy, mass spectrometry and elemental analysis. Selected ^1H NMR data for these compounds are collected in *Table 2.1*. The iminic proton (H^d) of all compounds is coupled to platinum, with values of 44.6-47.2 Hz for compounds **2** and 91.2-95.7 Hz for compounds **3**. These values are lower than those of the analogous platinum(II) compounds due to the

increase in the oxidation state, which implies a lower electronic density of the platinum centre. The difference in values for families **2** and **3** is again due to the difference in the *trans* influence of the ancillary ligands, with the same effect previously seen in platinum(II) compounds.

Table 2.1. Selected ^{1}H NMR data for platinum(IV) compounds[a]

Compound	δ(H^{d}) [^{3}J(Pt-H)]	δ(H^{a}) [^{3}J(Pt-H)]	δ(CH$_3$) [^{3}J(Pt-H)]
2a	8.49 [45.5]	7.01[b]	1.80 [59.6]
2b	8.37 [44.6]	7.02 [33.3]	1.99 [67.6]
2c	8.21 [47.2]	7.02 [38.2]	2.26 [68.3]
3a	8.19 [95.7]	7.78[b]	-
3b	8.09 [93.9]	7.97[b]	-
3c	7.96 [91.2]	8.25 [33.6]	-

[a] In $CDCl_3$, δ in ppm, J in Hz, labels as indicated in *Schemes 2.8* and *2.10*. [b] Not observed.

Furthermore, in compounds **2** the ancillary methyl also couples with platinum (^{2}J(Pt-H) = 59.6 - 68.3 Hz), a value which is significantly lower than that of its analogous platinum(II) precursor **1d**. Its chemical shift is downshifted as the size of the halido ligand increases (**2a**, δ = 1.80, **2b**, δ = 1.99, **2c**, δ = 2.26). This also affects the chemical shift of the iminic proton (H^{d}) which decreases for both series of compounds **2** and **3** as the halido size increases. Additionally, for compounds **3**, the chemical shift of the proton adjacent to the metalation site (H^{a}) increases with the increase in the bulk of the corresponding halide.

2.2.2. X-ray crystal structure determination

For platinum(II) compounds, three (**1b**) or two (**1b'**) independent molecules were found in the asymmetric unit with parameters equal within experimental error. Both compounds present the expected square planar environment around the platinum atom (*Figure 2.2*). In the cyclometallated platinum(II) compound **1b**, it is completed by the tridentate [C,N,N'] ligand and the bromido *trans* to the imine. The formation of a fused [6,5,6]-tricyclic system with a 5-membered platinacycle and a 6-membered chelate ring is confirmed.

Compound **1b'** presents the square planar coordination of the platinum completed by a [N,N'] bidentate ligand and two mutually *cis* bromido ancillary ligands. As previously observed by ^{1}H NMR spectra the imine adopts an *E* configuration with the phenyl ring close to the metal.

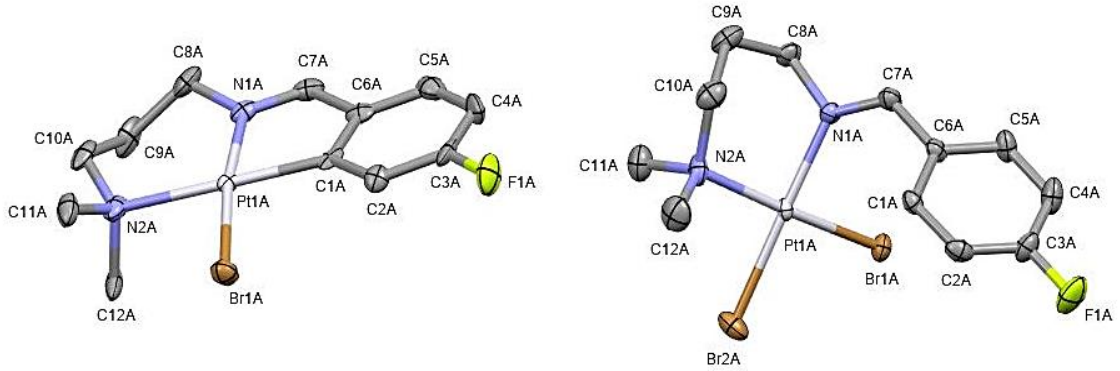

Figure 2.2. Molecular structure of compounds **1b** (molecule a) (left) and **1b'** (molecule a) (right). Selected bond lengths (Å) and angles (deg.) with estimated standard deviations. For **1b**: Pt(1A)-C(1A): 1.993(9); Pt(1A)-N(1A): 2.019(7); Pt(1A)-N(2A): 2.197(8); Pt(1A)-Br(1A): 2.4302(10); C(1A)-Pt(1A)-N(1A): 80.8(3); N(1A)-Pt(1A)-N(2A): 95.8(3); C(1A)-Pt(1A)-Br(1A): 92.7(3); N(2A)-Pt(1A)-Br(1A): 90.5(2). For **1b'**: Pt(1A)-N(1A): 2.016(2); Pt(1A)-N(2A): 2.093(2); Pt(1A)-Br(1A): 2.4248(3); Pt(1A)-Br(2A): 2.4238(3); N(1A)-Pt(1A)-N(2A): 89.27(10); N(1A)-Pt(1A)-Br(1A): 88.96(7); N(2A)-Pt(1A)-Br(2A): 92.36(7); Br(1A)-Pt(1A)-Br(2A): 89.361(11). The thermal ellipsoids are drawn at the 50% probability level. Hydrogens have been omitted for clarity.

Bond lengths and angles are in range of those reported in the literature for analogous compounds.[17,24,26] For both compounds **1b** and **1b'**, Pt-Br distances present no significant differences (2.4238 Å and 2.4302 Å) and Pt-amine distances are found to be longer than Pt-imine ones, due to the higher affinity of the latter in bonding to platinum. Furthermore, this Pt-amine distance is larger for the cyclometallated compound **1b** (2.197 Å) than for the coordination complex **1b'** (2.093 Å), because of the greater *trans* influence of the aryl versus the bromido ligand.

Most angles are close to the ideal value of 90°, being the smallest one the corresponding to the metallacyle C(1)-Pt-N(1) for **1b** (80.8(3)°) or the chelate N(1)-Pt-N(2) for **1b'** (89.27(10)°). For compound **1b**, as previously seen in analogous cyclometallated compounds[17,24] and in agreement with the flexibility of the propylamine chain, the chelate angle N(1)-Pt-N(2) increases up to 95.8(3)°.

The crystal structure of compound **1b** (*Figure 2.3*) revealed the presence of several intermolecular contacts shorter than the sum of van der Waals radii in its packing between bromide ligands and methyl protons (d(Br···H) = 2.854 Å) as well as different C··H contacts between aromatic and chelate rings (d(C···H) = 2.805-2.881 Å). Due to the non-planarity of the chelate ring and the steric hindrance of the methyl group, no Pt···Pt or π···π stacking interactions are observed.

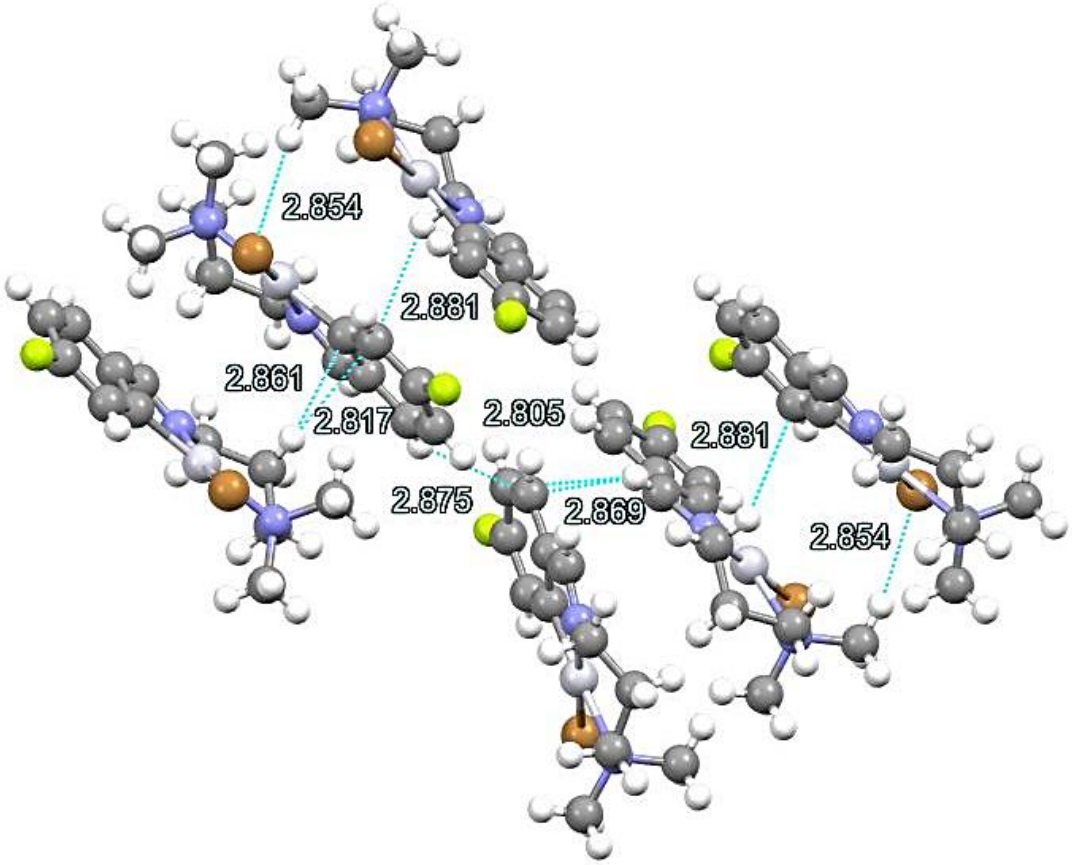

Figure 2.3. A view of the structure of compound **1b** with all intermolecular contacts shorter than the sum of van der Waals radii highlighted in blue: Br(1)-H(12): 2.854 Å, C(1)-H(9): 2.861 Å, C(2)-H(8): 2.881 Å, C(2)-H(9): 2.817 Å, C(4)-H(7): 2.805 Å, C(5)-H(5): 2.875, C(5)-H(7): 2.869 Å.

Cyclometallated platinum(IV) compounds **2b** and **3b** display an octahedral coordination around the platinum with a meridional tridentate [C,N,N'] ligand, an equatorial methyl and two (**2b**) or three (**3b**) bromido ligands completing the coordination sphere (*Figure 2.4*).

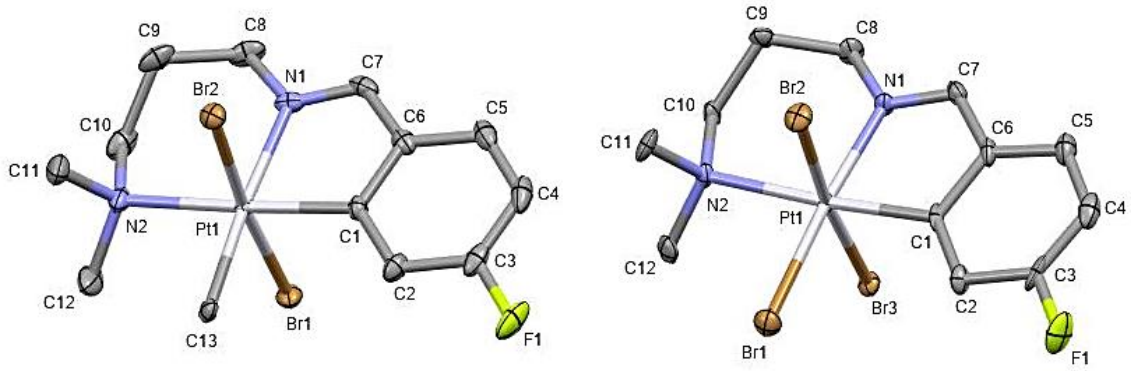

Figure 2.4. Molecular structure of compounds **2b** (molecule a) (left) and **3b** (molecule a) (right). Selected bond lengths (Å) and angles (deg.) with estimated standard deviations. For **2b**: Pt(1)-C(1), 2.007(3); Pt(1)-C(13), 2.135(3); Pt(1)-N(1), 2.141(2); Pt(1)-N(2), 2.258(3); Pt(1)-Br(1), 2.4485(3); Pt(1)-Br(2), 2.4675(3); C(1)-Pt(1)-C(13), 94.51(11); C(1)-Pt(1)-N(1), 79.97(11); C(13)-Pt(1)-N(2), 90.27(10); N(1)-Pt(1)-N(2), 95.28(10); C(1)-Pt(1)-Br(1), 86.43(8); C(13)-Pt(1)-Br(1), 91.27(8); N(1)-Pt(1)-Br(1), 89.37(7); N(2)-Pt(1)-Br(1), 90.95(7); C(1)-Pt(1)-Br(2), 87.53(8); C(13)-Pt(1)-Br(2), 89.49(8); N(1)-Pt(1)-Br(2), 89.29(7); N(2)-Pt(1)-Br(2), 95.05(7). For **3b**: Pt(1)-C(1), 2.027(9); Pt(1)-N(1), 2.032(8); Pt(1)-N(2), 2.276(8); Pt(1)-Br(1), 2.4496(10); Pt(1)-Br(3), 2.4624(9); Pt(1)-Br(2), 2.4636(10); C(1)-Pt(1)-N(1), 80.3(3); N(1)-Pt(1)-N(2), 96.2(3); C(1)-Pt(1)-Br(1), 94.5(3); N(2)-Pt(1)-Br(1), 89.07(19); C(1)-Pt(1)-Br(3), 89.8(2); N(1)-Pt(1)-Br(3), 88.1(2); N(2)-Pt(1)-Br(3), 91.9(2); Br(1)-Pt(1)-Br(3), 91.90(3); C(1)-Pt(1)-Br(2), 84.6(2); N(1)-Pt(1)-Br(2), 89.0(2); N(2)-Pt(1)-Br(2), 93.6(2); Br(1)-Pt(1)-Br(2), 90.58(4).The thermal ellipsoids are drawn at the 50% probability level. Hydrogens have been omitted for clarity.

Bond lengths and angles are within the range of values obtained for analogous compounds.[34] The metallacycle bite angle (**2b**, 79.97(11)°, **3b** 80.3(3)°) has the smallest value in the coordination sphere while the largest corresponds to the chelate ring. Axial bromido ligands present values close to the ideal linearity expected for an octahedral environment (**2b**, 173.947(11)°, **3b** 173.99(3)°) . As previously observed for compound **1b**, Pt-amine distances (**2b**, 2.258 Å, **3b**, 2.276 Å) are larger than for Pt-imine bonds (**2b**, 2.141 Å, **3b**, 2.032 Å). The latter is larger for compound **2b** (*trans* to a CH_3) than for compound **3b** (*trans* to a bromido), due to the higher *trans* influence of a C-donor ligand. This agrees with the lower coupling constant of the iminic proton with platinum observed by ^{1}H NMR for compound **2b**. When comparing to the platinum(II) precursor **1b** , Pt-amine, Pt-imine and Pt-C bond distances are slightly longer for the platinum(IV) derivatives.[34]

The packing arrangement for **2b** and **3b** are shown in *Figures 2.5* and 2.6, respectively. For **2b**, intramolecular short contacts C-F···Br-Pt and C-F···H_3CN are observed (d(F···Br) = 3.176 Å and d(F···H) = 2.509 Å). In addition, bromido ligands display

intramolecular interactions with aromatic and methyl protons (d(Br···H) = 2.959 Å and 3.115 Å, respectively). Analogous interactions of bromido ligands and aromatic and methylene protons are observed for **3b** (d(Br···H) = 2.933 Å and 3.045 Å, respectively). For **3b**, the fluoro substituent is not involved in intramolecular interactions while the axial bromido ligands lead to short contacts (d(Br···Br) = 3.674 Å). In both cases, the octahedral environment around the platinum with two axial ligands eliminates the possibility that the molecules establish Pt···Pt or π···π stacking interactions.

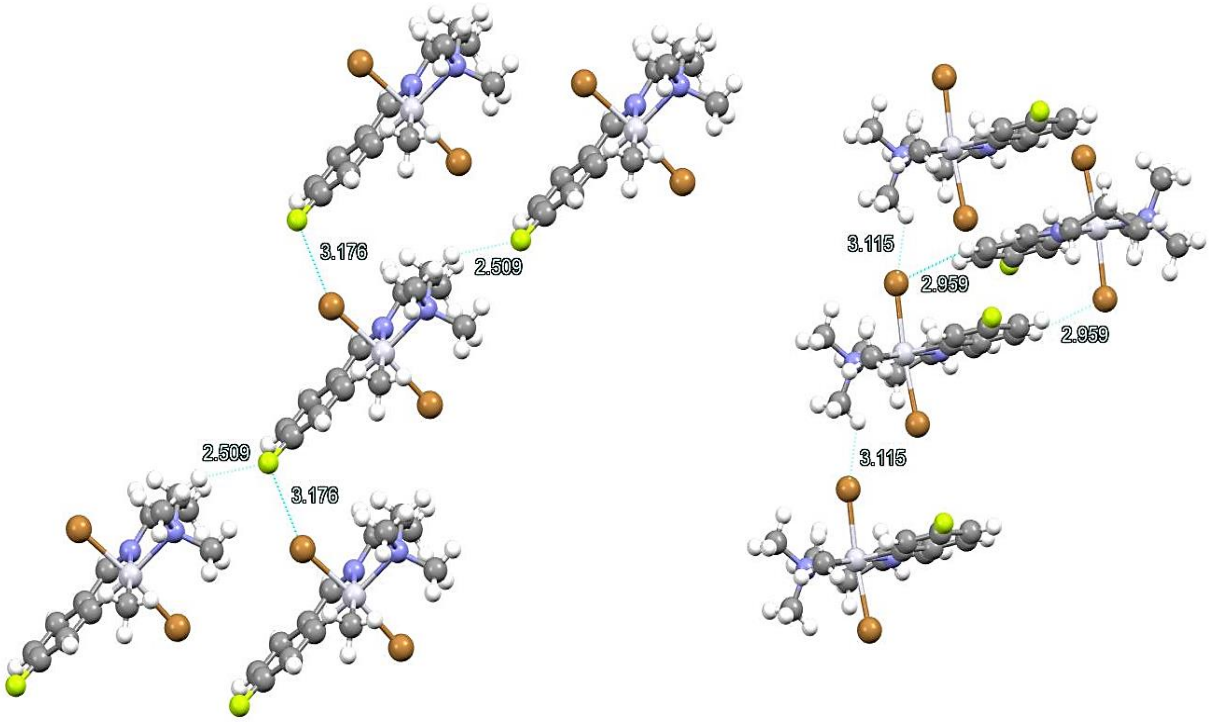

Figure 2.5. A view of the structure of compound **2a** with all intermolecular contacts shorter than the sum of van der Waals radii highlighted in blue: Br(1)-F(1): 3.176 Å, F(1)-H(10): 2.509 Å (left); Br(1)-H(11): 3.115 Å, Br(1)-H(5): 9.959 Å (right).

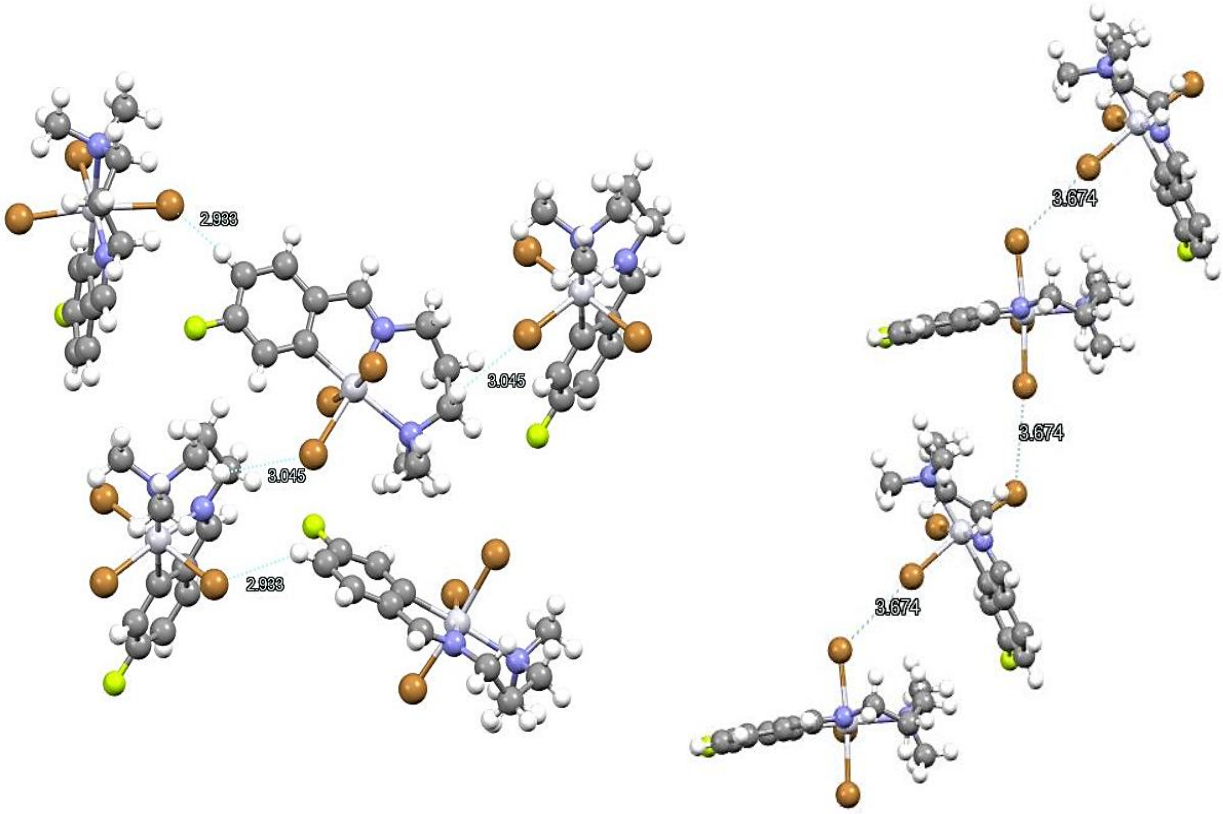

Figure 2.6. A view of the structure of compound **2b** with all intermolecular contacts shorter than the sum of van der Waals radii highlighted in blue: Br(3)-H(4): 2.933 Å, Br(1)-H(10): 3.045 Å (left); Br(2)-Br(3): 3.674 Å (right).

2.2.3. Photophysical characterisation

Absorption and emission spectra of all compounds were recorded in 10^{-4} M dichloromethane solutions at room temperature. The results are summarized in *Table 2.2*.

Table 2.2. Absorption and emission data for all compounds in dichloromethane solutions at 298 K.

Compound	Absorption λ_{max}/nm (ε/ M^{-1} cm^{-1})	Emission λ_{max}/nm	ϕ
L1	276 (1506), 286 (1060)	350	0.074[a]
1a	285 (3443), 311 (2563), 357 (2387), 374 (2618)	347 577, 620	0.056[a] 0.003[b]
1b	288 (4524), 318 (2713), 357 (2140), 378 (2618)	349 576, 622	0.044[a] 0.004[b]
1b'	296 (7941), 336 (3239)	349	0.016[a]
1c	295 (4194), 325 (2857), 386 (2731)	356	0.045[a]
1c'	300 (6520), 375 (3078)	344	0.014[a]
1d	285 (6548), 319 (3158), 364 (3104), 391 (3158)	345 574, 619	0.044[a] 0.001[b]
2a	274 (4929)	348	0.051[a]
2b	274 (8094)	351	0.064[a]
2c	267 (24526), 360 (1509)	-	-
3a	287 (3831)	349	0.051[a]
3b	286 (6353)	350	0.056[a]
3c	271 (23289), 379 (3449), 450 (3286)	-	-

[a] Quantum yields for emission in solution referred to naphthalene in cyclohexane. [b] Quantum yields for emission in solution referred to $[Ru(bipy)_3]Cl_3$ in water.

Cyclometallated platinum(II) compounds display several bands in the UV-Visible absorption spectra with moderate ε values (*Figure 2.7*). The lowest energy band (357-391 nm) can be assigned to a Pt(5d) → π* (L) metal-to-ligand charge transfer (MLCT) mixed

with intraligand transitions.[3,24,35,36] Higher energy bands are also observed in the 285-300 nm range, which are also recorded for the free ligand **L1** and therefore can be assigned to π-π* intraligand transitions intrinsic of the imine.

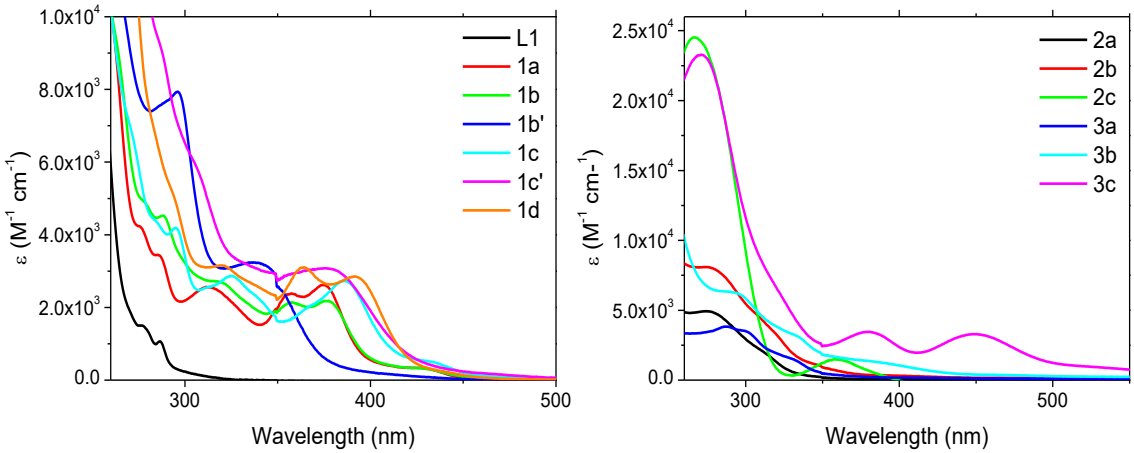

Figure 2.7. Absorption spectra for 10^{-4} M dichloromethane solutions of ligand **L1** and platinum(II) compounds **1** (left); and platinum(IV) compounds **2** and **3** (right).

For the platinum(IV) analogues, only the higher energy bands are observed (*Figure 2.7*). The loss of electron density of the platinum centre due to the oxidation results in the disappearance of the lower energy bands assigned to a MLCT mixed with IL transitions.[37] Additionally, compounds **2c** and **3c**, which contain iodido as an ancillary ligand, also present some lower energy bands in the 360-450 nm range. The possible origin of this band, according to the literature, is either a ligand-to-ligand charge transfer (LLCT, $I^- \rightarrow \pi^*$ (L1)) or a ligand-to-metal charge transfer (LMCT, $I^- \rightarrow d\sigma^*$ (Pt)) transition, caused by the π-donating character of the iodido ligand.[19]

All platinum compounds except **2c** and **3c** display a broad emission band centred at around 350 nm when excited at their high energy bands (270 -290 nm) (*Figure 2.8*). This emission is also observed upon excitation of the free ligand **L1** at the same wavelength and can therefore be assigned to intraligand (^{1}IL) transitions perturbed by the platinum atom.[38,39] This is evidenced in the decrease of the emission quantum yield with the addition of the platinum. This may be due to the metal orbital contribution of the emitting excited state in the complexes with a MLCT character, which causes a reduction in the radiative constant.[40,41]

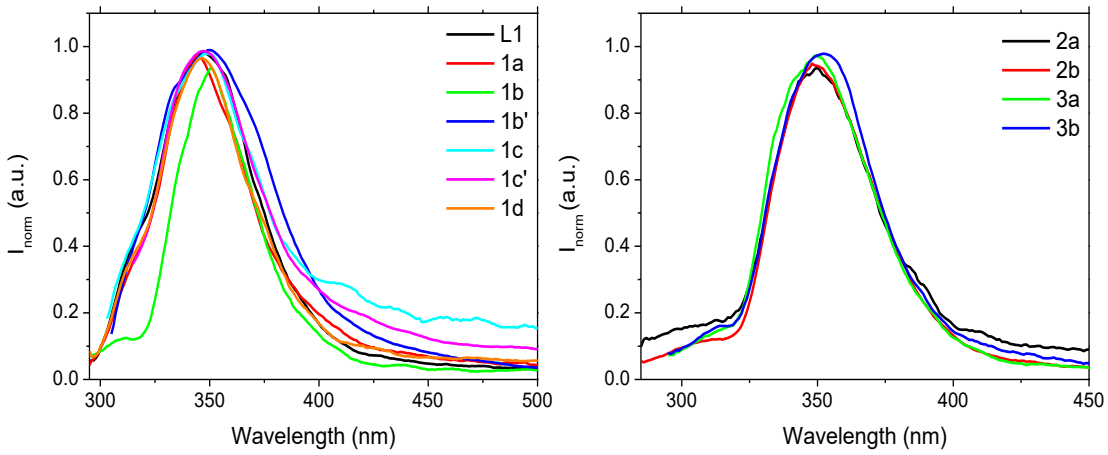

Figure 2.8. Normalized emission spectra for 10^{-4} M dichloromethane solutions of ligand **L1** and platinum(II) compounds **1** (left); and platinum(IV) compounds **2** and **3** (right) upon excitation at their high energy band (λ_{exc}= 350 nm).

The emission quantum yield for coordination compounds **1b'** and **1c'** is significantly lower than for their cyclometallated analogues **1b** and **1c**. The higher rigidity of the latter can be responsible for favouring the radiative emission versus the non-radiative energy loss.

Furthermore, when excited in their lower energy absorption bands, platinum(II) compounds **1a**, **1b** and **1d** display a structured emission band centred at 620 nm (*Figure 2.9*). The vibronic spacings of 1200 cm^{-1}, typical of ν(C=C) and ν(C=N) stretching frequencies in the excited state proves the involvement of the ligand character in the emission origin. This along with the large Stokes' shift and the significant quenching of the emission in the presence of oxygen indicates a phosphorescent ^{3}IL transition (*Figure 2.9*). Compound **1c** does not display this emission band, probably due to the heavy atom quenching effect from the iodide atom, which is in concordance with the non-emissive properties observed for its platinum(IV) analogues **2c** and **3c**.[42]

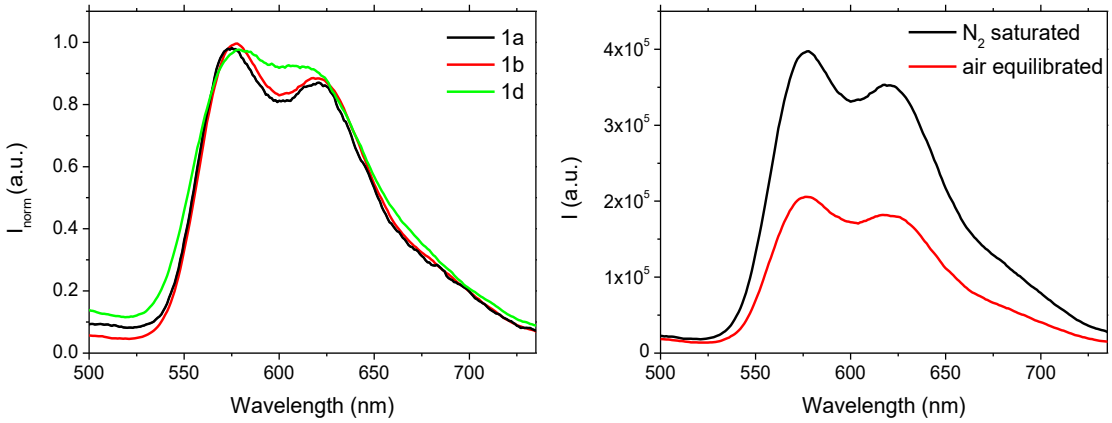

Figure 2.9. Normalized emission spectra for 10^{-4} M dichloromethane solutions of platinum(II) compounds **1a**, **1b** and **1d** upon excitation at their low energy band (λ_{exc}= 625 nm) (left) and comparison between air equilibrated and N_2 saturated emission spectra of compound **1b** (right).

In all cases, no excimeric or aggregates' bands that usually present a broad emission at higher wavelengths were recorded. This agrees with the fact that no Pt···Pt or π···π stacking interactions are observed in the crystal packing of the molecules.

2.3. Conclusions

A large series of compounds comprised of [N,N'] chelate platinum(II) compounds and tridentate [C,N,N'] cyclometallated platinum(II) and platinum(IV) compounds were successfully synthesized through a wide variety of synthetic methods. All of them were fully characterised by several techniques and for the bromide derivatives, X-ray crystal structures were obtained.

The photophysical study of these compounds revealed that most of them present luminescent properties. However, the emission quantum yields that were measured presented low values for all compounds, probably due to the high flexibility of the propylene chain, which favours non-radiative pathways.

It was also observed that the presence of iodine atoms as ancillary ligands quenches partially or completely the emission, making those compounds not suitable for optical applications.

Finally, it can be concluded that for this family of compounds, the oxidation to platinum(IV) resulted in the loss of the ^{3}IL phosphorescent band, due to the loss in electron density in the platinum. Therefore, they only presented the higher energy band that matches the fluorescence emission of the free ligand with perturbation from the platinum atom.

2.4. Experimental Section

2.4.1. General procedures

Commercial reagents 4-fluorobenzaldehyde (Sigma Aldrich, 98%), 3-dimethylamino-1-propylamine (Sigma Aldrich, 99%), sodium sulphate (Na_2SO_4, Panreac, 99%), sodium acetate (CH_3COONa, Carlo Erba, 99%), potassium bromide (KBr, Probus, 98%), bromine (Br_2, Sigma Aldrich, >99%) and iodine (I_2, Panreac, >99%); and solvents toluene (Scharlau, 99.9%), methanol (Sigma Aldrich, >99%), dichloromethane (CH_2Cl_2, Scharlau, 99%), acetone (Carlo Erba, >99%) and diethyl ether (Carlo Erba, 99%) were used as received.

Complexes *cis*-$[PtBr_2(DMSO)_2]$[43], *cis*-$[PtI_2(DMSO)_2]$[43], *cis*-$[PtCl_2(DMSO)_2]$[44], $[Pt_2(CH_3)_4\{\mu\text{-}S(CH_3)_2\}]$[45] and iodobenzene dichloride ($PhICl_2$)[46] were prepared as reported in the literature.

2.4.2. Physical measurements

NMR spectra were recorded in $CDCl_3$ at the *Unitat de RMN* of the *Universitat de Barcelona* with a Mercury 400 spectrometer (^1H, 400 MHz; ^{19}F, 376.5 MHz). Chemical shifts are given in δ values (ppm) relative to TMS (^1H) or $CFCl_3$ (^{19}F) and coupling constants J are given in Hz.

Electrospray mass spectra were performed at the *Unitat d'Espectrometria de Masses (Universitat de Barcelona)* in a LC/MSD-TOF spectrometer using H_2O-CH_3CN 1:1 to introduce the sample.

Microanalyses were performed at the *Centres Científics i Tecnològics (Universitat de Barcelona)* using a Carlo Erba model EA1108 elemental analyser.

UV/Vis spectra were recorded with a Cary 100 scan 388 Varian UV spectrometer. Emission and excitation spectra were recorded in a Horiba Jobin-Yvon SPEX Nanolog-TM spectrofluorimeter at 298 K using 10^{-4} M dichloromethane solutions.

Total luminescence quantum yields were measured at 298 K relative to $[Ru(bipy)_3]Cl_2$ in water ($\phi = 0.042$) and naphthalene in cyclohexane ($\phi = 0.23$) as standard references.

2.4.3. Synthesis and characterisation

Synthesis of 4-FC$_6$H$_4$CH=N(CH$_2$)$_3$N(CH$_3$)$_2$ (L1)

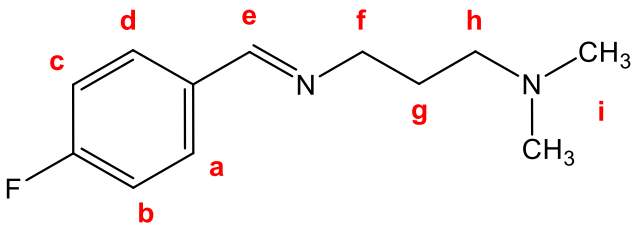

Ligand 4-FC$_6$H$_4$CH=N(CH$_2$)$_3$N(CH$_3$)$_2$ (**L1**)[24] was obtained by following the method described in the literature from the reaction of 0.618 g (4.980 mmols) of 4-fluorobenzaldehyde and 0.577 g (5.647 mmols) of 3-dimethylamino-1-propylamine in 20 ml of toluene. The mixture was stirred at room temperature for 2 hours and water was eliminated by adding sodium sulphate and filtering it off. The solvent was removed under vacuum to give a yellow oil. Yield: 0.898 g (87%).

^{1}H NMR (CDCl$_3$, 400 MHz): δ 8.25 [s, 1H, H^e]; 7.72 [m, 2H, H^{a,d}]; 7.08 [dd, 2H, ^{3}J(F-H) = 8.8, ^{4}J(H-H) = 2.4, H^{b,c}]; 3.63 [td, 2H, ^{3}J(H-H) = 7.2, ^{4}J(H-H) = 1.2, H^f]; 2.35 [t, 2H ^{3}J(H-H) = 7.2, H^h]; 2.24 [s, 6H, H^i]; 1.87 [qi, 2H, ^{3}J(H-H) = 7.2, H^g]. **^{19}F NMR** (CDCl$_3$, 376.5 MHz): δ -109.90 [m, 1F].

Synthesis of [PtBr$_2${(CH$_3$)$_2$N(CH$_2$)$_3$N=CH(4-FC$_6$H$_4$)}] (1b')

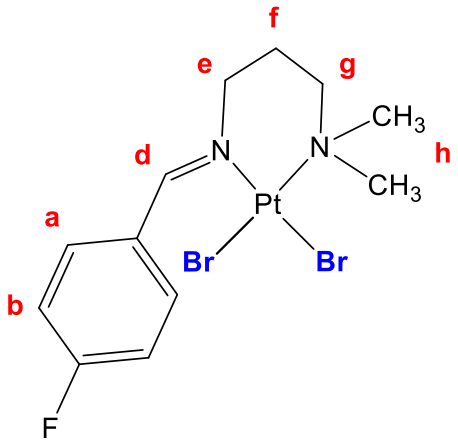

Compound [PtBr$_2${(CH$_3$)$_2$N(CH$_2$)$_3$N=CH(4-FC$_6$H$_4$)}] (**1b'**) was obtained from the reaction of 0.405 g (0.797 mmols) of *cis*-[PtBr$_2$(DMSO)$_2$] and 0.177 g (0.850 mmols) of 4-FC$_6$H$_4$CH=N(CH$_2$)$_3$N(CH$_3$)$_2$ (**L1**) in 25 ml of dry methanol. The mixture was refluxed at 65 ^{o}C for 4 hours. Half of the volume was removed, and the solution was left to

crystallise in the freezer. The yellow solid was filtered and dried under vacuum. Yield: 0.250 g (56%).

^{1}H NMR ($CDCl_3$, 400 MHz): δ 9.38 [m, 2H, H^a]; 8.43 [s, 1H, ^{3}J(Pt-H) = 115.6, H^d]; 7.27 [t, 2H, ^{3}J(F-H) = 8.0, H^b]; {4.93 [m, 1H]; 4.11 [m, 1H]; 3.49 [m, 1H]; 2.62 [m, 1H]; 2.17 [m, 1H]; 1.99 [m, 1H], $H^{e,f,g}$}; {2.95 [s, 3H]; 2.85 [s, 3H], H^h}. **^{19}F NMR** ($CDCl_3$, 376.5 MHz): δ -101.50 [m, 1F]. **MS-ESI$^+$**: m/z 483.02 $[M\text{-}Br]^+$. **Anal. Found** (calcd for $C_{12}H_{17}Br_2FN_2Pt$): C, 26.27 (25.59); H, 3.23 (3.04); N, 5.01 (4.97).

Synthesis of $[PtI_2\{(CH_3)_2N(CH_2)_3N{=}CH(4\text{-}FC_6H_4)\}]$ (1c')

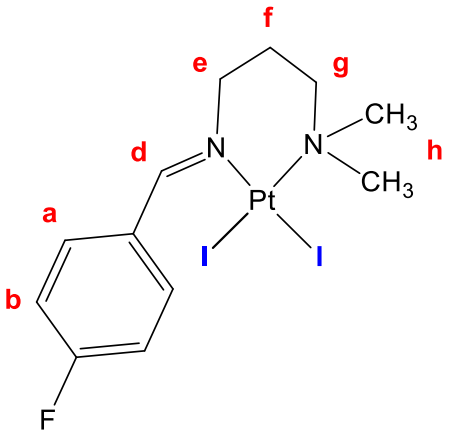

Compound $[PtI_2\{(CH_3)_2N(CH_2)_3N{=}CH(4\text{-}FC_6H_4)\}]$ (**1c'**) was prepared as a brown solid by following the same method from 0.255 g (0.372 mmols) of *cis*-$[PtI_2(DMSO)_2]$ and 0.082 g (0.394 mmols) of $4\text{-}FC_6H_4CH{=}N(CH_2)_3N(CH_3)_2$ (**L1**) in 25 ml of dry methanol. Yield: 0.100 g (41%).

^{1}H NMR ($CDCl_3$, 400 MHz): δ 9.45 [m, 2H, H^a]; 8.47 [s, 1H, ^{3}J(Pt-H) = 115.6, H^d]; 7.25 [t, 2H, ^{3}J(F-H) = 8.0, H^b]; {4.95 [m, 1H]; 4.13 [m, 1H]; 3.23 [m, 1H]; 2.72 [m, 1H]; 2.50 [m, 1H]; 1.97 [m, 1H], $H^{e,f,g}$}; {2.97 [s, 3H]; 2.84 [s, 3H], H^h}. **^{19}F NMR** ($CDCl_3$, 376.5 MHz): δ -101.50 [m, 1F]. **MS-ESI$^+$**: m/z 530.00 $[M\text{-}I]^+$. **Anal. Found** (calcd for $C_{12}H_{17}I_2FN_2Pt$): C, 21.56 (21.93); H, 2.67 (2.61); N, 4.07 (4.26).

Synthesis of [PtCl{$(CH_3)_2N(CH_2)_3N$=CH(4-FC_6H_3)}] (1a)

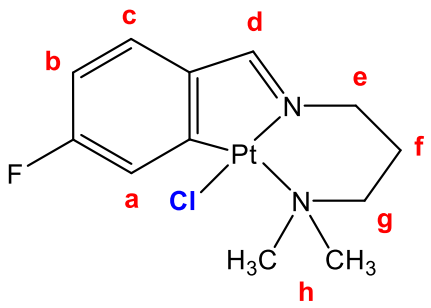

Compound [PtCl{$(CH_3)_2N(CH_2)_3N$=CH(4-FC_6H_3)}] (**1a**)[24] was obtained by following the method described in the literature from the reaction of 0.403 g (0.954 mmols) of *cis*-[$PtCl_2(DMSO)_2$], 0.222 g (1.066 mmols) of 4-FC_6H_4CH=$N(CH_2)_3N(CH_3)_2$ (**L1**) and 0.080 g (0.975 mmols) of anhydrous sodium acetate in 50 ml of dry methanol. The mixture was refluxed at 65 ºC for 72 hours and the solvent was removed under vacuum. The residue was extracted with 10 ml of CH_2Cl_2 and 10 ml of methanol were added. Half of the volume was removed under vacuum and the solution was left to crystallise in the freezer. The orange solid was filtered and dried under vacuum. Yield: 0.188 g (45%).

^{1}H NMR ($CDCl_3$, 400 MHz): δ 8.32 [t, 1H, ^{4}J(H-H) = 1.7, ^{3}J(Pt-H) = 141.9, H^d]; 7.72 [dd, 1H, ^{3}J(F-H) = 10.3, ^{4}J(H-H) = 2.5, ^{3}J(Pt-H) = 44.2, H^a]; 7.27 [m, 1H, H^c]; 6.70 [td, 1H, ^{3}J(F-H) = ^{3}J(H-H) = 8.5, ^{4}J(H-H) = 2.5, H^b]; 3.87 [m, 2H, ^{3}J(Pt-H) = 34.2, H^e]; 2.85 [m, 8H, $H^{g,h}$]; 2.02 [qi, 2H,^{3}J(H-H) = 5.1, H^f]. **^{19}F NMR** ($CDCl_3$, 376.5 MHz): δ -103.99 [m, 1F]. **MS-ESI$^+$**: m/z 439.07 $[M+H]^+$; 456.10 $[M+NH_4]^+$. **Anal. Found** (calcd for $C_{12}H_{16}ClFN_2Pt$): C, 32.00 (32.92); H, 3.70 (3.68); N, 6.30 (6.40).

Synthesis of [PtBr{$(CH_3)_2N(CH_2)_3N$=CH(4-FC_6H_3)}] (1b)

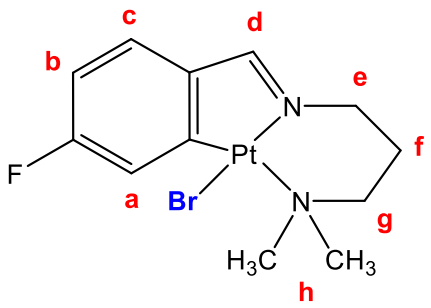

Compound [PtBr{$(CH_3)_2N(CH_2)_3N$=CH(4-FC_6H_3)}] (**1b**) was obtained from the reaction of 0.102 g (0.233 mmols) of [PtCl{$(CH_3)_2N(CH_2)_3N$=CH(4-FC_6H_3)}] (**1a**) and 0.116 g (0.975 mmols) of KBr in 10 ml of dry methanol. The mixture was refluxed at 65 ºC for

48 hours and the solvent was removed under vacuum. The residue was extracted with 10 ml of CH_2Cl_2 and 10 ml of methanol were added. Half of the volume was removed under vacuum and the solution was left to crystallise in the freezer. The orange solid was filtered and dried under vacuum. Yield: 0.039 g (35%).

^{1}H NMR ($CDCl_3$, 400 MHz): δ 8.33 [t, 1H, ^{4}J(H-H) = 1.5, ^{3}J(Pt-H) = 143.7, H^d]; 8.00 [dd, 1H, ^{3}J(F-H) = 10.7, ^{4}J(H-H) = 2.5, ^{3}J(Pt-H) = 46.6, H^a]; 7.26 [m, 1H, H^c]; 6.68 [td, 1H, ^{3}J(F-H) = ^{3}J(H-H) = 8.5, ^{4}J(H-H) = 2.5, H^b]; 3.86 [t, 2H, ^{3}J(H-H) = 5.1, ^{3}J(Pt-H) = 35.2, H^e]; 2.86 [m, 8H, $H^{g,h}$]; 2.03 [qi, 2H, ^{3}J(H-H) = 5.6, H^f]. **^{19}F NMR** ($CDCl_3$, 376.5 MHz): δ -103.85 [m, 1F]. **MS-ESI$^+$**: m/z 438.02 $[M+H]^+$; 402.10 $[M-Br]^+$. **Anal. Found** (calcd for $C_{12}H_{16}BrFN_2Pt$): C, 30.00 (29.89); H, 3.45 (3.34); N, 5.70 (5.81).

Synthesis of [PtI{$(CH_3)_2N(CH_2)_3N$=CH(4-FC_6H_3)}] (1c)

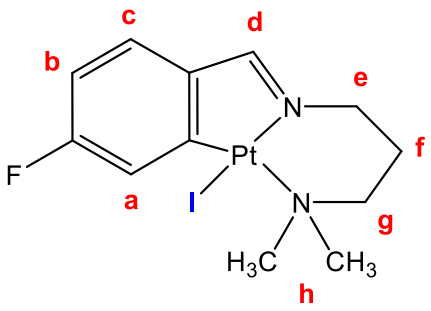

Compound [PtI{$(CH_3)_2N(CH_2)_3$N=CH(4-FC_6H_3)}] (**1c**) was obtained from the reaction of 0.306 g (0.504 mmols) of *cis*-[$PtI_2(DMSO)_2$], 0.133 g (0.639 mmols) of 4-FC_6H_4CH=$N(CH_2)_3N(CH_3)_2$ (**L1**) and 0.053 g (0.646 mmols) of anhydrous sodium acetate in 50 ml of dry methanol. The mixture was refluxed at 65 ^{o}C for 72 hours and the solvent was removed under vacuum. The residue was extracted with 10 ml of CH_2Cl_2 and 10 ml of methanol were added. Half of the volume was removed under vacuum and the solution was left to crystallise in the freezer. The red solid was filtered and dried under vacuum. Yield: 0.081 g (30%).

^{1}H NMR ($CDCl_3$, 400 MHz): δ 8.45 [dd, 1H, ^{3}J(F-H) = 11.4, ^{4}J(H-H) = 2.5, ^{3}J(Pt-H) = 39.8, H^a]; 8.38 [t, 1H, ^{4}J(H-H) = 1.7, ^{3}J(Pt-H) = 135.8, H^d]; 7.26 [m, 1H, H^c]; 6.65 [td, 1H, ^{3}J(F-H) = ^{3}J(H-H) = 8.4, ^{4}J(H-H) = 2.6, H^b]; 3.83 [t, 2H, ^{3}J(H-H) = 5.6, H^e]; 3.01 [s, 6H, ^{3}J(Pt-H) =16.7, H^h]; 2.81 [m, 2H, H^g]; 2.05 [qi, 2H, ^{3}J(H-H) = 5.7, H^f]. **^{19}F NMR** ($CDCl_3$, 376.5 MHz): δ -103.71 [m, 1F]. **MS-ESI$^+$**: m/z 530.01 $[M+H]^+$; 443.12 [M-

I+$CH_3CN]^+$; 401.09 $[M-I]^+$; 402.09 $[M-I]^+$. **Anal. Found** (calcd for $C_{12}H_{16}IFN_2Pt$): C, 27.08 (27.23); H, 3.13 (3.05); N, 5.23 (5.29).

Synthesis of [Pt(CH_3){(CH_3)$_2$N(CH_2)$_3$N=CH(4-FC_6H_3)}] (1d)

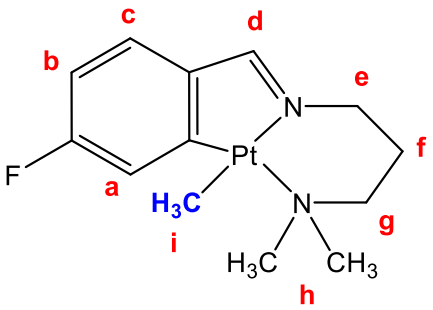

Compound [Pt(CH_3){(CH_3)$_2$N(CH_2)$_3$N=CH(4-FC_6H_3)}] **(1d)**[24] was obtained by following the method described in the literature from the reaction of 0.327 g (0.569 mmols) of [$Pt_2(CH_3)_4${μ-S(CH_3)$_2$}] and 0.265 g (1.272 mmols) of 4-FC_6H_4CH=N(CH_2)$_3$N(CH_3)$_2$ (**L1**) in 20 ml of toluene. The mixture was refluxed at 100 ^oC for 1 hour. The solvent was removed under vacuum and the residue obtained was treated with diethyl ether for a few minutes. The dark orange solid was filtered and dried under vacuum. Yield: 0.327 g (69%).

^{1}H NMR ($CDCl_3$, 400 MHz): δ 8.53 [s, 1H, ^{3}J(Pt-H) = 60.1, H^d]; 7.36 [dd, 1H, ^{3}J(F-H) = 10.9, ^{4}J(H-H) = 2.5, ^{3}J(Pt-H) =78.7, H^a]; 7.25 [m, 1H, H^c]; 6.64 [td, 1H, ^{3}J(F-H) = ^{3}J(H-H) =8.5, ^{4}J(H-H) =2.5, H^b]; 3.84 [t, 2H, ^{3}J(H-H) = 5.0, H^e]; 2.91 [m, 2H, H^g]; 2.74 [s, 6H, ^{3}J(Pt-H) = 23.2, H^h]; 2.02 [qi, 2H,^{3}J(H-H) = 5.1, H^f]; 0.97 [s, 3H, ^{2}J(Pt-H) =79.7, H^i]. **^{19}F NMR** ($CDCl_3$, 376.5 MHz): δ -107.55 [m, 1F]. **MS-ESI$^+$**: m/z 443.12 $[M-H+CH_3CN]^+$. **Anal. Found** (calcd for $C_{13}H_{19}FN_2Pt\cdot 2H_2O$)**:** C, 34.50 (34.44); H, 4.8 (5.11); N, 6.00 (6.17).

Synthesis of [Pt(CH_3)Cl_2){(CH_3)$_2$N(CH_2)$_3$N=CH(4-FC_6H_3)}] (2a)

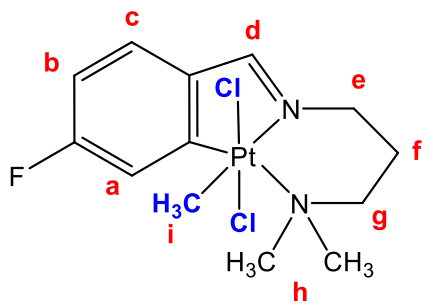

Compound [Pt(CH_3)Cl_2{(CH_3)$_2$N(CH_2)$_3$N=CH(4-FC_6H_3)}] (**2a**) was obtained from the reaction of 0.076 g (0.182 mmols) of [Pt(CH_3){(CH_3)$_2$N(CH_2)$_3$N=CH(4-FC_6H_3)}] (**1d**) and 0.051 g (0.185 mmols) of iodobenzene dichloride ($PhICl_2$) in 8 ml of acetone. The mixture was stirred at room temperature for 1 hour and the solvent was removed under vacuum. The residue was treated with diethyl ether and the yellow solid was filtered and dried under vacuum. Yield: 0.071 g (80%).

^{1}H NMR ($CDCl_3$, 400 MHz): δ 8.49 [s, 1H, ^{3}J(Pt-H) = 45.5, H^d]; 7.43 [dd, 1H, ^{3}J(H-H) = 8.3, ^{3}J(F-H) = 5.6, H^c]; 7.01 [dd, 1H, ^{3}J(F-H) = 8.9, ^{4}J(H-H) = 2.4, H^a]; 6.83 [td, 1H, ^{3}J(F-H) = ^{3}J(H-H) = 8.4, ^{4}J(H-H) = 2.4, H^b]; 4.26 [m, 1H, H^e]; 3.90 [m, 1H, H^e]; 2.94 [m, 2H, H^g]; 2.65 [s, 3H, H^h]; 2.48 [s, 3H, H^h]; 2.27 [m, 1H, H^f]; 2.12 [m, 1H, H^f]; 1.80 [s, 3H, ^{2}J(Pt-H) = 59.6, H^i]. **^{19}F NMR** ($CDCl_3$, 376.5 MHz): δ -101.46 [m, 1F]. **MS-ESI$^+$**: m/z 494.11 [M-Cl+CH_3CN]$^+$; 453.09 [M-Cl]$^+$; 416.11 [M-2Cl-H]$^+$. **Anal. Found** (calcd for $C_{13}H_{19}Cl_2FN_2Pt\cdot 2H_2O$)**:** C, 29.80 (29.78); H, 3.78 (4.42); N, 5.27 (5.34).

Synthesis of [Pt(CH_3)Br_2{(CH_3)$_2$N(CH_2)$_3$N=CH(4-FC_6H_3)}] (2b)

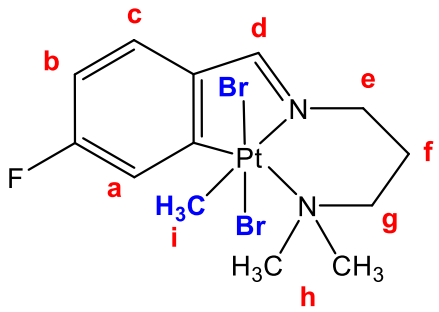

Compound [Pt(CH_3)Br_2{(CH_3)$_2$N(CH_2)$_3$N=CH(4-FC_6H_3)}] (**2b**) was prepared as an orange solid by following the same method from 0.078 g (0.187 mmols) of [Pt(CH_3){(CH_3)$_2$N(CH_2)$_3$N=CH(4-FC_6H_3)}] (**1d**) and 0.060 g (0.375 mmols) of Br_2. Yield: 0.082 g (76%).

^{1}H NMR ($CDCl_3$, 400 MHz): δ 8.37 [s, 1H, ^{3}J(Pt-H) = 44.6, H^d]; 7.43 [dd, 1H, ^{3}J(H-H) = 8.3, ^{3}J(F-H) = 5.8, H^c]; 7.02 [dd, 1H, ^{3}J(F-H) = 9.9, ^{4}J(H-H) = 2.3, ^{3}J(Pt-H) = 33.3, H^a]; 6.76 [td, 1H, ^{3}J(F-H) = ^{3}J(H-H) = 8.5, ^{4}J(H-H) = 2.4, H^b]; 4.01 [m, 2H, H^e]; 2.98 [m, 2H, H^g]; 2.87 [s, 6H, ^{3}J(Pt-H) = 15.1, H^h]; 2.21 [m, 2H, H^f]; 1.99 [s, 3H, ^{2}J(Pt-H) = 67.6, H^i]. **^{19}F NMR** ($CDCl_3$, 376.5 MHz): δ -102.43 [m, 1F]. **MS-ESI$^+$**: m/z 538.06 [M-Br+CH_3CN]$^+$; 497.03 [M-Br]$^+$; 416.11 [M-2Br-H]$^+$. **Anal. Found** (calcd for $C_{13}H_{19}Br_2FN_2Pt\cdot H_2O$): C, 25.69 (26.23); H, 3.20 (3.19); N, 4.53 (4.71).

Synthesis of [Pt(CH$_3$)I$_2${(CH$_3$)$_2$N(CH$_2$)$_3$N=CH(4-FC$_6$H$_3$)}] (2c)

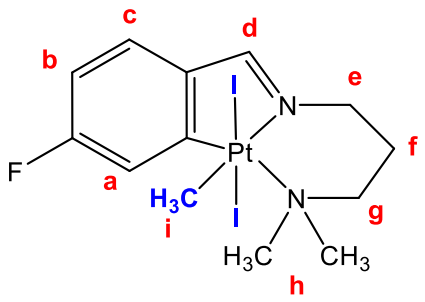

Compound [Pt(CH$_3$)I$_2${(CH$_3$)$_2$N(CH$_2$)$_3$N=CH(4-FC$_6$H$_3$)}] (**2c**) was prepared as a dark brown solid by following the same method from 0.073 g (0.175 mmols) of [Pt(CH$_3$){(CH$_3$)$_2$N(CH$_2$)$_3$N=CH(4-FC$_6$H$_3$)}] (**1d**) and 0.055 g (0.217 mmols) of I$_2$. Yield: 0.061 g (52%).

^{1}H NMR (CDCl$_3$, 400 MHz): δ 8.21 [t, 1H, ^{4}J(H-H) = 1.7, ^{3}J(Pt-H) = 47.2, H^d]; 7.45 [dd, 1H, ^{3}J(H-H) = 8.3, ^{3}J(F-H) = 5.7, H^c]; 7.02 [dd, 1H, ^{3}J(F-H) = 9.7, ^{4}J(H-H) = 2.4, ^{3}J(Pt-H) = 38.2, H^a]]; 6.64 [td, 1H, ^{3}J(F-H) = ^{3}J(H-H) = 8.5, ^{4}J(H-H) = 2.3, H^b]; 4.06 [t, 2H, ^{3}J(H-H) = 4.6, H^e]; 3.18 [s, 6H, ^{3}J(Pt-H) = 17.4, H^h]; 3.05 [m, 2H, H^g]; 2.26 [s, 3H, ^{2}J(Pt-H) = 68.3, H^i], 2.22 [m, 2H, H^f]. **^{19}F NMR** (CDCl$_3$, 376.5 MHz): δ -102.63 [m, 1F]. **MS-ESI$^+$**: m/z 688.96 [M+NH$_4$]$^+$; 544.02 [M-I]$^+$; 415.11 [M-2I-H]$^+$. **Anal. Found** (calcd for C$_{13}$H$_{19}$I$_2$FN$_2$Pt·½I$_2$): C, 19.14 (19.56); H, 2.16 (2.40); N, 3.17 (3.51).

Synthesis of [PtCl$_3${(CH$_3$)$_2$N(CH$_2$)$_3$N=CH(4-FC$_6$H$_3$)}] (3a)

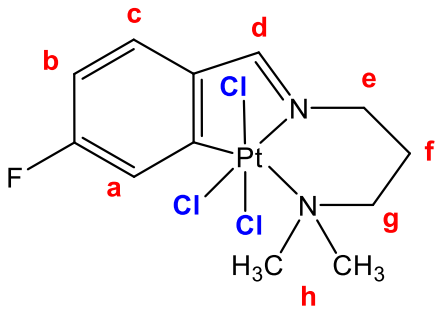

Compound [PtCl$_3${(CH$_3$)$_2$N(CH$_2$)$_3$N=CH(4-FC$_6$H$_3$)}] (**3a**) was obtained by following the method described in the literature from the reaction of 0.096 g (0.219 mmols) of [PtCl{(CH$_3$)$_2$N(CH$_2$)$_3$N=CH(4-FC$_6$H$_3$)}] (**1a**) and 0.072 g (0.262 mmols) of iodobenzene dichloride (PhICl$_2$) in 10 ml of acetone. The mixture was stirred for 10 minutes and the solvent was removed under vacuum. The residue was treated with diethyl ether and the yellow solid was filtered and dried under vacuum. Yield: 0.035 g (31%).

^{1}H NMR ($CDCl_3$, 400 MHz): δ 8.19 [s, 1H, ^{3}J(Pt-H) = 95.7, H^{d}]; 7.78 [dd, 1H, ^{3}J(F-H) = 9.0, ^{4}J(H-H) = 2.5, H^{a}]; 7.53 [dd, 1H, ^{3}J(H-H) = 5.7, ^{4}J(F-H) = 2.6, H^{c}]; 6.95 [td, 1H, ^{3}J(F-H) = ^{3}J(H-H) = 8.4, ^{4}J(H-H) = 2.4, H^{b}]; 3.98 [t, 2H, ^{3}J(H-H) = 5.4, H^{e}]; 2.97 [s, 6H, ^{3}J(Pt-H) = 10,2 H^{h}]; 2.96 [m, 2H, H^{g}]; 2.25 [m, 2H, H^{f}]. **^{19}F NMR** ($CDCl_3$, 376.5 MHz): δ -101.46 [m,1F]. **MS-ESI^{+}**: m/z 526.04 $[M+NH_4]^{+}$; 508.01 $[M+H]^{+}$; 472.03 $[M-Cl]^{+}$; 436.06 $[M-2Cl-H]^{+}$. **Anal. Found** (calcd for $C_{12}H_{16}Cl_3FN_2Pt$)**:** C, 28.32 (28.33); H, 3.24 (3.17); N, 5.32 (5.51).

Synthesis of [$PtBr_3${$(CH_3)_2N(CH_2)_3N=CH(4-FC_6H_3)$}] (3b)

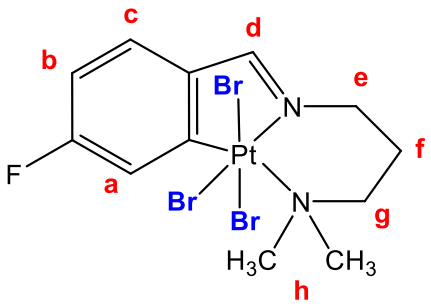

Compound [$PtBr_3${$(CH_3)_2N(CH_2)_3N=CH(4-FC_6H_3)$}] (**3b**) was prepared as a brown solid by following the same method from 0.029 g (0.060 mmols) of [$PtBr${$(CH_3)_2N(CH_2)_3N=CH(4-FC_6H_3)$}] (**1b**) and 0.050 g (0.313 mmols) of Br_2. Yield: 0.039 g (86%).

^{1}H NMR ($CDCl_3$, 400 MHz): δ 8.09 [s, 1H, ^{3}J(Pt-H) = 93.9, H^{d}]; 7.97 [dd, 1H, ^{3}J(F-H) = 9.5, ^{4}J(H-H) = 2.6, H^{a}]; 7.52 [dd, 1H, ^{3}J(H-H) = 8.9, ^{4}J(F-H) = 5.4, H^{c}]; 6.85 [td, 1H, ^{3}J(F-H) = ^{3}J(H-H) = 8.2, ^{4}J(H-H) = 2.1, H^{b}]; 3.99 [t, 2H, ^{3}J(H-H) = 5.1, H^{e}]; 3.17[s, 6H, ^{3}J(Pt-H) = 13.4, H^{h}]; 2.94 [m, 2H, H^{g}]; 2.28 [m, 2H, H^{f}]. **^{19}F NMR** ($CDCl_3$, 376.5 MHz): δ -101.75 [m, 1F]. **MS-ESI^{+}**: m/z 642.85 $[M+H]^{+}$; 562.90 $[M-Br]^{+}$; 483.02 $[M-2Br+H]^{+}$. **Anal. Found** (calcd for $C_{12}H_{16}Br_3FN_2Pt$)**:** C, 22.38 (22.45); H, 2.65 (2.51); N, 3.99 (4.36).

Synthesis of [PtI_3{$(CH_3)_2N(CH_2)_3N=CH(4\text{-}FC_6H_3)$}] (3c)

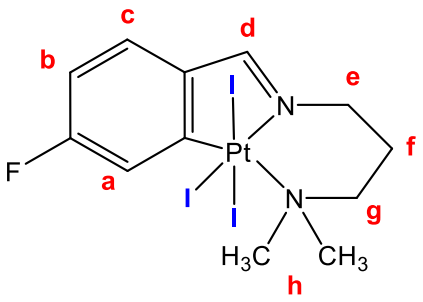

Compound [PtI_3{$(CH_3)_2N(CH_2)_3N=CH(4\text{-}FC_6H_3)$}] (**3c**) was prepared as a dark brown solid by following the same method from 0.035 g (0.058 mmols) of [PtI{$(CH_3)_2N(CH_2)_3N=CH(4\text{-}FC_6H_3)$}] (**1c**) and 0.059 g (0.232 mmols) of I_2. Yield: 0.043 g (93%).

^{1}H NMR ($CDCl_3$, 400 MHz): δ 8.25 [dd, 1H, ^{3}J(Pt-H) = 33.6, ^{3}J(F-H) = 10.3, ^{4}J(H-H) = 2.4, H^a]; 7.96 [s, 1H, ^{3}J(Pt-H) = 91.2, H^d]; 7.52 [dd, 1H, ^{3}J(H-H) = 8.2, ^{4}J(F-H) = 5.9, H^c]; 6.66 [td, 1H, ^{3}J(F-H) = ^{3}J(H-H) = 8.3, ^{4}J(H-H) = 2.4, H^b]; 3.96 [t, 2H, ^{3}J(H-H) = 5.6, H^e]; 3.55 [s, 6H, ^{3}J(Pt-H) = 16.6, H^h]; 2.92 [m, 2H, H^g]; 2.32 [qi, 2H, ^{3}J(H-H) = 5.2, H^f]. **^{19}F NMR** ($CDCl_3$, 376.5 MHz): δ -97.45 [m, 1F]. **MS-ESI$^+$**: m/z 783.82 $[M+H]^+$, 655.90 $[M-I]^+$, 529.00 $[M-2I-H]^+$. **Anal. Found** (calcd for $C_{12}H_{16}I_3FN_2Pt$)**:** C, 15.44 (15.84); H, 1.87 (1.77); N, 2.82 (3.08).

2.4.4. X-Ray Diffraction

Suitable crystals of compounds **1b'**, **1b**, **2b** and **3b** were grown at room temperature in dichloromethane-methanol. X-ray diffraction data were collected for prism-like specimens on a D8 VENTURE system equipped with a multilayer monochromator and a Mo high brilliance Incoatec Microfocus Source (λ = 0.71073 Å) at 100 K (**1b'**, **2b**, **3b**) or at 293 K (**1b**). The structures were solved and refined using the Bruker SHELXTL Software package.[48] Crystallographic details are given in *Tables A1* and *A2*.

2.5. References

1. Kalinowski, J.; Fattori, V.; Cocchi, M.; Williams, J.A.G. *Coord. Chem. Rev.* **2011**, *255*, 2401–2425.
2. Fleetham, T.; Li, G.; Li, J. *Adv. Mater.* **2017**, *29*, 2401–2425.
3. Kourkoulos, D.; Karakus, C.; Hertel, D.; Alle, R.; Schmeding, S.; Hummel, J.; Risch, N.; Holder, E.; Meerholz, K. *Dalton Trans.* **2013**, *42*, 13612–13621.
4. Li, Z.; Badaeva, E.; Ugrinov, A.; Kilina, S.; Sun, W. *Inorg. Chem.* **2013**, *52*, 7578–7592.
5. Gareth Williams, J.A.; Develay, S.; Rochester, D.L.; Murphy, L. *Coord. Chem. Rev.* **2008**, *252*, 2596–2611.
6. Huo, S.; Carroll, J.; Vezzu, D.A.K. *Asian J. Org. Chem.* **2015**, *4*, 1210–1245.
7. Brooks, J.; Babayan, Y.; Lamansky, S.; Djurovich, P.I.; Tsyba, I.; Bau, R.; Thompson, M.E. *Inorg. Chem.* **2002**, *41*, 3055–3066.
8. Scaffidi-Domianello, Y.Y.; Nazarov, A.A.; Haukka, M.; Galanski, M.; Keppler, B.K.; Schneider, J.; Du, P.; Eisenberg, R.; Kukushkin, V.Y. *Inorg. Chem.* **2007**, *46*, 4469–4482.
9. Pandya, S.U.; Moss, K.C.; Bryce, M.R.; Batsanov, A.S.; Fox, M.A.; Jankus, V.; Al Attar, H.A.; Monkman, A.P. *Eur. J. Inorg. Chem.* **2010**, 1963–1972.
10. Anderson, C.M.; Weinstein, M.A.; Morris, J.; Kfoury, N.; Duman, L.; Balema, T.A.; Kreider-Mueller, A.; Scheetz, P.; Ferrara, S.; Chierchia, M.; Tanski, J.M. *J. Organomet. Chem.* **2013**, *723*, 188–197.
11. Crespo, M.; Martinez, M.; Sales, J.; Solans, X.; Font-Bardía, M. *Organometallics* **1992**, *11*, 1288–1295.
12. Crespo, M.; Font-Bardía, M.; Pérez, S.; Solans, X. *J. Organomet. Chem.* **2002**, *642*, 171–178.
13. Anderson, C.M.; Crespo, M.; Jennings, M.C.; Laugh, A.J.; Ferguson, G.; Puddephatt, R.J. *Organometallics* **1991**, *10*, 2672–2679.
14. Anderson, C.; Crespo, M. *J. Organomet. Chem.* **2004**, *689*, 1496–1502.

15. Crespo, M.; Evangelio, E. *J. Organomet. Chem.* **2004**, *689*, 1956–1964.

16. Estevan, F.; González, G.; Lahuerta, P.; Martinez, M.; Peris, E.; Van Eldik, R. *J. Chem. Soc., Dalton Trans.* **1996**, 1045–1050.

17. Capapé, A.; Crespo, M.; Granell, J.; Font-Bardía, M.; Solans, X. *J. Organomet. Chem.* **2005**, *690*, 4309–4318.

18. Juliá, F.; Bautista, D.; González-Herrero, P. *Chem. Commun.* **2016**, *52*, 1657–1660.

19. Juliá, F.; García-Legaz, M.D.; Bautista, D.; González-Herrero, P. *Inorg. Chem.* **2016**, *55*, 7647–7660.

20. Berenguer, J.R.; Lalinde, E.; Moreno, M.T. *Coord. Chem. Rev.* **2018**, *366*, 69–90.

21. Rendina, L.M.; Puddephatt, R.J. *Chem. Rev.* **1997**, *97*, 1735–1753.

22. Wilson, J.J.; Lippard, S.J. *Chem. Rev.* **2014**, *114*, 4470–4495.

23. Nabavizadeh, S.M.; Amini, H.; Rashidi, M.; Pellarin, K.R.; McCready, M.S.; Cooper, B.F.T.; Puddephatt, R.J. *J. Organomet. Chem.* **2012**, *713*, 60–67.

24. Gandioso, A.; Valle-Sistac, J.; Rodríguez, L.; Crespo, M.; Font-Bardía, M. *Organometallics* **2014**, *33*, 561–570.

25. Crespo, M. *Organometallics* **2012**, *31*, 1216–1234.

26. Crespo, M.; Font-Bardia, M.; Granell, J.; Martínez, M.; Solans, X. *J. Chem. Soc., Dalton Trans.* **2003**, *3*, 3763–3769.

27. Crespo, M.; Font-Bardía, M.; Solans, X. *J. Organomet. Chem.* **2006**, *691*, 444–454.

28. Bernhardt, P. V.; Calvet, T.; Crespo, M.; Font-Bardía, M.; Jansat, S.; Martínez, M. *Inorg. Chem.* **2013**, *52*, 474–484.

29. Crespo, M.; Font-Bardía, M.; Solans, X. *J. Organomet. Chem.* **2006**, *691*, 1897–1906.

30. Kaupp, M.; Malkina, O.L.; Malkin, V.G.; Pyykkö, P. *Chem. Eur. J.* **1998**, *4*, 118–126.

31. Johnstone, T.C.; Alexander, S.M.; Wilson, J.J.; Lippard, S.J. *Dalton Trans.* **2015**, *44*, 119–129.

32. Solé, M.; Balcells, C.; Crespo, M.; Quirante, J.; Badia, J.; Baldomà, L.; Font-Bardia, M.; Cascante, M. *Dalton Trans.* **2018**, *47*, 8956–8971.

33. Calvet, T.; Crespo, M.; Font-Bardía, M.; Jansat, S.; Martínez, M. *Organometallics* **2012**, *31*, 4367–4373.

34. Bauer, E.; Domingo, X.; Balcells, C.; Polat, I.H.; Crespo, M.; Quirante, J.; Badía, J.; Baldomà, L.; Font-Bardia, M.; Cascante, M. *Dalton Trans.* **2017**, *46*, 14973–14987.

35. Hight, L.M.; McGuire, M.C.; Zhang, Y.; Bork, M.A.; Fanwick, P.E.; Wasserman, A.; McMillin, D.R. *Inorg. Chem.* **2013**, *52*, 8476–8482.

36. Song, C.; Tang, J.; Li, J.; Wang, Z.; Li, P.; Zhang, H. *Inorg. Chem.* **2018**, *57*, 12174–12186.

37. Zhang, Y.; Meng, F.; You, C.; Yang, S.; Xiong, L.; Xiong, W.; Zhu, W.; Wang, Y.; Pei, Y.; Su, S. *Dyes Pigm.* **2017**, *142*, 457–464.

38. Li, K.; Wan, Q.; Yang, C.; Chang, X.Y.; Low, K.H.; Che, C.M. *Angew. Chem. Int. Ed.* **2018**, *57*, 14129–14133.

39. Puttock, E. V.; Walden, M.T.; Williams, J.A.G. *Coord. Chem. Rev.* **2018**, *367*, 127–162.

40. Li, J.; Djurovich, P.I.; Alleyne, B.D.; Yousufuddin, M.; Ho, N.N.; Thomas, J.C.; Peters, J.C.; Bau, R.; Thompson, M.E. *Inorg. Chem.* **2005**, *44*, 1713–1727.

41. Juliá, F.; González-Herrero, P. *Dalton Trans.* **2016**, *45*, 10599–10608.

42. Martinho, J.M.C. *J. Phys. Chem* **1989**, *93*, 6687–6692.

43. Al-Allaf, T.A.K.; Rashan, L.J.; Abu-Surrah, A.S.; Fawzi, R.; Steimann, M. *Transit. Met. Chem.* **1998**, *23*, 403–406.

44. Kukushkin, V.Y.; Lovqvist, K.; Norin, B.; Oskarsson, A.; Elding, L.I.; Cox, ; E G; Saenger, H.; Wardlaw, W. *Inorg. Synth.* **1998**, *32*, 153–158.

45. Hill, G.S.; Irwin, M.J.; Levy, C.J.; Rendina, L.M.; Puddephatt, R.J. *Inorg. Synth.* **1998**, *32*, 149–153.

46. Zhao, X.F.; Zhang, C. *Synthesis* **2007**, 551–557.

48. Sheldrick, G.M. *Acta Crystallogr. Sect. C Struct. Chem.* **2015**, *71*, 3–8.

CHAPTER 3

Anticancer activity of luminescent platinacycles against multiplatinum-resistant metastatic CRC and CRPC cell models

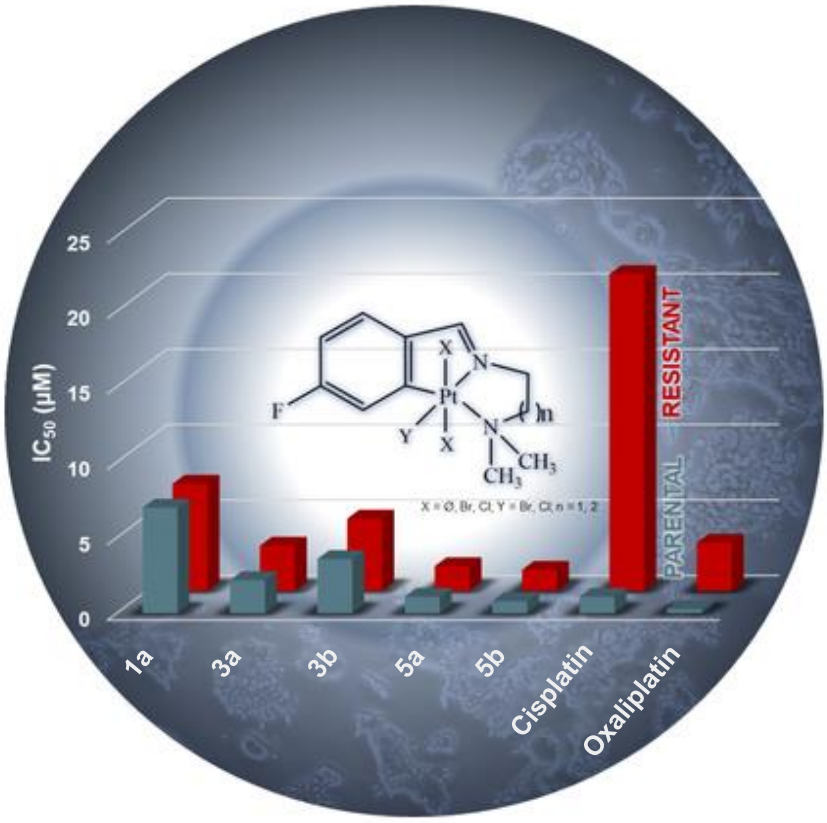

Part of this chapter has been published in: Lázaro, A.; Balcells, C.; Quirante, J.; Badia, J.; Baldomà, L.; Ward, J. S., Rissanen, K.; Font-Bardia, M.; Rodríguez, L.; Crespo, M.; Cascante, M. *Chem. Eur. J.*, **2020**, *26*, 1947-1952.

3. Anticancer activity of luminescent platinacycles against multiplatinum-resistant metastatic CRC and CRPC cell models

3.1. Introduction

Platinum based chemotherapy remains to be the only effective treatment against a wide variety of tumours. However, the acquisition of platinum resistance is very common which makes conventional platinum drugs ineffective in time against cancer cells. Therefore, it is necessary to find alternatives that are both effective and non-cross resistant. Nowadays, the strategy is to administer simultaneously several drugs that proceed through different mechanisms to avoid the adaptation of the cell to one action route. Then, it becomes crucial to find alternatives to conventional drugs with different mechanisms.[1–3]

Platinum(IV) compounds have attracted a great interest as they are kinetically inert compared to platinum(II) analogues due to their d^6 low spin configuration and present two extra coordination positions that allow the tuning of their properties.[4–6] Particularly, a lot of interest has been devoted to multiple action platinum(IV) compounds derived from cisplatin which contain bioactive ligands in the axial positions.[7–9]

It is generally assumed that platinum(IV) compounds can act as prodrugs if they have the ability to undergo reductive elimination under cellular media to give the platinum(II) active species as well as the two axial ligands (*Scheme 3.1*). This allows them to remain inert until reaching the target cells without causing secondary effects in other parts of the body. This could mean they could even be administered orally which would improve the quality of life of patients in treatment.[10,11]

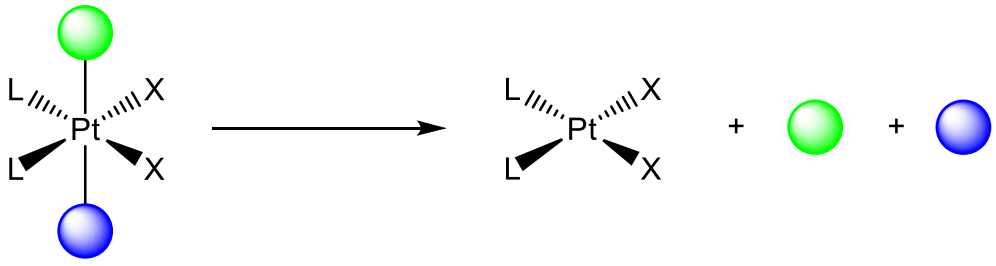

Scheme 3.1. Scheme of the reduction of platinum(IV) compounds in cellular media.

Specifically, cancer cells present a hypoxic environment with a high concentration of reducing agents. So, reduction is a key step in the mechanism of action of the prodrug, as it should not be reduced before reaching the cells or neither be too resistant to reduction as it would then become inactive.[12–14]

In spite of the attention that platinum(IV) compounds and cyclometallated platinum(II) compounds have attracted, less studies have been performed in cyclometallated platinum(IV) analogues. They present the combined properties of a platinum(IV) centre with the higher stability provided by the presence of a Pt-C bond and the higher lability of the ligand in *trans* to it, which could enhance their anticancer properties.[15]

A previous study of compounds with the general formulae [PtX(C,N,N')] and [PtXYZ(C,N,N')] depicted in *Figure 3.1* revealed that although remarkable antiproliferative activity in selected cancer lines was observed for both platinum(II) and platinum(IV) derivatives, the latter were not able to reduce under cellular media if they contain C-donor ligands such as methyl or aryl in addition to the cyclometallated imine. Furthermore, compounds with more than one iodido ligand presented low solubility which did not allow to perform analogous studies.[16,17]

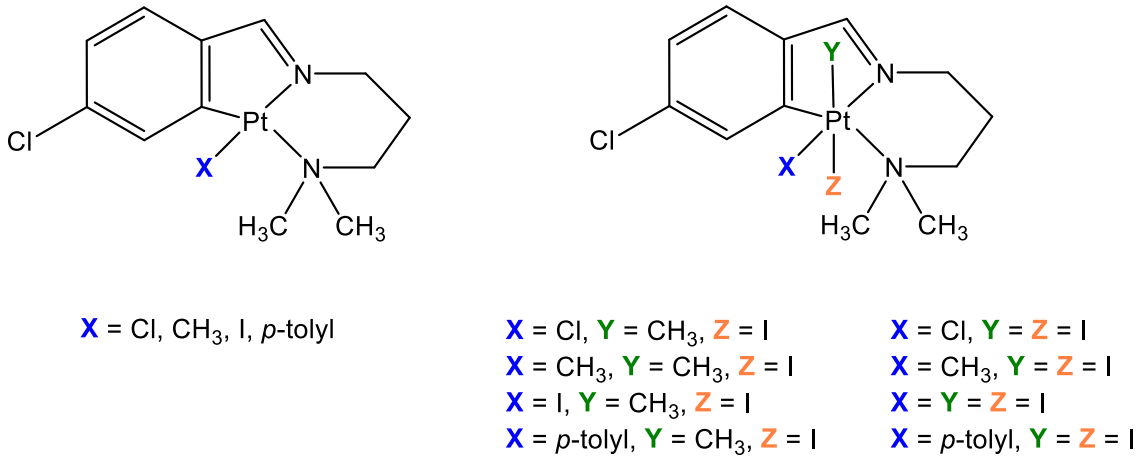

Figure 3.1. Structure of the cyclometallated [C,N,N'] compounds previously studied.

Therefore, in this work, it has been attempted to optimize these structures to maximise their efficacy and selectivity against cancer cells as well as to achieve the synthesis of cyclometallated platinum(IV) compounds that are able to get reduced in the cell so they can act as prodrugs. For this, a new family of [C,N,N'] cyclometallated compounds derived from ligand 4-$FC_6H_4CH=N(CH_2)_2N(CH_3)_2$ has been synthesised. Compounds

differ in the nature of the ancillary ligand (chlorido or bromido) and the oxidation state of the platinum centre. The effect of the length of the aliphatic chain of the ligand in the resulting properties was also assessed by evaluating the antiproliferative effect of their longer chain analogues derived from ligand 4-$FC_6H_4CH=N(CH_2)_3N(CH_3)_2$ depicted in *Chapter 2*.

Their antiproliferative activity has been evaluated in a wide cancer cells panel as well as for tumour cells that have acquired platinum resistance and healthy cells to evaluate their selectivity. To further understand their mechanism of action, several studies such as DNA interaction, reduction under cellular media, their effect in cell cycle phase distribution, apoptosis and ROS production were performed.

Additionally, the luminescent properties of all compounds were also evaluated, as it could be of remarkable interest for their application for in vivo cell imaging, as DNA probes or as a mean to track their cellular uptake and distribution by fluorescence microscopy.[18–21]

3.2. Results and Discussion

3.2.1. Synthesis and characterisation

Ligand 4-$FC_6H_4CH=N(CH_2)_2N(CH_3)_2$ (**L2**) was synthesised by Schiff condensation of 4-fluorobenzaldehyde and 2-dimethylamino-1-ethanamine in toluene, an analogous procedure than the one depicted in *Chapter 2* for ligand **L1** (*Scheme 3.2*). As well as its derivative with the longer chain (**L1**), characterisation by ^{1}H and ^{19}F NMR confirms the formation of a single isomer which is attributed to the more stable *E* configuration around the C=N bond.[22]

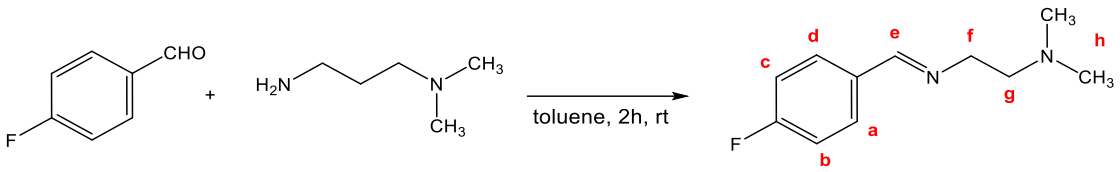

Scheme 3.2. Synthesis of ligand **L2**.

All cyclometallated compounds were also synthesised *via* the same methods described in *Chapter 2* for their longer chain analogues. Compound [PtCl{$(CH_3)_2N(CH_2)_2N=CH(4-FC_6H_3)$}] (**4a**) was prepared by the cyclometallation of **L2** with cis-[$PtCl_2(DMSO)_2$] as a metallating agent, which proceeds through electrophilic activation of the C-H bond in *ortho* position of the aryl ring in the presence of a base (*Scheme 3.3*).[23,24] In this case, the reaction time required for the complete formation of the cyclometallated compound without traces of the [N,N'] coordination compound is 24 hours longer than its analogue with the longer propylene chain **1a**.

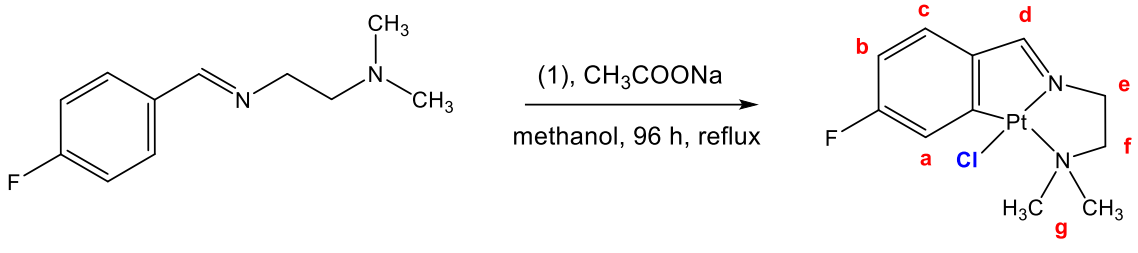

Scheme 3.3. Synthesis of compound **4a.** (1) cis-[$PtCl_2(DMSO)_2$].

Compound [PtBr{$(CH_3)_2N(CH_2)_3N=CH(4-FC_6H_3)$}] (**4b**) was synthesised by ligand substitution from compound **4a** using an excess of KBr in methanol (*Scheme 3.4*).

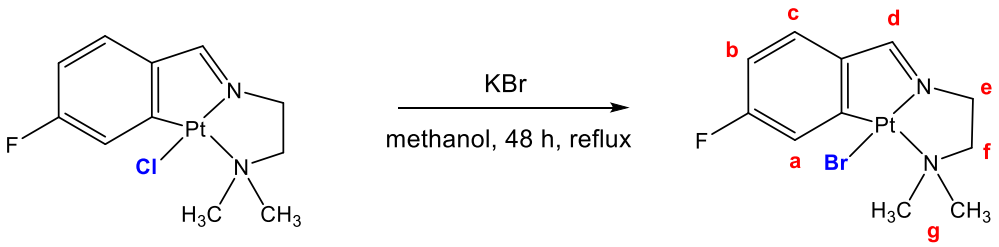

Scheme 3.4. Synthesis of compound **4b**.

Oxidative halogenation reactions were performed on compounds **4a** and **4b** to obtain the corresponding cyclometallated platinum(IV) compounds [PtX_3{$(CH_3)_2N(CH_2)_3N$=CH(4-FC_6H_3)}] (**5a**, X = Cl; **5b**, X = Br) using iodobenzene dichloride ($PhICl_2$) and Br_2, respectively (*Scheme 3.5*).

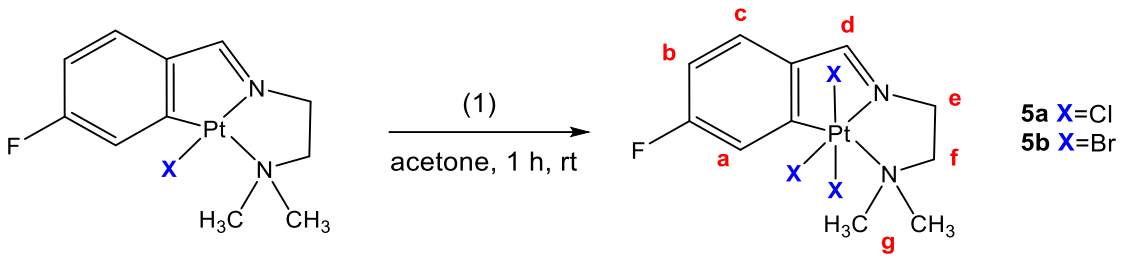

Scheme 3.5. Synthesis of compounds **5a** and **5b**. (1) $PhICl_2$ (**5a**); Br_2 (**5b**).

All compounds were characterised by elemental analyses, mass spectrometry and ^{1}H and ^{19}F NMR spectroscopy, matching the desired structures. For the compounds under study, the dimethylamino protons appear as a singlet integrating for 6 H coupled to platinum. As expected, the ^{3}J(Pt-H) values for the imine proton are significantly smaller for platinum(IV) derivatives **5a** and **5b** (^{3}J(Pt-H) = 89-90 Hz) than for the parent platinum(II) compounds (^{3}J(Pt-H) = 141-143 Hz). For **4b** and **5b,** the coupling of the proton adjacent to the metallated carbon H^a to ^{195}Pt is also observed and the value of the coupling constant is also reduced upon increase of the oxidation state from 50.8 Hz (**4b**) to 27.5 Hz (**5b**).

3.2.2. X-ray crystal structure determination

Single crystals suitable for X-ray diffraction were obtained for all compounds with, in all cases, one single molecule present in the asymmetric unit. Both cyclometallated platinum(II) compounds **4a** and **4b** (*Figure 3.2*) present the expected square-planar environment around the platinum atom completed with a tridentate [C,N,N'] ligand and a halido (**4a**, X = Cl, **4b** X = Br). As a result, fused [6,5,5]-tricyclic systems containing

an *ortho*-metallated phenyl group, a five-membered platinacycle and a five-membered chelate ring with two nitrogen atoms coordinated to platinum are formed. In these systems, both the platinacycle and the chelate rings are nearly coplanar with the coordination plane leading to more rigid structures than those reported in the previous chapter for compounds **1a** and **1b** containing the longer propylene chain.[25,26]

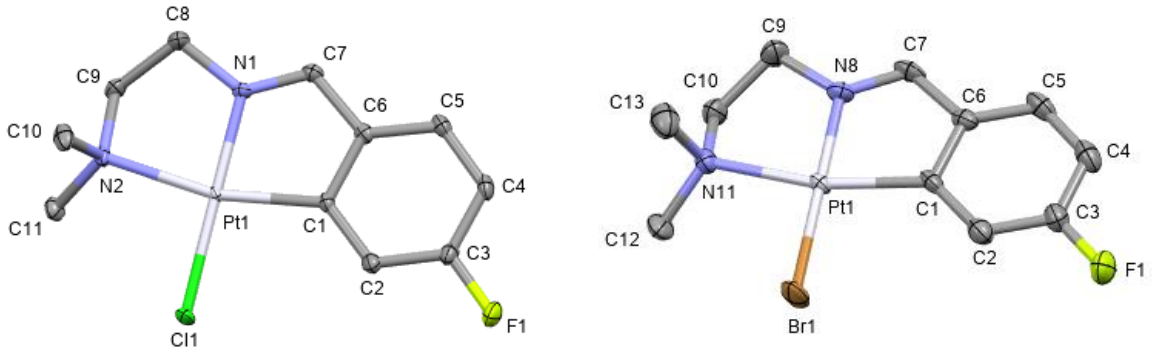

Figure 3.2. Molecular structure of compounds **4a** (left) and **4b** (right). Selected bond lengths (Å) and angles (deg.) with estimated standard deviations. For **4a**: Pt(1)–N(1): 1.962(2); Pt(1)–N(2): 2.157(3); Pt(1)–C(1): 1.986 (3); Pt(1)–Cl(1): 2.3119 (10); C(1)–Pt–N(1): 81.33(11); N(1)–Pt–N(2): 83.52(10); N(2)–Pt–Cl(1): 97.07(7); Cl(1)–Pt–C(1): 98.10(9). For **4b**: Pt(1)–N(8): 1.958(6); Pt(1)–N(11): 2.151(6); Pt(1)–C(1): 1.996(7); Pt(1)–Br(1): 2.4224 (8); C(1)–Pt–N(8): 81.4(3); N(8)–Pt–N(11): 83.2(2); N(11)–Pt–Br(1): 97.15(17); Br(1)–Pt–C(1): 98.3(2).

Bond lengths and angles are well within the range of values obtained for analogous compounds.[22,23] For both compounds, bond lengths around the platinum are very similar except for the Pt-Br bond in **4b** which is longer (2.4224 Å) than the Pt-Cl bond (2.3119 Å) in **4a**. As seen in the previous chapter, Pt-amine distances are larger than Pt-imine distances in agreement with the weaker ligating ability of amines for platinum. Most angles around the platinum are close to the ideal value of 90º, with the smallest angles corresponding to the metallacycle C-Pt-N (81.33(11)º for **4a** and 81.4(3)º for **4b**) and to the chelate angle N-Pt-N (83.52(10)º for **4a** and 83.2(2)º for **4b**). The latter is in contrast with the fact that for compounds **1b** and **1b**, containing a more flexible propanediamine chain, the chelate angle has a larger value in the range 95-97º.[26]

For platinum(IV) compounds **5a** and **5b**, the platinum atom displays an octahedral coordination with a meridional tridentate [C,N,N'] ligand (*Figure 3.3*). Three chlorido (**5a**) or bromido (**5b**) ligands complete the coordination around the platinum. As observed

for the parent platinum(II) compounds, Pt-amine distances are larger than Pt-imine distances and the smallest angles correspond to the metallacycle (C-Pt-N (81.6(3)º for **5a** and 82.8(8)º for **5b**) and to the chelate angle N-Pt-N (82.2(3)º for **5a** and 82.0(6)º for **5b**). The axial ligands form a Cl-Pt-Cl angle of 175.86(8) (**5a**) or a Br-Pt-Br of 173.85(8) (**5b**). As previously observed, a comparison of the bond distances of the cyclometallated platinum(IV) compounds with those of the platinum(II) precursors reveals that the Pt-N_{imine}, Pt-N_{amine} and Pt-C bond lengths are moderately longer for the platinum(IV) compounds.[16]

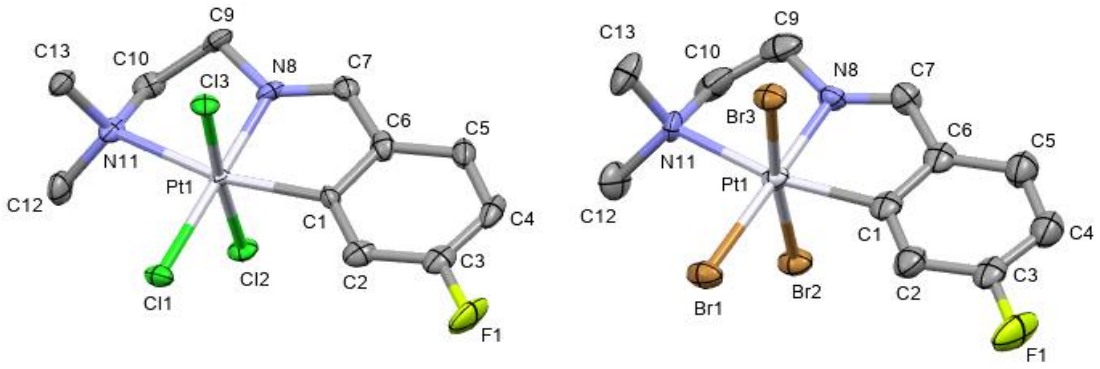

Figure 3.3. Molecular structure of compound **5a** (left) and **5b** (right). Selected bond lengths (Å) and angles (deg.) with estimated standard deviations. For **5a**: Pt(1)–N(8): 1.984(8); Pt(1)–N(11): 2.253(8); Pt(1)–C(1): 2.019(9); Pt(1)–Cl(1): 2.320(2); Pt(1)–Cl(2): 2.313(2); Pt(1)–Cl(3): 2.322(2); C(1)–Pt–N(8): 81.6(3); N(8)–Pt–N(11): 82.2(3); N(11)–Pt–Cl(1): 97.8(2); Cl(1)–Pt–C(1): 98.4(3); Cl(2)–Pt–Cl(1): 90.02(8); Cl(2)–Pt–N(8): 90.6(2); Cl(2)–Pt–N(11): 90.0(2); Cl(2)–Pt–C(1): 87.0(3); Cl(3)–Pt–Cl(1): 90.78(8); Cl(3)–Pt–N(8): 88.6(2); Cl(3)–Pt–N(11): 93.9(2); Cl(3)–Pt–C(1): 88.8(3). For **5b**: Pt(1)–N(8): 1.986(14); Pt(1)–N(11): 2.231(16); Pt(1)–C(1): 2.03(2); Pt(1)–Br(1): 2.4507(19); Pt(1)–Br(2): 2.4563(19); Pt(1)–Br(3): 2.4668(182); C(1)–Pt–N(8): 82.8(8); N(8)–Pt–N(11): 82.0(6); N(11)–Pt–Br(1): 97.6(4); Br(1)–Pt–C(1): 98.3(6); Br(2)–Pt–Br(1): 90.01(6); Br(2)–Pt–N(8): 90.6(4); Br(2)–Pt–N(11): 91.2(5); Br(2)–Pt–C(1): 86.0(5); Br(3)–Pt–Br(1): 90.80(7); Br(3)–Pt–N(8): 88.7(5); Br(3)–Pt–N(11): 94.7(5); Br(3)–Pt–C(1): 87.8(5).

As shown in *Figures 3.4* and *3.5*, all four crystal structures reveal the presence of intermolecular contacts shorter than the sum of van der Waals radii. For square-planar platinum(II) compounds **4a** and **4b**, the fluorine substituent is involved in these interactions leading to F···H_{imine} (**4a**, d(F···H) = 2.622 Å and 2.569 Å; **4b**, d(F···H) = 2.637 Å) and F···F (**4a**, d(F···F) = 2.810 Å; **4b**, d(F···F) = 2.900 Å) interactions, in addition to X··· H_3C (**4a**, X = Cl, **4b**, X = Br) and several C···H interactions.

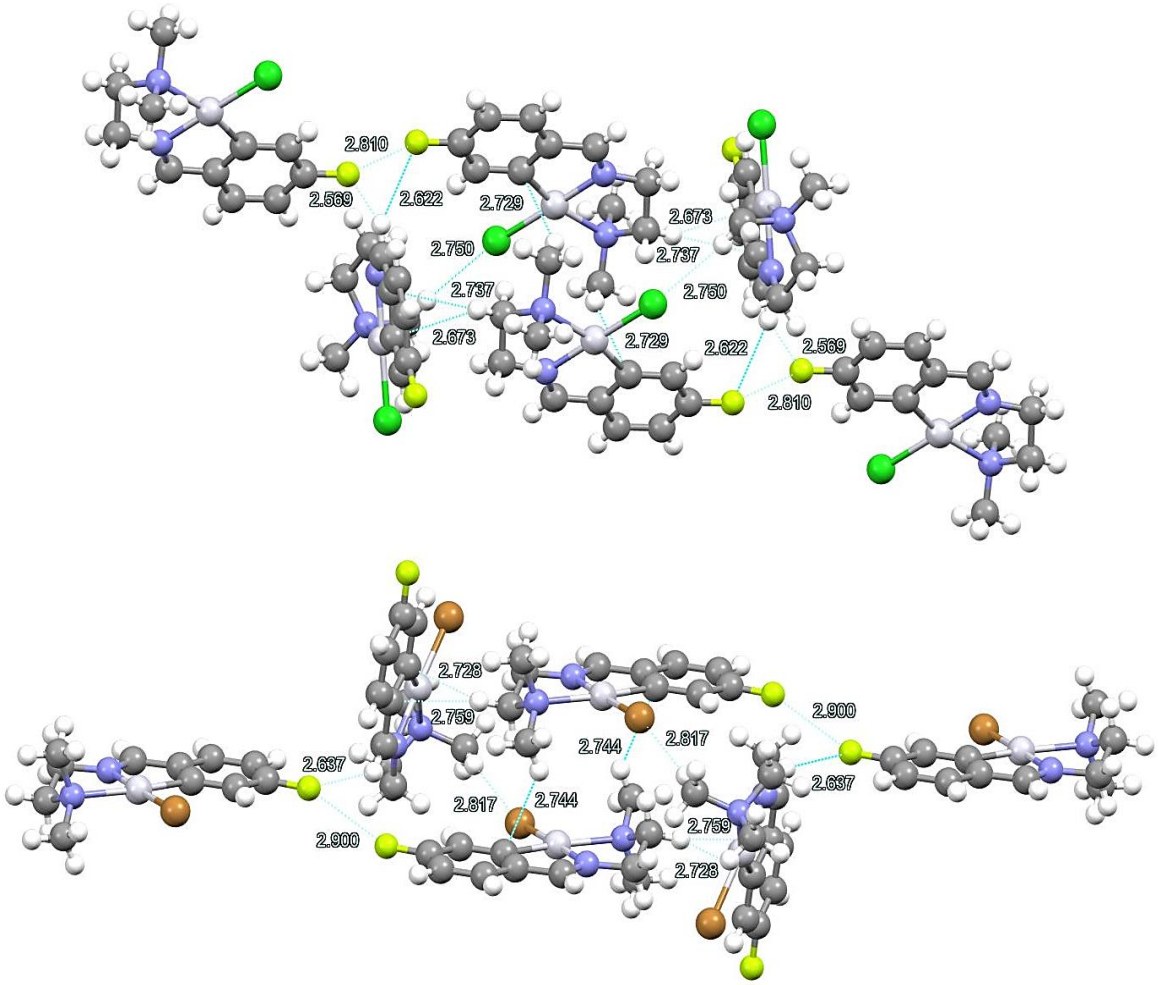

Figure 3.4. A view of the structure of compounds **4a** (top) and **4b** (bottom) with all intermolecular contacts shorter than the sum of van der Waals radii highlighted in blue. For **4a**: F(1)-H(7): 2.569 Å; F(1)-F(1): 2.810 Å; H(10A)-Cl(1): 2.750 Å; C(1)-H(9): 2.673 Å; C(6)-H(9): 2.737 Å; C(1)-H(11): 2.729 Å. For **4b**: F(1)-H(7): 2.637 Å; F(1)-F(1): 2.900 Å; H(10)-C(1): 2.728 Å; C(1)-H(12): 2.744 Å; C(6)-H(10): 2.759 Å ; Br(1)-H(13): 2.817 Å.

In contrast, for the octahedral platinum(IV) compounds **5a** and **5b**, the fluorine is not involved in these short contacts which consist mainly on intermolecular interactions of the halido ligand (**5a**, X = Cl, **5b**, X = Br) with aromatic (**5a**, d(Cl···H) = 2.848 Å; **5b**, d(Br···H) = 2.963 Å) and methyl protons (**5a**, d(Cl···H) = 2.887 Å; **5b**, d(Br···H) = 3.047 Å) in addition to C···H interactions for compound **5a** (d(C···H) = 2.828 Å) and a Br···Br interaction between the axial bromido ligands for compound **5b** (d(Br···Br) = 3.533 Å).

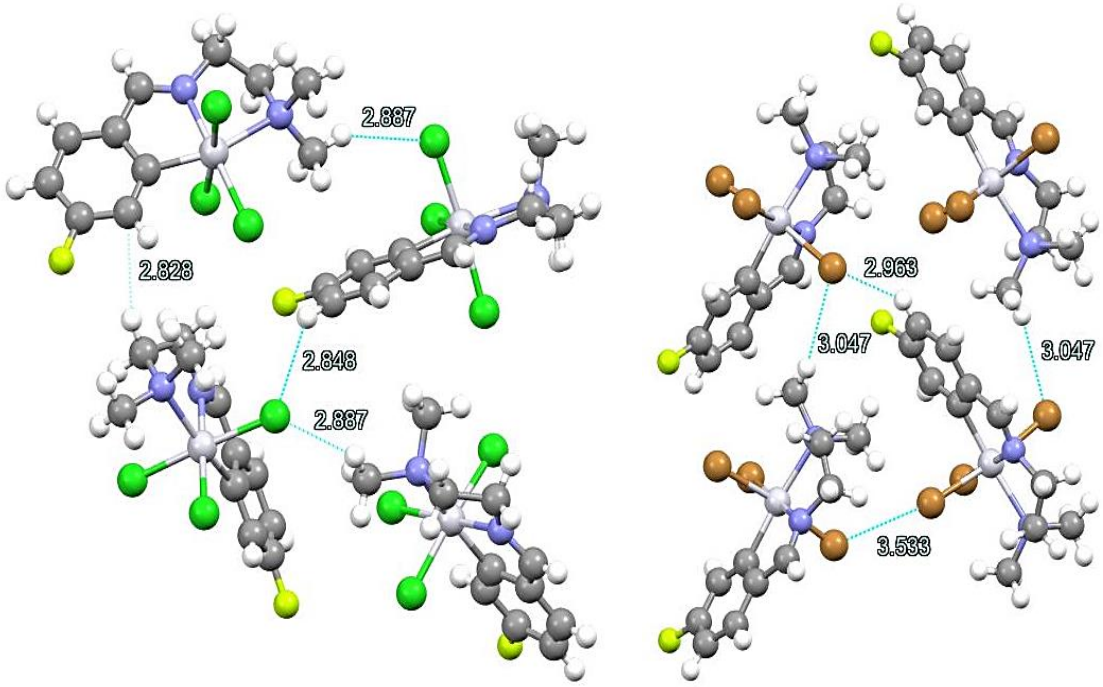

Figure 3.5. A view of the structure of compounds 5a (left) and 5b (right) with all intermolecular contacts shorter than the sum of van der Waals radii highlighted in blue. For **5a**: Cl(3)-H(12) = 2.887 Å, Cl(3)-H(4) = 2.848 Å, C(2)-H(10) = 2.828 Å. For **5b**: Br(2)-Br(3) = 3.533 Å, Br(3)-H(12) = 3.047 Å, Br(3)-H(4) = 2.963 Å.

3.2.3. Photophysical characterisation

Absorption and emission spectra of all compounds were recorded in $5 \cdot 10^{-5}$ M dichloromethane solutions at room temperature. The results are summarized in *Table 3.1*.

Table 3.1. Absorption and emission data for all compounds in dichloromethane solutions at 298K.

Compound	**Absorption λ_{max}/nm (ε/ M^{-1} cm^{-1})**	**Emission λ_{max}/nm**	**ϕ**
L2	275 (1994), 286 (1295)	350	0.059[a]
4a	277 (7524), 288 (5960), 324 (4843), 383 (4203)	347 577, 630	0.069[a] 0.005[b]
4b	280 (7645), 291 (6901), 326 (5898), 386 (5396)	350 576, 625	0.065[a] 0.006[b]
5a	270 (22702), 336 (2655)	352	0.123[a]
5b	280 (12290), 301 (9805), 340 (4097), 380 (2228)	351 578, 628	0.046[a] 0.002[b]

[a] Quantum yields for emission in solution referred to naphthalene in cyclohexane. [b] Quantum yields for emission in solution referred to $[Ru(bipy)_3]Cl_3$ in water.

All compounds show several bands in the 270-301 nm range in the UV-Visible absorption spectra with high ε values. These bands can be attributed to π→π* intraligand transitions as they match the absorption of the free ligand **L2** (*Figure 3.6*). Additionally, cyclometallated platinum(II) compounds **4a** and **4b** and platinum(IV) compound **5b** show bands in the lower energy range (380-386 nm) that can be assigned as Pt(5d) → π* (L) metal-to-ligand charge transfer (MLCT) mixed with intraligand transitions.[26–28]

Upon excitation at their high energy absorption bands, all compounds display a broad emission band around 350 nm for both **L2** and the resulting cyclometallated complexes (*Figure 3.6*). Therefore, it can be attributed to an intraligand (^{1}IL) transition that can be perturbed by the presence of the platinum.[29,30]

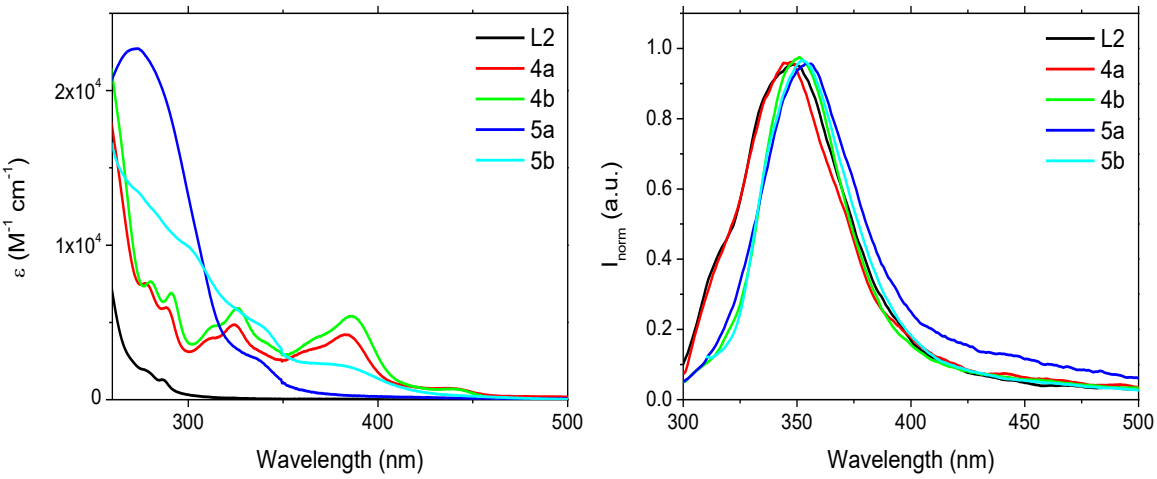

Figure 3.6. Absorption spectra (left) and normalized emission spectra upon excitation at their high energy band (λ_{exc}= 350 nm, right) for $5 \cdot 10^{-5}$ M dichloromethane solutions of ligand **L2** and platinum compounds **4** and **5**.

When excited at their lower energy absorption bands, a vibronically structured band in the 576-630 nm range is observed for compounds **4** and **5b**. As seen previously, it can be attributed to phosphorescence ^{3}IL emission due to the large Stokes' shift and the quenching of the emission in the presence of oxygen (*Figure 3.7*).[22,26] In all cases, no excimer's or aggregates' bands that usually present a broad emission at higher wavelengths were recorded. This agrees with the fact that no Pt···Pt or π···π stacking interactions are observed in the crystal packing of the molecules.

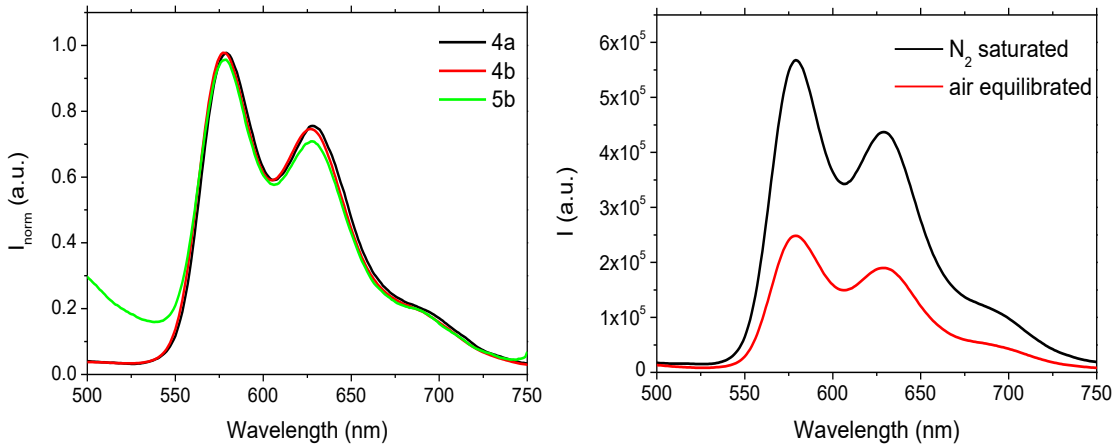

Figure 3.7. Normalized emission spectra for $5 \cdot 10^{-5}$ M dichloromethane solutions of platinum compounds **4a**, **4b** and **5b** upon excitation at their low energy band (λ_{exc}= 625 nm, left) and comparison between air equilibrated and N_2 saturated emission spectra of compound **4a** (right).

The quantum yield values for all emission bands are summarized in *Table 3.2* for all compounds and their analogues (compounds **1a**, **1b**, **3a**, **3b**) depicted in *Chapter 2*.

Table 3.2. Absorption and emission data for all compounds

1a X = Cl, n= 2
4a X = Cl, n= 1
1b X = Br, n= 2
4b X = Br, n= 1

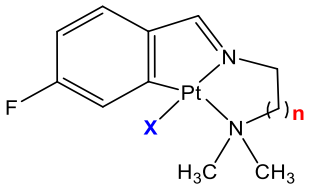

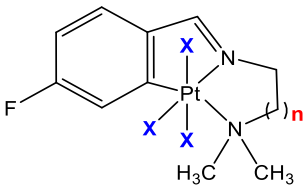

3a X = Cl, n= 2
5a X = Cl, n= 1
3b X = Br, n= 2
5b X = Br, n= 1

Compound	ϕ_F[a] (λ_{em} = 350 nm)	ϕ_{Ph}[b] (λ_{em} = 576-630 nm)
1a	0.056	0.003
4a	0.069	0.005
1b	0.044	0.004
4b	0.065	0.006
3a	0.051	-
5a	0.123	-
3b	0.056	-
5b	0.046	0.002

[a] Quantum yields for emission in solution referred to naphthalene in cyclohexane. [b] Quantum yields for emission in solution referred to $[Ru(bipy)_3]Cl_3$ in water.

We can observe that for the emission band at 350 nm, quantum yield values are higher for those compounds that derive from the more rigid ethylene chain (**4** and **5**, ϕ = 0.046-0.123) than their analogues depicted in *Chapter 2* containing a propylene chain (**1** and **3**, ϕ = 0.044-0.064). As an exception, compound **5b** presents a lower quantum yield regarding its analogue **3b**, which is explained by the presence of the previously not observed band at higher wavelengths. For the emission band at higher wavelength, the same tendency can be observed when comparing compounds **1** and **4**. Therefore, it can be concluded that the higher rigidity in compounds **4** and **5** restricts their vibrations which results in an increase in the radiative pathways versus non-radiative ones.

3.2.4. Cell viability assays

All compounds along with their analogues with a longer aliphatic chain depicted in *Chapter 2* were selected to study their anticancer properties (*Figure 3.8*). Compounds containing a methyl as an ancillary ligand (**2a**-**2c**) were discarded for these studies as it has been previously stated that the presence of more Pt-C bonds prevents platinum(IV) compounds reduction under cellular media and therefore the possibility of them acting as prodrugs.[25,31] Additionally, those containing iodido ligands (**1c**, **3c**) were not selected as it has been observed that they present a low solubility which does not allow the performance of this studies in biological media.[16]

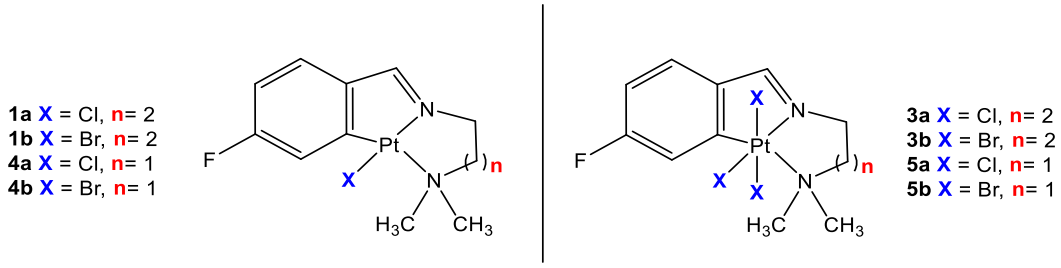

Figure 3.8. Molecular structure of the selected compounds for biological studies.

The antiproliferative activity of all compounds was assessed against a wide panel of cancer cell lines including SW620 (colorectal cancer), PC-3 (prostate cancer), A549 (lung adenocarcinoma) and MCF-7 (breast adenocarcinoma). The resulting IC_{50} values are summarised in *Table 3.3*.

Table 3.3. Antiproliferative activity (IC_{50}, μM) on A549 lung, SW620 colorectal, MCF-7 breast and PC-3 prostate cancer cell lines for the studied compounds, cisplatin and oxaliplatin.

Compound[a]	A549	SW620	MCF-7	PC-3
1a	5 ± 2	5.7 ± 1.1	6 ± 2	1.1 ± 0.6
1b	5 ± 2	5.5 ± 0.4	7 ± 2	2.1 ± 1.3
4a	57 ± 3	4.6 ± 0.8	>100	19 ± 5
4b	48 ± 5	3.1 ± 1.1	>100	66 ± 13
3a	1.4 ± 0.5	0.9 ± 0.3	3.3 ± 0.5	0.9 ± 0.2
3b	3.39 ± 0.12	1.8 ± 0.7	6.6 ± 0.8	1.46 ± 0.13
5a	4.1 ± 0.3	0.41 ± 0.04	5.4 ± 1.0	1.2 ± 0.5
5b	4 ± 2	0.7 ± 0.4	8.0 ± 0.8	1.46 ± 0.11
Cisplatin[b]	5.5 ± 0.2	1.4 ± 0.5	25.6 ± 0.7	1.5 ± 0.4
Oxaliplatin[b]	1.3 ± 0.2	0.3 ± 0.2	23.4 ± 0.2	1.2 ± 0.3

[a] Results shown correspond to mean ± standard deviation of two experiments performed in triplicates. [b] Cisplatin and oxaliplatin are taken as reference compounds.

Remarkably, all compounds except **4a** and **4b** present significantly lower IC_{50} values than both reference compounds (cisplatin and oxaliplatin) in the breast cancer cell line MCF-7. Additionally, some platinum(IV) compounds display values in the nanomolar range, being compound **5a** the most effective against SW620 (0.41 μM), whereas compound **3a** presented the highest efficiency against the remaining cancer cell lines (PC-3, 0.9 μM; A549, 1.4 μM; MCF-7; 3.3 μM). The latter reaches for A549 a similar efficacy than oxaliplatin, and all platinum(IV) derivatives are slightly more potent than cisplatin in this cell line. On the other hand, platinum(II) compound **1a** has a similar effect in PC-3 than platinum(IV) derivatives.

The heterogeneity of these results, except for the less active compounds **4a** and **4b**, suggests the existence of more than one mechanism of action for the studied compounds. Platinum(IV) compounds **3a** and **5a** were selected as lead compounds as well as platinum(II) compound **1a**, which also presents a competitive efficiency.

For these compounds, their antiproliferative effect on normal human foreskin fibroblast cells (BJ) was also evaluated to test their selectivity at the range of concentrations where they completely stop the proliferation of all cancer cell lines. As it can be seen in

Figure 3.9, compound **3a** is highly selective for all cell lines at 5 μM concentration, as well as at 1 μM for PC-3 and SW620, a concentration where the proliferation of BJ was completely unaffected. On the other hand, compound **5a** presents selectivity for all cell lines at 5 μM without compromising the viability of the healthy cells at this higher concentration and also displays a high selectivity for SW620 at 1 mM concentration. Compound **1a** also presents similar selectivity with the advantage that it does not present any effect in BJ cells at none of the concentrations. This implies that though its IC_{50} values are indeed higher than those of platinum(IV) compounds, they could display a better toxicity profile with lower secondary effects.

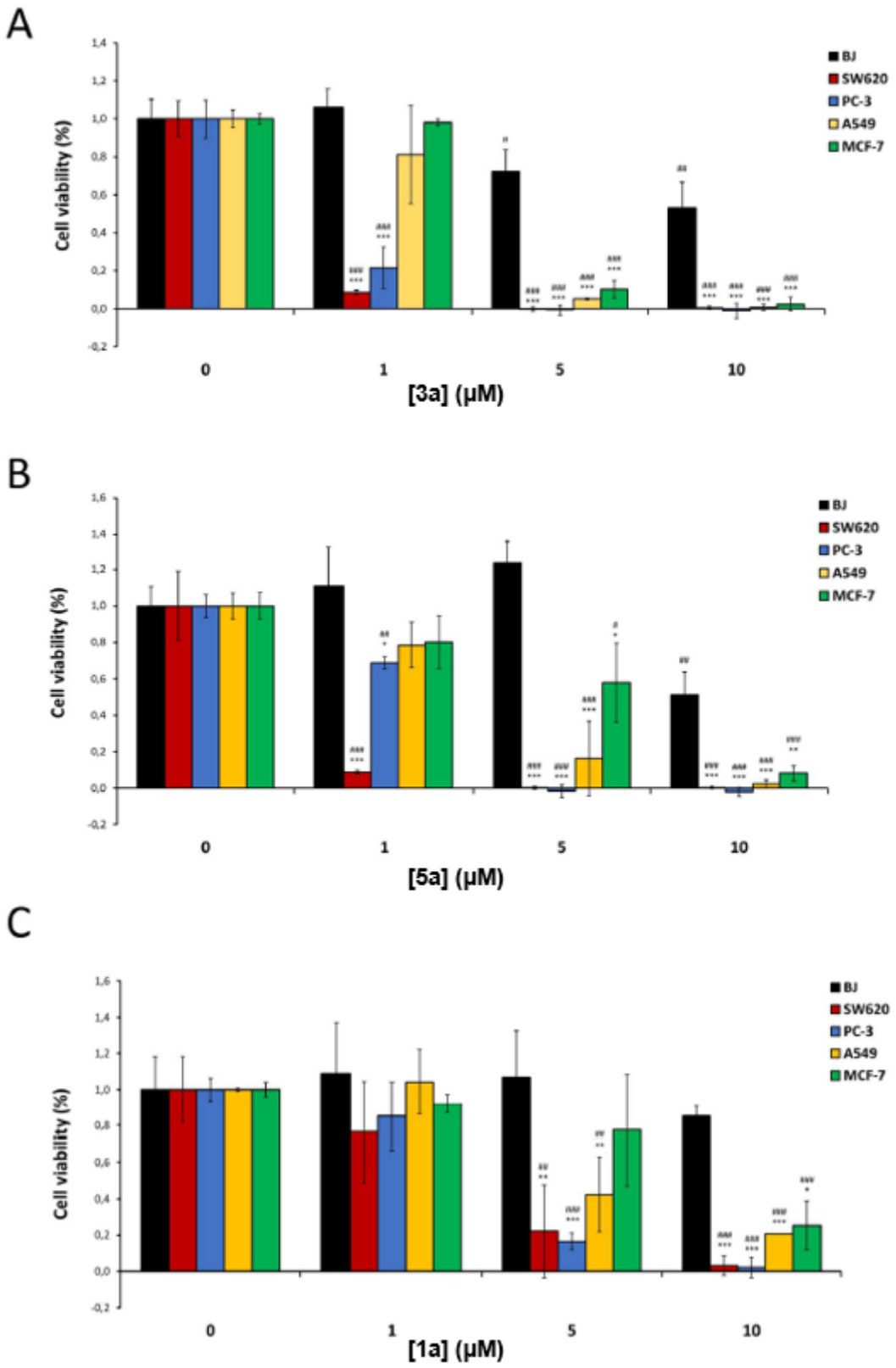

Figure 3.9. Normalized cell viability after 72 h incubation with 0, 1, 5 or 10 μM of compounds **3a** (A), **5a** (B) and **1a** (C) in BJ healthy foreskin fibroblasts, SW620 colorectal cancer, PC-3 metastatic prostate adenocarcinoma, A549 lung adenocarcinoma and MCF-7 breast cancer cells determined by MTT antiproliferative assay.

Afterwards, the effect of platinum(IV) compounds **3** and **5** against metastatic tumours that have acquired multiplatinum resistance (MPR) was evaluated by testing them for prostate PC-3-MPR and colorectal SW620-MPR and their age matched controls (PC-3-O and SW620-O). Surprisingly, all compounds present a complete absence of cross-resistance, as they exhibit similar antiproliferative effect in both metastatic resistant cell models, with resistance indexes (RI_{resist}) close to 1 (*Tables 3.4 and 3.5*).

Table 3.4. Antiproliferative activity (IC_{50}, μM) and resistance index (RI) of the studied compounds, cisplatin and oxaliplatin on the generated colorectal cancer (CRC) model of multiplatinum resistance (SW620-MPR) and its age-matched control (SW620-O).

Compound[a]	SW620-O	SW620-MPR	RI_{aging}	RI_{resist}	RI_{total}
1a	7 ± 3	7.1 ± 0.6	1.2	**1**	1.3
3a	2.2 ± 0.3	3 ± 2	2.4	**1.2**	2.8
3b	3.6 ± 1.2	4.8 ± 1.4	2	**1.3**	2.7
5a	1.1 ± 0.7	1.64 ± 0.01	2.8	**1.4**	4
5b	0.8 ± 0.4	1.4 ± 0.7	1.2	**1.7**	2
Cisplatin	1.1 ± 0.9	21 ± 4	0.8	**19**	15
Oxaliplatin	0.3 ± 0.2	3.2 ± 1.1	1	**10**	10

[a] Results shown correspond to mean ± standard deviation of two experiments performed in triplicates. [b] RI_{aging} corresponds to the ratio of IC_{50} between SW620-O (age-matched control) and SW620 (parental). [c] RI_{resist} corresponds to the ratio of IC_{50} between SW620-MPR (resistant) and SW620-O (age-matched control). [d] RI_{total} corresponds to the ratio of IC_{50} between SW620-MPR (resistant) and SW620 (parental).

Table 3.5 . Antiproliferative activity (IC_{50}, μM) and resistance index (RI) of the studied compounds, cisplatin and oxaliplatin on the generated colorectal cancer (CRC) model of multiplatinum resistance (PC-3-MPR) and its age-matched control (PC-3-O).

Compound[a]	PC-3-O	PC-3-MPR	RI_{aging}	RI_{resit}	RI_{total}
1a	0.67 ± 0.11	1.6 ± 0.2	0.6	**2.5**	1.5
3a	1.4 ± 0.8	1.5 ± 0.3	1.5	**1**	1.6
3b	5.3 ± 0.3	3.7 ± 1.3	3.7	**0.7**	2.5
5a	2 ± 2	2.9 ± 0.4	1.9	**1.3**	2.4
5b	4 ± 2	3.7 ± 0.4	2.4	**1**	2.5
Cisplatin	2.5 ± 0.9	23 ± 9	1.7	**9**	15
Oxaliplatin	0.69 ± 0.02	51 ± 12	0.6	**74**	42

[a] Results shown correspond to mean ± standard deviation of two experiments performed in triplicates. [b] RI_{aging} corresponds to the ratio of IC_{50} between PC-3-O (age-matched control) and PC-3 (parental). [c] RI_{resist} corresponds to the ratio of IC50 between PC-3-MPR (resistant) and PC-3-O (age-matched control). [d] RI_{total} corresponds to the ratio of IC_{50} between PC-3-MPR (resistant) and PC-3 (parental).

Although other examples of low cross-resistance have been reported in the literature, they are usually related to the presence of bioactive agents as axial ligands that upon their release can act in combination with the resulting platinum(II) compound.[7,9,32] In our case, having halogen groups in the axial positions, the absence of cross-resistance must arise from the platinacycle itself. This is confirmed by the similar RI_{resist} values observed for platinum(II) compound **1a** against these cell lines.

To further understand the mechanism of action of these compounds, compound **5a** and cisplatin as a reference were selected to study their effect in the cell cycle progression, apoptosis and intracellular ROS levels in both SW620-O and SW620-MPR (*Figure 3.10*).

The cell cycle is a series of tightly and sequential events that cells undergo before being divided by mitosis. It consists in a G0/G1 phase where a cell can be either quiescent (G0) or preparing for DNA replication (G1); the duplication of its genome (synthesis, S) and G2/Mitosis (M) where an exact copy of the cell is generated. In healthy cells, several checkpoints exist that allow them to avoid uncontrolled proliferation or proliferation of damaged cells. It is the malfunction of these checkpoints what is key to oncogenic proliferation and therefore, inhibiting this proliferation through cell cycle arrest is one approach for anticancer therapy.[33] Another appealing therapeutic window is to counteract

the anti-apoptotic oncogenic activation that allows cancer cells to avoid apoptotic stimuli by activating oncogenes that promote cell survival. Therefore, it is of interest to analyse the effect of our compounds in these phases to understand the origin of their cancer activity.

Additionally, the concentration of reactive oxygen species (ROS), which are oxidant by-products of cell metabolism (superoxide, O_2^-; hydrogen peroxide; H_2O_2; hydroxyl radical, ·OH and singlet oxygen, $^1O_2$), is usually low in healthy cells and contributes to the cell survival and proliferation. On the other hand, high ROS levels are attributed to stress and pathological conditions which produce damage to DNA leading to apoptosis. This is of interest as cancer cells can evade these apoptotic programs while maintaining a high ROS level, which is why the mechanism of action of cisplatin consists in further increase the ROS production to an extent where the cancer cells can no longer evade apoptosis.[34]

The effect in the cell cycle was completely different for both compounds. While cisplatin causes a significant G2/M arrest in SW620-O at its IC_{50} value, as previously observed, its effect in SW620-MPR is much lower.[35] On the other hand, compound **5a** induced an S arrest in SW620-O but had no interference in the cell cycle of SW620-MPR. This implies that, considering that its IC_{50} values are the same for both resistant and non-resistant cell lines, compound **5a** should perform through a different mechanism than conventional platinum drugs, for which SW620-MPR has not developed resistance.

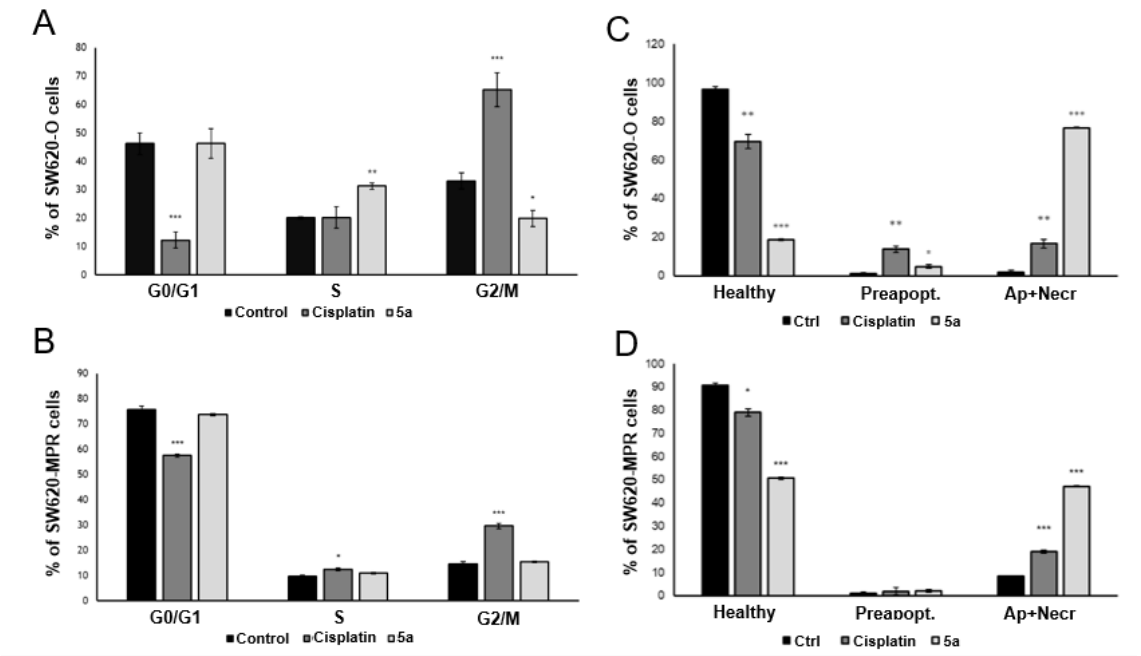

Figure 3.10. Cell cycle phase distribution at 72 h incubation with cisplatin or **5a** at their IC_{50} concentration in (A) SW620-O and (B) SW620-MPR. Percentage variations of alive, early apoptotic and late apoptotic/necrotic cell populations at 72 h incubation with cisplatin or **5a** at their IC_{50} concentrations in (C) SW620-O and (D) SW620-MPR cells.

In this regard, it was observed that while cisplatin causes a significant increase in ROS production in SW620-O with lesser effect in SW620-MPR, compound **5a** presented this effect in the multiplatinum resistant cell line but not in SW620-O.

Finally, compound **5a** was able to significantly induce apoptosis in both SW620-O and SW620-MPR cell lines while cisplatin had a more modest effect. These apoptosis levels do not correlate with the ROS accumulation in the cells treated with either cisplatin or compound **5a**.

Therefore, in general terms, the results indicate that although multiplatinum resistant cells have adapted to and minimised the effect of conventional platinum compounds that cause a cell cycle disruption, they are vulnerable to the induction of apoptosis caused by compound **5a**.

3.2.5. DNA migration assays

The ability of all compounds to modify the mobility of the supercoiled close (sc) and the open circular (oc) forms of pBluescript SK + plasmid DNA was tested in agarose gel by electrophoresis (*Figure 3.11*). It can be observed that platinum(II) compounds cause

significant changes in the mobility of plasmid DNA at concentrations as low as 10 µM for compounds **1** and an even lower concentration of 5 µM for compounds **4**. However, for platinum(IV) compounds, only **5b** presents some interaction with DNA at a high concentration of 100 µM, while the rest were not efficient at all at modifying its mobility. This lack of effect could be an indicator that these compounds are in fact acting as pro-drugs and are only activated upon reduction to platinum(II) in cellular media.

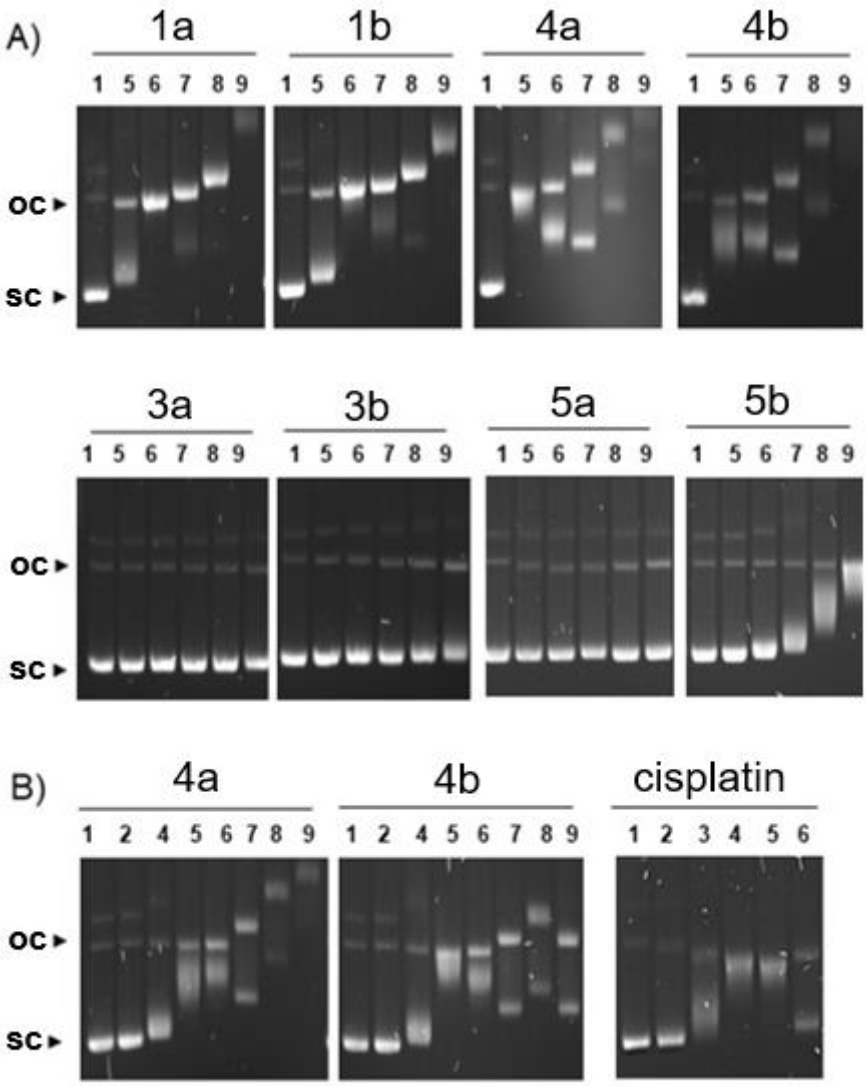

Figure 3.11. Interaction of pBluescript SK+ plasmid DNA (0.3 µg) with increasing concentrations of compounds under study. A) All compounds were analysed from 10 to 200 µM concentration Lane 1: DNA only. Lane 5: 10 µM. Lane 6: 25 µM. Lane 7: 50 µM. Lane 8: 100 µM. Lane 9: 200 µM. B) Compounds 4a and 4b were also analysed at lower concentrations and compared with cisplatin as a standard reference. Lane 1: 0 µM. Lane 2: 1 µM. Lane 3: 2.5 µM. Lane 4: 5 µM. Lane 5: 10 µM. Lane 6: 25 µM. Lane 7: 50 µM. Lane 8: 100 µM. Lane 9: 200 µM; sc = supercoiled closed circular DNA; oc = open circular DNA.

3.2.6. NMR stability studies

The stability of platinum(IV) compound **3a** in the aqueous biological media was assessed by performing ^{1}H-NMR spectra at time periods up to one week. A solution of compound **3a** at a 1 mM concentration was prepared in a 50 mM phosphate buffer in D_2O (pD = 7.40) and two drops of d^6-DMSO to allow solubilisation of the compound.

The most informative resonances of the resulting spectra are those in the imine region, as previously reported for previous stability studies performed by ^{1}H-NMR in similar compounds.[16,17] As depicted in *Figure 3.12*, a major product which gives a singlet in this region (δ = 8.44 ppm) remains stable up to one week is observed. No coupling with platinum is observed for these nor for the other minor compounds, which suggest the formation of a mixture of solvato complexes where the solvents used (D_2O or d^6-DMSO) might have replaced the more labile N-donor or chlorido ligands. This agrees with the aquation of equatorial ligands recently observed in the literature.[36]

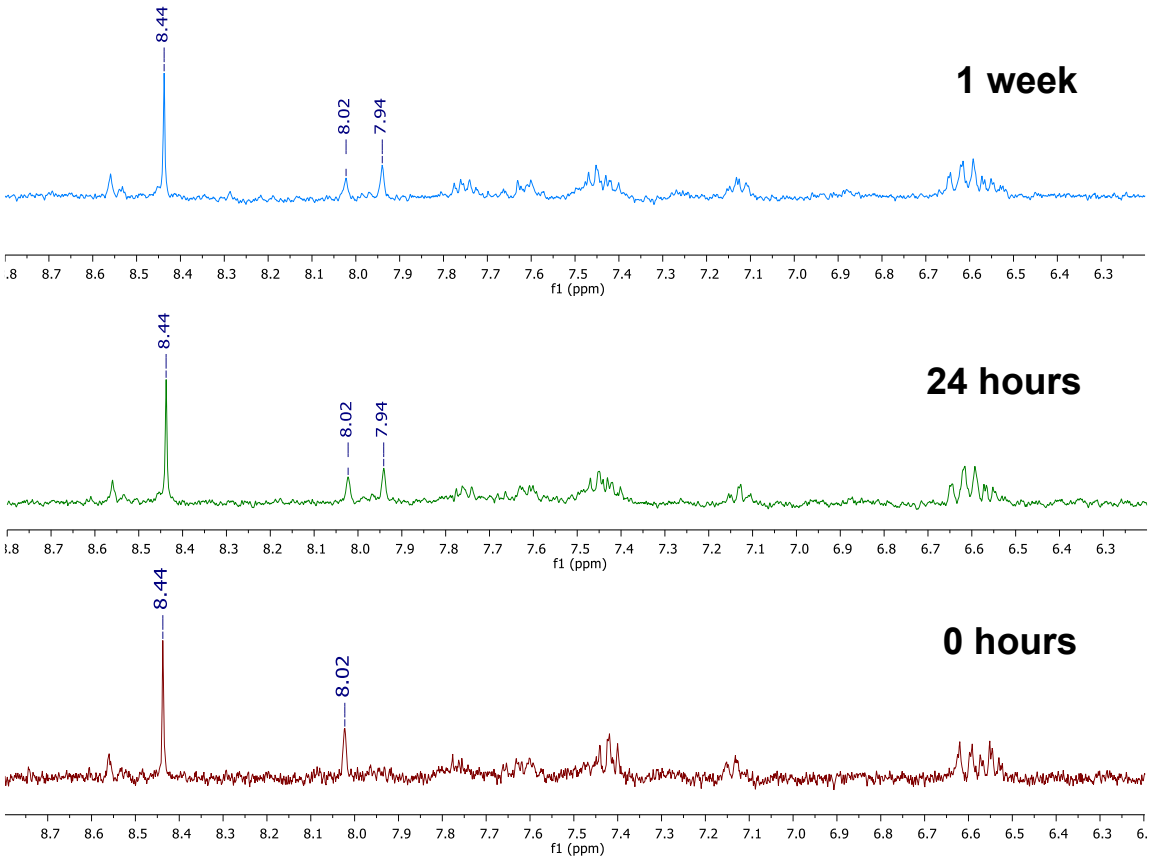

Figure 3.12. Partial view of the ^{1}H NMR spectrum of a solution of compound **3a** (1 mM) in 50 mM phosphate buffer (in D_2O, pH 7.40) and -DMSO-d^6, freshly prepared, after 24 h and 1 week of storage at 298 K.

To investigate our hypothesis that these platinum(IV) compounds can be rapidly reduced under biological conditions by reducing agents present in cell media, the reactions of compound **3a** with glutathione, ascorbic acid and cysteine were monitored by ^{1}H NMR spectroscopy under analogous conditions. A mixture containing 1 mM concentration of compound **3a** and 25 mM of the corresponding reductant were prepared in a 50 mM phosphate buffer (D_2O, pD = 7.40) and two drops of DMSO-d^{6} and were measured at several time periods up to one week. As previously mentioned, the imine region was analysed as it easily provides information, and it avoids the interference of the signals corresponding to the reductants.

The aromatic and imine region of the ^{1}H NMR corresponding to reaction with cysteine is shown in *Figure 3.13*, as it was the most conclusive. This is in agreement with recent studies that suggest that cysteine is the most effective in the reduction of platinum(IV) anticancer prodrugs under physiological conditions and that its reactivity is highly dependent on pH.[37,38]

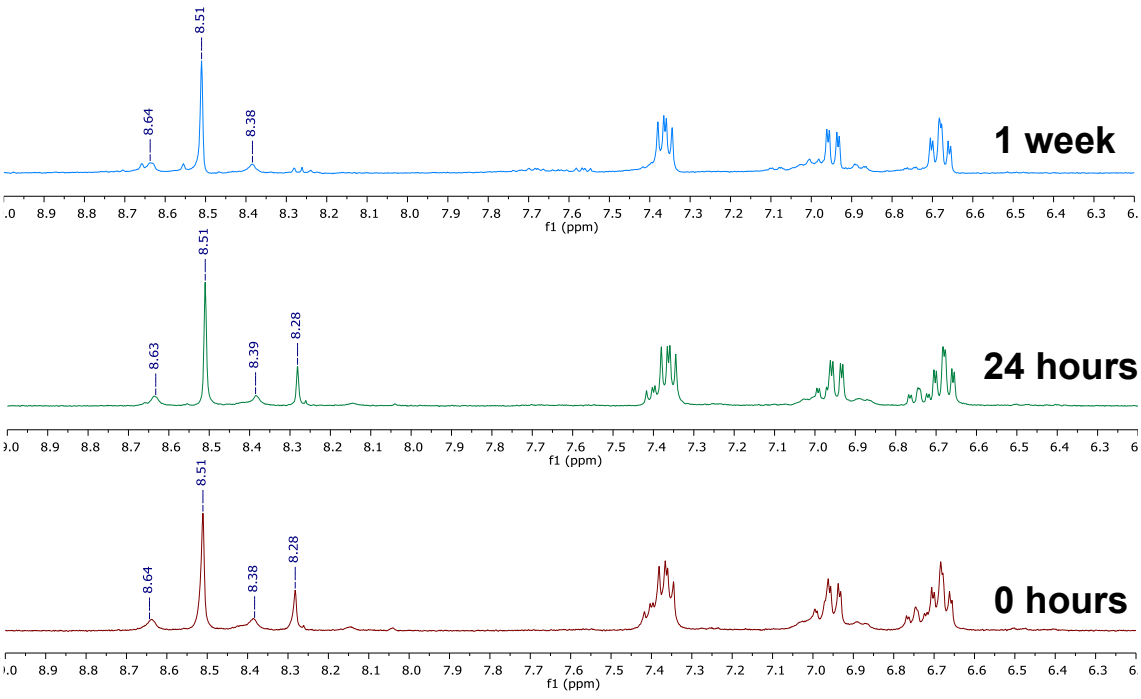

Figure 3.13. Partial view of ^{1}H NMR spectrum of a solution of compound **3a** (1 mM) in 50 mM phosphate buffer (in D_2O, pH 7.40) and d6-DMSO containing 25 mM L-cysteine, freshly prepared, and after 24 h and 1 week of storage at 298 K.

This reaction produces from the early stages a compound that is stable in solution up to one week and its signal at δ = 8.51 ppm with a coupling constant ^{3}J(H-Pt) = 100 Hz can

be assigned to platinum(II) compound **1a-cys**. The coupling constant value confirms the substitution of the chlorido ligand by cysteine, as it depends not only on the oxidation state of platinum, with higher values for platinum(II) compounds, but also on the *trans* influence of the ancillary ligand in equatorial position. Therefore, it presents a lower value than the chlorido derivative **1a** (^{3}J(Pt-H)= 141 Hz), in agreement with its higher *trans* influence.[39]

Additionally, the proposed mechanism depicted in *Scheme 3.6* matches kinetic studies reported in the literature for analogous compounds, where it was found that the reaction of this kind of cyclometallated platinum(IV) compounds consists in two consecutive steps. First, cysteine reduces the compound to platinum(II) (step 1, *Scheme 3.6*) which is followed by the substitution of the remaining chlorido ligand for a cysteine deprotonated moiety (step 2, *Scheme 3.6*).[40]

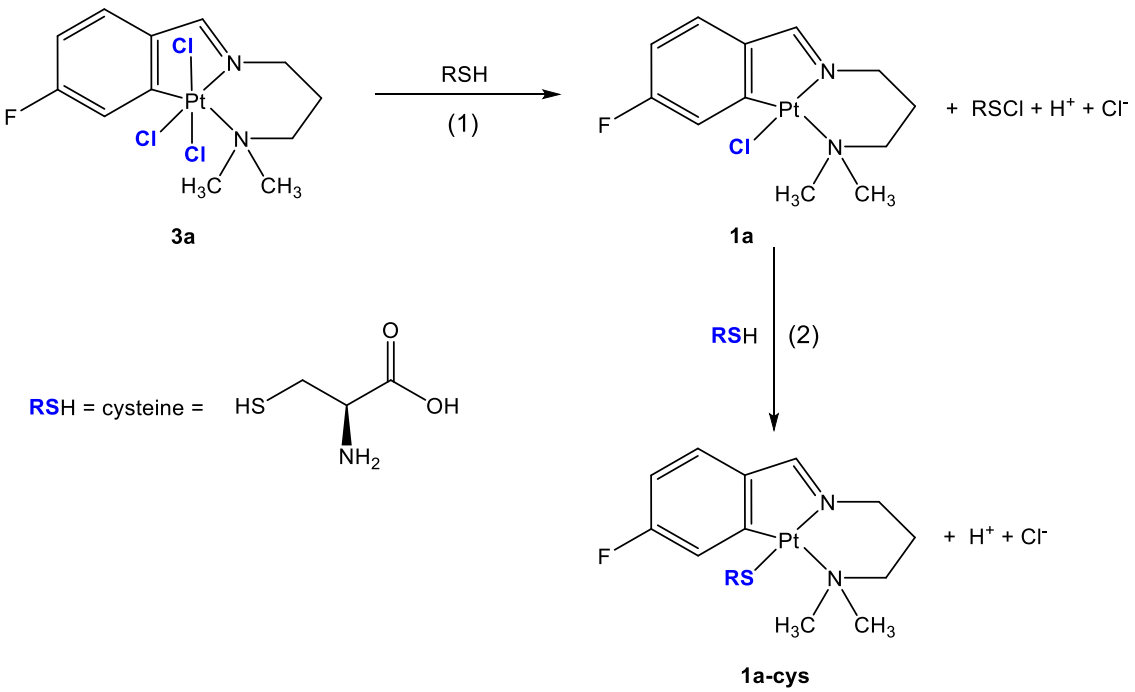

Scheme 3.6. Proposed mechanism for the reaction of compound **3a** with cysteine in aqueous biological medium.

3.3. Conclusions

The anticancer and photophysical properties of a new family of [C,N,N'] cyclometallated platinum(II) and platinum(IV) with differences in the nature of the ancillary ligand and the length of the aliphatic chain have been analysed. Their luminescent properties were slightly enhanced regarding their analogues with a propylene chain depicted in *Chapter 2*, thanks to the increase in rigidity that the shorter ethylene chain provides. This favours the radiative pathways and a subsequent increase in their luminescence quantum yields, which still present moderate values.

The antiproliferative studies for all compounds including their analogues from *Chapter 2* revealed that they present high efficacy and selectivity against a broad cancer cells panel. Specifically, platinum(IV) compounds display an enhanced effect and a complete absence of cross-resistance in multiplatinum resistant cell models. This property has been found to be intrinsic of the platinacycle and cell phase distribution and apoptosis studies have proved that they undergo a different mechanism than conventional platinum compounds.

In addition, DNA interaction and NMR studies have proved the ability of platinum(IV) compounds to be reduced under cellular media, and that this appears to be a key point in their antiproliferative activity. As a whole, these compounds offer a high potential to be developed as pro-drugs in cancer chemotherapies as second-line treatments for platinum-resistant tumours.

3.4. Experimental Section

3.4.1. General procedures

Commercial reagents 4-fluorobenzaldehyde (Sigma Aldrich, 98%), 2-dimethylamino-1-ethanamine (Sigma Aldrich, 95%), sodium sulphate (Na_2SO_4, Panreac, 99%), sodium acetate (CH_3COONa, Carlo Erba, 99%), potassium bromide (KBr, Probus, 98%), bromine (Br_2, Sigma Aldrich, >99%) and iodine (I_2, Panreac, >99%); and solvents methanol (Sigma Aldrich, >99%), dichloromethane (CH_2Cl_2, Scharlau, 99%), acetone (Carlo Erba, >99%) and hexane (Sigma Aldrich, >98%) were used as received.

Complexes cis-$[PtCl_2(DMSO)_2]$[41] and iodobenzene dichloride ($PhICl_2$)[42] were prepared as reported in the literature.

3.4.2. Physical measurements

NMR spectra were recorded in $CDCl_3$ at the *Unitat de RMN* of the *Universitat de Barcelona* with a Mercury 400 spectrometer (^1H, 400 MHz; ^{19}F, 376.5 MHz). Chemical shifts are given in δ values (ppm) relative to TMS (^1H) or $CFCl_3$ (^{19}F) and coupling constants J are given in Hz.

Electrospray mass spectra were performed at the *Unitat d'Espectrometria de Masses (Universitat de Barcelona)* in a LC/MSD-TOF spectrometer using H_2O-CH_3CN 1:1 to introduce the sample.

Microanalyses were performed at the *Centres Científics i Tecnològics (Universitat de Barcelona)* using a Carlo Erba model EA1108 elemental analyser.

UV/Vis spectra were recorded with a Cary 100 scan 388 Varian UV spectrometer. Emission and excitation spectra were recorded in a Horiba Jobin-Yvon SPEX Nanolog-TM spectrofluorimeter at 298 K using $5 \cdot 10^{-5}$ M dichloromethane solutions.

Total luminescence quantum yields were measured at 298K relative to $[Ru(bipy)_3]Cl_2$ in water ($\phi = 0.042$) and naphthalene in cyclohexane ($\phi = 0.23$) as standard references.

3.4.3. Synthesis and characterisation

Synthesis of 4-$FC_6H_4CH=N(CH_2)_2N(CH_3)_2$ (L2)

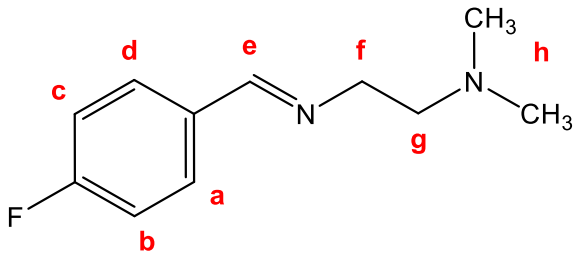

Ligand $4\text{-}FC_6H_4CH=N(CH_2)_2N(CH_3)_2$ (**L2**)[22] was obtained by following the method described in the literature from the reaction of 0.782 g (6.301 mmols) of 4-fluorobenzaldehyde and 0.626 g (7.102 mmols) of 2-dimethylamino-1-ethanamine in 20 ml of toluene. The mixture was stirred at room temperature for 2 hours and water was eliminated by adding sodium sulphate and filtering it off. The solvent was removed under vacuum to give a yellow oil. Yield: 1.044 g (85%).

^{1}H NMR ($CDCl_3$, 400 MHz): δ 8.26 [s, 1H, H^e]; 7.70 [dd, 2H, ^3J(H-H) = 8.8, ^4J(F-H) = 5.6, $H^{a,d}$]; 7.07 [t, 2H, ^3J(F-H) = ^3J(H-H) = 8.8, $H^{b,c}$]; 3.71 [t, 2H, ^3J(H-H) = 6.8, H^f]; 2.62 [t, 2H, ^3J(H-H) = 6.8, H^g]; 2.29 [s, 6H, H^h]. **^{19}F NMR** ($CDCl_3$, 376.5 MHz): δ -109.90 [m, 1F].

Synthesis of $[PtCl\{(CH_3)_2N(CH_2)_2N=CH(4\text{-}FC_6H_3)\}]$ (4a)

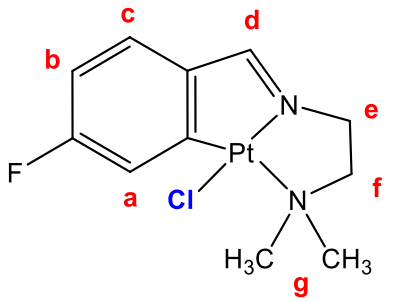

Compound $[PtCl\{(CH_3)_2N(CH_2)_2N=CH(4\text{-}FC_6H_3)\}]$ (**4a**)[22] was obtained by slight modification of the method described in the literature from the reaction of 0.402 g (0.951 mmols) of cis-$[PtCl_2(DMSO)_2]$, 0.222 g (1.067 mmols) of $4\text{-}FC_6H_4CH=N(CH_2)_2N(CH_3)_2$ (**L2**) and 0.079 g (0.975 mmols) of anhydrous sodium acetate in 50 ml of dry methanol. The mixture was refluxed at 65 ^oC for 96 hours and the solvent was removed under vacuum. The residue was extracted with 10 ml of CH_2Cl_2 and 10 ml of methanol were

added. Half of the volume was removed under vacuum and the solution was left to crystallise in the freezer. The orange solid was filtered and dried under vacuum. Yield: 0.174 g (42%).

^{1}H NMR ($CDCl_3$, 400 MHz): δ 8.26 [s, 1H, ^{3}J(Pt-H) = 141.2, H^{d}]; 7.41 [dd, 1H, ^{3}J(F-H) = 9.5, ^{4}J(H-H) = 2.8, ^{3}J(Pt-H) = 50.8, H^{a}]; 7.24 [dd, 1H, ^{3}J(H-H) = 8.0, ^{4}J(F-H) = 5.6, H^{c}]; 6.69 [td, 1H, ^{3}J(F-H) = ^{3}J(H-H) = 8.8, ^{4}J(H-H) = 2.8, H^{b}]; 4.06 [t, 2H, ^{3}J(H-H) = 6.0, H^{e}]; 3.11 [t, 2H, ^{3}J(H-H) = 6.0, H^{f}]; 2.90 [s, 6H, H^{g}]. **^{19}F NMR** ($CDCl_3$, 376.5 MHz): δ -102.92 [m, 1F]. **MS-ESI^{+}**: *m/z* 442.08 $[M+NH_4]^{+}$. **Anal. Found** (calcd for $C_{11}H_{14}ClFN_2Pt$): C, 30.70 (31.20); H, 3.40 (3.33); N, 6.70 (6.62).

Synthesis of [PtBr{$(CH_3)_2N(CH_2)_2N$=CH(4-FC_6H_3)}] (4b)

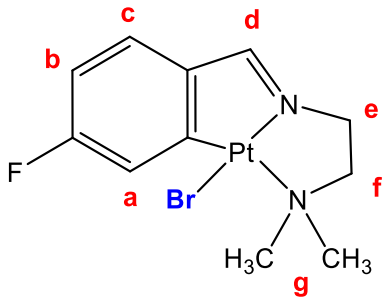

Compound [PtBr{$(CH_3)_2N(CH_2)_3$N=CH(4-FC_6H_3)}] (**4b**) was obtained from the reaction of 0.260 g (0.614 mmols) of [PtCl{$(CH_3)_2N(CH_2)_2$N=CH(4-FC_6H_3)}] (**4a**) and 0.309 g (2.597 mmols) of KBr in 25 ml of dry methanol. The mixture was refluxed at 65 ºC for 48 hours and the solvent was removed under vacuum. The residue was extracted with 10 ml of CH_2Cl_2 and 10 ml of methanol were added. Half of the volume was removed under vacuum and the solution was left to crystallise in the freezer. The orange solid was filtered and dried under vacuum. Yield: 0.131 g (46%).

^{1}H NMR ($CDCl_3$, 400 MHz): δ 8.28 [s, 1H, ^{3}J(Pt-H) = 143.4, H^{d}]; 7.60 [dd, 1H, ^{3}J(F-H) = 9.6, ^{4}J(H-H) = 2.6, ^{3}J(Pt-H) = 50.8, H^{a}], 7.24-7.28 [m, 1H, H^{c}], 6.67 [td, 1H, ^{3}J(F-H) = ^{3}J(H-H) = 8.6, ^{4}J(H-H) = 2.5, H^{b}], 4.06 [t, 2H, ^{3}J(H-H) = 5.8, H^{e}], 3.10 [t, 2H, ^{3}J(H-H) = 6.1, H^{f}], 2.93 [s, 6H, ^{3}J(Pt-H) = 14.7, H^{g}]. **^{19}F NMR** ($CDCl_3$, 376.5 MHz): δ -102.8 [m, 1F]. **MS-ESI^{+}**: *m/z* 469.00 $[M + H]^{+}$.

Synthesis of [$PtCl_3${$(CH_3)_2N(CH_2)_2N=CH(4\text{-}FC_6H_3)$}] (5a)

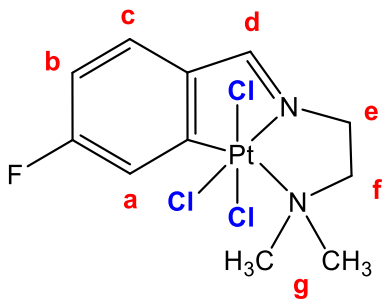

Compound [$PtCl_3${$(CH_3)_2N(CH_2)_3N=CH(4\text{-}FC_6H_3)$}] (**5a**) was obtained from the reaction of 0.051 g (0.120 mmols) of [$PtCl${$(CH_3)_2N(CH_2)_2N=CH(4\text{-}FC_6H_3)$}] (**4a**) and 0.034 g (0.124 mmols) of iodobenzene dichloride ($PhICl_2$) in 7 ml of acetone. The mixture was stirred at room temperature for 10 minutes and the solvent was removed under vacuum. The residue was treated with hexane and the yellow solid was filtered and dried under vacuum. Yield: 0.050 g (84%).

^{1}H NMR ($CDCl_3$, 400 MHz): δ 8.16 [s, 1H, ^{3}J(Pt-H) = 89.4, H^d]; 7.53 [m, 2H, $H^{a,c}$], 6.94 [td, 1H, ^{3}J(F-H) = ^{3}J(H-H) = 8.5, ^{4}J(H-H) = 2.5, H^b], 4.17 [t, 2H, ^{3}J(H-H) = 5.8H^e], 3.38 [t, 2H, ^{3}J(H-H) = 5.7, H^f], 3.06 [s, 6H, ^{3}J(Pt-H) = 10.1, H^g]. **^{19}F NMR** ($CDCl_3$, 376.5 MHz): δ -94.8 [m, 1F]. **MS-ESI$^+$**: *m/z* 494.99 $[M + H]^+$. **Anal. Found** (calcd $C_{11}H_{14}Cl_3FN_2Pt{\cdot}H_2O$): C, 25.62 (25.75); H, 3.00 (3.15); N, 5.52 (5.46).

Synthesis of [$PtBr_3${$(CH_3)_2N(CH_2)_2N=CH(4\text{-}FC_6H_3)$}] (5b)

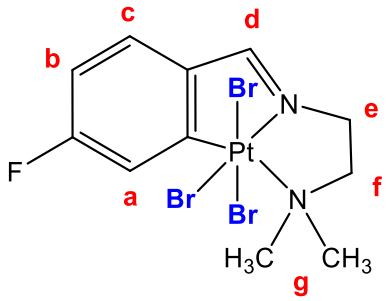

Compound [$PtBr_3${$(CH_3)_2N(CH_2)_2N=CH(4\text{-}FC_6H_3)$}] (**5b**) was prepared as a brown solid by following the same method from 0.050 g (0.107 mmols) of [$PtBr${$(CH_3)_2N(CH_2)_2N=CH(4\text{-}FC_6H_3)$}] (**4b**) and 0.103 g (0.642 mmols) of Br_2. Yield: 0.054 g (81%).

^{1}H NMR ($CDCl_3$, 400 MHz): δ 8.05 [s, 1H, ^{3}J(Pt-H) = 90.4, H^d]; 7.62 [dd, 1H, ^{3}J(F-H) = 8.5, ^{4}J(H-H) = 2.4, ^{3}J(Pt-H) = 27.5, H^a], 7.50 [dd, 1H, ^{3}J(H-H) = 8.4, ^{4}J(F-H) = 5.4, H^c],

6.84 [td, 1H, ^{3}J(F-H) = ^{3}J(H-H) = 8.5, ^{4}J(H-H) = 2.4, H^{b}], 4.18 [t, 2H, ^{3}J(H-H) = 5.6, H^{e}], 3.45 [t, 2H, ^{3}J(H-H) = 5.5, H^{f}], 3.21 [s, 6H, ^{3}J(Pt-H) = 12.0, H^{g}]. **^{19}F NMR** ($CDCl_3$, 376.5 MHz): δ -95.2 [m, 1F]. **MS-ESI^{+}**: *m/z* 628.83 $[M + H]^{+}$. **Anal. Found** (calcd for $C_{11}H_{14}Br_3FN_2Pt \cdot H_2O$): C, 20.16 (20.44); H, 2.23 (2.50); N, 4.03 (4.34).

3.4.4. X-ray Diffraction

Suitable crystals of compounds **4a**, **4b**, **5a** and **5b** were grown at room temperature in dichloromethane-methanol (**4a**, **5a** and **5b**) or dichloromethane-hexane (**4b**). X-ray diffraction data were collected on a D8 VENTURE system equipped with a multilayer monochromator and a Mo high brilliance Incoatec Microfocus Source (λ = 0.71073 Å) at 293 K (**4a**) or on a Bruker-Nonius KappaCCD system with an APEX-II CCD detector with graphite-monochromatised Mo-Kα (λ = 0.71073 Å) radiation. The structures were solved and refined using the Bruker SHELXTL Software package.[43] Crystallographic details are given in Tables A3-A4.

3.4.5. Biological assays

Cell culture and viability assays

Human lung adenocarcinoma A-549 cells and lymph node metastasis of colorectal SW620 cells were grown in minimum essential medium (DMEM (Dulbecco's Modified Eagle Medium). Human breast adenocarcinoma MCF-7 cells were cultured in DMEM without phenol red, containing 1 mM sodium pyruvate, 0.01 $mg \cdot ml^{-1}$ insulin, and 1% non-essential amino acids. Bone metastasis of CRPC PC-3 cells were cultured in RPMI-1640. 10% Foetal Bovine Serum (FBS) and 0.1% streptomycin/penicillin were added to all culture media, and cells were cultured in standard culture conditions (humidified air with 5% CO_2 at 37°C). Cell viability assays were performed by a variation of the MTT (3-(4,5-dimethylthiazol-2-yl)-2,5-diphenyltetrazolium bromide) assay described previously.[44] Relative cell viability, compared to the viability of untreated cells, was measured by absorbance at 550 nm on an ELISA plate reader (Tecan Sunrise MR20-301, TECAN, Salzburg, Austria). Concentrations that inhibited cell growth by 50% (IC_{50}) after 72 h of treatment were subsequently calculated by sigmoidal fitting with GraphPad Prism 6 software.

Generation of multiplatinum-resistant cell models and age-matched controls

PC-3 and SW620 cells were cultured for about eight months either with or without incremental doses of cisplatin, obtaining cell models that are resistant to cisplatin and cross-resistant to oxaliplatin, thus termed multiplatinum-resistant (PC-3-MPR or SW620-MPR), and their age-matched/old controls (PC-3-O or SW620-O). Cell viability and IC_{50} progression for the four cell lines were regularly monitored until passage 43-45, in which cells were frozen and preserved in liquid nitrogen. Upon use, cells were defrozen and used through passages 45 to 60, routine culturing MPR cell lines under the presence of 5.5 μM cisplatin (SW620-MPR) and 1 μM cisplatin (PC-3-MPR).

Flow cytometry-based cell cycle, apoptosis and ROS analyses

Cells in triplicates for each condition were seeded in 6-well plates. After 24 h, cell culture medium was removed and fresh medium with each compound at the previously determined IC_{50} for each cell line (*Table 3.3*) was added to the plates, and cells were incubated for 72 h. For cell cycle, cells were trypsinized mildly, collected, fixed in 70% ethanol and stored at −20°C until measure. Right before measuring, fixed cells were incubated for 1 h with PBS containing 50 $mg \cdot ml^{-1}$ propidium iodide (PI) and 10 $mg \cdot ml^{-1}$ DNase-free RNase. For apoptosis, trypsinized and collected cells were double stained with PI and annexin-V in binding buffer (10 mM HEPES/NaOH, pH 7.40, 140 mM NaCl, 2.5 mM $CaCl_2$) and incubated in darkness for 30 min at room temperature. For ROS analysis, attached cells after 72 h with each condition were incubated with 5 μM 2',7'-dichlorofluorescein diacetate (DCFH-DA, Invitrogen) in PBS supplemented with 10 mM glucose and 2 mM glutamine for 30 min at 37°C, and further incubated for another 30 min with full culture medium. Finally, cells were trypsinised and resuspended thoroughly in 0.4 mL of PBS containing DCFH-DA (50 μM) and PI (20 $\mu g \cdot ml^{-1}$). For all three assays, fluorescence data of 10^4 cells was collected on a CyAn flow cytometer (Beckman Coulter) and analysed using FlowJo v10 software.

Data analysis

For each compound, a minimum of three independent experiments with triplicate values were conducted to measure cell viability. A minimum of two independent experiments in triplicates were performed for cell cycle analysis and assessment of apoptosis. Significant differences compared to control were assessed by Student's t-test where $p < 0.05$(#), $p <$

0.01(##) or $p < 0.001$(###) were taken into consideration. Data are given as the mean ± standard deviation (SD).

DNA migration assays

DNA migration studies were performed as described before.[17] Compounds under study were prepared in high purity DMSO at 10 mM concentration and then serial dilutions with MilliQ water (1:1) were made. pBluescript SK+ plasmid DNA-drug interaction was analysed by agarose gel electrophoresis. Plasmid DNA aliquots (0.3 μg) were incubated in TE buffer (10 mM Tris-HCl, 1 mM EDTA, pH 7.5) with different concentrations of compounds under study ranging from 0 μM to 200 μM at 37 ºC for 24 h. Cisplatin was used as a reference control. Samples were then subjected to 1% agarose gel electrophoresis in TAE buffer, stained in TAE buffer containing ethidium bromide (0.5 mg ml^{-1}) and visualized and photographed under UV light. All compounds under study were firstly analysed between 10 and 200 μM concentration. Compounds **4a** and **4b** which show the higher retardation at 10 μM concentration were also analysed at lower concentration and interaction with DNA was also observed at 5 μM.

3.5. References

1. Kenny, R.G.; Chuah, S.W.; Crawford, A.; Marmion, C.J. *Eur. J. Inorg. Chem.* **2017**, 1596–1612.
2. Gibson, D. *J. Inorg. Biochem.* **2019**, *191*, 77–84.
3. Johnstone, T.C.; Wilson, J.J.; Lippard, S.J. *Inorg. Chem.* **2013**, *52*, 12234–12249.
4. Wang, Z.; Deng, Z.; Zhu, G. *Dalton Trans.* **2019**, *48*, 2536–2544.
5. Johnstone, T.C.; Suntharalingam, K.; Lippard, S.J. *Chem. Rev.* **2016**, *116*, 3436–3486.
6. Gibson, D. *Dalton Trans.* **2016**, *45*, 12983–12991.
7. Petruzzella, E.; Sirota, R.; Solazzo, I.; Gandin, V.; Gibson, D. *Chem. Sci.* **2018**, *9*, 4299–4307.
8. Kenny, R.G.; Marmion, C.J. *Chem. Rev.* **2019**, *119*, 1058–1137.
9. Kostrhunova, H.; Petruzzella, E.; Gibson, D.; Kasparkova, J.; Brabec, V. *Chem. Eur. J.* **2019**, *25*, 5235–5245.
10. Hall, M.D.; Hambley, T.W. *Coord. Chem. Rev.* **2002**, *232*, 49–67.
11. Hall, M.D.; Mellor, H.R.; Callaghan, R.; Hambley, T.W. *J. Med. Chem.* **2007**, *50*, 3403–3411.
12. Guo, S.X.; Mason, D.N.; Turland, S.A.; Lawrenz, E.T.; Kelly, L.C.; Fallon, G.D.; Gatehouse, B.M.; Bond, A.M.; Deacon, G.B.; Battle, A.R.; Hambley, T.W.; Rainone, S.; Webster, L.K.; Culliane, C. *J. Inorg. Biochem.* **2012**, *115*, 226–239.
13. Ellis, L.T.; Er, H.M.; Hambley, T.W. *Aust. J. Chem* **1995**, *48*, 793–806.
14. Choi, S.; Filotto, C.; Bisanzo, M.; Delaney, S.; Lagasee, D.; Whitworth, J.L.; Jusko, A.; Li, C.; Wood, N.A.; Willingham, J.; Schwenker, A.; Spaulding, K. *Inorg. Chem.* **1998**, *37*, 2500–2504.
15. Crespo, M. *J. Organomet. Chem.* **2019**, *879*, 15–26.
16. Bauer, E.; Domingo, X.; Balcells, C.; Polat, I.H.; Crespo, M.; Quirante, J.; Badía, J.; Baldomà, L.; Font-Bardia, M.; Cascante, M. *Dalton Trans.* **2017**, *46*, 14973–

14987.

17. Solé, M.; Balcells, C.; Crespo, M.; Quirante, J.; Badia, J.; Baldomà, L.; Font-Bardia, M.; Cascante, M. *Dalton Trans.* **2018**, *47*, 8956–8971.

18. Zhang, Y.; Luo, Q.; Zheng, W.; Wang, Z.; Lin, Y.; Zhang, E.; Lü, S.; Xiang, J.; Zhao, Y.; Wang, F. *Inorg. Chem. Front.* **2018**, *5*, 413–424.

19. Zou, T.; Liu, J.; Lum, C.T.; Ma, C.; Chan, R.C.T.; Lok, C.-N.; Kwok, W.M.; Che, C.M. *Angew. Chem.* **2014**, *126*, 10283–10287.

20. Berenguer, J.R.; Pichel, J.G.; Giménez, N.; Lalinde, E.; Moreno, M.T.; Piñeiro-Hermida, S. *Dalton Trans.* **2015**, *44*, 18839–18855.

21. Mauro, M.; Aliprandi, A.; Septiadi, D.; Kehr, N.S.; De Cola, L. *Chem. Soc. Rev.* **2014**, *43*, 4144–4166.

22. Gandioso, A.; Valle-Sistac, J.; Rodríguez, L.; Crespo, M.; Font-Bardía, M. *Organometallics* **2014**, *33*, 561–570.

23. Capapé, A.; Crespo, M.; Granell, J.; Font-Bardía, M.; Solans, X. *J. Organomet. Chem.* **2005**, *690*, 4309–4318.

24. Crespo, M.; Font-Bardia, M.; Granell, J.; Martínez, M.; Solans, X. *Dalton Trans.* **2003**, *3*, 3763–3769.

25. Escolà, A.; Crespo, M.; Quirante, J.; Cortés, R.; Jayaraman, A.; Badía, J.; Baldomà, L.; Calvet, T.; Font-Bardía, M.; Cascante, M. *Organometallics* **2014**, *33*, 1740–1750.

26. Lázaro, A.; Serra, O.; Rodríguez, L.; Crespo, M.; Font-Bardia, M. *New J. Chem.* **2019**, *43*, 1247–1256.

27. Millán, G.; Giménez, N.; Lara, R.; Berenguer, J.R.; Moreno, M.T.; Lalinde, E.; Alfaro-Arnedo, E.; López, I.P.; Pineiro-Hermida, S.; Pichel, J.G. *Inorg. Chem.* **2019**, *58*, 1657–1673.

28. Song, C.; Tang, J.; Li, J.; Wang, Z.; Li, P.; Zhang, H. *Inorg. Chem.* **2018**, *57*, 12174–12186.

29. Li, K.; Wan, Q.; Yang, C.; Chang, X.Y.; Low, K.H.; Che, C.M. *Angew. Chem.*

2018, *57*, 14129–14133.

30. Puttock, E. V.; Walden, M.T.; Williams, J.A.G. *Coord. Chem. Rev.* **2018**, *367*, 127–162.

31. Escolà, A.; Crespo, M.; López, C.; Quirante, J.; Jayaraman, A.; Polat, I.H.; Badía, J.; Baldomà, L.; Cascante, M. *Bioorg. Med. Chem.* **2016**, *24*, 5804–5815.

32. Petruzzella, E.; Braude, J.P.; Aldrich-Wright, J.R.; Gandin, V.; Gibson, D. *Angew. Chem.* **2017**, *56*, 11539–11544.

33. Diaz-Moralli, S.; Tarrado-Castellarnau, M.; Miranda, A.; Cascante, M. *Pharmacol. Ther.* **2013**, *138*, 255–271.

34. Dasari, S.; Bernard Tchounwou, P. *Eur. J. Pharmacol.* **2014**, *740*, 364–378.

35. Sarin, N.; Engel, F.; Kalayda, G. V.; Mannewitz, M.; Cinatl, J.; Rothweiler, F.; Michaelis, M.; Saafan, H.; Ritter, C.A.; Jaehde, U.; Frötschl, R. *PLoS One* **2017**, *12*, e0181081.

36. Kastner, A.; Poetsch, I.; Mayr, J.; Burda, J. V.; Roller, A.; Heffeter, P.; Keppler, B.K.; Kowol, C.R. *Angew. Chem.* **2019**, *131*, 7542–7547.

37. Dong, J.; Huo, S.; Shen, S.; Xu, J.; Shi, T.; Elding, L.I. *Bioorg. Med. Chem. Lett.* **2016**, *26*, 4261–4266.

38. Chipman, A.; Yates, B.F.; Canty, A.J.; Ariafard, A. *Chem. Commun.* **2018**, *54*, 10491–10494.

39. Bernhardt, P. V.; Calvet, T.; Crespo, M.; Font-Bardía, M.; Jansat, S.; Martínez, M. *Inorg. Chem.* **2013**, *52*, 474–484.

40. Crespo, M.; Font-Bardia, M.; Hamidizadeh, P.; Martínez, M.; Nabavizadeh, S.M. *Inorg. Chim. Acta* **2019**, *486*, 8–16.

41. Al-Allaf, T.A.K.; Rashan, L.J.; Abu-Surrah, A.S.; Fawzi, R.; Steimann, M. *Transit. Met. Chem.* **1998**, *23*, 403–406.

42. Zhao, X.F.; Zhang, C. *Synthesis* **2007**, 551–557.

43. Sheldrick, G.M. *Acta Crystallogr. C Struct. Chem.* **2015**, *71*, 3–8.

44. Matito, C.; Mastorakou, F.; Centelles, J.J.; Torres Simón, J.L.; Serratosa, M.C. *Eur. J. Nutr.* **2003**, *42*, 43–49.

CHAPTER 4

Effect of the axial ligands on the anticancer activity of novel cyclometallated platinum(IV) compounds against colorectal cancer cells lines

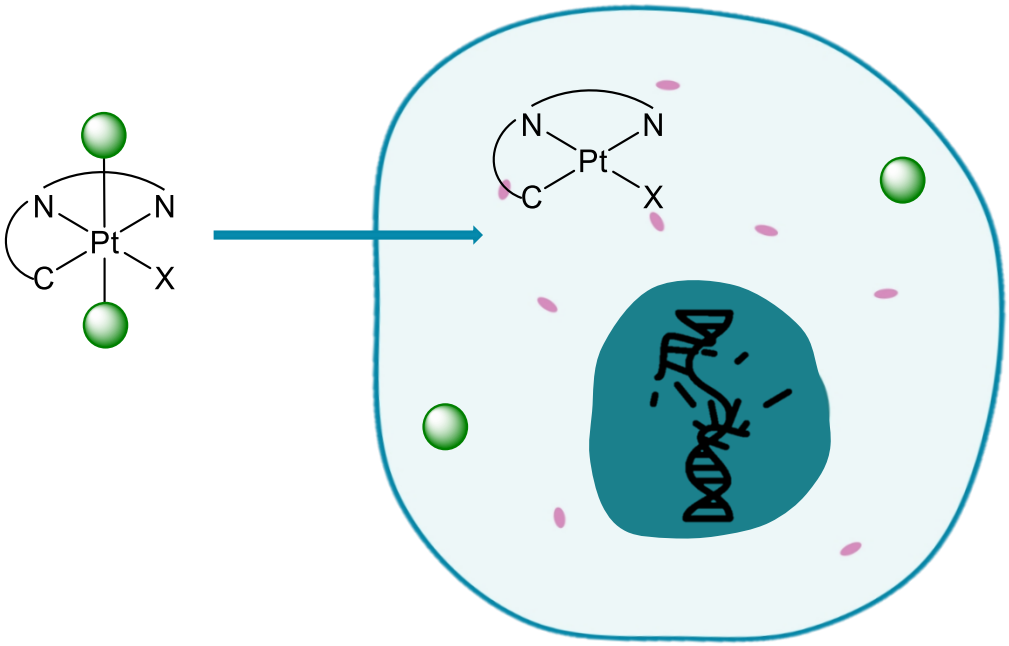

4. Effect of the axial ligands on the anticancer activity of novel cyclometallated platinum(IV) compounds against colorectal cancer cells lines

4.1. Introduction

In the recent years, platinum complexes with non-classical structures such as platinum(IV) compounds or with different mechanisms of action than cisplatin have been thoroughly investigated.[1–3] The platinum(IV) compounds include two axial ligands that can dissociate after biological reduction and their nature can modulate the reduction parameters, kinetic stability, lipophilicity, and pharmacological properties of the prodrug.[4–6]

Upon these parameters, the reduction potential is key to predict the activity of these compounds. Very high redox potentials might lead to straightforward fast reduction and severe side effects while a lack of anticancer activity might be related to a lower reduction rate, which can prevent the compound from giving the active platinum(II) species. These potentials are mainly affected by the electron donating properties of the ancillary axial ligands.[7–9]

However, no straightforward correlation has been established between the reduction potential of platinum(IV) compounds and their biological activity, as the ability of the coordination sphere to associate with the reducing agents present in cellular media also plays a major role in facilitating the electron transfer.[10,11] This is why more studies are being aimed at disclosing their reactivity and understanding the precise mechanisms of the reduction process and therefore develop a rational design of new compounds.[12]

Several compounds derived from the oxidation of platinum(II) clinically approved drugs such as cisplatin and derivatives have been reported so far.[13,14] Among them, iproplatin, satraplatin and tetraplatin, shown in *Figure 4.1*, have undergone clinical trials but none of them or other platinum(IV) structures have been yet approved for their use.[15,16]

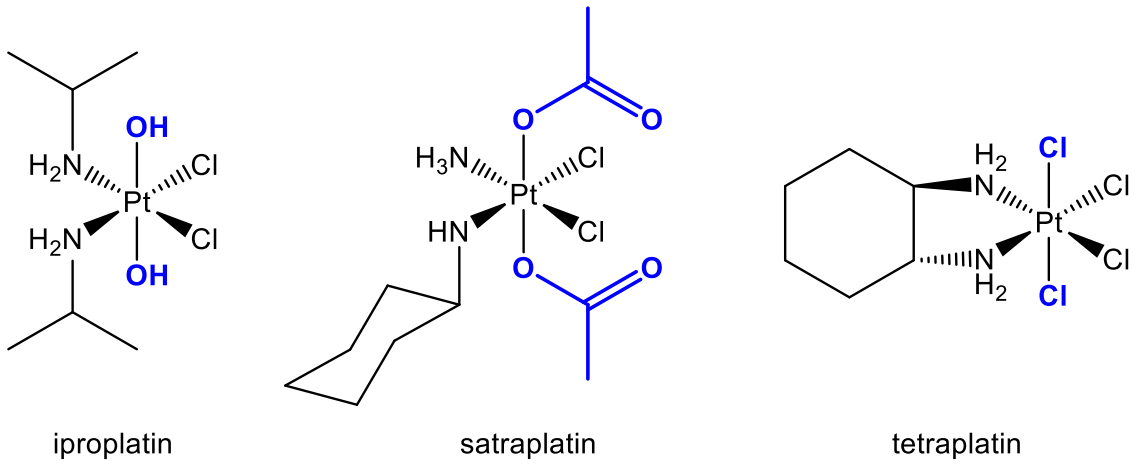

iproplatin satraplatin tetraplatin

Figure 4.1. Structure of the described platinum(IV) compounds.

Most reported platinum(IV) prodrugs bear axial chlorido, hydroxido or carboxylato ligands because of the synthetic ease with which they can be introduced. Hydrogen peroxide or several species releasing chlorine such as iodobenzene dichloride can be used with platinum(II) compounds to give the *trans* oxidative addition products.[15]

Specifically, hydroxido derivatives are interesting as upon reduction, the release of hydrogen peroxide can increase the reactive oxygen species (ROS) level in cellular media which is known to induce cell death.[17] Additionally, the metal-bound hydroxido ligands are sufficiently nucleophilic to attack carboxylic acid anhydrides to yield platinum(IV) carboxylates (*Scheme 4.1*).[18]

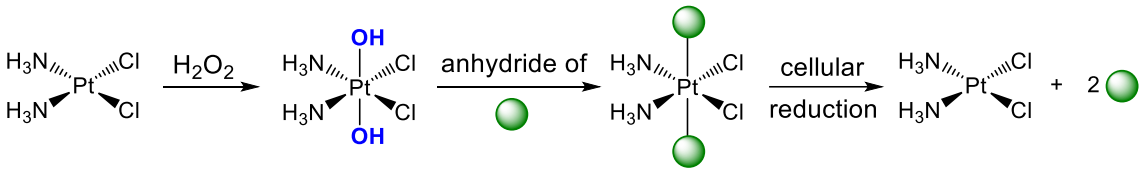

Scheme 4.1. Scheme of the preparation of the described compounds from cisplatin and their reduction under cellular media.

Upon all the reported examples of compounds containing these axial ligands, it has been established that the ease of reduction is higher for chlorido than for hidroxido ligands, with intermediate values for several carboxylato moieties.[19–21] This reduction potentials have been widely determined by the use of cyclic voltammetry (CV) techniques, which reveal an irreversible reduction peak for all platinum(IV) derivatives.[22]

Nevertheless, the synthesis and biological activity of cyclometallated analogues of these compounds has been less studied. This is why in this chapter, a family of cyclometallated platinum(IV) compounds with variations in the nature of the axial ancillary ligands was synthesised. Among all the structures reported in *Chapter 3*, compound $[PtCl_3\{(CH_3)_2N(CH_2)_3N{=}CH(4\text{-}FC_6H_3)\}]$ (**5a**), containing chlorido as axial ligands, presented the most remarkable biological activity and therefore the structure of its platinacycle was selected for the preparation of the new compounds and chosen as a reference for comparison purposes. An hydroxido derivative was prepared to study its biological activity and reduction potentials as well as to serve as a precursor for different carboxylato derivatives. Dichloroacetate (DCA) and trifluoroacetate (TFA) were used to synthesise two different carboxylato compounds to also study the effect of their nature in the properties of the final compounds (*Figure 4.2*).

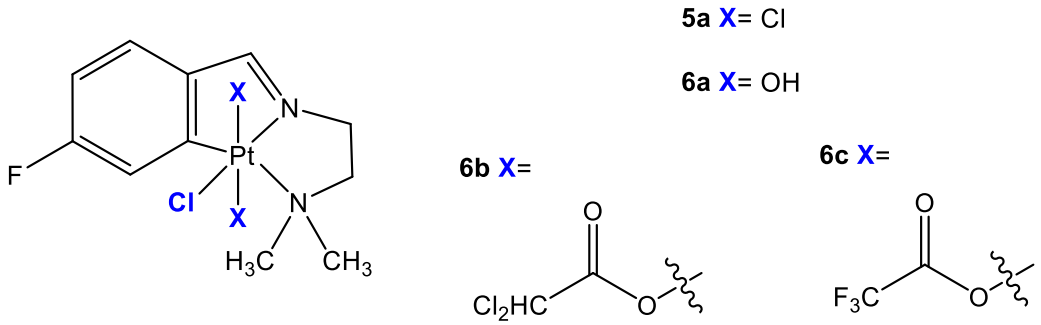

Figure 4.2. Structure of the compounds studied in this chapter.

DCA is a known anticancer agent that inhibits a key enzyme (pyruvate dehydrogenase kinase), which is present in cancer cells. Platinum(IV) compounds containing DCA ligands act as dual-action compounds which upon entry in the cell release a platinum(II) species and two molecules of DCA which target the mitochondria in the cell.[23,24]

Finally, TFA does not display any biological activity, but was selected as compounds with this axial ligand are known to reduce more rapidly and be more cytotoxic than those containing acetato moieties.[25] This has been attributed also to the enhanced intracellular accumulation of the first, resulting from the higher lipophilicity of the fluorinated complexes.[21] Furthermore, the presence of fluorine atoms allows an easy tracking of its behaviour in the cell, as the ^{19}F isotope is NMR sensitive with a large chemical shift range and avoids the difficulties of interpreting ^{1}H NMR in the crowded cellular environment.[26,27]

4.2. Results and Discussion

4.2.1. Synthesis and characterisation

Compound [PtCl(OH)$_2${(CH$_3$)$_2$N(CH$_2$)$_2$N=CH(4-FC$_6$H$_3$)}] (**6a**) was synthesised by slight modification of the method reported in the literature by the addition of hydrogen peroxide (H_2O_2) to the platinum(II) compound [PtCl{(CH$_3$)$_2$N(CH$_2$)$_2$N=CH(4-FC$_6$H$_3$)}] (**4a**) in dichloromethane to allow the oxidative addition of two hydroxyl axial ligands to obtain the final cyclometallated platinum(IV) compound (*Scheme 4.2*).[8]

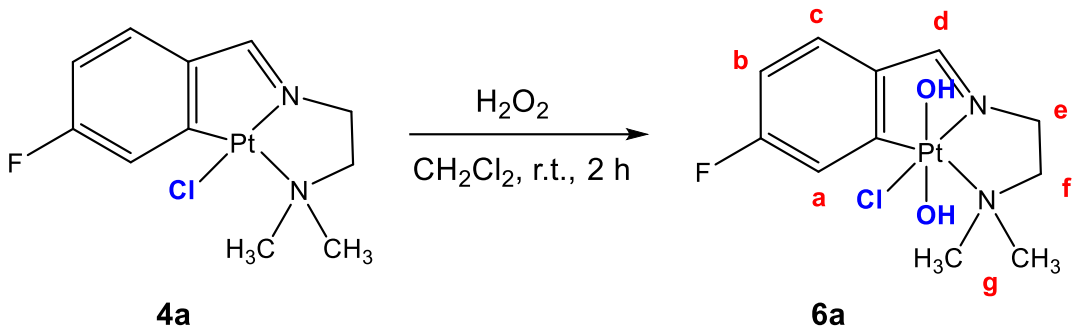

Scheme 4.2. Synthesis of compound **6a**.

Compounds [PtCl(CHCl$_2$COO)$_2${(CH$_3$)$_2$N(CH$_2$)$_2$N=CH(4-FC$_6$H$_3$)}] (**6b**) and [PtCl(CF$_3$COO)$_2${(CH$_3$)$_2$N(CH$_2$)$_2$N=CH(4-FC$_6$H$_3$)}] (**6c**) were obtained by the reaction depicted in *Scheme 4.3* between the hydroxyl axial groups of compound [PtCl(OH)$_2${(CH$_3$)$_2$N(CH$_2$)$_2$N=CH(4-FC$_6$H$_3$)}] (**6a**) and the corresponding anhydride (dichloroacetic anhydride, **6b**; trifluoroacetic anhydride, **6c**).

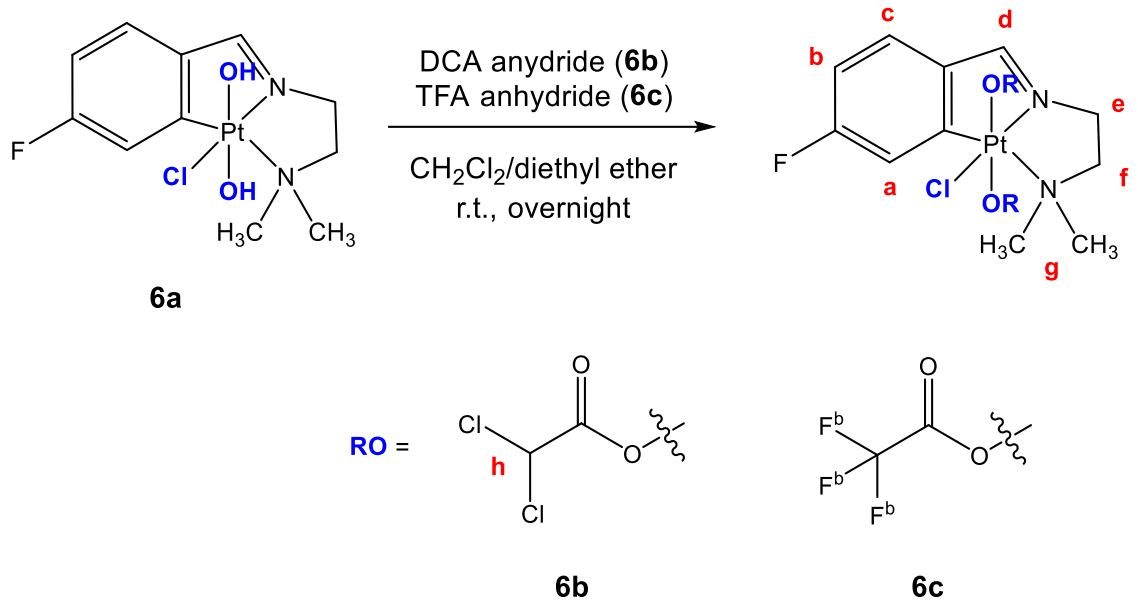

Scheme 4.3. Synthesis of compounds **6b** and **6c**.

All final compounds were characterised by ^{1}H and ^{19}F NMR spectra, mass spectrometry and infrared spectroscopy matching the desired structures.

^{1}H NMR spectra of all compounds present the expected signals for the fused [6,5,5]-tricyclic system with no significant differences between the different derivatives, except for an additional singlet signal at 5.85 ppm for compound **6b** corresponding to the protons from the dichloroacetate moieties. Upon comparison with the platinum(II) precursor **4a**, it can be observed that the coupling constant of the iminic proton (H^{d}) is significantly reduced from 141 Hz to values between 89 - 100 Hz for compounds **6**. This is due to the increase in the oxidation state, which implies a lower electronic density of the platinum centre.[28] Furthermore, the chemical shift of this proton is not significantly affected by the presence of different ancillary ligands, as it is directly influenced by the nature of the ligand in *trans* to the imine bond, which corresponds to a chlorido in all cases.[29] As expected, upon oxidation with H_2O_2, which occurs in *trans*, compound **6a** retains this disposition in solution without further isomerisation, which would result in the doubling of the signals of the $N(CH_3)_2$ and the $(CH_2)_2$ protons in the ^{1}H NMR, as they would become diastereotopic.[30]

Additionally, compound **6a** presents one single signal as a multiplet in its ^{19}F NMR spectra (δ = -96.50 ppm) which appears shifted regarding its platinum(II) precursor **4a** (δ = -102.92 ppm), as previously observed upon change of the oxidation state of analogous

compounds.[30] This signal is also present in the ^{19}F NMR spectra for compounds **6b** and **6c** at a similar position (δ = -95.49 ppm, **6b**, δ = -94.71 ppm, **6c**), in agreement with the lesser effect of the nature of the axial ancillary ligands in its chemical shift.[31] Compound **6c** presents an additional singlet signal at -74.42 ppm that integrates to 6 fluorine atoms, corresponding to the two equivalent trifluoroacetato axial ligands.

Infrared spectroscopy allowed to identify the most characteristic bands of all compounds. Compound **6a** displays a broad band centred at 3471 cm^{-1} attributed to the O-H stretching of the hydroxyl group while compounds **6b** and **6c** present an intense band at 1705 cm^{-1} and 1736 cm^{-1}, respectively, characteristic of the C=O vibration band of an ester group. Finally, all the protonated molecular peaks were found by mass spectrometry further confirming the successful formation of the desired products.

4.2.2. Electrochemistry

Cyclic voltammetry was performed for 10^{-3} M solutions in dimethyl sulfoxide/water (1:1) of all compounds **6** along with their chloride analogue [$PtCl_3${$(CH_3)_2N(CH_2)_3N$=CH(4-FC_6H_3)}] (**5a**) to evaluate their ease to be reduced to platinum(II). All compounds show an irreversible reduction peak, which is a common feature for platinum(IV) compounds upon loss of the axial ligands.[22] This is shown in *Figure 4.3* for compound **5a** as an example.

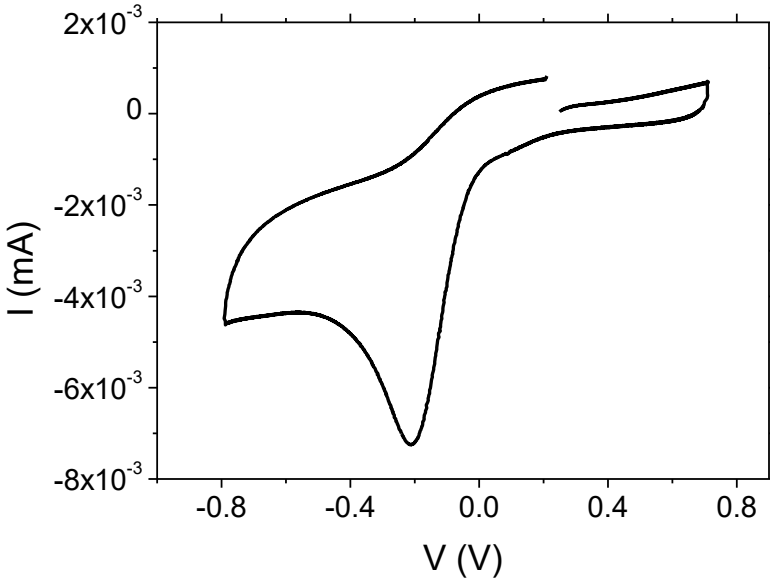

Figure 4.3. First cycle of the cyclic voltammogram of compound **5a** in a dimethyl sulfoxide/water (1:1) solution at a scan rate of 100 mV/s.

As previously observed for non-cyclometallated similar compounds, the reduction process occurs more readily for chlorido (**5a**) than for hydroxido (**6a**) axial ligands, with intermediate values for carboxylato ligands (**6b**, **6c**) (*Table 4.1*). Additionally, it has been observed that variations in the nature of the latter only results in small changes in the reduction potential, but with a higher reduction potential for trifluoracetate derivatives.[19]

Table 4.1. Reduction potentials versus SHE for compounds **5a** and **6**.

Compound	E^o (mV)
5a	-209
6a	-261
6b	-234
6c	-226

4.2.3. Cell viability assays

The antiproliferative activity of all compounds was assessed against the HCT116 colorectal cancer cell line. The resulting IC_{50} values are summarised in *Table 4.2*.

Table 4.2. Antiproliferative activity (IC_{50}, μM) on the HCT116 colorectal cancer cell line for the studied compounds and cisplatin.

Compound[a]	HCT116
5a	1.85 ± 0.52
6a	19.15 ± 2.79
6b	8.87 ± 0.55
6c	4.92 ± 1.52
Cisplatin[b]	21.10 ± 1.34

[a] Results shown correspond to mean ± standard deviation of two experiments performed in triplicates.
[b] Cisplatin is taken as a reference compound.

The new compounds display significantly lower IC_{50} values than the reference compound (cisplatin) for this cell line, with only a slightly lower value for the hydroxido compound **6a**. Despite most of them presenting high efficacy, they do not display improved values when compared to that of the chlorido derivative **5a**. Compound **6c**, containing TFA ligands displays the lowest IC_{50}. Some studies have shown that platinum(IV) with axial

trifluoroacetato ligands were more potent than their analogues with acetato ligands. This has been attributed to the enhanced intracellular accumulation, which results from the higher lipophilicity of the fluorinated complexes.[21]

On the other hand, the lower efficacy of compound **6a** could be related to the higher difficulty to be reduced previously confirmed by cyclic voltammetry, under the assumption that these compounds act as pro-drugs and are only activated upon reduction under cellular media. Finally, compound **6b** which present bioactive DCA ligands, does not benefit from these and shows an intermediate value, which could again be hypothesised to be related to its higher reduction potential. In summary, even though more studies should be performed for the understanding of their mechanism of action, their antiproliferative activity seems to follow a trend, with higher activity upon a higher tendency to reduce, as expected for platinum(IV) prodrugs.

However, further testing in different cancer cell lines could give rise to different results and provide more information on their selectivity. Additionally, their antiproliferative effect against healthy cells should also be evaluated, as they could display a better toxicity profile with lower secondary effects which could be an advantage even if they present higher IC_{50} values.

4.2.4. DNA migration assays

The ability of all compounds to modify the mobility of the supercoiled close (sc) and the open circular (oc) forms of pBluescript SK + plasmid DNA was tested in agarose gel by electrophoresis (*Figure 4.4*).

Interestingly, compounds **6** cause significant changes in the mobility at concentrations of 25 µM (**6a**), 50 µM (**6b**) and 100 µM (**6c**). These values, although they correspond to higher concentrations than the reference compounds, such as cisplatin (2.5 µM), show that the presence of hydroxido or carboxylato ligands allows these compounds to interact with DNA, which is not observed for compound **5a** with only chlorido as ancillary ligands.

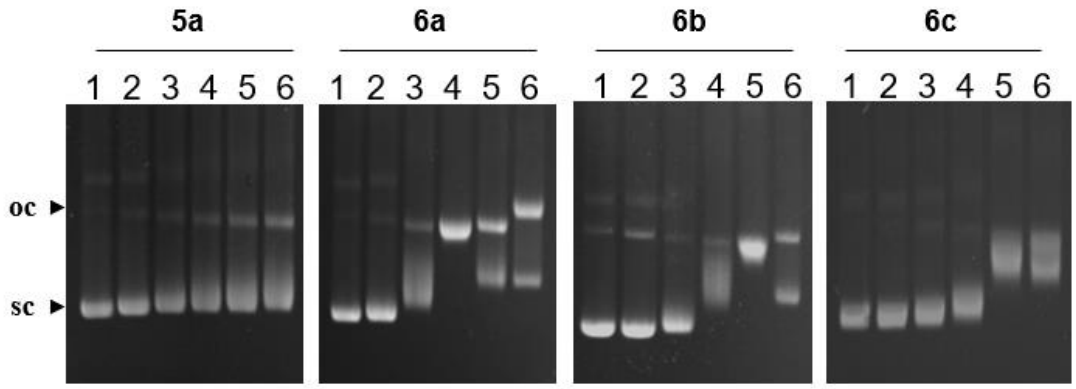

Figure 4.4. Interaction of pBluescript SK+ plasmid DNA (0.3 μg) with increasing concentrations of compounds under study. All compounds were analysed from 10 to 200 μM concentration Lane 1: DNA only. Lane 2: 10 μM. Lane 3: 25 μM. Lane 4: 50 μM. Lane 5: 100 μM. Lane 6: 200 μM. sc = supercoiled closed circular DNA; oc = open circular DNA.

The lack of interaction for compound **5a** despite its high effectivity against cancer cell lines was previously attributed to its action as a pro-drug which only becomes active upon reduction under biological media to give the active platinum(II) species.[31] The fact that the new compounds **6** can interact with DNA prior to its reduction, could be attributed to a coordination mediated by the presence of hydrogen bonding with the hydroxido or carboxylato ligands. The mode in which this interactions work could be determined by further studies on molecular docking, but from the presented data, they appear to be more favourable for compound **6a** containing two hydroxido ligands as it is able to modify the mobility of plasmid DNA at lower concentrations.

Upon comparison of these results with the IC_{50} values indicated above, compounds that present none or less interaction with DNA display the highest antiproliferative activity. This also suggests an alternative mechanism that involves platinum(IV) compounds interacting with DNA prior to reduction which could compete in a less effective manner with the expected pro-drug behaviour.

4.3. Conclusions

The anticancer properties of a family of [C,N,N'] cyclometallated platinum(IV) compounds upon variation of the ancillary ligands (chlorido, hydroxido or carboxylato) have been studied.

Cyclic voltammetry studies revealed that all compounds present an irreversible reduction peak, with reduction potentials following the trend Cl > TFA > DCA > OH, as previously reported for non-cyclometallated analogues, suggesting that their tendency to be reduced under cellular media should follow this trend.

Antiproliferative studies for all compounds reveal a range of IC_{50} values for the colorectal cancer cell line HCT116, being all of them lower than the reference compound (cisplatin). Their anticancer properties seem to follow a trend, with higher activity upon a higher tendency to reduce, which would agree with them acting as pro-drugs.

Finally, DNA interaction studies revealed that hydroxido and carboxylato derivatives are able to interact with plasmid DNA prior to reduction, whereas the chlorido derivative does not interact at all. This suggests an interaction likely based in hydrogen bonding and interestingly, the higher the IC_{50} values the lower is the compound interaction. This could suggest an alternative mechanism that could be competing with the expected pro-drug behaviour.

4.4. Experimental Section

4.4.1. General procedures

Commercial reagents hydrogen peroxide (H_2O_2, Panreac, 33%), dichloroacetic anhydride (Acros Organics, 98%) and trifluoroacetic anhydride (Sigma Aldrich, >99%); and solvents dichloromethane (CH_2Cl_2, Scharlau, 99%), diethyl ether (Carlo Erba, 99%) and acetone (Carlo Erba, >99%) were used as received.

Compounds $[PtCl\{(CH_3)_2N(CH_2)_2N=CH(4\text{-}FC_6H_3)\}]$ (**4a**)[32] and $[PtCl_3\{(CH_3)_2N(CH_2)_2N=CH(4\text{-}FC_6H_3)\}]$ (**5a**)[31] were prepared as reported in the literature.

4.4.2. Physical measurements

NMR spectra were recorded in $CDCl_3$ at the *Unitat de RMN* of the *Universitat de Barcelona* with a Mercury 400 spectrometer (^1H, 400 MHz; ^{19}F, 376.5 MHz). Chemical shifts are given in δ values (ppm) relative to TMS (^1H) or $CFCl_3$ (^{19}F) and coupling constants J are given in Hz.

Infrared spectra were recorded in a Thermo Scientific FT-IR Nicolet iS5 spectrometer with an iD7 ATR accessory.

Electrospray mass spectra were performed at the *Unitat d'Espectrometria de Masses (Universitat de Barcelona)* in a LC/MSD-TOF spectrometer using H_2O-CH_3CN 1:1 to introduce the sample.

4.4.3. Synthesis and characterisation

Synthesis of [PtCl(OH)$_2${(CH$_3$)$_2$N(CH$_2$)$_2$N=CH(4-FC$_6$H$_3$)}] (6a)

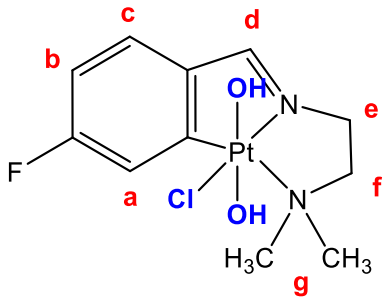

Compound [PtCl(OH)$_2${(CH$_3$)$_2$N(CH$_2$)$_2$N=CH(4-FC$_6$H$_3$)}] (**6a**)[8] was obtained by slight modifications of the method reported in the literature from the reaction of 0.050 g (0.118 mmols) of [PtCl{(CH$_3$)$_2$N(CH$_2$)$_2$N=CH(4-FC$_6$H$_3$)}] (**4a**) and 0.004 g (0.118 mmols) of H$_2$O$_2$ in 10 ml of dichloromethane. The mixture was stirred at room temperature for 2 hours and the solvent was removed under vacuum. The residue was treated with diethyl ether and the yellow solid was filtered and dried under vacuum. Yield: 0.031 g (57%).

^{1}H NMR (CDCl$_3$, 400 MHz): δ 8.19 [s, 1H, ^{3}J(Pt-H) = 103.9, H^d]; 7.45-7.56 [m, 2H, H^{a,c}], 6.94 [td, 1H, ^{3}J(F-H) = ^{3}J(H-H) = 8.5, ^{4}J(H-H) = 2.4, H^b], 4.14 [t, ^{3}J(H-H) = 5.7, 2H, H^e], 3.28 [t, 2H, ^{3}J(H-H) = 5.7, H^f], 3.06 [s, 6H, ^{3}J(Pt-H) = 10.4, H^g]. **^{19}F NMR** (CDCl$_3$, 376.5 MHz): δ -96.50 [m, 1F]. **MS-ESI$^+$**: *m/z* 459.02 [M + H]$^+$. **IR**: υ 3471.24 (O-H).

Synthesis of [PtCl(CHCl$_2$COO)$_2${(CH$_3$)$_2$N(CH$_2$)$_2$N=CH(4-FC$_6$H$_3$)}] (6b)

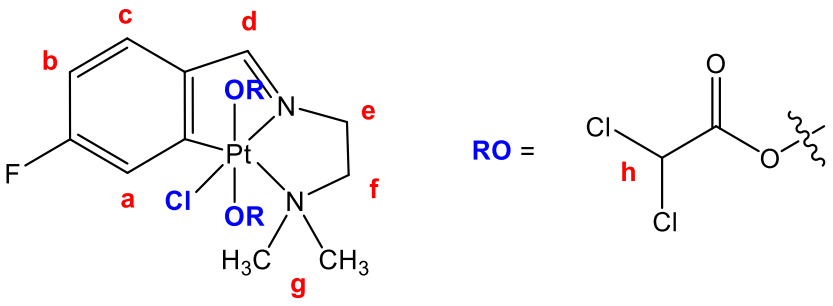

Compound [PtCl(CHCl$_2$COO)$_2${(CH$_3$)$_2$N(CH$_2$)$_2$N=CH(4-FC$_6$H$_3$)}] (**6b**) was obtained from the reaction of 0.020 g (0.044 mmols) of [PtCl(OH)$_2${(CH$_3$)$_2$N(CH$_2$)$_2$N=CH(4-FC$_6$H$_3$)}] (**6a**) and 0.027 g (0.109 mmols) of dichloroacetic anhydride in 10 ml of dichloromethane/diethyl ether (1:1). The mixture was stirred at room temperature overnight and the solvent was removed under vacuum. The residue was dissolved in

acetone and diethyl ether was added. The yellow solid was filtered and dried under vacuum. Yield: 0.017 g (57%).

^{1}H NMR ($CDCl_3$, 400 MHz): δ 8.09 [s, 1H, ^{3}J(Pt-H) = 92.1, H^{d}]; 7.44-7.56 [m, 2H, $H^{a,c}$], 6.95 [td, 1H, ^{3}J(F-H) = ^{3}J(H-H) = 8.4, ^{4}J(H-H) = 2.3, H^{b}], 5.84 [s, 2H, H^{h}], 4.11 [t, ^{3}J(H-H) = 5.3, 2H, H^{e}], 3.39 [t, 2H, ^{3}J(H-H) = 5.3, H^{f}], 3.06 [s, 6H, ^{3}J(Pt-H) = 10.2 H^{g}]. **^{19}F NMR** ($CDCl_3$, 376.5 MHz): δ -95.49 [m, 1F]. **MS-ESI^{+}**: *m/z* 680.92 $[M + H]^{+}$. **IR**: υ 1705.79 (C≡O).

Synthesis of Synthesis of $[PtCl(CF_3COO)_2\{(CH_3)_2N(CH_2)_2N{=}CH(4\text{-}FC_6H_3)\}]$ (6c)

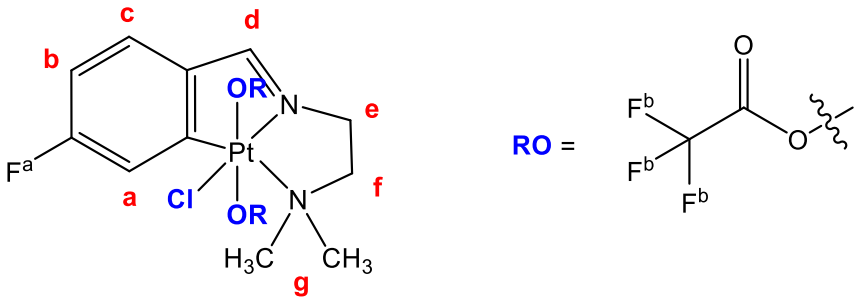

Compound $[PtCl(CF_3COO)_2\{(CH_3)_2N(CH_2)_2N{=}CH(4\text{-}FC_6H_3)\}]$ (**6c**) was prepared as a yellow solid by following the same method from 0.020 g (0.044 mmols) of $[PtCl(OH)_2\{(CH_3)_2N(CH_2)_2N{=}CH(4\text{-}FC_6H_3)\}]$ (**6a**) and 0.023 g (0.109 mmols) of trifluoroacetic anhydride. Yield: 0.014 g (49%).

^{1}H NMR ($CDCl_3$, 400 MHz): δ 8.16 [s, 1H, ^{3}J(Pt-H) = 88.9, H^{d}]; 7.49-7.55 [m, 2H, $H^{a,c}$], 6.94 [td, 1H, ^{3}J(F-H) = ^{3}J(H-H) = 8.5, ^{4}J(H-H) = 2.5, H^{b}], 4.17 [t, 2H, ^{3}J(H-H) = 5.9, H^{e}], 3.38 [t, 2H, ^{3}J(H-H) = 5.8, H^{f}], 3.06 [s, 6H, ^{3}J(Pt-H) = 9.9, H^{g}]. **^{19}F NMR** ($CDCl_3$, 376.5 MHz): δ -74.42 [s, 6F, F^{b}], -94.71 [m, 1F, F^{a}]. **MS-ESI^{+}**: *m/z* 650.17 $[M + H]^{+}$. **IR**: υ 1736.15 (C≡O).

4.4.4. Electrochemistry

Electrochemistry experiments were carried out with a BioLogic SP150 instrument using a glassy carbon working electrode, a Ag/AgCl (3 M KCl) reference electrode, and platinum wire counter electrode; potential values are given versus SHE.[33] The samples were dissolved in 1:1 a water-DMSO mixture at the $1 \cdot 10^{-3}$ M level concentration and using 0.1 M $(Bu_4N)ClO_4$ as supporting electrolyte.

4.4.5. Biological assays

Cell culture and viability assays

Human colorectal carcinoma HCT116 cells were cultured in a DMEM/HAM F12 (1 : 1 volume) mixture containing 10% FBS, 4 mM L-glutamine, 12.5 mM D-glucose and 0.1% streptomycin/penicillin. Cell viability assays were performed by a variation of the MTT (3-(4,5-dimethylthiazol-2-yl)-2,5-diphenyltetrazolium bromide) assay described previously. Relative cell viability, compared to the viability of untreated cells, was measured by absorbance at 550 nm on an ELISA plate reader (Tecan Sunrise MR20-301, TECAN, Salzburg, Austria). Concentrations that inhibited cell growth by 50% (IC_{50}) after 72 h of treatment were subsequently calculated by sigmoidal fitting with GraphPad Prism 6 software.

Data analysis

For each compound, a minimum of three independent experiments with triplicate values were conducted to measure cell viability. Significant differences compared to control were assessed by Student's t-test where $p < 0.03$(#), $p < 0.004$(##) or $p < 0.0005$(###) were taken into consideration. Data are given as the mean ± standard deviation (SD).

DNA migration assays

DNA migration studies were performed as described before.[34] Compounds under study were prepared in high purity DMSO at 10 mM concentration and then serial dilutions with MilliQ water (1:1) were made. pBluescript SK+ plasmid DNA-drug interaction was analysed by agarose gel electrophoresis. Plasmid DNA aliquots (0.3 µg) were incubated in TE buffer (10 mM Tris-HCl, 1 mM EDTA, pH 7.5) with different concentrations of compounds under study ranging from 0 µM to 200 µM at 37 ºC for 24 h. Cisplatin was used as a reference control. Samples were then subjected to 1% agarose gel electrophoresis in TAE buffer, stained in TAE buffer containing ethidium bromide (0.5 mg ml^{-1}) and visualized and photographed under UV light. All compounds under study were analysed between 10 and 200 µM concentration.

4.5. References

1. Alassadi, S.; Pisani, M.J.; Wheate, N.J. *Dalton Trans.* **2022**, *51*, 10835–10846.
2. Kenny, R.G.; Chuah, S.W.; Crawford, A.; Marmion, C.J. *Eur. J. Inorg. Chem.* **2017**, 1596–1612.
3. Cai, L.; Yu, C.; Ba, L.; Liu, Q.; Qian, Y.; Yang, B.; Gao, C. *Appl. Organomet. Chem.* **2018**, *32*, 1–17.
4. Gibson, D. *Dalton Trans.* **2016**, *45*, 12983–12991.
5. Yap, S.Q.; Chin, C.F.; Hong Thng, A.H.; Pang, Y.Y.; Ho, H.K.; Ang, W.H. *ChemMedChem* **2017**, *12*, 300–311.
6. Johnstone, T.C.; Suntharalingam, K.; Lippard, S.J. *Chem. Rev.* **2016**, *116*, 3436–3486.
7. Reithofer, M.R.; Bytzek, A.K.; Valiahdi, S.M.; Kowol, C.R.; Groessl, M.; Hartinger, C.G.; Jakupec, M.A.; Galanski, M.; Keppler, B.K. *J. Inorg. Biochem.* **2011**, *105*, 46–51.
8. Crespo, M.; Font-Bardia, M.; Hamidizadeh, P.; Martínez, M.; Nabavizadeh, S.M. *Inorg. Chim. Acta* **2019**, *486*, 8–16.
9. Reshetnikov, V.; Daum, S.; Mokhir, A. *Chem. Eur. J.* **2017**, *23*, 5678–5681.
10. Sinisi, M.; Intini, F.P.; Natile, G. *Inorg. Chem.* **2012**, *51*, 9694–9704.
11. Zhang, J.Z.; Wexselblatt, E.; Hambley, T.W.; Gibson, D. *Chem. Commun.* **2012**, *48*, 847–849.
12. Wexselblatt, E.; Gibson, D. *J. Inorg. Biochem.* **2012**, *117*, 220–229.
13. Wheate, N.J.; Walker, S.; Craig, G.E.; Oun, R. *Dalton Trans.* **2010**, *39*, 8113–8127.
14. Mi, Q.; Shu, S.; Yang, C.; Gao, C.; Zhang, X.; Luo, X.; Bao, C.; Zhang, X.; Niu, J. *Int. J. Med. Physics, Clin. Eng. Radiat. Oncol.* **2018**, *07*, 231–247.
15. Wilson, J.J.; Lippard, S.J. *Chem. Rev.* **2014**, *114*, 4470–4495.
16. Gibson, D. *J. Inorg. Biochem.* **2021**, *217*, 111353.

17. Aggarwal, V.; Tuli, H.S.; Varol, A.; Thakral, F.; Yerer, M.B.; Sak, K.; Varol, M.; Jain, A.; Khan, M.A.; Sethi, G. *Biomolecules* **2019**, *9*, 735.

18. Johnstone, T.C.; Alexander, S.M.; Wilson, J.J.; Lippard, S.J. *Dalton Trans.* **2015**, *44*, 119–129.

19. Ellis, L. T., Er, H. M., Hambley, T.W. *Aust. J. Chem.* **1995**, *48*, 793-806.

20. Nakabayashi, Y.; Erxleben, A.; Létinois, U.; Pratviel, G.; Meunier, B.; Holland, L.; Lippert, B. *Chem. Eur. J.* **2007**, *13*, 3980–3988.

21. Wexselblatt, E.; Raveendran, R.; Salameh, S.; Friedman-Ezra, A.; Yavin, E.; Gibson, D. *Chem. Eur. J.* **2015**, *21*, 3108–3114.

22. Hall, M.D.; Hambley, T.W. *Coord. Chem. Rev.* **2002**, *232*, 49–67.

23. Michelakis, E.D.; Webster, L.; Mackey, J.R. *Br. J. Cancer* **2008**, *99*, 989–994.

24. Petruzzella, E.; Sirota, R.; Solazzo, I.; Gandin, V.; Gibson, D. *Chem. Sci.* **2018**, *9*, 4299–4307.

25. Choi, S.; Filotto, C.; Bisanzo, M.; Delaney, S.; Lagasee, D.; Whitworth, J.L.; Jusko, A.; Li, C.; Wood, N.A.; Willingham, J.; Schwenken, A.; Spaulding, K. *Inorg. Chem.* **1998**, *37*, 2500–2504.

26. Yuan, S.; Zhu, Y.; Dai, Y.; Wang, Y.; Jin, D.; Liu, M.; Tang, L.; Arnesano, F.; Natile, G.; Liu, Y. *Angew. Chem. Int. Ed.* **2022**, *61*, e202114250.

27. Chen, H.; Viel, S.; Ziarelli, F.; Peng, L. *Chem. Soc. Rev.* **2013**, *42*, 7971–7982.

28. Bernhardt, P. V.; Calvet, T.; Crespo, M.; Font-Bardía, M.; Jansat, S.; Martínez, M. *Inorg. Chem.* **2013**, *52*, 474–484.

29. Crespo, M.; Font-Bardía, M.; Solans, X. *J. Organomet. Chem.* **2006**, *691*, 1897–1906.

30. Lázaro, A.; Serra, O.; Rodríguez, L.; Crespo, M.; Font-Bardia, M. *New J. Chem.* **2019**, *43*, 1247–1256.

31. Lázaro, A.; Balcells, C.; Quirante, J.; Badia, J.; Baldomà, L.; Ward, J.S.; Rissanen, K.; Font-Bardia, M.; Rodríguez, L.; Crespo, M.; Cascante, M. *Chem. Eur. J.* **2020**, *26*, 1947–1952.

32. Gandioso, A.; Valle-Sistac, J.; Rodríguez, L.; Crespo, M.; Font-Bardía, M. *Organometallics* **2014**, *33*, 561–570.

33. Song, M.; Daniels, K.E.; Kiani, A.; Rashid-Nadimi, S.; Dickey, M.D. *Adv. Intell. Syst.* **2021**, *3*, 2100024.

34. Solé, M.; Balcells, C.; Crespo, M.; Quirante, J.; Badia, J.; Baldomà, L.; Font-Bardia, M.; Cascante, M. *Dalton Trans.* **2018**, *47*, 8956–8971.

CHAPTER 5

Phosphorescent cyclometallated platinum(II) compounds containing different chromophores as efficient singlet oxygen photosensitisers

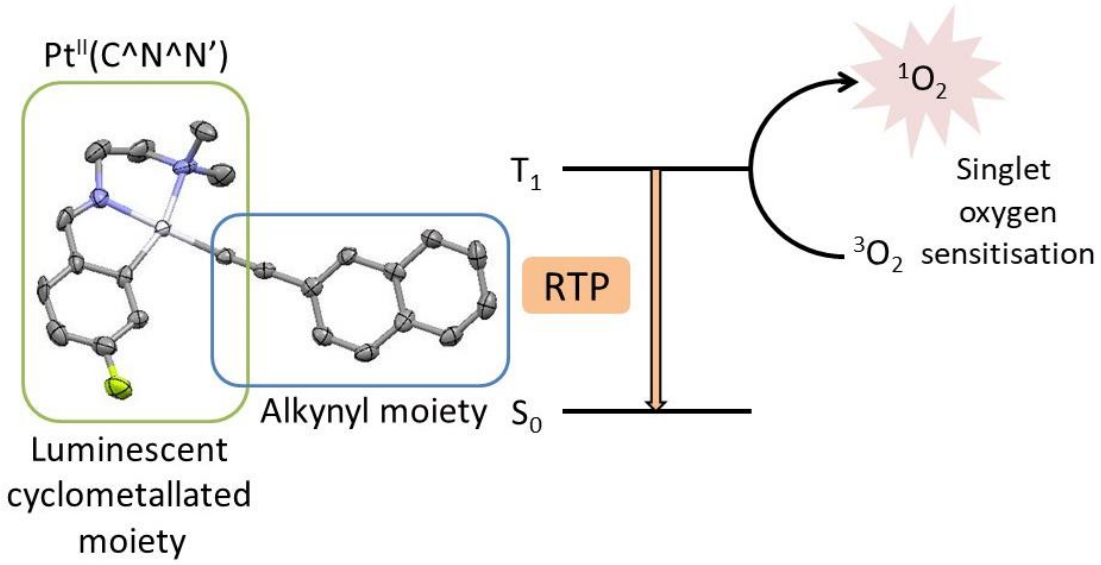

Part of this chapter has been published in: Lázaro, A.; Cunha, C.; Bosque, R.; Pina, J.; Ward, J.S.; Truong, K.N.; Rissanen, K.; Lima, J.C.; Seixas de Melo, J. S.; Crespo, M.; Rodríguez, L. *Inorg. Chem.* **2020**, *59*, 8220-8230.

5. Phosphorescent cyclometallated platinum(II) compounds containing different chromophores as efficient singlet oxygen photosensitisers

5.1. Introduction

Cyclometallated platinum(II) are widely studied as luminescent materials for their application in optical devices, sensors or electronic displays, among others.[1,2] In these areas, phosphorescent compounds attract a special interest in more specific fields such as the fabrication of organic light-emitting diodes (OLEDs), photodynamic therapy, bioimaging or oxygen sensing.[3–5] In particular, the latter persists at the forefront of research, as the generated singlet oxygen ($^1O_2$) is considered a reactive oxygen species (ROS) that therefore can be used for synthetic or biological purposes.[6–8]

Uncommonly, oxygen is a molecule whose electronic ground state has a triplet spin state ($^3O_2$ ($^3\Sigma g^-$)) and whose two lowest energy excited states have a singlet nature ($^1O_2$ ($^1\Delta g$)); $^1O_2$ ($^1\Sigma g^+$)). In solution, the second singlet excited state decays to the first one before reacting to another molecule.[9]

Taking this into account, the presence of a molecule, called photosensitiser, with a populated first triplet excited state (T_1) is necessary for the $^1O_2$ formation, as it arises from the energy transfer from this state allowed due to the same spin multiplicity (*Figure 5.1*). The presence and efficiency of this singlet oxygen production can be determined as singlet oxygen returns to its triplet ground state by emitting phosphorescence centred at 1270 nm.[10,11]

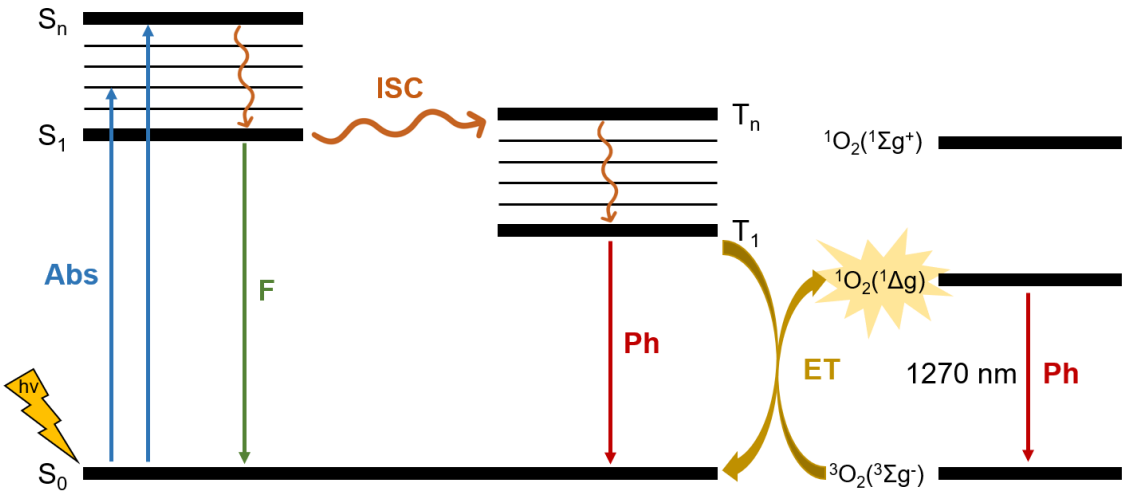

Figure 5.1. Jablonski diagram illustrating the formation of singlet oxygen.

Laser flash photolysis is a pump-probe technique used to detect singlet oxygen. It consists of a strong pump laser that gives short flashes that allow a high concentration of excited states in the sample, and a weak broad probe with a time delay that allows their spectroscopic analysis.[12] The specific method that is used is called transient absorption, which allows to determine the absorption of the singlet (fs-TA, $S_1 \rightarrow S_n$) or triplet (ns-TA, $T_1 \rightarrow T_n$) excited states by analysing the change in the absorption of the probe. From the transient absorption spectra, kinetic data can be obtained which helps illustrate both the radiative and non-radiative processes through which these excited states are deactivated, including the formation of singlet oxygen. This also provides an in-depth photophysical study of the analysed compounds with a further understanding of their luminescent properties.[13,14]

As previously mentioned, a populated triplet state is crucial for the obtention of singlet oxygen. Thus, the photosensitiser needs to present an efficient intersystem crossing (ISC) which can be enhanced by the presence of a transition metal, such as platinum, in the molecules' structure, thanks to its high spin orbit coupling.[15,16] Therefore, the first report on cyclometallated platinum(II) compounds as photosensitisers for singlet oxygen generation was contributed by Weinstein and co-workers, with some later examples published to date.[6,17]

Taking all of this into consideration, in this Chapter, a series of new cyclometallated platinum(II) compounds with the general structure [Pt(C≡CR){$(CH_3)_2N(CH_2)_2N$=CH(4-

FC_6H_3)}] containing a tridentate [C,N,N'] ligand and an alkynyl chromophoric unit occupying the fourth position has been reported. An exhaustive photophysical study has been performed for all compounds and their ability to produce singlet oxygen has also been evaluated.

Although the luminescence of cyclometallated platinum(II) compounds with alkynyl aromatic ligands has been widely studied, in all the reported examples the [C,N,N'] positions belong to an aromatic cycle.[18–20] In this case, the structure derives from imine 4-$FC_6H_4CH=N(CH_2)_2N(CH_3)_2$, which results in a compound with an aromatic and a chelate ring. The photophysical properties of compounds derived from this ligand and containing halido ancillary ligands were already described in *Chapter 3*. Nevertheless, the change in this fourth ligand to an alkynyl aromatic moiety could have a significant effect in the resulting luminescent properties.[21]

5.2. Results and Discussion

5.2.1. Synthesis and characterisation

Compounds [Pt(C≡CR){$(CH_3)_2N(CH_2)_2N$=CH(4-FC_6H_3)}] (**7**) were synthesised by following the strategy described in *Scheme 5.1* from compound [PtCl{$(CH_3)_2N(CH_2)_2N$=CH(4-FC_6H_3)}] (**4a**) previously reported in *Chapter 3*. It consists in a slight modification of a Sonogashira method reported in the literature where the corresponding R-C≡C-H ligand is deprotonated with a base (sodium acetate) followed by the substitution of the chlorido ligand with CuI as a catalyst.[22] The reaction was also assayed with 1-ethynylpyrene, and the final compound was isolated in a pure form. However, its high instability did not make it a suitable candidate for photophysical studies and therefore was discarded.

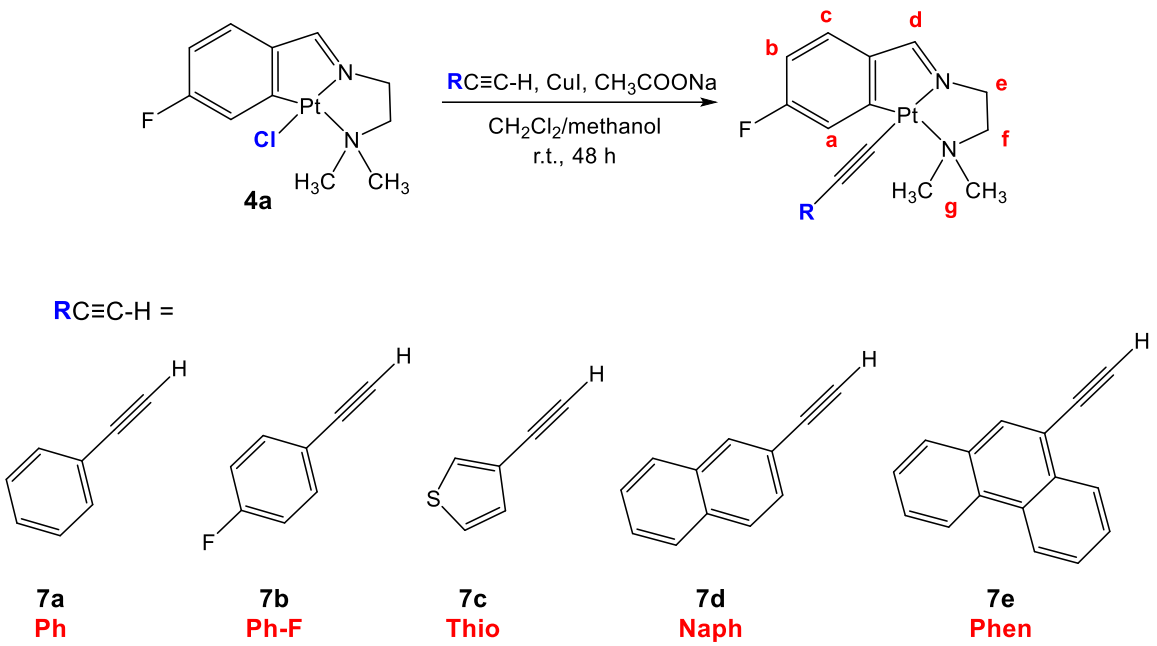

Scheme 5.1. Synthesis of compounds **7**. The letters in red are used for NMR assignment.

All compounds were characterised by ^{1}H and ^{19}F NMR spectroscopy, mass spectrometry and infrared spectroscopy confirming the correct formation of the desired products. The disappearance of the alkynyl terminal proton as well as the presence of the new aromatic signals with significant shifts regarding the free alkynyl ligand were observed by ^{1}H NMR. As seen in previous compounds with an analogous cyclometallated structure, the dimethylamino protons appear as a singlet (δ = 3 ppm) coupled to platinum

(^{3}J(Pt-H) = 20 Hz) as is the proton adjacent to the metallated carbon (H^a) with a coupling constant around 70 Hz. The iminic proton (H^d) for all compounds appears as a singlet coupled to platinum with coupling constants ranging between 79 to 81 Hz. This value is significantly lower than that of their precursor **4a** (^{3}J(Pt-H) = 141 Hz), which agrees with the higher *trans* influence of an alkynyl ligand *versus* a chlorido, which results in the weakening of the Pt-N bond in *trans*.[23]

Additionally, one single peak was observed in ^{19}F NMR which is not significantly affected by the exchange of the chlorido for the alkynyl moiety. A second signal is present for compound **7b** due to the presence of the *p*-fluorobenzene group. Furthermore, all molecular peaks were identified by ESI(+) mass spectrometry as well as the identification of the C≡C vibration band around 2100 cm^{-1} observed by IR spectroscopy, where the absence of the C≡*C-H* stretch was confirmed.

Elemental analyses were performed for all compounds, obtaining results that matched the desired structure only for compounds **7a**, **7b** and **7c**. This could be due to the difficulty in the analyses of fluorinated compounds previously reported in the literature.[24] However, all other techniques along with the following photophysical studies can support the purity of all compounds.

5.2.2. X-ray crystal structure determination

Single crystals suitable for X-ray diffraction were obtained for compounds **7b**, **7c** and **7d**. One single molecule is present in the asymmetric unit of compounds **7b** and **7d** while three independent molecules are observed in the asymmetric unit of compound **7c** (*Figure 5.2*). As expected for these compounds, the platinum adopts a square planar geometry completed by the tridentate [C,N,N'] ligand and the alkynyl aromatic group *trans* to the imine.

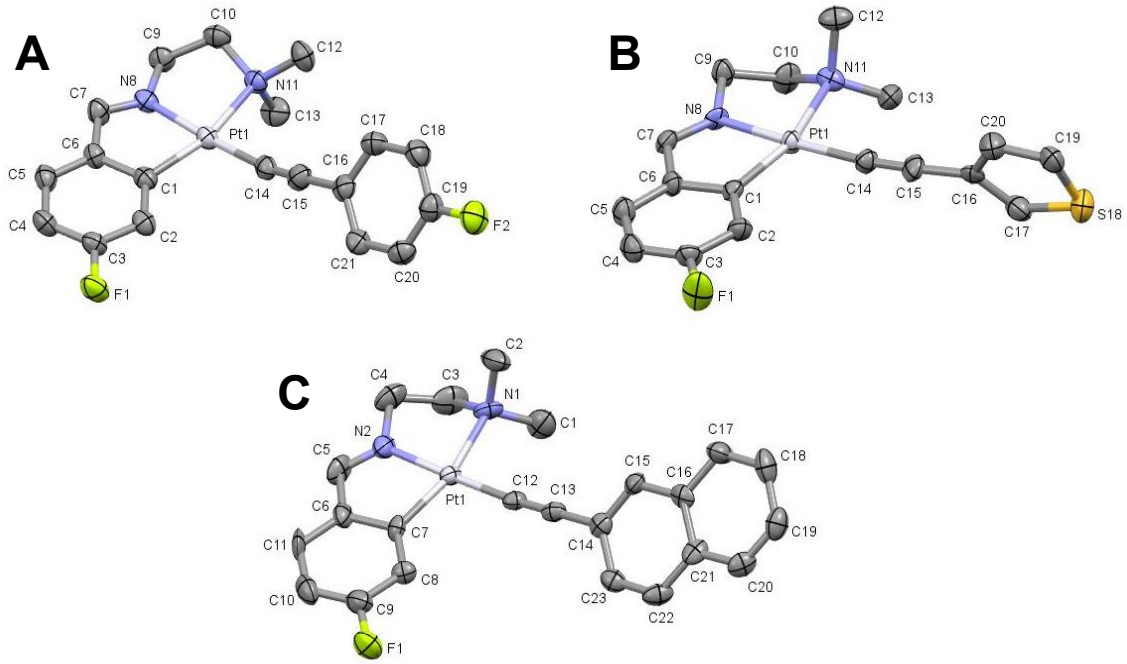

Figure 5.2. Molecular structure of compounds **7b** (A), **7c** (B) and **7d** (C). Selected bond lengths (Å) and angles (deg.) with estimated standard deviations. For **7b**: Pt(1)–N(8): 2.010(6); Pt(1)–N(11): 2.176(5); Pt(1)–C(14): 2.002(7); Pt(1)–C(1): 1.999(6); C(14)–C(15): 1.161(9); N(8)–Pt(1)–N(11): 81.9(2); C(1)–Pt(1)–N(8): 81.5(2); C(1)–Pt(1)–C(14): 97.2(3); C(14)–Pt(1)–N(11): 99.1(2); Pt(1)-C(14)-C(15): 170.05. For **7c**: Pt(1)–N(8): 2.001(11); Pt(1)–N(11): 2.157(12); Pt(1)–C(14): 1.992(15); Pt(1)–C(1): 1.984(14); C(14)–C(15): 1.180(2); N(8)–Pt(1)–-N(11): 81.6(5); C(1)–Pt(1)–N(8): 81.6(5); C(1)–Pt(1)–C(14): 100.0(6); C(14)–Pt(1)–N(11): 96.7(5); Pt(1)-C(14)-C(15): 174.03. For **7d**: Pt(1)–N(2): 1.990(11); Pt(1)–N(1): 2.161(11); Pt(1)–C(12): 1.963(13); Pt(1)–C(7): 2.005(14); C(12)–C(13): 1.199(18); N(2)–Pt(1)–N(1): 82.4(5); C(7)–Pt(1)–N(2): 81.5(5); C(7)–Pt(1)–C(12): 98.1(5); C(12)–Pt(1)–N(1): 98.1(5); Pt(1)-C(14)-C(15): 174.72. The thermal ellipsoids are drawn at the 50% probability level. Hydrogens have been omitted for clarity.

Bond lengths and angles are in the same range of those reported in the literature for analogous compounds.[23,25,26] No significant differences in the distances around the platinum atom were observed between compounds with different alkynyl aromatic bonds. However, Pt-N_{imine} distances are larger for compounds **7** (2.010 Å for **7b**, 2.001 Å for **7c** and 1.990 Å for **7d**) when compared to their precursor **4a** (1.962 Å). This is consistent with the higher *trans* influence of the alkynyl group and agrees with the lower platinum coupling constant observed by ^{1}H NMR for these new family of compounds.

The alkynyl chromophore is at a nearly linear conformation with the platinum atom with angles between 170º and 175º for all compounds and its aromatic ring is nearly perpendicular to the tridentate [C,N,N']-platinum coordination plane.

The crystalline packing of compounds **7c** and **7d** (*Figures 5.3 and 5.4*) shows intermolecular short contacts involving the fluorine atom (**7c**, d(F···H) = 2.551 Å; **7d**, d(F···H) = 2.552 Å), while for **7b** the most relevant intermolecular short contacts involve the alkynyl moiety or the platinum atom (d(C···H) = 2.689 Å) and d(Pt···H) = 2.782 Å (*Figure 5.5*). The latter are known as σ-hole interactions where uncommonly, the platinum centre acts as a nucleophile and displays an intermolecular interaction with a hydrogen donor, the aromatic proton in this case. This has been reported in the literature for several compounds.[27]

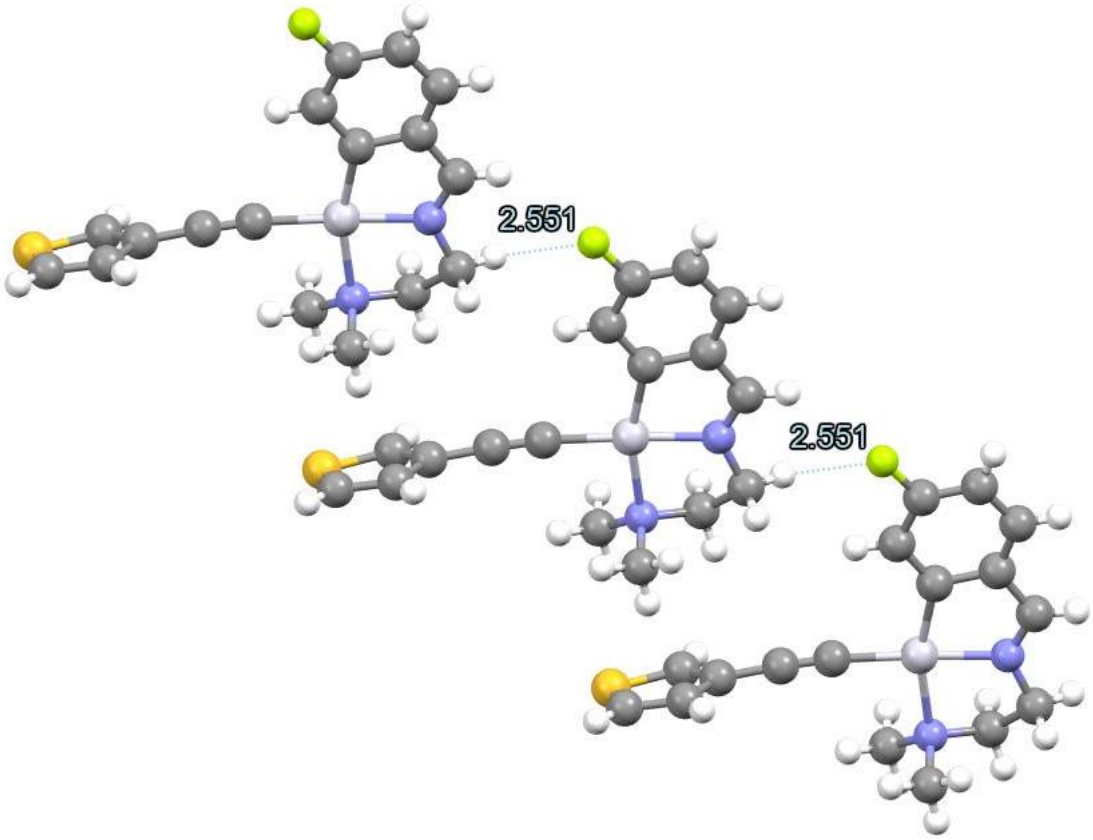

Figure 5.3. A view of the structure of compound **7c** with relevant intermolecular short contacts highlighted in blue: F(1)-H(9): 2.551 Å.

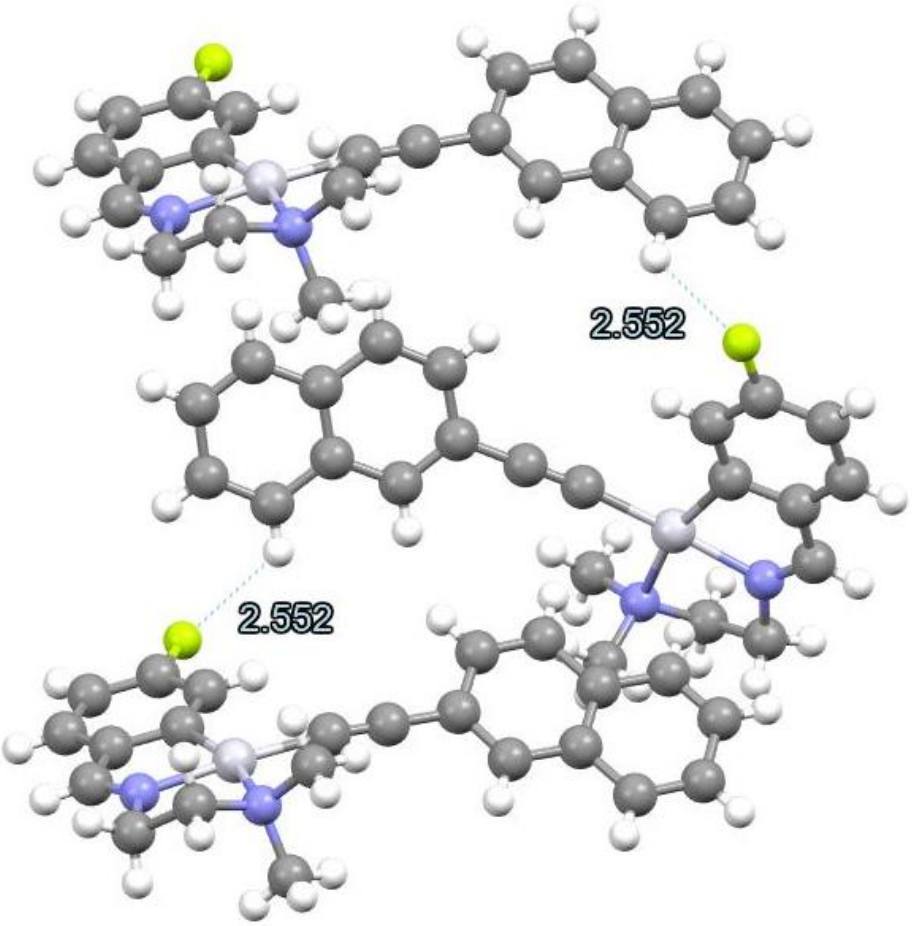

Figure 5.4. A view of the structure of compound **7d** with relevant intermolecular short contacts highlighted in blue: F(1)-H(17): 2.552 Å.

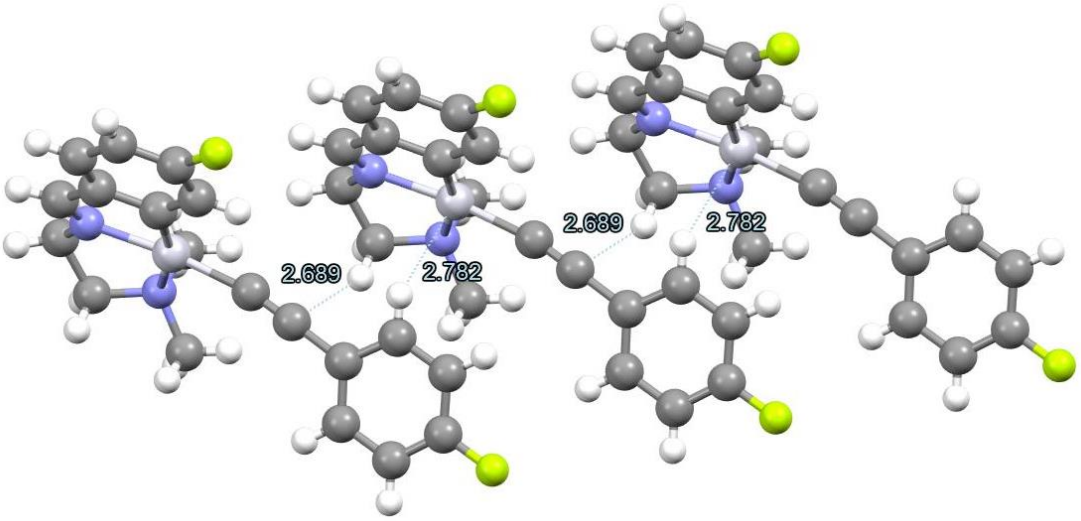

Figure 5.5. A view of the structure of compound **7b** with relevant intermolecular short contacts highlighted in blue: Pt(1)-H(21): 2.782 Å; C(15)-H(9B): 2.689 Å.

5.2.3. Photophysical characterization

Absorption and emission spectra of all the compounds were recorded in $1.3 \cdot 10^{-5}$ M acetonitrile solutions at room temperature. The results are summarized in *Table 5.1*.

Table 5.1. Spectral data for all compounds in acetonitrile solutions at 298 K.

Compound	Absorption λ_{max}/nm (ε x 10^{-3}/ M^{-1} cm^{-1})	Emission λ_{max}/nm	ϕ_{Ph} (with O_2)[a]	ϕ°_{Ph} (N_2 sat.)[a]	τ°_{Ph} (ns) (N_2 sat.)[b]
4a	378 (7.7)	629	0.005	0.016	353
7a	282 (21.6), 342 (6.6), 382 (7.6)	624	0.005	0.023	438
7b	278 (21.2), 342 (6.9), 382 (7.7)	625	0.007	0.023	491
7c	280 (14.7), 342 (5.6), 382 (6.2)	626	0.009	0.018	557
7d	297 (8.0), 309 (8.2), 386 (3.4)	626	0.008	0.025	464
7e	333 (10.1), 380 (3.5)	624	0.008	0.028	579

[a] Phosphorescence quantum yields ϕ_{Ph} obtained in aerated (with O_2) or degassed (N_2 saturated, N_2 sat.) acetonitrile solutions. [B] Phosphorescence lifetimes τ_{Ph}^{o} obtained in degassed (N_2 saturated, N_2 sat.) acetonitrile solutions using time-correlated single-photon counting technique.

Several bands are present in the absorption spectra of compounds **7** and their precursor **4a** with moderate molar extinction coefficients ε values (*Figure 5.6*). According to previous data, the lowest energy absorption band centred around 380 nm can be attributed to a Pt(5d)→π*(ligand) metal to ligand charge transfer (MLCT) mixed with intraligand transition. A higher energy absorption band in the 280-300 nm range is also recorded for all compounds. This band is also recorded for the free imine as it was recorded in *Chapter 3*, and therefore can be assigned to a π-π* intraligand transition intrinsic of the cyclometallated ligand.[28–30] Furthermore, compounds **7d** and **7e** present additional bands at 309 nm and 333 nm, respectively, which correspond to transitions typical of the naphthyl and phenanthryl chromophores and that are also observed in the corresponding free alkynyl ligand.

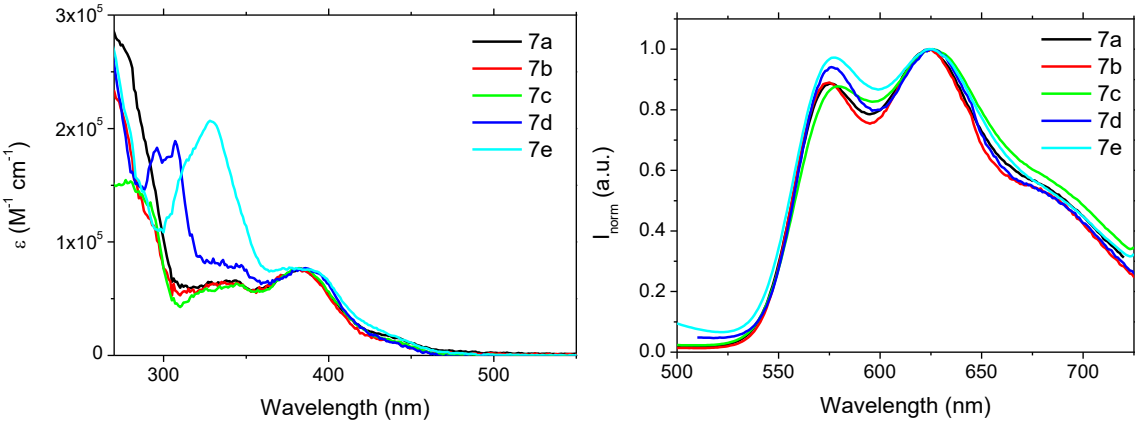

Figure 5.6. Absorption spectra (left) and normalized emission spectra (right) for $1.3 \cdot 10^{-5}$ M acetonitrile solutions of compounds **7** at 298 K (λ_{exc} = 625 nm).

Emission spectra for all compounds show a vibronically structured band centred at ca. 625 nm, with progressional spacings of 1200 cm^{-1}, typical of ν(C=N) and ν(C=C) stretching frequencies, which demonstrates the involvement of the cyclometallated ligand character in the emission origin, as previously observed for compounds derived from the same structure. The large Stokes' shift and the quenching in the emission intensity by the presence of oxygen indicates a triplet origin for this luminescence. This is typical of platinum compounds due to its heavy atom effect, which favours the intersystem crossing enhancing the triplet population and therefore, the phosphorescence emission. Specifically, in accordance with the literature, it can be assigned to a ^{3}IL transition mixed with ^{3}MLCT transitions involving the cyclometallating ligand, supported by the obtention of the same emission profile independent of the alkynyl aromatic chromophore.[23,25,26]

Phosphorescence lifetimes (τ_{Ph}^{o}) were also recorded for nitrogen saturated solutions using a time-correlated single-photon counting technique (ns-TCSPC) (*Table 5.1*). The values, between 430-580 ns for the new compounds **7**, with a lower value for their precursor **4a** (τ_{Ph}^{o} = 353 ns), support a triplet origin where the $T_1 \rightarrow S_0$ transition is allowed thanks to the spin orbit coupling provided by the platinum atom. As previously mentioned, the phosphorescence quantum yields for compounds **4a** and **7** increase in the absence of oxygen, still presenting moderate values, which are slightly lower for the chlorido analogue **4a** (*Table 5.1*). Higher values have been recorded for other cyclometallated platinum(II) compounds with aromatic alkynyl ligands, but they usually present a

completely aromatic structure in contrast with the flexible ethylene chain present in the cyclometallating imine in these compounds.[31]

5.2.4. ns-transient absorption

Time-resolved transient absorption experiments were performed to further understand the characteristics of the excited states of all compounds. Firstly, transient triplet-triplet absorption spectra were recorded by flash photolysis at 355 nm (ns-TA) for degassed acetonitrile solutions for all derivatives (*Figure 5.7*). The spectra show, besides the ground state depletion in the 380-410 nm range, intense broad triplet-triplet absorption bands in the 420-700 nm range for all compounds. This allows to confirm that, as the transient triplet-triplet absorption maxima ($\lambda_{max}^{T_1 \rightarrow T_n}$, *Table 5.2*) are constant for the different alkynyl aromatic derivatives **7** and their precursor **4a**, the triplet state is much more localised in the cyclometallated unit.

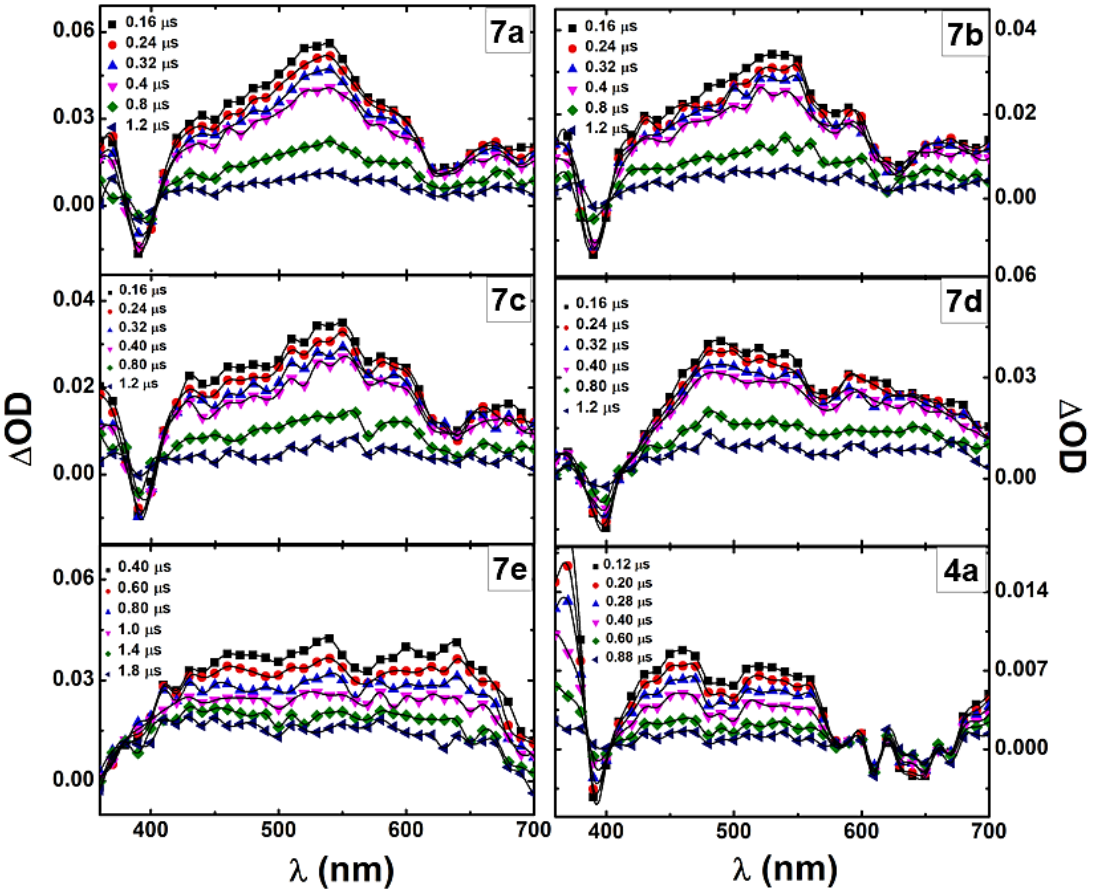

Figure 5.7. Room temperature time-resolved transient triplet-triplet absorption spectra for compounds **7** and their precursor **4a** collected by laser flash photolysis at 355 nm (ns-TA) in degassed acetonitrile solutions.

Therefore, this allows us to confirm that the phosphorescence emission of compounds **7** arises from a triplet state were the alkynyl aromatic moiety is not participating, which supports the previous assignment of the phosphorescence emission band as an ^{3}IL transition mixed with ^{3}MLCT intrinsic of the cyclometallated unit. Upon further analysis of these data, triplet state lifetimes (τ_T) were also recorded for all compounds (*Table 5.2*), with values ranging from 630 to 1200 ns for compounds **7**, with a slightly lower value for compound **4a** (τ_T = 423 ns). This implies that the triplet deactivation occurs faster for the precursor with a chlorido ligand than for the aromatic alkynyl derivatives, with further investigation required to understand the specific deactivation pathways.

Table 5.2. ns-TA data for all compounds[a]

Compound	$\boldsymbol{\lambda_{max}^{T_1 \rightarrow T_n}}$**(nm)**	$\boldsymbol{\tau_T}$ **(ns) (N_2 sat.)**
4a	460	423
7a	540	630
7b	540	700
7c	540	650
7d	490	700
7e	540	1200

[a] Transient $T_1 \rightarrow T_n$ maxima and triplet-state lifetimes τ_T obtained from ns-ms laser flash photolysis in deareated (N_2 saturated, N_2 sat.) acetonitrile solutions.

5.2.5. fs-transient absorption

Femtosecond transient absorption (fs-TA) experiments were performed to acquire additional information on the excited state formation and deactivation processes. The obtained data is shown in *Figure 5.8* for compound **7a** as an example. For all compounds **7** and their precursor **4a**, the spectra show a positive overlapped transient absorption band between 430 and 690 nm that corresponds to the convolution of the single excited state absorption ($ESA^{(S_1-S_n)}$) and the triplet excited state absorption ($ESA^{(T_1-T_n)}$) (*Figure 5.8 A*). Although the overlapping between these bands is strong, due to their spectral

resemblance at longer delay times with the triplet-triplet absorption spectra (*Figure 5.7*) and their long-lived nature (kinetic traces not decaying at the fs-TA time window, 7.6 ns), we can assign them to the excited state absorption, following intersystem crossing.

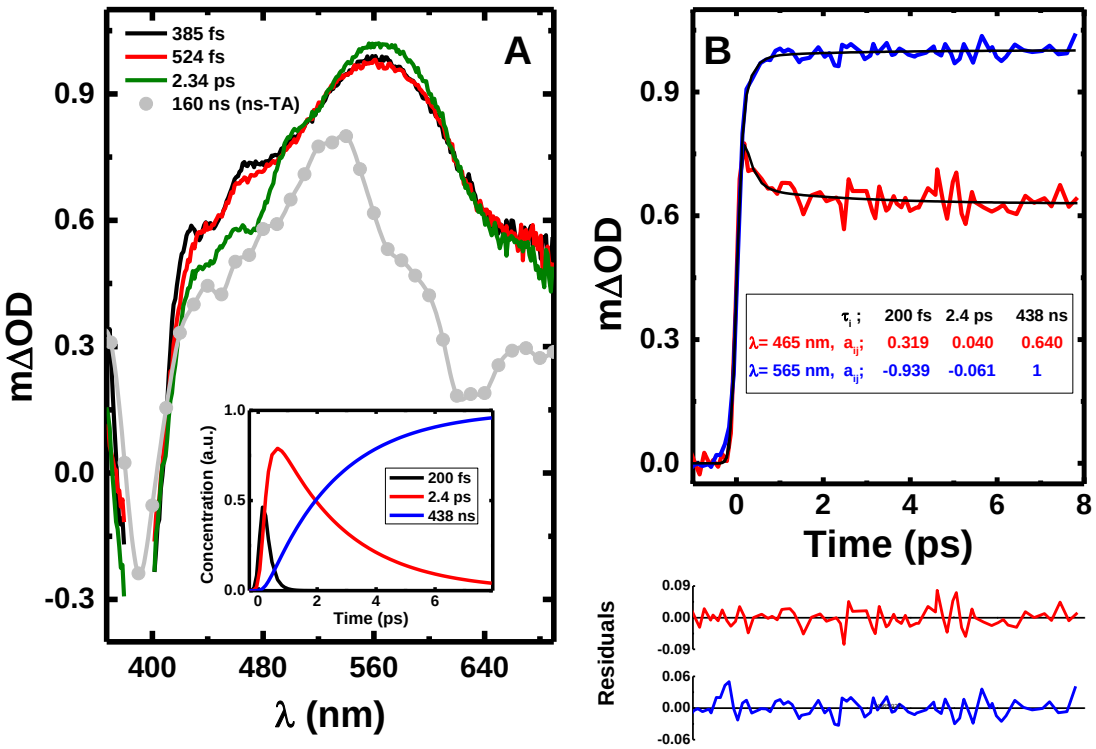

Figure 5.8. (A) Room temperature femtosecond time-resolved transient absorption data for compound **7a** collected in an aerated acetonitrile solution with excitation at 390 nm, together with the normalized ns-ms transient absorption spectra collected at 160 ns after laser flash photolysis; as inset the concentration profiles of the time constants obtained from the analysis to the transient absorption data are presented; the fs-TA data in the spectral range 380-400 nm is not shown because it is disturbed by the scattered pump beam. **(B)** Representative kinetic traces with fits, lifetimes and pre-exponential values resulting from the analysis of the transient absorption data; for a better judgment of the quality of the fits the residuals are also shown.

The best fitting results and kinetic data are shown in *Table 5.3* for all compounds and the decay profile is shown in *Figure 5.8 B* for compound **7a** as an example.

For all cases, the kinetic traces fit well with a tri-exponential decay consisting of a fast decay transient with values around 200 fs, a second decay with values from 0.5 ps to 3.8 ps and a long-lived transient decay associated to the deactivation of the triplet excited state that was fitted to the previously obtained values (ns-TA).

The fastest lifetime can be attributed to solvation dynamics as it agrees with the solvent relaxation time of acetonitrile (0.26 ps)[32] while the second can be attributed to the decay

of the singlet excited state which undergoes a rapid intersystem crossing ($\tau^{S_1 \sim \rightarrow T_1}$) to then give the observed long-lived triplet state. Interestingly, it can be observed that this rapid intersystem crossing is even faster for the precursor **4a** than for compounds **7** (*Table 5.3*). The fact that this triplet state is formed at the expense of the singlet excited state is supported by the observed negative values associated with the 0.5-3.8 ps lifetime in the wavelength where the $ESA^{(T_1-T_n)}$ occurs (565 nm, *Figure 5.8 B*) together with the concentration profiles and the distinct rise of the long-lived 438 ns time constant (*Figure 5.8 A*). This confirms that the presence of the enhanced spin-orbit coupling induced by the platinum atom is indeed allowing the decay of the triplet state with a $T_1 \rightarrow S_0$ transition.

Table 5.3. Intersystem crossing rate constants[a]

Compound	$\tau^{S_1 \sim \rightarrow T_1}$ (ps)	$k'^{S_1 \sim \rightarrow T_1}_{ISC}$ x10^{11} (s)
4a	0.5	9.4
7a	2.4	0.8
7b	3.2	0.3
7c	2.9	1.0
7d	1.1	1.1
7e	3.8	0.4

[a] Obtained from the results of the global fit analysis to the fs-TA data in aerated acetonitrile solutions of all compounds at 293 K.

In addition, the intersystem crossing (ISC) rate constants $k'^{S_1 \sim \rightarrow T_1}_{ISC}$ were also calculated by assuming a unitary singlet oxygen sensitisation efficiency ($S_\Delta = \frac{\Phi_T}{\Phi_\Delta}$), which implies that the triplet state formation quantum yield (ϕ_T) can be approximated to the singlet oxygen sensitization quantum yield (ϕ_Δ, *Table 5.4*) ($\phi_T \cong \phi_\Delta$), using the following equation:

$$k'^{S_1 \sim \rightarrow T_1}_{ISC} = \frac{\Phi_T}{\tau_{S_1 \sim \rightarrow T_1}} \quad (1)$$

where the decay lifetime and quantum yield were determined in aerated acetonitrile solutions. The fast triplet state formation is again supported by these values for all compounds, with a higher rate constant for the precursor **4a** (*Table 5.3*).

5.2.6. Singlet oxygen production

Singlet oxygen sensitisation quantum yields (ϕ_Δ) were determined by comparison of the near-infrared phosphorescence signal of $^1O_2$ at 1270 nm of all compounds in aerated acetonitrile solutions with that obtained for 1H-phenalenone in toluene as a reference (*Table 5.4*). These signals were measured by flash photolysis upon excitation at 355 nm and ϕ_Δ were calculated using the following equation:

$$\Phi_\Delta = \frac{slope_{cp}}{slope_{ref}} x \frac{Abs_{ref}}{Abs_{cp}} x \frac{n^2_{solv,cp}}{n^2_{solv,ref}} x \Phi_\Delta^{ref} \qquad (2)$$

where slope is obtained by plotting the photosensitized singlet oxygen phosphorescence intensity at 1270 nm as a function of the laser energy, Abs corresponds to the absorption value at 355 nm, n^2_{solv} refers to the refraction index of the corresponding solvent and Φ_Δ^{ref} is the known singlet oxygen sensitisation quantum yield for the reference (ϕ_Δ (1H-phenalenone, toluene, 298 K) = 0.93).

The obtained results present moderate values but in the range of those reported in the literature for some platinum complexes.[33,34] However, the complexes that present the higher singlet oxygen sensitisation are those where the platinum is directly attached to a macrocyclic structure such as a porphyrin or a calixarene.[35–38] For all of them, it is agreed that the presence of the platinum heavy atom, which increases the efficiency of the intersystem crossing and allows a long-lived triplet state, is crucial for this generation of $^1O_2$.[39]

Table 5.4. Singlet oxygen sensitisation, internal conversion quantum yields and calculated rate constants in aerated acetonitrile solutions at 298 K.

Compound	Φ_Δ (with O_2)[a]	$\Phi_{IC}^{S_1 \rightarrow S_0}$ [b]	k_{ET} x10^6 (s)[b]	k_{Ph} x10^6(s)[b]	$k_{ISC}^{T_1 \rightarrow S_0}$ x10^6(s)[b]
4a	0.47	0.53	6.23	0.07	2.76
7a	0.21	0.79	8.21	0.20	2.09
7b	0.11	0.89	4.66	0.30	1.74
7c	0.29	0.71	1.80	0.06	1.74
7d	0.12	0.88	4.58	0.31	1.85
7e	0.16	0.84	4.32	0.22	1.51

[a] Singlet oxygen sensitization quantum yields (ϕ_Δ). [b] Internal conversion quantum yields (ϕ_{IC}) and associated rate constants, k_{ET}, radiative phosphorescence decay, k_{Ph}, and intersystem crossing, $k_{ISC}^{T_1 \sim \rightarrow S_0}$. $\Phi_{IC}^{S_1 \rightarrow S_0} = 1 - \phi_F - \phi_T$, assuming $\phi_F \rightarrow 0$ and unitary singlet oxygen sensitization efficiency $S_\Delta = \frac{\Phi_T}{\Phi_\Delta}$ and therefore $\phi_T \cong \phi_\Delta$.

To calculate the pseudo-unimolecular rate constant of energy transfer that leads to the formation of singlet oxygen (k_{ET}), the following Stern-Volmer type relation can be retrieved (assuming a negligible effect of oxygen in the singlet lifetime as can be seen in the fs-TA data):

$$\frac{\Phi_{Ph}^{\circ}}{\Phi_{Ph}} = 1 + \tau_{Ph}^{\circ} k_{ET} \qquad (3)$$

where Φ_{Ph} and Φ_{Ph}° are the phosphorescence quantum yields recorded in acetonitrile in the presence and absence of oxygen and τ_{Ph}° is the phosphorescence decay obtained in deaerated acetonitrile. The values of k_{ET} calculated with this equation are summarized in *Table 3.4*.

Afterwards, the following relation can be established between the singlet oxygen sensitisation quantum yield (Φ_Δ) and the phosphorescence quantum yield (Φ_{Ph}) obtained in the presence of oxygen:

$$\frac{\Phi_\Delta}{\Phi_{Ph}} = \frac{k_{ET}}{k_{Ph}} \qquad (4)$$

where k_{Ph} is the radiative constant for phosphorescence that can be obtained once k_{ET} is known.

Finally, the non-radiative rate constant for intersystem crossing between $T_1 \sim \rightarrow S_0$, $k_{ISC}^{T_1 \sim \rightarrow S_0}$, can be calculated using the following two equations:

$$k_{ISC}^{T_1 \sim \rightarrow S_0} = \frac{1}{\tau_{Ph}} - k_{Ph} - k_{ET} \quad (5) \qquad \text{or} \qquad k_{ISC}^{T_1 \sim \rightarrow S_0} = \frac{1}{\tau_{Ph}^{o}} - k_{Ph} \quad (6)$$

Upon analysis of all the calculated parameters (*Table 5.4*), in the absence of O_2, the main deactivation pathway corresponds to the radiationless internal conversion process ($\Phi_{IC}^{S_1 \rightarrow S_0} = 1 - \phi_F - \phi_T$) for all compounds. This agrees with previously observed low phosphorescence quantum yields even in the deaerated conditions.

The pathway leading to the formation of $^1O_2$ (k_{ET}) is always predominant among the rate constants, being higher in all cases than the internal conversion process ($k_{ISC}^{T_1 \sim \rightarrow S_0}$). Both k_{ET} and the radiative rate constant for the triplet emission (k_{Ph}) are affected by the change in the ancillary ligand from a chlorido to an alkynyl aromatic moiety, except for the tiophene derivative. Compounds **7** present a significant increase in the k_{Ph}, being still significantly lower than the internal conversion, regarding their precursor **4a**.

5.2.7. Theoretical studies

Theoretical calculations were performed at the DFT/B3LYP level to further understand the photophysical properties of all compounds. Firstly, the optimisation of the geometry revealed that the minimum energy conformation consists in a perpendicular disposition between the square planar geometry around the platinum and the aromatic alkynyl moiety, which agrees with the obtained X-ray crystal structures and validates the theoretical model.

To confirm that this conformation is maintained in solution, the absorption spectra of compound **7a** was calculated in the perpendicular, oblique, and parallel disposition between the metallacycle and the aromatic chromophore. As it can be seen in *Figure 5.9.*, the perpendicular disposition is the one that better reproduces the experimental spectra and, therefore, it was chosen to perform the calculations of all spectra in acetonitrile.

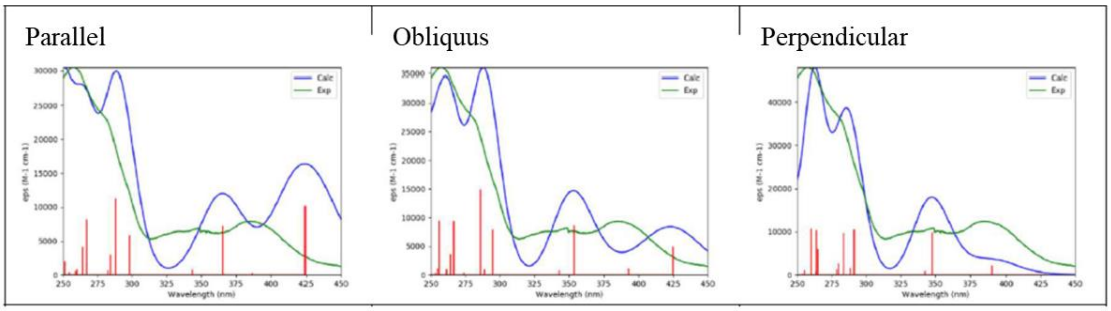

Figure 5.9. Calculations of the UV-visible spectrum of compound **7a** taking into consideration the different possible conformations in solution. Each graphic contains the experimental data (green), calculated transitions (red) and the calculated spectrum (blue).

The molecular orbitals involved in the main transitions were calculated for all compounds and are shown in *Figure 5.10* for compound **7a** as an example along with its absorption transitions in *Table 5.5*. In all cases, the HOMO orbital is in the platinum-alkynyl moiety, with the closest occupied orbitals HOMO-1 and HOMO-2 located in the Pt-alkynyl bond and the aryl ring of the cyclometallated unit, and HOMO-3 mainly located at the metal. The lowest occupied molecular orbital (LUMO) is mainly centred in the π* orbital of the phenyl ring of the metallacycle. Therefore, the lower energy absorption bands can be assigned to ^{1}LLCT (C≡C → C^N) /^{1}MLCT transitions. Several high energy transitions between 260-290 nm can be observed. The most intense one corresponds to a HOMO → LUMO +4 transition, where both orbitals correspond mainly to the alkynyl group with a small contribution of the d-orbitals of the metal. Additionally, the cyclometallated fragments is also contributing to LUMO+4. Thus, these can be regarded as mainly π-π* intraligand transitions.

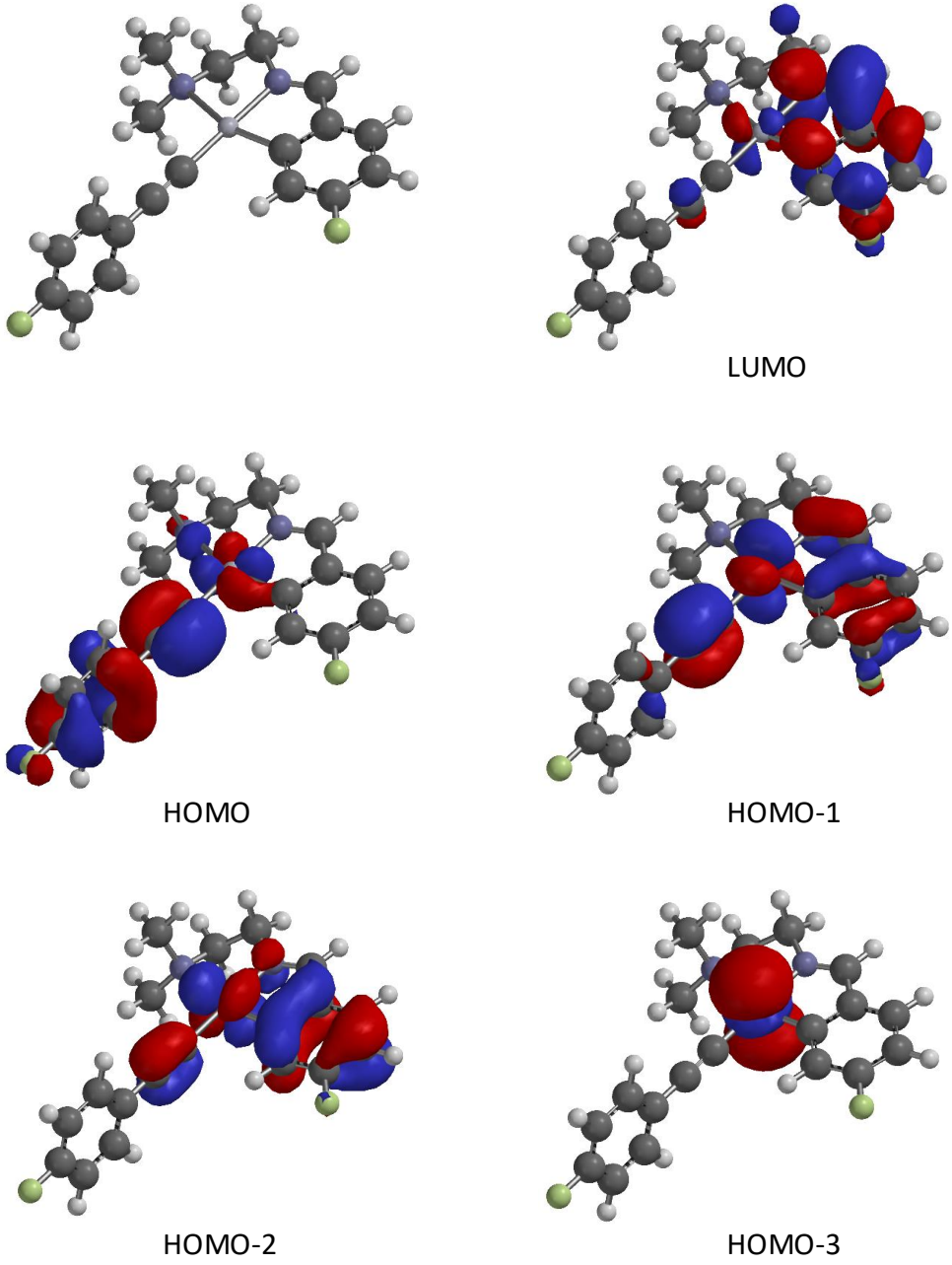

Figure 5.10. Selected frontier molecular orbitals involved in the transitions of compound 7**a** in the ground state.

Table 5.5. Absorption transitions (experimental and calculated) and corresponding calculated force strength (f) and assigned transitions for compound **7a**.

λ_{exp} (nm)	λ_{calc} (nm) (f)	Assignation
450	420.3 (0.0011)	HOMO → LUMO
385	385.8 (0.0349)	HOMO-1 → LUMO
344	345.7 (0.1997)	HOMO-2 → LUMO
284sh	289.8 (0.1377)	HOMO → LUMO+1
	287.7 (0.0744)	HOMO-1 → LUMO+1
	283.2 (0.2100)	HOMO-4 → LUMO
	277.4 (0.0660)	HOMO → LUMO+2
269	264.5 (0.0510)	HOMO-1 → LUMO+4
	262.1 (0.2403)	HOMO → LUMO+4
	258.5 (0.2075)	HOMO-1 → LUMO+2

Finally, the vertical energies corresponding to the transitions between the first singlet (fluorescence) or triplet (phosphorescence) excited states were calculated to further understand the luminescence results using in each case the optimised geometry in the corresponding excited state. The calculations predict a triplet emission from the LUMO+1/LUMO to HOMO/HOMO-1 orbitals (*Table 5.6*), with predicted wavelengths in agreement with the experimental data, which confirms the phosphorescent origin of the emission. Furthermore, both HOMO-1 and HOMO present contribution from the metal as well as from the alkynyl moiety, with the LUMO mainly located in the cyclometallating ligand. This confirms and supports the assignment of the phosphorescence band to a mixture of ^{3}IL and ^{3}MLCT transitions.

Table 5.6. Predicted singlet and triplet transitions for all complexes including the expected wavelength and the orbitals involved in the transition.

Compound	Singlet λ_{em} (nm) (f) / transition	Triplet λ_{em} (nm) / transition
4a	457 (0.0174) LUMO → HOMO (88%)	629 LUMO → HOMO (81%)
7a	491 (0.0008) LUMO → HOMO (98%)	607 LUMO → HOMO-1 (77%) 522 LUMO → HOMO (97%)
7b	496 (0.0012) LUMO → HOMO (98%)	496 LUMO → HOMO-1 (75%) 429 LUMO → HOMO (96%)
7c	507 (0.0018) LUMO → HOMO (98%)	608 LUMO → HOMO-1 (76%) 548 LUMO → HOMO (97%)
7d	482 (0.2675) LUMO → HOMO (96%)	609 LUMO → HOMO-1 (78%) 536 LUMO+1 → HOMO (77%) 531 LUMO → HOMO (90%)
7e	514 (0.0226) LUMO → HOMO (96%)	608 LUMO → HOMO-1 (75%) 591 LUMO+1 → HOMO (88%) 550 LUMO → HOMO (96%)

5.3. Conclusions

The photophysical analysis of this family of [C,N,N'] cyclometallated platinum(II) compounds derived from the same structure as those reported in *Chapter 3* but with the introduction of an alkynyl aromatic chromophore as an ancillary ligand has been described.

These new compounds present similar luminescent properties as their analogues containing halido ligands, presenting a phosphorescent emission that can be assigned to a ^{3}IL mixed with ^{3}MLCT transition, with slightly higher quantum yield values for the alkynyl derivatives. Additionally, this assignment has been confirmed by DFT calculations that have determined the orbitals involved in both this and the absorption transitions.

Thanks to the use of flash photolysis techniques, a more in depth photophysical analysis has provided further information in the formation and deactivation pathways of the triplet state of all compounds. Both these phenomena have been observed to be faster for the chlorido precursor that the alkynyl aromatic final compounds.

Additionally, all compounds have proved to be able to efficiently sensitise molecular oxygen with singlet oxygen sensitisation quantum yield values ranging from 11 to 47%, the latter corresponding to the chlorido derivative, which therefore could potentially have some biological or photocatalytic applications.

Although this generation of singlet oxygen is the preferred deactivation pathway for all compounds, the new compounds present a significant increase in the phosphorescence rate constant regarding their chlorido precursor. Overall, it could be stated that the substitution of the halido by an alkynyl aromatic moiety results in an enhancement in the efficiency of the phosphorescence emission of the resulting compounds.

5.4. Experimental Section

5.4.1. General procedures

Commercial reagents phenylacetylene (Sigma Aldrich, 98%), copper iodide (CuI, Riedel de Haën, >99%), sodium acetate (CH_3COONa, Carlo Erba, 99%), 1-ethynyl-4-fluorobenzene (Sigma Aldrich, 99%), 3-ethynyltiophene (Sigma Aldrich, 96%), 2-ethynylnaphthalene (Sigma Aldrich, 97%) and 9-ethynylphenanthrene (Sigma Aldrich, 97%); and solvents methanol (Sigma Aldrich, >99%), dichloromethane (CH_2Cl_2, Scharlau, 99%) and hexane (Sigma Aldrich, >98%) were used as received.

Compound $[PtCl\{(CH_3)_2N(CH_2)_2N{=}CH(4\text{-}FC_6H_3)\}]$ (**4a**)[23] was prepared as reported in the literature.

5.4.2. Physical measurements

NMR spectra were recorded in $CDCl_3$ at the Unitat de RMN of the Universitat de Barcelona with a Mercury 400 spectrometer (^1H, 400 MHz; ^{19}F, 376.5 MHz). Chemical shifts are given in δ values (ppm) relative to TMS (^1H) or $CFCl_3$ (^{19}F) and coupling constants J are given in Hz.

Infrared spectra were recorded in a Thermo Scientific FT-IR Nicolet iS5 spectrometer with an iD7 ATR accessory. IR frequencies ν are given in cm^{-1}.

Electrospray mass spectra were performed at the *Unitat d'Espectrometria de Masses (Universitat de Barcelona)* in a LC/MSD-TOF spectrometer using H_2O-CH_3CN 1:1 to introduce the sample.

Microanalyses were performed at the *Centres Científics i Tecnològics (Universitat de Barcelona)* using a Carlo Erba model EA1108 elemental analyser.

5.4.3. Synthesis and characterisation

Synthesis of [Pt(C≡CPh){$(CH_3)_2N(CH_2)_2N$=CH(4-FC_6H_3)}] (7a)

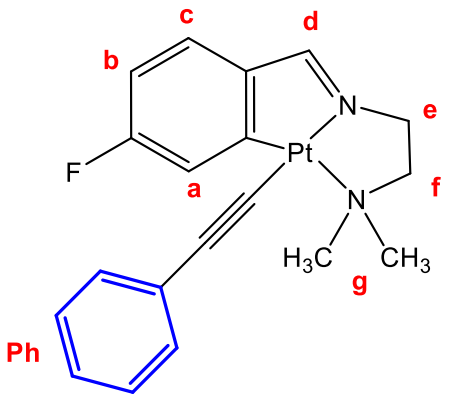

Compound [Pt(C≡CPh){$(CH_3)_2N(CH_2)_2N$=CH(4-FC_6H_3)}] (**7a**) was obtained from the reaction of 0.103 g (0.243 mmols) of [PtCl{$(CH_3)_2N(CH_2)_2N$=CH(4-FC_6H_3)}] (**4a**), 0.025 g (0.249 mmols) of phenylacetylene, 0.010 g (0.053 mmols) of CuI and 0.061 g (0.744 mmols) of sodium acetate in CH_2Cl_2/methanol (10:1). The mixture was stirred at room temperature under nitrogen and protected from light for 48 hours. The solvent was removed under vacuum and the residue was treated with hexane. The orange solid was filtered and dried under vacuum. Yield: 0.091 g (76%).

^{1}H NMR ($CDCl_3$, 400 MHz): δ 8.32 [s, 1H, ^{3}J(Pt-H) = 81.2, H^d]; 7.55 [dd, 1H, ^{3}J(F-H) = 9.6, ^{4}J(H-H) = 2.3, ^{3}J(Pt-H) = 70.2, H^a], 7.48 [d, 2H, ^{3}J(H-H) = 7.1, H^{Ph}], 7.22-7.24 [m, 3H, $H^{c,Ph}$], 7.15 [t, 1H, ^{3}J(H-H) = 7.4, H^{Ph}], 6.66 [td, 1H, ^{3}J(F-H) = ^{3}J(H-H) = 8.8, ^{4}J(H-H) = 2.6, H^b], 4.01 [t, 2H, ^{3}J(H-H) = 11.7, H^e], 3.15 [t, 2H, ^{3}J(H-H) = 6.0 Hz, H^f], 3.06 [s, 6H, ^{3}J(Pt-H) = 20.2, H^g]. **^{19}F NMR** ($CDCl_3$, 376.5 MHz): δ -108.44 [s, 1F]. **MS-ESI$^+$**: *m/z* 490.12 $[M + H]^+$. **IR**: υ 2097 (C≡C). **Anal. Found** (calcd for $C_{19}H_{19}FN_2Pt \cdot 0.5\ CH_2Cl_2$): C 44.86 (44.03); H 3.52 (3.79); N 5.24 (5.27).

Synthesis of [Pt(C≡CPh-F){$(CH_3)_2N(CH_2)_2N$=CH(4-FC_6H_3)}] (7b)

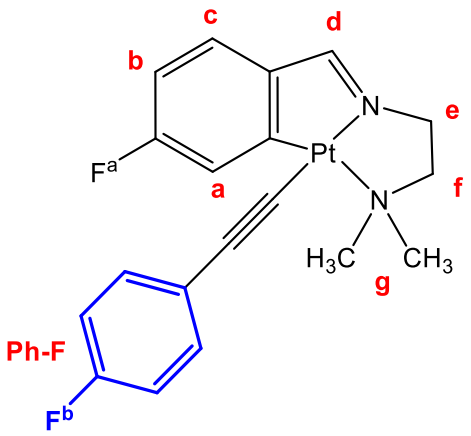

Compound [Pt(C≡CPh-F){$(CH_3)_2N(CH_2)_2N$=CH(4-FC_6H_3)}] (**7b**) was prepared as an orange solid by following the same method from 0.102 g (0.241 mmols) of [PtCl{$(CH_3)_2N(CH_2)_2N$=CH(4-FC_6H_3)}] (**4a**), 0.030 g (0.249 mmols) of 1-ethynyl-4-fluorobenzene, 0.010 g (0.053 mmols) of CuI and 0.063 g (0.768 mmols) of sodium acetate. Yield: 0.070 g (57%).

^{1}H NMR ($CDCl_3$, 400 MHz): δ 8.34 [s, 1H, ^{3}J(Pt-H) = 81.3, H^d], 7.53 [dd, 1H, ^{3}J(F-H) = 9.4, ^{4}J(H-H) = 2.7, ^{3}J(Pt-H) = 71.1, H^a], 7.43 [dd, J = 8.9, 5.5 Hz, 2H, H^{Ph-F}], 7.23 [m, 1H, H^c], 6.93 [t, 2H, ^{3}J(F-H) = ^{3}J(H-H) = 8.9 , H^{Ph-F}], 6.67 [td, 1H, ^{3}J(F-H) = ^{3}J(H-H) = 8.6, ^{4}J(H-H) = 2.6, H^b], 4.03 [t, 2H, ^{3}J(H-H) = 5.9 ,H^e], 3.15 [t, 2H, ^{3}J(H-H) = 6.0, H^f], 3.04 [s, 6H, ^{3}J(Pt-H) = 20.2, H^g]. **^{19}F NMR** ($CDCl_3$, 376.5 MHz): δ -103.98 [s, $1F^a$]; -115.55 [s, 1F, F^b]. **MS-ESI$^+$**: *m/z* 508.12 $[M + H]^+$. **IR**: υ 2100 (C≡C). **Anal. Found** (calcd for $C_{19}H_{18}F_2N_2Pt \cdot 0.5\ CH_2Cl_2$): C 42.59 (42.59); H 3.29 (3.48); N 5.12 (5.09).

Synthesis of [Pt(C≡CThio){$(CH_3)_2N(CH_2)_2N$=CH(4-FC_6H_3)}] (7c)

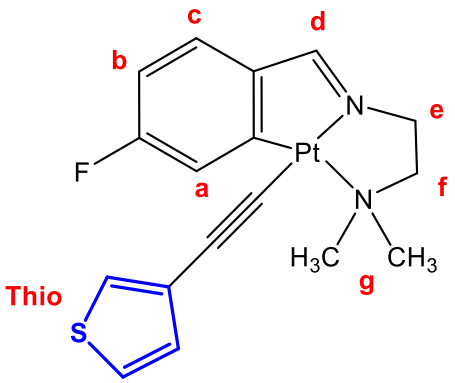

Compound [Pt(C≡CThio){$(CH_3)_2N(CH_2)_2N$=CH(4-FC_6H_3)}] (**7c**) was prepared as an orange solid by following the same method from 0.099 g (0.243 mmols) of [PtCl{$(CH_3)_2N(CH_2)_2N$=CH(4-FC_6H_3)}] (**4a**), 0.027 g (0.249 mmols) of 3-ethynyltiophene, 0.010 g (0.053 mmols) of CuI and 0.060 g (0.731 mmols) of sodium acetate. Yield: 0.086 g (74%).

^{1}H NMR ($CDCl_3$, 400 MHz): δ 8.35 [s, 1H, ^{3}J(Pt-H) = 80.9, H^d], 7.56 [dd, 1H, ^{3}J(F-H) = 9.6, ^{4}J(H-H) = 2.7, ^{3}J(Pt-H) = 70.7, H^a], 7.24 [m, 2H, $H^{c,Tioph}$], 7.19 [dd, 1H, ^{3}J(H-H) = 4.9, ^{3}J(H-H) = 3.0, H^{Tioph}], 7.14 [dd, 1H, ^{3}J(H-H) = 4.9, ^{3}J(H-H) = 1.1, H^{Tioph}], 6.66 [td, 1H, ^{3}J(F-H) = ^{3}J(H-H) = 8.6, ^{4}J(H-H) = 2.5, H^b], 4.03 [t, 2H, ^{3}J(H-H) = 6.4, H^e], 3.14 [t, 2H, ^{3}J(H-H) = 6.0, H^f], 3.04 [s, 6H, ^{3}J(Pt-H) = 20.5, H^g]. **^{19}F NMR** ($CDCl_3$, 376.5 MHz): δ -104.17 [s, 1F]. **MS-ESI$^+$**: *m/z* 496.08 $[M + H]^+$. **IR**: υ 2104 (C≡C). **Anal. Found** (calcd. for $C_{17}H_{17}FN_2PtS \cdot 0.5\ CH_2Cl_2$): C 39.07 (39.52); H 3.34 (3.37); N 5.31 (5.21); S 5.77 (5.96).

Synthesis of [Pt(C≡CNaph){$(CH_3)_2N(CH_2)_2N$=CH(4-FC_6H_3)}] (7d)

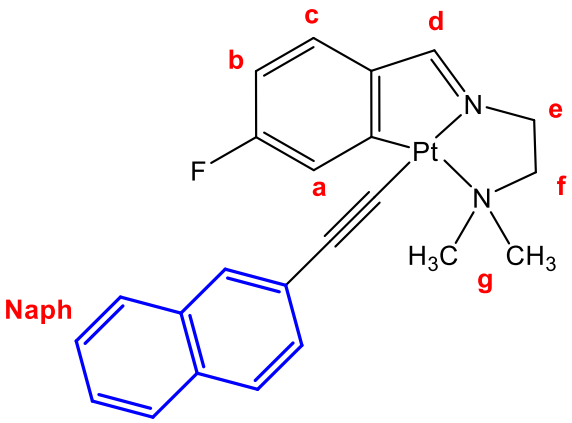

Compound [Pt(C≡CNaph){$(CH_3)_2N(CH_2)_2N$=CH(4-FC_6H_3)}] (**7d**) was prepared as an orange solid by following the same method from 0.051 g (0.120 mmols) of [PtCl{$(CH_3)_2N(CH_2)_2N$=CH(4-FC_6H_3)}] (**4a**), 0.019 g (0.125 mmols) of 2-ethynylnaphthalene, 0.005 g (0.026 mmols) of CuI and 0.029 g (0.359 mmols) of sodium acetate. Yield: 0.050 g (77%).

^{1}H NMR ($CDCl_3$, 400 MHz): δ 8.36 [s, 1H, ^{3}J(Pt-H) = 79.5, H^d], 7.92 [s, 1H, H^{Naph}]; 7.74 [t, 2H, ^{3}J(H-H) = 6.7, H^{Naph}]; 7.70 [d, 1H, ^{3}J(H-H) = 8.4, H^{Naph}]; 7.64 [d, 1H, ^{3}J(F-H) = 10.4, H^a]; 7.57 [d, 1H, ^{3}J(H-H) = 8.4, H^{Naph}]; 7.39 [m, 2H, H^{Naph}]; 7.26 [m, 1H, H^c]; 6.68 [t, 1H, ^{3}J(F-H) = ^{3}J(H-H) = 8.8, H^b], 4.04 [t, 2H, ^{3}J(H-H) = 6.2, H^e], 3.17 [t, 2H, ^{3}J(H-H) = 5.4, H^f], 3.10 [s, 6H, ^{3}J(Pt-H) = 19.6, H^g]. **^{19}F NMR** ($CDCl_3$, 376.5 MHz): δ -104.16 [s, 1F]. **MS-ESI$^+$**: *m/z* 539.14 $[M + H]^+$. **IR**: υ 2099 (C≡C).

Synthesis of [Pt(C≡CPhen){$(CH_3)_2N(CH_2)_2N$=CH(4-FC_6H_3)}] (7e)

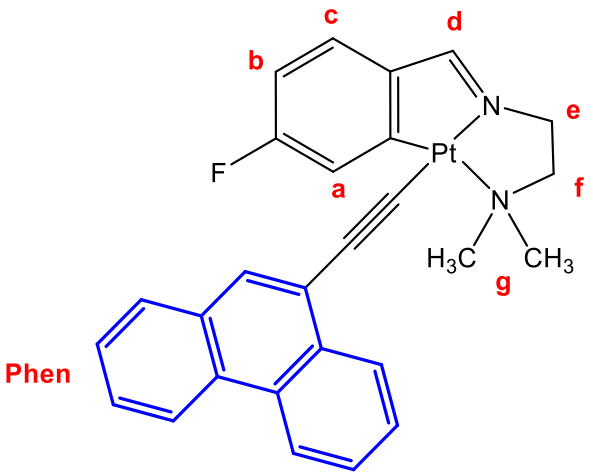

Compound [Pt(C≡CPhen){$(CH_3)_2N(CH_2)_2N$=CH(4-FC_6H_3)}] (**7e**) was prepared as an orange solid by following the same method from 0.052 g (0.123 mmols) of [PtCl{$(CH_3)_2N(CH_2)_2N$=CH(4-FC_6H_3)}] (**4a**), 0.025 g (0.125 mmols) of 9-ethynylphenanthrene, 0.005 g (0.026 mmols) of CuI and 0.031 g (0.378 mmols) of sodium acetate. Yield: 0.061 g (84%).

^{1}H NMR ($CDCl_3$, 400 MHz): δ 8.81 [m, 1H, H^{Phen}]; 8.65 [m, 1H, H^{Phen}]; 8.61 [d, ^{3}J(H-H) = 7.8, 1H, H^{Phen}]; 8.30 [s, 1H, ^{3}J(Pt-H) = 81.9, H^d], 7.96 [s, 1H, H^{Phen}]; 7.79 [d, ^{3}J(H-H) = 7.3, 1H, H^a]; 7.68 [dd, 1H, ^{3}J(H-H) = 9.6, ^{4}J(H-H) = 2.3, H^{Phen}], 7.63 [m, 2H, H^{Phen}]; 7.55 [m, 2H, H^{Phen}]; 7.26 [m, 1H, H^c], 6.68 [td, 1H, ^{3}J(F-H) = ^{3}J(H-H) = 8.5, ^{4}J(H-H) = 2.6, H^b], 4.53 [t, 2H, ^{3}J(H-H) = 6.2, H^e], 3.18 [t, 2H, ^{3}J(H-H) = 5.9, H^f], 3.12 [s, 6H, ^{3}J(Pt-H) = 19.3, H^g]. **^{19}F NMR** ($CDCl_3$, 376.5 MHz): δ -103.86 [s, 1F]. **MS-ESI$^+$**: *m/z* 590.16 $[M + H]^+$. **IR**: υ 2078 (C≡C).

5.4.4. X-ray Diffraction

Single crystals suitable for X-ray diffraction analysis were grown for **7b**, **7c**, and **7d** by slow diffusion of hexane in a dichloromethane solution of the compounds. The crystal data and experimental details for the data collections are given below. Single crystal X-ray data for **7b**, **7c**, and **7d** were collected at 170 K on a Bruker-Nonius KappaCCD diffractometer with an APEX-II detector with graphite-monochromatised Mo−Kα (λ = 0.71073 Å) radiation. Data collection was carried out using the program COLLECT,[40] with data reduction performed using HKL DENZO and SCALEPACK,[41] with intensities absorption corrected using SADABS.[42] All structures were solved using ShelXT,[43] and

refined by full-matrix least-squares on F^2 using SHELXL[44] in the OLEX2 program package.[45] Anisotropic displacement parameters were assigned to non-H atoms. Positional disorder in the structures was treated by gently restraining geometric and anisotropic displacement parameters. All hydrogen atoms were refined using riding models with Ueq(H) of 1.5Ueq(C). Crystallographic details are given in Tables A5-A6.

5.4.5. Photophysical studies

Absorption spectra were obtained in a 5 mm or 10 mm quartz cuvette for $1.3 \cdot 10^{-5}$ M acetonitrile solutions on a Cary 5000 UV-vis-NIR or Shimadzu UV-2450 spectrophotometer. The emission spectra of the compounds in solution were obtained in fluorescence quartz cuvette of 5 mm or 10 mm path length, using a Horiba-Jobin-Vonn Fluorolog 3.22 or Fluoromax spectrometers. Phosphorescence spectra and decays were obtained with the D1934 unit of Fluoromax 3.22 spectrometer. All the fluorescence and phosphorescence spectra were corrected for the wavelength response of the system with the appropriate correction files obtained for the instrument.

Emission quantum yield determinations and laser flash photolysis experiments

All measured solutions were degassed using a cuvette specially designed and described elsewhere for 20−30 min with N_2 or Ar.[46] Emission quantum yields were measured with a Hamamatsu Quantaurus QY absolute photoluminescence quantum yield spectrometer model C11437 (integration sphere). Transient absorption spectra were measured using a flash photolysis setup composed of a LKS 60 ns laser photolysis spectrometer from Applied Photophysics, pumped with third harmonic, 355 nm, of a Spectra Physics Quanta-Ray Nd:YAG laser. The transient spectra were obtained by monitoring the optical density change at 5−10 nm intervals, averaging at least 10 decays at each wavelength.

Singlet oxygen yields

Room-temperature singlet oxygen NIR phosphorescence was detected using a Hamamatsu R5509−42 photomultiplier in the Applied Photophysics laser flash photolysis apparatus described above. A Newport RG1000 filter was used to eliminate the harmonic contribution of sensitizer emission from the infrared signal. The singlet oxygen formation quantum yields were determined by plotting the photosensitized singlet oxygen phosphorescence intensity at 1270 nm of optically matched aerated solutions of the

samples and reference compound as a function of the laser energy[47] and comparing the slopes using eq 2:

$$\Phi_{\Delta} = \frac{slope_{cp}}{slope_{ref}} x \frac{Abs_{ref}}{Abs_{cp}} x \frac{n^2_{solv,cp}}{n^2_{solv,ref}} x \Phi^{ref}_{\Delta} \quad (2)$$

with Φ^{ref}_{Δ} being the singlet oxygen formation quantum yield of the reference compound-1H-Phenal-1-one in toluene (ϕ_{Δ}= 0.93) was used as the standard.

TCSPC

Phosphorescence decays were obtained either in aerated or degassed acetonitrile solutions and were measured with two different custom-built time-correlated single-photon counting equipment (TCSPC). For the Pt−Ar (**7a**−**e**) and Pt−Cl (**4a**) compounds, ns-TCSPC was carried out as elsewhere reported except that a NanoLED (excitation at 373 nm) IBH was used as the excitation source.[48] Deconvolution of the phosphorescence decay curves was performed using the modulating function method, as implemented by G. Striker in the SAND program.[49]

fs-TA

The experimental setup for ultrafast spectroscopic and kinetic measurements was described elsewhere[50] and consists of a broadband HELIOS pump−probe fs-TA (350−1600 nm) spectrometer from Ultrafast Systems equipped with an amplified femtosecond Spectra-Physics Solstice-100F laser (800 nm central wavelength displaying a pulse width of 128 fs at 1 kHz repetition rate) that is coupled with a Spectra-Physics TOPAS Prime F optical parametric amplifier (195−22 000 nm) for pulse pump generation. Probe light in the UV range was generated by passing a small portion of the 800 nm light from the Solstice-100F laser through a computerized optical delay (with a time window up to 8 ns) and focusing on a vertical translating CaF_2 crystal to generate a white-light continuum (350−750 nm). All measurements were obtained in a 2 mm quartz cuvette with absorptions lower than 0.3 at the pump excitation wavelength. The instrumental response function of the system was assumed to be equal to that of the pump−probe cross-correlation determined from the measurement of the instantaneous stimulated Raman signal from the pure solvent (in an analogous 2 mm cuvette). Typical values for the IRF of the system were found to be better than 250 fs. The solutions were stirred during the experiments or kept moving using a motorized translating sample holder

to avoid photodegradation. The spectral chirp of the data was corrected using Surface Xplorer PRO program from Ultrafast Systems. Global analysis of the data (using a sequential model) was performed after single value decomposition using Glotaran software.[51]

5.4.6. Theoretical calculations

DFT calculations have been performed using the Q-Chem[52] software implemented in Spartan'18,[53] with the B3LYP[54,55] functional and the following basis set: 6- 31G*,[56,57] including polarization for non-hydrogen atoms, for C, H, N, and Cl and LANL2DZ[58] for Pt. Solvation effects have been included using the CPCM method.[59]

UV/vis transitions have been calculated at the TD-DFT level using the same functional and basis set; this methodology has provided satisfactory results in our previous work.[60] To estimate the emission spectra, we have optimized the geometries corresponding to the first singlet (for fluorescence) and triplet (for phosphorescence) states and calculated the transitions between the ground state and the excited states using the corresponding excited state geometries.

5.5. References

1. Goswami, S.; Winkel, R.W.; Schanze, K.S. *Inorg. Chem.* **2015**, *54*, 10007–10014.
2. Giménez, N.; Lalinde, E.; Lara, R.; Moreno, M.T. *Chem. Eur. J.* **2019**, *25*, 5514–5526.
3. Geist, F.; Jackel, A.; Irmler, P.; Linseis, M.; Malzkuhn, S.; Kuss-Petermann, M.; Wenger, O.S.; Winter, R.F. *Inorg. Chem.* **2017**, *56*, 914–930.
4. McKenzie, L.K.; Bryant, H.E.; Weinstein, J.A. *Coord. Chem. Rev.* **2019**, *379*, 2–29.
5. Herberger, J.; Winter, R.F. *Coord. Chem. Rev.* **2019**, *400*, 1–34.
6. Jiang, X.; Zhu, N.; Zhao, D.; Ma, Y. *Sci. China Chem.* **2016**, *59*, 40–52.
7. Davies, M.J. *Biochem. Biophys. Res. Commun.* **2003**, *305*, 761–770.
8. Redmond, R.W.; Kochevar, I.E. *Photochem. Photobiol.* **2006**, *82*, 1–178.
9. Halliwell, B.; Gutteridget, J.M.C. *Biochem. J* **1984**, *219*, 1–14.
10. Jiménez-Banzo, A.; Ragàs, X.; Kapusta, P.; Nonell, S. *Photochem. Photobiol. Sci.* **2008**, *7*, 1003–1010.
11. Pereira, N.A.M.; Laranjo, M.; Casalta-Lopes, J.; Serra, A.C.; Piñeiro, M.; Pina, J.; Seixas de Melo, J.S.; Senge, M.O.; Botelho, M.F.; Martelo, L.; Burrows, H.D.; Pinho e Melo, T.M.V.D. *ACS Med. Chem. Lett.* **2017**, *8*, 310–315.
12. Benasson, R. V.; Land, E.J.; Trusott, T.G. *Flash Photolysis and Pulse Radiolysis*; **1983**. Ed: Pergamon.
13. Berera, R.; van Grondelle, R.; Kennis, J.T.M. *Photosynth. Res.* **2009**, *101*, 105–118.
14. Ruckebusch, C.; Sliwa, M.; Pernot, P.; de Juan, A.; Tauler, R. *J. Photochem. Photobiol. C* **2012**, *13*, 1–27.
15. Cooper, T.M.; Haley, J.E.; Krein, D.M.; Burke, A.R.; Slagle, J.E.; Mikhailov, A.; Rebane, A. *J. Phys. Chem. A* **2017**, *121*, 5442–5449.
16. Mei, J.; Ogawa, K.; Kim, Y.G.; Heston, N.C.; Arenas, D.J.; Nasrollahi, Z.;

McCarley, T.D.; Tanner, D.B.; Reynolds, J.R.; Schanze, K.S. *ACS Appl. Mater. Interfaces* **2009**, *1*, 150–161.

17. Shavaleev, N.M.; Adams, H.; Best, J.; Edge, R.; Navaratnam, S.; Weinstein, J.A. *Inorg. Chem.* **2006**, *45*, 9410–9415.

18. Zhang, W.; Luo, Y.; Xu, Y.; Tian, L.; Li, M.; He, R.; Shen, W. *Dalton Trans.* **2015**, *44*, 18130–18137.

19. Lu, W.; Mi, B.X.; Chan, M.C.W.; Hui, Z.; Che, C.M.; Zhu, N.; Lee, S.T. *J. Am. Chem. Soc.* **2004**, *126*, 4958–4971.

20. Savel, P.; Latouche, C.; Roisnel, T.; Akdas-Kilig, H.; Boucekkine, A.; Fillaut, J.L. *Dalton Trans.* **2013**, *42*, 16773–16783.

21. Huo, S.; Carroll, J.; Vezzu, D.A.K. *Asian J. Org. Chem.* **2015**, *4*, 1210–1245.

22. Sonogashira, K.; Fujikura, Y.; Yatake, T.; Toyoshima, N.; Takahashi, S.; Hagihara, N. *J. Organomet. Chem.* **1978**, *145*, 101–108.

23. Lázaro, A.; Balcells, C.; Quirante, J.; Badia, J.; Baldomà, L.; Ward, J.S.; Rissanen, K.; Font-Bardia, M.; Rodríguez, L.; Crespo, M.; Cascante, M. *Chem. Eur. J.* **2020**, *26*, 1947–1952.

24. Fadeeva, V.P.; Tikhova, V.D.; Nikulicheva, O.N. *J. Anal. Chem.* **2008**, *63*, 1094–1106.

25. Lázaro, A.; Serra, O.; Rodríguez, L.; Crespo, M.; Font-Bardia, M. *New J. Chem.* **2019**, *43*, 1247–1256.

26. Gandioso, A.; Valle-Sistac, J.; Rodríguez, L.; Crespo, M.; Font-Bardía, M. *Organometallics* **2014**, *33*, 561–570.

27. Ivanov, D.M.; Bokach, N.A.; Yu. Kukushkin, V.; Frontera, A. *Chem. Eur. J.* **2022**, *28*.

28. Millán, G.; Giménez, N.; Lara, R.; Berenguer, J.R.; Moreno, M.T.; Lalinde, E.; Alfaro-Arnedo, E.; López, I.P.; Pineiro-Hermida, S.; Pichel, J.G. *Inorg. Chem.* **2019**, *58*, 1657–1673.

29. Puttock, E. V.; Walden, M.T.; Williams, J.A.G. *Coord. Chem. Rev.* **2018**, *367*,

127–162.

30. Li, K.; Wan, Q.; Yang, C.; Chang, X.Y.; Low, K.H.; Che, C.M. *Angew. Chem. Int. Ed.* **2018**, *57*, 14129–14133.

31. Haque, A.; Xu, L.; Al-Balushi, R.A.; Al-Suti, M.K.; Ilmi, R.; Guo, Z.; Khan, M.S.; Wong, W.Y.; Raithby, P.R. *Chem. Soc. Rev.* **2019**, *48*, 5547–5563.

32. Horng, M.L.; Gardecki, J.A.; Papazyan, A.; Maroncelli, M. *J. Phys. Chem.* **1995**, *99*, 17311-17337.

33. Xue, X.; Zhu, C.; Chen, H.; Bai, Y.; Shi, X.; Jiao, Y.; Chen, Z.; Miao, Y.; He, W.; Guo, Z. *Inorg. Chem.* **2017**, *56*, 3754–3762.

34. Shi, H.; Clarkson, G.J.; Sadler, P.J. *Inorg. Chim. Acta* **2019**, *489*, 230–235.

35. Pushpanandan, P.; Maurya, Y.K.; Omagari, T.; Hirosawa, R.; Ishida, M.; Mori, S.; Yasutake, Y.; Fukatsu, S.; Mack, J.; Nyokong, T.; Furuta, H. *Inorg. Chem.* **2017**, *56*, 12572–12580.

36. Lai, S.W.; Liu, Y.; Zhang, D.; Wang, B.; Lok, C.N.; Che, C.M.; Selke, M. *Photochem. Photobiol.* **2010**, *86*, 1414–1420.

37. Jana, A.; McKenzie, L.; Wragg, A.B.; Ishida, M.; Hill, J.P.; Weinstein, J.A.; Baggaley, E.; Ward, M.D. *Chem. Eur. J.* **2016**, *22*, 4164–4174.

38. Hu, X.; Ogawa, K.; Kiwada, T.; Odani, A. *J. Inorg. Biochem.* **2017**, *170*, 1–7.

39. Kim, S.; Ohulchanskyy, T.Y.; Bharali, D.; Chen, Y.; Pandey, R.K.; Prasad, P.N. *J. Phys. Chem. C* **2009**, *113*, 12641–12644.

40. Hooft, R.W.W. COLLECT Nonius BV: Delft, The Netherlands, **1998**.

41. Otwinowski, Z.; Minor, W. *Methods Enzymol.* **1997**, *276*, 307–326.

42. Sheldrick, G.M. SADABS, version 2008/2; University of Göttingen, Germany **1996**.

43. Sheldrick, G.M. *Acta Crystallogr., Sect. A: Found Adv.* **2015**, A*71*, 3–8.

44. Sheldrick, G.M. *Acta Crystallogr. Sect. C Struct. Chem.* **2015**, C*71*, 3–8.

45. Dolomanov, O. V.; Bourhis, L.J.; Gildea, R.J.; Howard, J.A.K.; Puschmann, H. *J.*

Appl. Crystallogr. **2009**, *42*, 339–341.

46. Seixas De Melo, J. *Chem. Educ.* **2005**, *10*, 29–35.

47. Kristiansen, M.; Scurlock, R.D.; Iu, K.-K.; Ogilby, P.R. *J. Phys. Chem* **1991**, *95*, 5190–5197.

48. Seixas De Melo, J.; Fernandes, P.F. *J. Mol. Struct.* **2001**, *565–566*, 69–78.

49. Striker, G.; Subramaniam, V.; Seidel, C.A.M.; Volkmer, A. *J. Phys. Chem. B* **1999**, *103*, 8612–8617.

50. Pina, J.; Seixas De Melo, J.S.; Eckert, A.; Scherf, U. *J. Mater. Chem. A* **2015**, *3*, 6373–6382.

51. Snellenburg, J.J.; Laptenok, S.P.; Seger, R.; Mullen, K.M.; Van Stokkum, I.H.M. *J. Stat. Softw.* **2012**, *49*, 1–22.

52. Shao, Y.; Gan, Z.; Epifanovsky, E.; Gilbert, A.T.B.; Wormit, M.; Kussmann, J.; Lange, A.W.; Behn, A.; Deng, J.; Feng, X.; et al. *Mol. Phys.* **2015**, *113*, 184–215.

53. Spartan'18 v 1.4.0.; Wavefunction, Inc.: Irvine, CA, **2019**.

54. Becke, A.D. *J. Chem. Phys.* **1993**, *98*, 5648–5652.

55. Lee, C.; Yang, W.; Parr, R.G. *Phys. Rev. B. Condens. Matter Mater. Phys.* **1988**, *37*, 785–789.

56. Hariharan, P.C.; Pople, J.A. *Theor. Chim. Acta* **1973**, *28*, 213–222.

57. Francl, M.M.; Pietro, W.J.; Hehre, W.J.; Binkley, J.S.; Gordon, M.S.; DeFrees, D.J.; Pople, J.A. *J. Chem. Phys.* **1982**, *77*, 3654–3665.

58. Hay, P.J.; Wadt, W.R. *J. Chem. Phys.* **1985**, *82*, 299–310.

59. Cossi, M.; Rega, N.; Scalmani, G.; Barone, V. *J. Comput. Chem.* **2003**, *24*, 669–681.

60. Bartocci, S.; Sabaté, F.; Bosque, R.; Keymeulen, F.; Bartik, K.; Rodríguez, L.; Dalla Cort, A. *Dyes Pigm.*. **2016**, *135*, 94–101.

CHAPTER 6

Cyclometallated [N,C,N] platinum(II) compounds toward a red-shifted emission with excimers' formation and aggregation induced emission

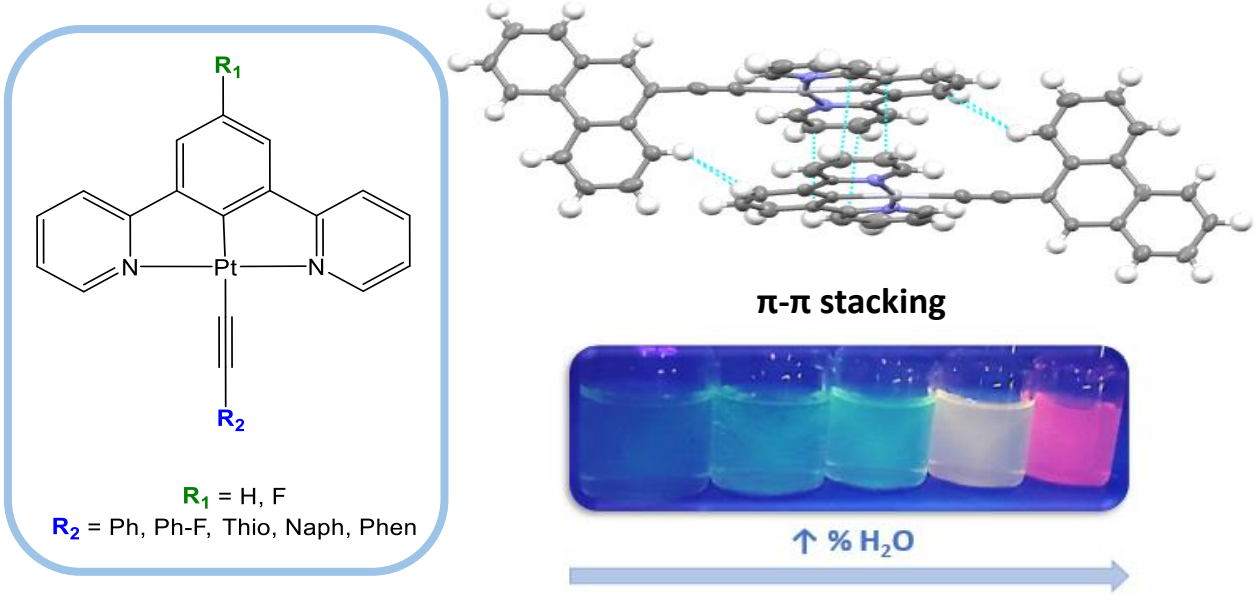

Part of this chapter has been published in: Lázaro, A.; Bosque, R.; Ward, J.S.; Rissanen, K.; Crespo, M.; Rodríguez, L. *Inorg. Chem.* **2023**, *62*, 2000-2012.

6. Cyclometallated [N,C,N] platinum(II) compounds toward a red-shifted emission with excimers' formation and aggregation induced emission.

6.1. Introduction

An interesting tangent in the field of optical materials is the modulation of the chemical structures and assemblies to shift the emission to the red since, for example, OLEDs and materials that emit in the red or near-infrared (NIR) region represent a challenging target, due to the favored deactivation processes in low-energy emissive populated states.[1] Red-shifted and NIR emission are of vital importance in several relevant applications such as full-color displays, remote sensing of environmental conditions, night-vision displays, bio-chemosensors and *in vivo* imaging, Light-Fidelity (Li-Fi) communication or security authentication devices and it is mostly explored with pure organic molecules.[2–5]

One strategy to modulate the photophysical properties and achieve a red shift in the emission is to study molecules that present supramolecular self-assembly properties. In this area, platinum(II) compounds are of great interest as they present square-planar geometries that can undergo face-to-face intermolecular interactions through ligand–ligand and Pt···Pt interactions, that can give rise to new electronic excited states that produce red-shifted emission from triplet metal-metal-to-ligand charge-transfer (^{3}MMLCT) or excimeric ^{3}IL excited states in addition to the one arising from the mononuclear platinum(II) moiety.[6–10] These excimers are dimers formed thanks to the presence of these intermolecular interactions that are non-existing in the ground state. Their energy is lower compared to the monomeric singlet excited state and therefore present a less energetic emission that results in a higher wavelength thus shifting the molecule's emission to the red (*Figure 6.1*).[11,12]

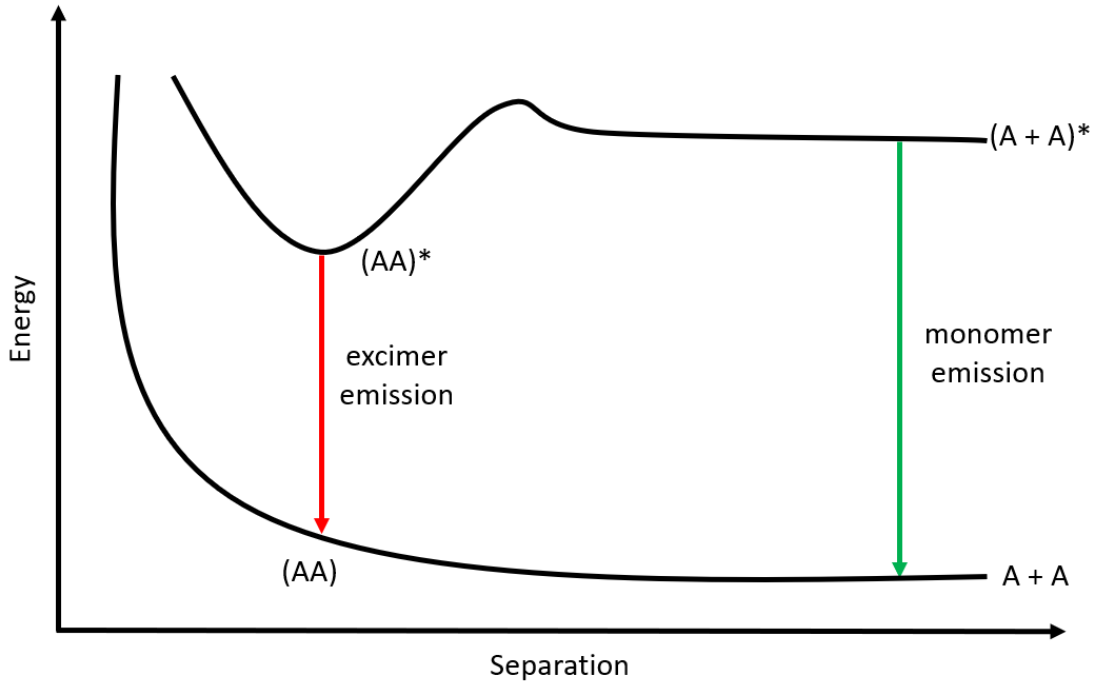

Figure 6.1. Diagram illustrating the energy of an excimer emission.

Additionally, the aggregation of platinum(II) compounds can also be present in the ground state and can either be tuned by structural or environment modifications, such as the polarity of the solvent or the introduction of a bad solvent were the studied compounds present a lower solubility. In this case, aggregates are found in the ground state and can absorb and emit light in a different manner than the monomeric species. Furthermore, this aggregation can result in a decrease in the non-radiative emission pathways due to the loss of vibrational movement in the aggregate, which gives rise to more efficient radiative pathways (aggregation induced emission, AIE).[13–15]

Specifically, cyclometallated platinum(II) compounds are currently relevant in this field as their rigidity allows to achieve high luminescence (mainly from the triplet excited state, i.e., phosphorescence) quantum yields, color tunability and stability.[10,16] For this, the nature of the cyclometallated ligands, ancillary ligands and the ionic or neutral character of the molecules are extremely relevant to modulate the absorption and emission properties.[17] Among them, [N,C,N] cyclometallated compounds, especially those derived from a completely planar ligand, have been observed to exhibit intense luminescence and versatile emissive excited states, including not only intraligand (IL) (π–π^*) excited states but also excimeric excited states and emissive aggregates.[18–20] The aromaticity and

planarity of these compounds is a key aspect to their ability to establish efficient intermolecular interactions which influence the resulting luminescence properties. However, less efforts have been paid on the analysis of the ancillary ligand that occupies the fourth coordination position at the platinum(II) center, even though they can also play an influence on their resulting assemblies and luminescent properties.[21]

In this chapter, two series of cyclometallated platinum(II) compounds containing planar tridentate [N,C,N] ligands with an alkynyl-chromophore as the co-ligand occupying the fourth coordination position have been synthesised. Different chromophores have been chosen to evaluate how the electrowithdrawing character (fluorine), soft atom (sulfur in thiophene) or extended aromaticity (benzene, naphthalene and phenanthrene) can affect the resulting packing through intermolecular contacts and the resulting influence in their luminescent properties. Additionally, the two series of compounds differ on the presence of a H or F atom at the central benzyl ring, that could confer also different intermolecular forces in the packing. The differences on the resulting photophysical properties depending on the [N,C,N] ligand and co-ligands have been analyzed in detail together with their ability to exhibit a red-shifted excimeric or aggregates' emission.

6.2. Results and Discussion

6.2.1. Synthesis and characterisation

Ligands 1,3-di(2-pyridyl)benzene (**L3**) and 2,2'-(5-fluoro-1,3-phenylene)dipyridine (**L4**) were synthesised by following the method described in the literature shown in *Scheme 6.1*.[22] It consists in a microwave-accelerated palladium catalysed Stille coupling using CuO as a base. The use of the microwave significantly reduces the reaction time from days to minutes without compromising the resulting reaction yields when compared to the traditional synthesis carried out under reflux.[23]

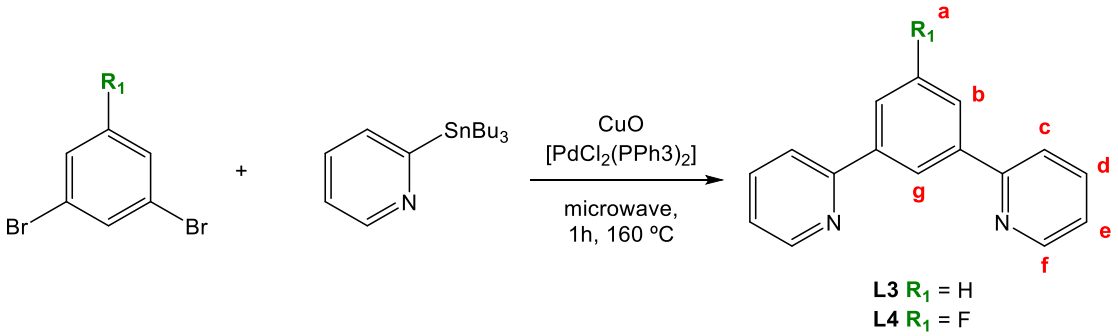

Scheme 6.1. Synthesis of ligands **L3** and **L4**.

An analogous strategy was used to perform cyclometallation on these two ligands with K_2PtCl_4 in order to obtain two [PtCl(N,C,N)] precursors [PtCl{2,6-$(C_5H_4N)_2$-C_6H_3}] (**8**) and [PtCl{2,6-$(C_5H_4N)_2$-4-FC_6H_2}] (**9**) to further perform the substitution of the chlorido ligand (*Scheme 6.2*). As it is reported, the reaction time *versus* the same procedure performed under reflux is reduced from 3 days to 30 minutes.[22]

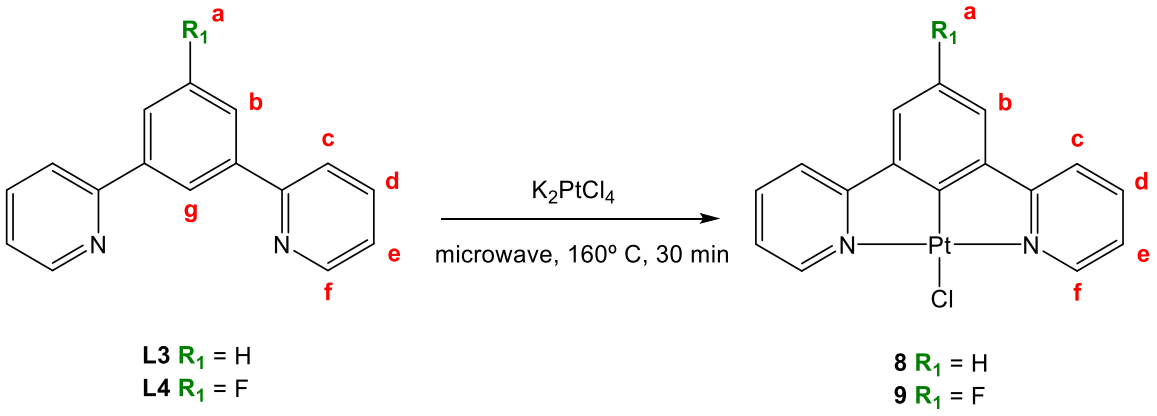

Scheme 6.2. Synthesis of compounds **8** and **9**.

Both the ligands and the chlorido precursors were successfully obtained, which was confirmed as their ^{1}H NMR spectra matched those reported in the literature.

All the final [PtC≡CR$_2$(N,C,N)] compounds were syntesised through the reaction depicted in *Scheme 6.3*. As reported in the literature, the corresponding precursors **8** or **9** were reacted with an excess of different alkynyl aromatic ligands which were previously deprotonated using sodium hydroxide as a base.[24] Final compounds [Pt(C≡CR$_2$){2,6-(C$_5$H$_4$N)$_2$-C$_6$H$_3$}] (**8x**) and [Pt(C≡CR$_2$){2,6-(C$_5$H$_4$N)$_2$-4-FC$_6$H$_2$}] (**9x**) were isolated as orange solids after precipitation and washing with water, methanol and hexane.

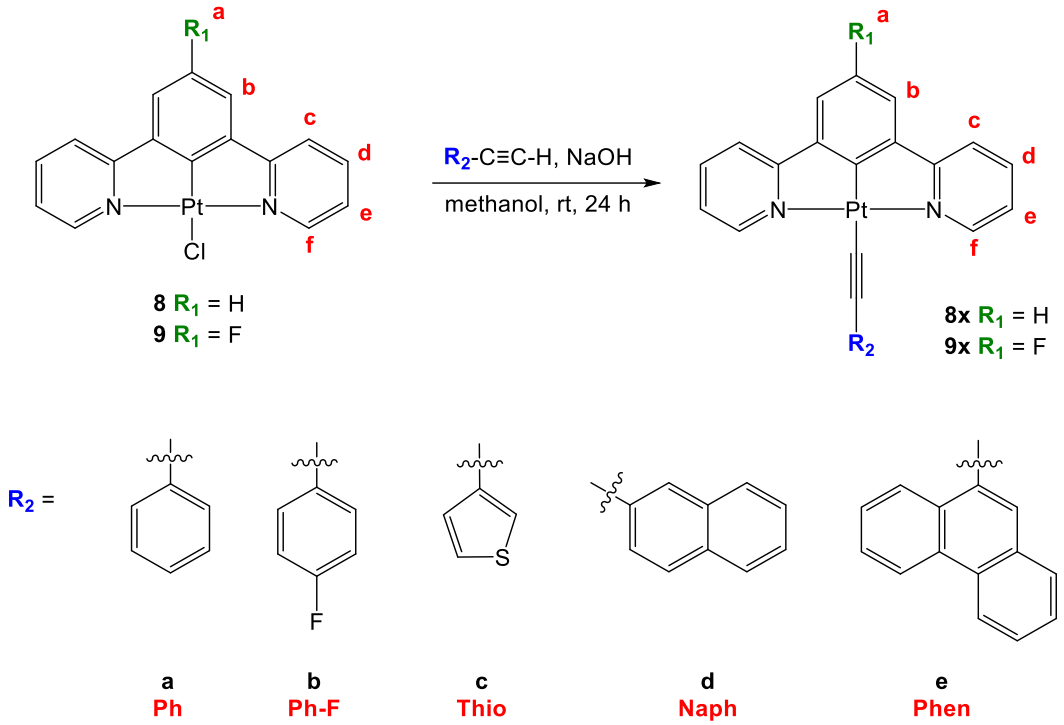

Scheme 6.3. Synthesis of compounds **8x** and **9x**. The letters in red are used for NMR assignment.

Characterisation by ^{1}H NMR showed the disappearance of the terminal alkynyl proton from the corresponding aromatic R$_2$C≡C-*H* chromophore as well as the presence of the aromatic protons from the [N,C,N] tridentate ligand confirming the formation of the desired products. This is also supported by a significant shift of the protons that belong to the cyclometallated unit, with a downfield shift in the pyridine proton (H^{f}) of *ca.* 0.10-0.25 ppm when compared to that of the precursors. As expected, no significant changes were observed in the coupling constants of this proton with platinum between the precursors and the final compounds, as the ligand in *trans* with the nitrogen of the

pyridine bond is not exchanged. Additionally, compounds **9x** were also characterised by ^{19}F NMR, showing only one signal as a triplet assigned to the fluorine in the central position of the aromatic ring which is coupled with the two adjacent aromatic protons. Compound **9b**, due to the aromatic *p*-fluorobenzene moiety, presents a second signal as a multiplet. This signal can also be observed when performing the ^{19}F NMR spectrum of compound **8b**, which also contains this moiety.

Infrared spectroscopy was also useful to detect the C≡C stretching vibration (around 2070 cm^{-1}) for all compounds along with the absence of the band assigned to the stretching of the terminal proton of the free alkynyl aromatic ligand (around 3300 cm^{-1}). Finally, all the protonated molecular peaks were found by mass spectrometry further confirming the successful formation of the desired products.

6.2.2. X-ray crystal structure determination

Single crystals suitable for X-ray diffraction were grown for compounds **8e** and **9c** by slow diffusion of hexane into a concentrated dichloromethane solution with one (**8e**, *Figure 6.2*) or two (**9c**, *Figure 6.3*) crystallographically independent molecules present in the asymmetric unit. For both cases, the platinum adopts the expected square-planar environment completed with the corresponding tridentate [N,C,N] cyclometallating ligand and the alkynyl aromatic ancillary group. Bond distances and angles are in the range of those reported in the literature for analogous cyclometallated platinum(II) complexes and no significant differences can be observed in the bond lengths between the two compounds.[25,26] However, the aromatic ring of the alkynyl ligand is almost perpendicular to the planar cyclometallated unit for compound **8e** (85.3º) while compound **9c** presents two different conformations in the two different molecules present in the asymmetric unit with angles of 52.1º and 83.3º.

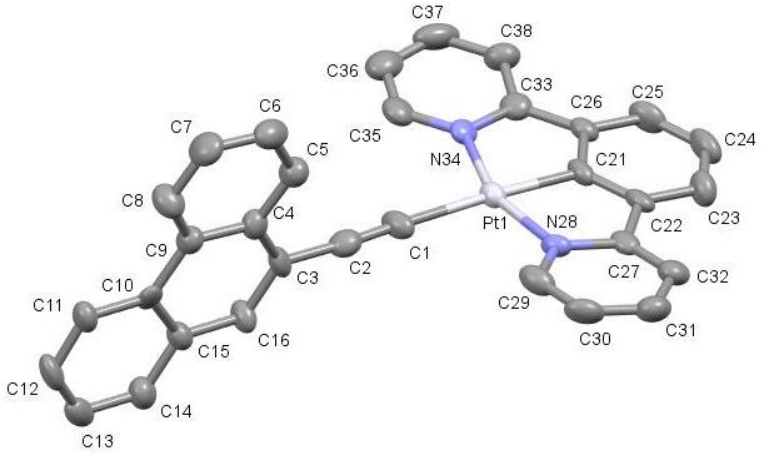

Figure 6.2. Molecular structure of compound **8e**. Selected bond lengths (Å) and angles (°) with estimated standard deviations: Pt(1)–N(34): 2.038(7); Pt(1)–C(21): 1.939(7); Pt(1)–N(28): 2.035(7); Pt(1)–C(1): 2.077(8); C(1)–C(2): 1.181(11); N(34)–Pt(1)–C(21): 79.4(3); C(21)–Pt(1)–N(28): 79.7(3); N(28)–Pt(1)–C(1): 100.2(3); C(1)–Pt(1)–N(34): 100.9(3); Pt(1)-C(1)-C(2): 177.71(9). The thermal ellipsoids are drawn at the 50% probability level and hydrogen atoms omitted for clarity

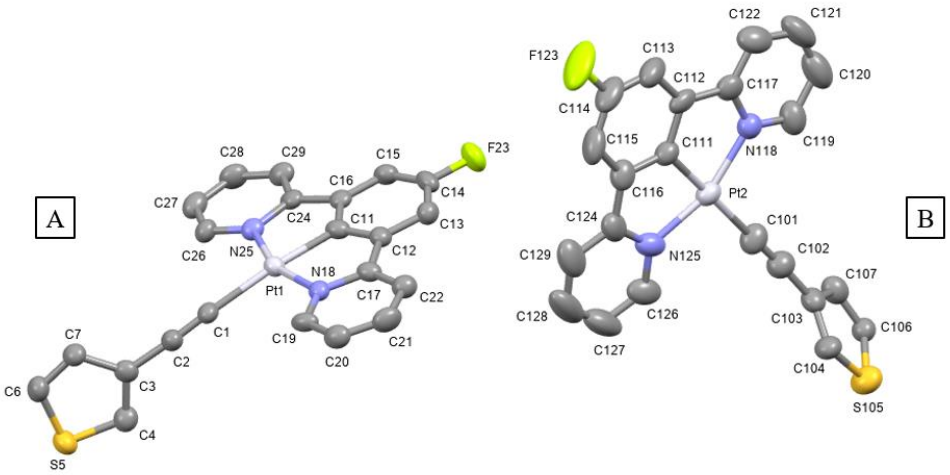

Figure 6.3. Molecular structure of compound **9c** (two crystallographically independent molecules present in the asymmetric unit cell, A and B). Selected bond lengths (Å) and angles (°) with estimated standard deviations: (**A**) Pt(1)–N(18): 2.033(5); Pt(1)–C(11): 1.942(7); Pt(1)–N(25): 2.035(5); Pt(1)–C(1): 2.099(7); C(1)–C(2): 1.179(9); N(18)–Pt(1)–C(11): 80.0(3); C(11)–Pt(1)–N(25): 80.1(3); N(25)–Pt(1)–C(1): 98.0(2); C(1)–Pt(1)–N(18): 101.7(2); Pt(1)-C(1)-C(2): 165.2(6). (**B**) Pt(2)–N(118): 2.040(5); Pt(2)–C(111): 1.930(8); Pt(2)–N(125): 2.038(7); Pt(2)–C(101): 2.054(8); C(101)–C(102): 1.185(10); N(118)–Pt(2)–C(111): 80.1(3); C(11)–Pt(2)–N(125): 79.3(3); N(125)–Pt(2)–C(101): 99.9(3); C(101)–Pt(2)–N(118): 100.8(3); Pt(2)-C(101)-C(102): 178.7(6). The thermal ellipsoids are drawn at the 50% probability level and hydrogen atoms omitted for clarity.

The packing of compound **8e** presents a zig-zag conformation held together by the stacking of two cyclometallated moieties (*Figure 6.4*). However, since these dimeric structures are arranged in a head-to-tail fashion, the presence of metallophilic interactions are not permitted with a Pt···Pt distance of 5.052 Å. Instead, π-π stacking interactions (d(C···C) = 3.5-3.36 Å) are the ones responsible for the presence of these dimer-like structures along with additional C···H intermolecular contacts (d(C···H) = 2.849 Å). This results in an interplanar distance of 3.0 Å between platinacycles of the two stacked molecules.

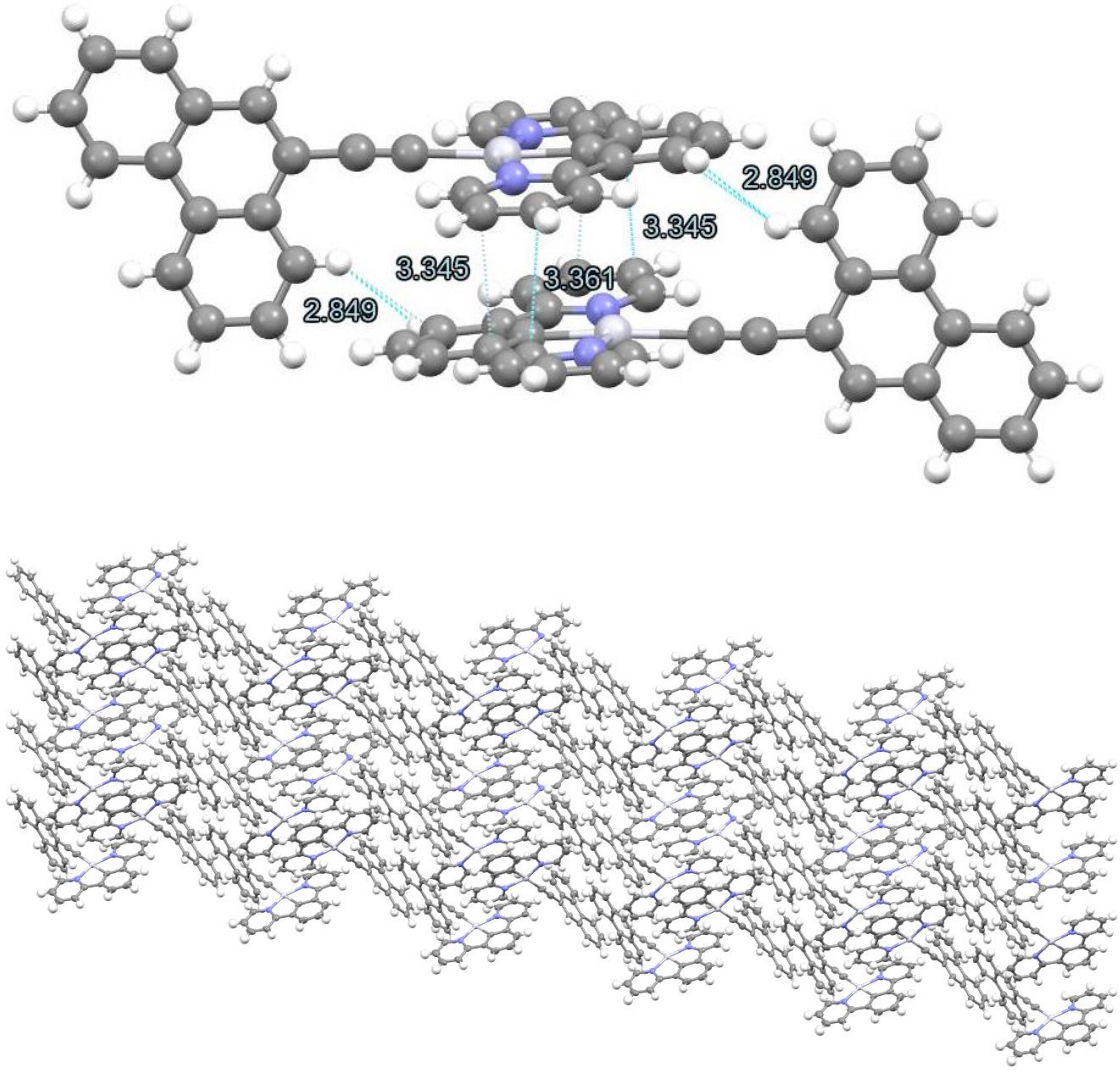

Figure 6.4. A view of the relevant intermolecular short contacts highlighted in blue: C(31)-C(33):3.361 Å; C(20)-C(26) = 3.345 Å; C(23)-H(5): 2.849 Å (top) and the general packing for compound **8e** (bottom)**.**

For compound **9c**, the packing also displays a zig-zag conformation with the stacking of two cyclometallated moieties (*Figure 6.5*). However, only F···H (2.449 Å) and C···H (3.345 Å) interactions can be observed in the stacking of these dimers, which are in a head to tail disposition with a Pt(2)···Pt(2) distance of 4.988 Å. The lack of interactions between the cyclometallated moieties leads to a higher interplanar distance of 3.2 Å compared to compound **8e**.

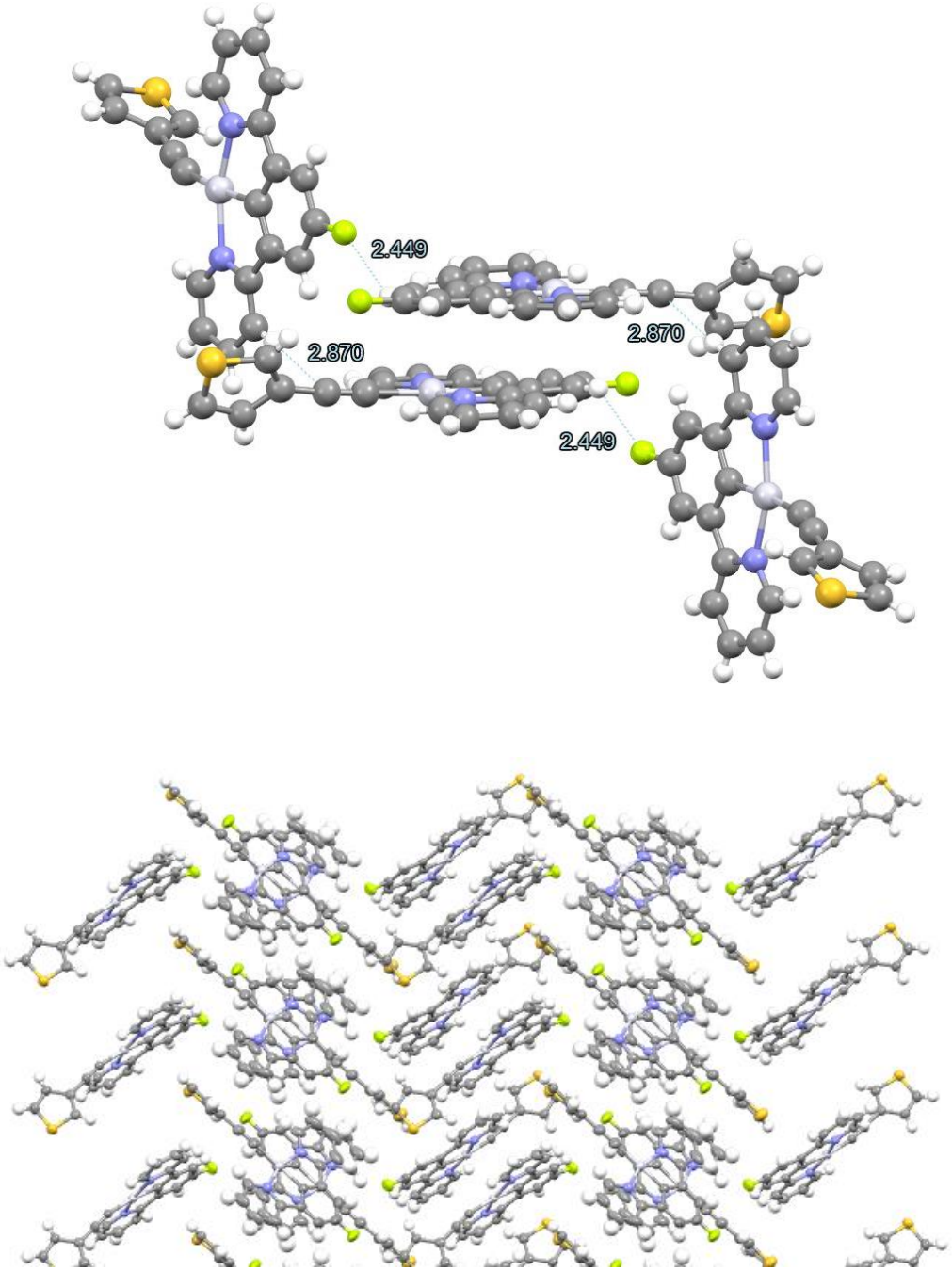

Figure 6.5. A view of the relevant intermolecular short contacts highlighted in blue: F(23)-H(115): 2.449 Å; C(102)-H(22) = 3.345 Å (top) and the general packing for compound **9c** (bottom).

Interestingly, as two crystallographic independent molecules are present in the asymmetric unit, a second kind of stacking can be observed where the Pt(1)···Pt(1) distance (3.466 Å) is just below the combined van der Waals radii (3.5 Å) and can therefore be considered a platinophilic interaction.[24] The different arrangements are depicted in *Figure 6.6*. This ability to present stacked structures, in a different fashion for each compound, suggests the possibility that they can aggregate in solution and that the differences in the aggregation mode could potentially lead to the observation of different emissive properties.

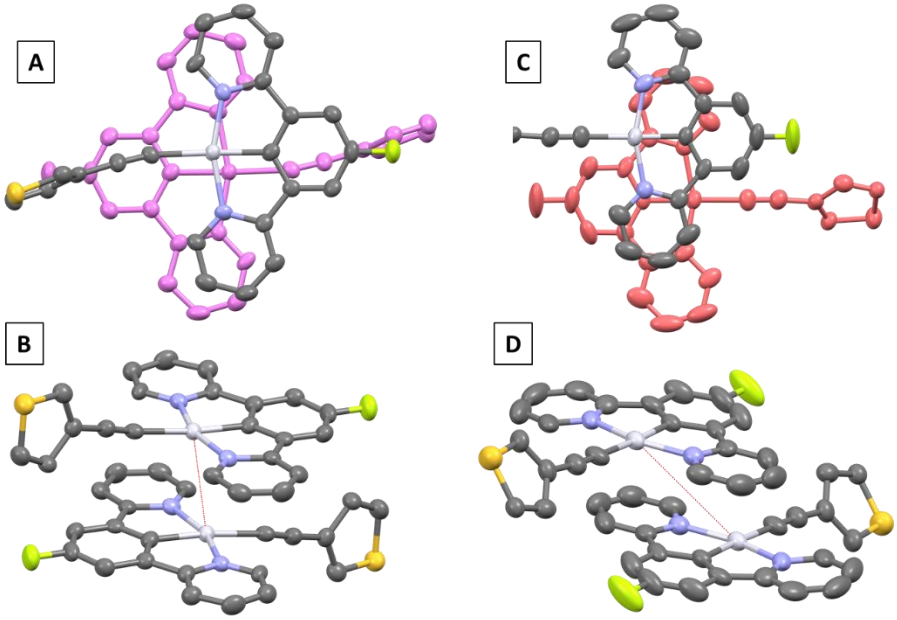

Figure 6.6. Disposition of the two different Pt···Pt contacts for compound **9c**: Pt(1)-Pt(1) = 3.466 Å (A and B); Pt(2)-Pt(2) = 5.052 Å (C and D).

6.2.3. Photophysical characterisation

The absorption spectra of all compounds and ligands were recorded in $5 \cdot 10^{-5}$ M dichloromethane solutions at room temperature and the results are shown in *Table 6.1* and *Figure 6.7*.

Table 6.1. Spectral data including absorption and phosphorescence emission maxima in dichloromethane solutions at 298 K.

Compound	**λ_{abs}, nm (ε x 10^{-3}, M^{-1} cm^{-1})**	**λ_{em} (nm)**
L3	280 (8.6)	341
L4	279 (8.9)	337
8	290 (18.4), 333 (5.8), 380 (7.2), 402 (5.9)	490
9	290 (12.5), 378 (4.2), 422 (4.7)	505
8a	291 (17.0), 389 (4.6)	497, 702
8b	290 (18.2), 388 (5.5)	495, 692
8c	292 (25.5), 391 (7.0)	501, 698
8d	288 (8.7), 309 (5.8), 389 (2.3)	490, 693
8e	289 (28.4), 319 (22.3), 334 (24.0), 391 (7.7)	547, 698
9a	289 (10.1), 380 (3.5), 421 (3.5)	507, 692
9b	292 (20.6), 390 (5.5), 422 (5.7)	511, 694
9c	291 (10.8), 391 (2.7), 424 (2.8)	513, 696
9d	294 (31.5), 310 (2.5), 392 (6.8), 427 (7.5)	520, 699
9e	290 (32.1), 319 (25.6), 333 (26.6), 425 (8.2)	547, 700

Compounds **8x** and **9x** present intense absorption bands in the high energy region (ca. 290 nm) that can be assigned to $^{1}\pi$-π^* transitions intrinsic of the cyclometallated (1,3-di(2-pyridyl)benzene or 2,2'-(5-fluoro-1,3-phenylene)dipyridine) ligand as they are also recorded in the absorption of the free ligands **L3** and **L4** (*Figure 6.7*) In the lower energy region (380-430 nm), less intense bands, which are also present in the precursors **8** and **9**, are observed that can correspond to mixed charge transfer and ligand centred transitions according to the literature.[7,8,15,27,28]

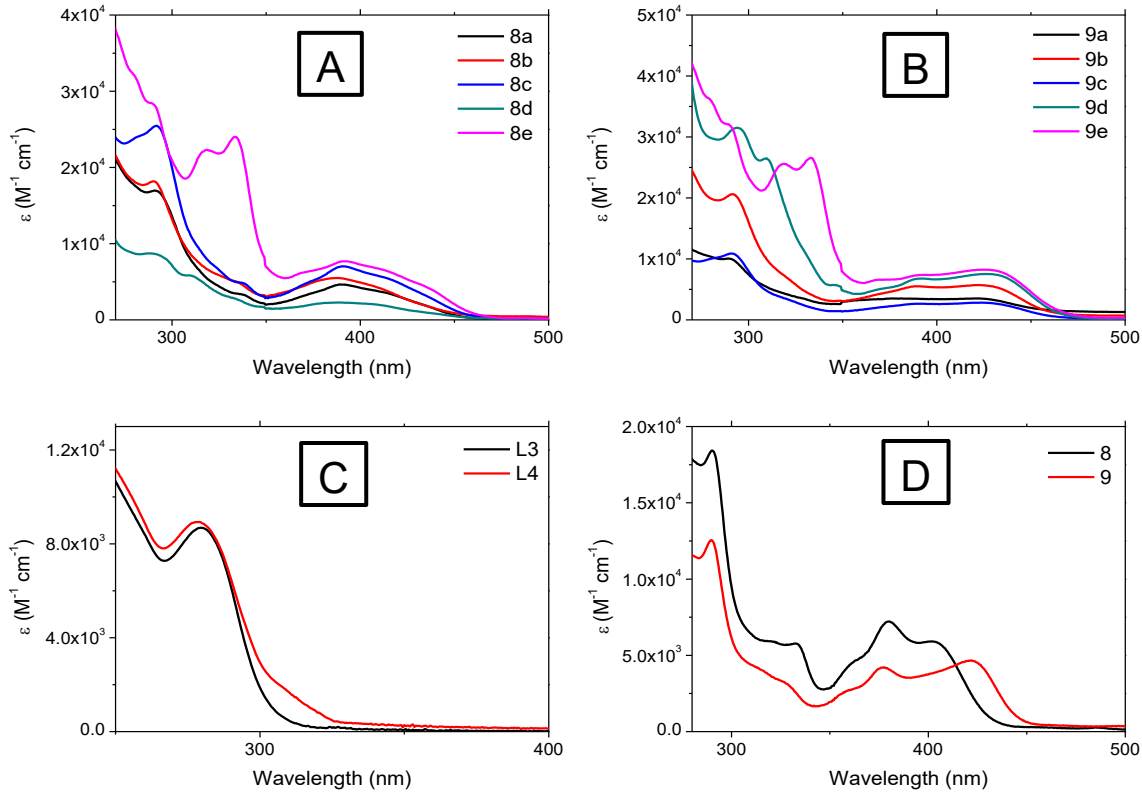

Figure 6.7. Absorption spectra for $5 \cdot 10^{-5}$ M dichloromethane solutions of compounds **8x** (A) and **9x** (B), ligands **L3** and **L4** (C) and compounds **8** and **9** (D) at 298 K.

All final compounds present a vibronically structured band with maxima around 500 nm when excited at their lower energy absorption band. This band is attributed to a mainly ligand centred $^{3}\pi$-π^* transition from the [N,C,N] cyclometallated ligand that can be mixed with metal-to-ligand or intraligand charge transfer transitions (^{3}MLCT or ^{3}ILCT). For the chlorido precursors, the same pattern can be observed (*Figure 6.8*).[18,29–31]

The phosphorescent assignment is supported by the large Stokes' shift and the quenching of the emission in the presence of oxygen for both compounds **8x** and **9x** and their

precursors. Ligands **L3** and **L4** present a broad emission around 350 nm (*Figure 6.8*) when excited at their only absorption band (280 nm) that can be assigned to a fluorescent $^1\pi$-π^* intraligand transition not quenched by the presence of oxygen, which indicates that the phosphorescence is induced thanks to the perturbation of the platinum atom in the emission.

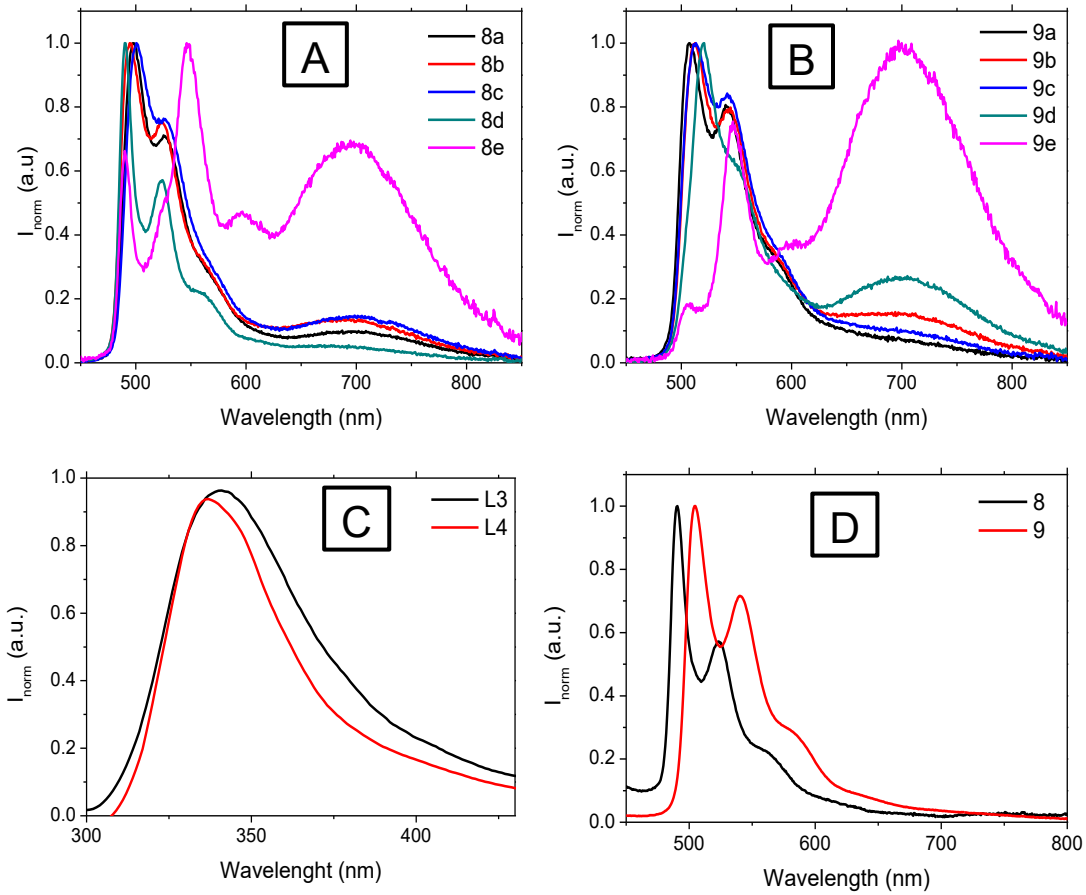

Figure 6.8. Normalized emission spectra (right) for $5 \cdot 10^{-5}$ M dichloromethane solutions of of compounds **8x** (A) and **9x** (B) (λ_{exc} = 390 nm), ligands **L3** and **L4** (C) (λ_{exc} = 280 nm) and compounds **8** and **9** (D) (λ_{exc} = 380 nm) at 298 K.

An additional band at 700 nm is observed for all the final compounds **8x** and **9x**, which can be attributed to an excimer formation.[13,32] This is supported by the recording of the excitation spectra of compound **9e**, as an example, at the two emission maxima (500 and 700 nm) which resemble the same pattern that matches the absorption spectra (*Figure 6.9*). This fact confirms that the emitting species is indeed not present in the ground state and discards the possibility of an emission coming from aggregates.

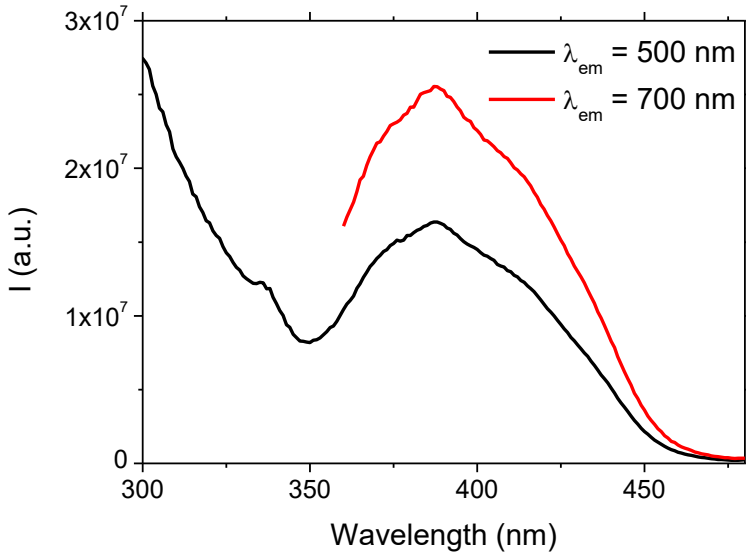

Figure 6.9. Excitation spectra of compound **2e** in dichloromethane at the two different emission maxima at 298 K.

The lack of excimer formation in the precursors **8** and **9** along with the different excimer intensities along compounds **8x** and **9x** indicates an important role of the alkynyl aromatic moiety and the substituent in the central benzene ring in the resulting emissive properties. The excimer formation is generally more favoured in compounds **9x** and mainly for the bigger chromophore, phenanthrene, in compounds **8e** and **9e**. In fact, the presence of the excimer in compounds analogous to **8** and **9**, where the ancillary ligand is a chlorido, has only been observed in the literature at higher concentrations.[12]

Global phosphorescence quantum yields were recorded and are displayed in *Table 6.2* along with the splitting into the contribution of the monomer and the excimer emission. The total values increase in the absence of oxygen up to a 60 %, in the range of those reported in the literature for analogous compounds.[12,24,33] In most cases, the monomer emission is the major radiative deactivation pathway, with a larger excimer contribution for compounds containing a phenanthrene as an alkynyl aromatic moiety (**8e** and **9e**), being almost dominant for compound **9e**. This could be attributed to the establishment of π-π stacking intermolecular interactions in solution that have been observed in the crystal structure of compound **8e**.

Table 6.2. Phosphorescence quantum yields recorded in air-equilibrated (with O_2) or degassed (N_2 sat.) in dichloromethane solutions at 298 K.

Compound	Φ_{Ph} (with O_2)	Φ°_{Ph} (N_2 sat.)	Φ°_{Ph} monomer (N_2 sat.)	Φ°_{Ph} excimer (N_2 sat.)
L3	0.004	0.004	0.004	-
L4	0.007	0.007	0.007	-
8	0.03	0.61	0.61	-
9	0.03	0.66	0.66	-
8a	0.04	0.61	0.46	0.15
8b	0.05	0.56	0.39	0.17
8c	0.03	0.52	0.36	0.16
8d	0.04	0.55	0.45	0.10
8e	0.01	0.34	0.13	0.21
9a	0.04	0.60	0.49	0.11
9b	0.03	0.49	0.34	0.15
9c	0.03	0.59	0.46	0.13
9d	0.03	0.50	0.27	0.23
9e	0.01	0.37	0.07	0.30

Therefore, although no significant differences are observed in the global quantum yields in general, a variation can be observed when they are split into the two contributions (monomer and excimer). The main effect seems to arise from an extended aromaticity, as it can be seen for compounds **8e** and **9e**, but also the hydrogen or fluorine atom in the central position of the [N,C,N] ligand, with a larger excimer formation in the presence of a fluorine as it can be seen by comparing the naphthalene and phenanthrene derivatives of both families. This could be attributed to the less electronic density present in the aromatic rings which could favour the establishment of intermolecular contacts.

Phosphorescence emission lifetimes were recorded for both the monomer and excimer emission and are displayed in *Table 6.3*. For all final compounds and the precursors, the values are of hundreds of nanoseconds and increase to a few microseconds in deaerated solutions, which are in the range of those reported for similar compounds supporting a triplet emission origin.[12,34,35] Phenanthrene derivatives are again a particular case as they display longer decay time values than the rest of compounds, which has been previously observed in other cyclometallated platinum(II) compounds containing this chromophore.[17]

Table 6.3. Phosphorescence lifetimes of the compounds recorded in air-equilibrated (with O_2) or degassed (N_2 sat.) dichloromethane solutions.

Compound	τ (μs) monomer (with O_2)	τ (μs) excimer (with O_2)	τ^o (μs) monomer (N_2 sat.)	τ^o(μs) excimer (N_2 sat)
L3	$3.91 \cdot 10^{-3}$	-	-	-
L4	$2.26 \cdot 10^{-3}$	-	-	-
8	0.4	-	8.3	-
9	0.4	-	6.9	-
8a	0.3	0.2	5.3	2.9
8b	0.4	0.2	7.4	3.3
8c	0.2	0.1	4.6	3.0
8d	0.2	0.1	4.9	2.9
8e	0.4	0.3	41.4	5.3
9a	0.5	0.2	5.9	3.1
9b	0.4	0.2	7.0	3.0
9c	0.4	0.2	5.4	2.7
9d	0.5	0.2	7.2	3.7
9e	0.6	0.3	34.4	6.9

For these two compounds (**8e** and **9e**), time resolved spectra were performed and the resulting kinetics show the clear predominance of the monomer emission regarding the excimer at increasing times in agreement with the longer recorded decay times (*Figure 6.10*)

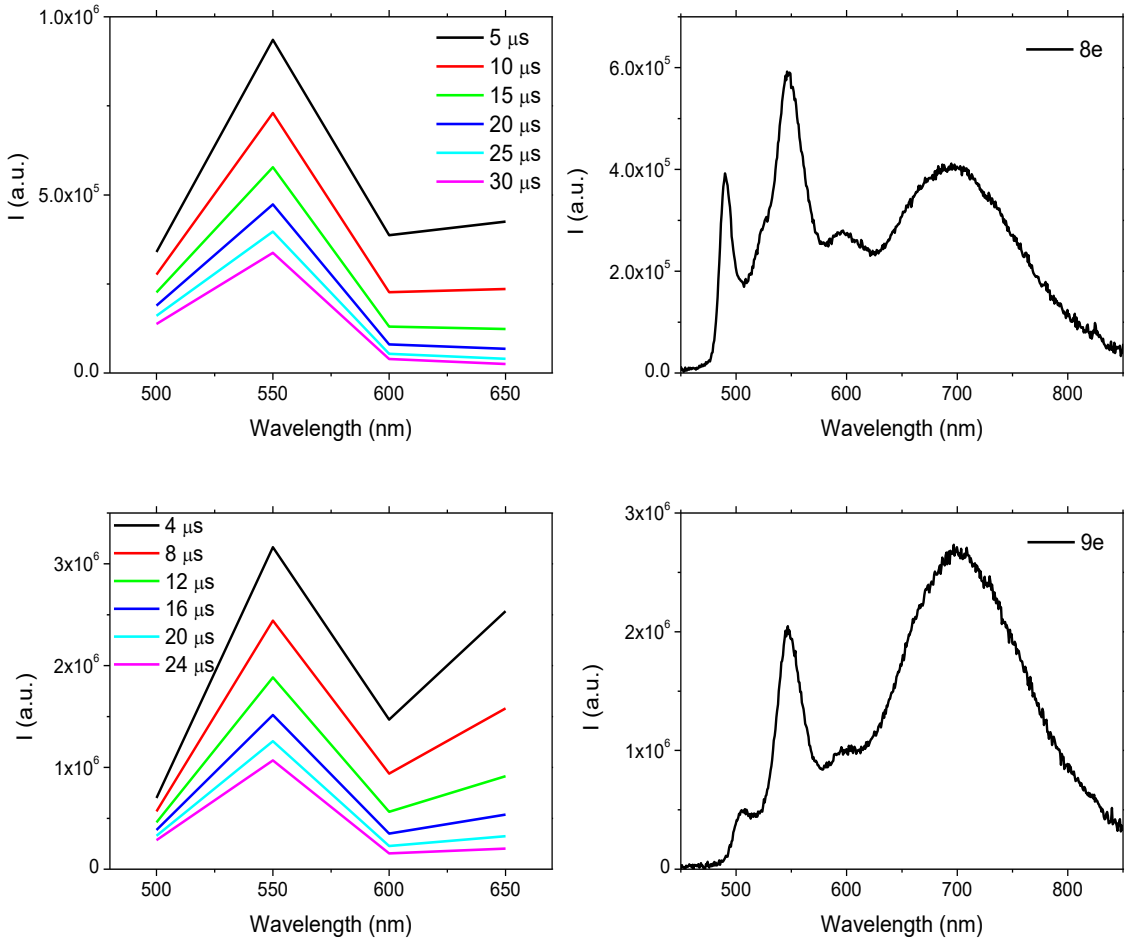

Figure 6.10. Time-resolved phosphorescence spectra (left) and emission spectra (right) in dearated dichloromethane solutions at 298 K of compounds **8e** and **9e**.

Radiative and non-radiative constants were calculated from the experimental quantum yields and lifetime values (*Table 6.4*). According to the values, the increase in the monomer emission quantum yield is attributed to a decrease in the non-radiative deactivation pathways rate, as the non-radiative constant values (k_{nr}) are of one order of magnitude smaller than in air-equilibrated samples while radiative constants (k_r) stay the same. Additionally, in the excimer emission band, we can observe that the k_{nr} values for the phenanthrene derivatives **8e** and **9e** are smaller than those calculated for the rest of

compounds, in agreement with the significant increase in the emission intensity of this band in these compounds.

Table 6.4. Spectral data including radiative and non-radiative rate constants obtained in air-equilibrated (with O_2) or degassed (N_2 sat.) dichloromethane solutions.

Compound	k_r (μs^{-1}) monomer (with O_2)	k_{nr} (μs^{-1}) monomer (with O_2)	k_r (μs^{-1}) monomer (N_2 sat.)	k_{nr} (μs^{-1}) monomer (N_2 sat.)	k_r (μs^{-1}) excimer (N_2 sat.)	k_{nr} (μs^{-1}) excimer (N_2 sat.)
L3	1.02	254.73	-	-	-	-
L4	3.08	439.38	-	-	-	-
8	0.08	2.32	0.07	0.05	-	-
9	0.08	2.51	0.10	0.05	-	-
8a	0.12	3.04	0.09	0.10	0.05	0.29
8b	0.10	2.17	0.05	0.08	0.05	0.25
8c	0.14	4.34	0.08	0.14	0.05	0.28
8d	0.18	4.28	0.09	0.11	0.03	0.31
8e	0.03	2.62	0.03	0.21	0.04	0.15
9a	0.07	1.77	0.08	0.09	0.04	0.29
9b	0.07	2.33	0.05	0.10	0.05	0.28
9c	0.09	2.65	0.09	0.10	0.05	0.33
9d	0.06	2.15	0.04	0.10	0.06	0.21
9e	0.02	1.66	0.02	0.27	0.04	0.10

In solid state, all compounds present a broad emission band centred between 579 and 626 nm (*Figure 6.11*) which can be assigned to the emission of the π-π stacked forms that are in accordance with the observation of the dimer formation in the obtained crystalline structures.[24]

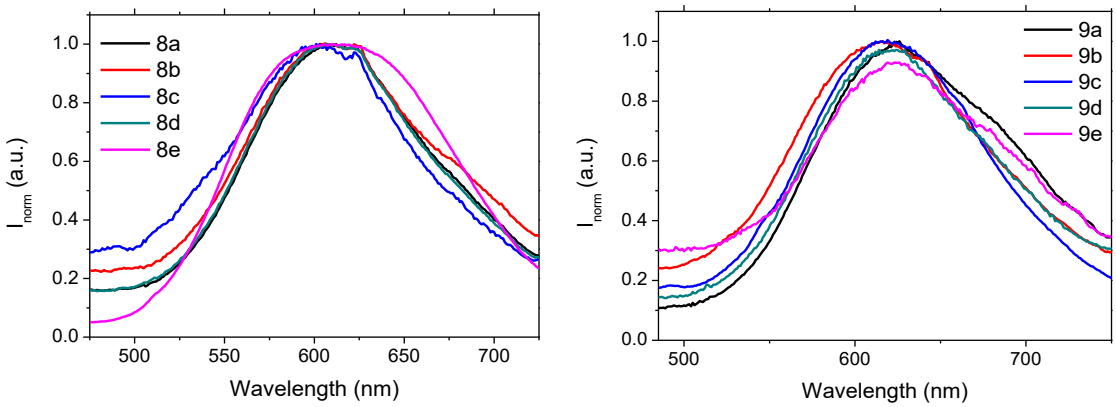

Figure 6.11. Normalized emission spectra in solid state of compounds **8x (left)** and **9x** (right) at 298 K (λ_{exc} = 390 nm).

Phosphorescence quantum yields have moderate values up to 12 % and the corresponding lifetimes are of hundreds of nanoseconds, in agreement with a triplet state emission origin (*Table 6.5*). It can be observed that quantum yields for compounds **8x** in the solid state are larger than in solution while in the case of compounds **9x** these values are in the same order as those previously recorded in dichloromethane. This can be rationalized to the more efficient intermolecular packing in the absence of the fluorine atom at the cyclometallated ligand that seems to favor the π-π stacking and the formation of aggregates, as previously observed in the packing in the X-ray diffraction determined structures. Interestingly, the calculated k_r and k_{nr} values show an enhancement of the radiative deactivation channels with k_r values larger for compounds **8x** and **9x** and k_{nr} smaller (**8x**) or similar (**9x**) than those previously obtained in air-equilibrated solution samples.

Table 6.5. Electronic absorption and emission data including absorption and emission maxima and phosphorescence quantum yields recorded in solid state (powder).

Compound	λ_{em}^{max} (nm)	ϕ_{Ph}	τ (µs)	k_r (µs^{-1})	k_{nr} (µs^{-1})
L3	357	0.005	-	-	-
L4	390	0.008	-	-	-
8	559	0.03	0.7	0.05	1.39
9	506	0.02	0.5	0.04	2.01
8a	612	0.14	0.4	0.35	2.20
8b	611	0.09	0.5	0.18	1.75
8c	601	0.05	0.6	0.08	1.60
8d	610	0.10	0.6	0.18	1.51
8e	609	0.12	0.7	0.17	1.23
9a	626	0.03	0.4	0.07	2.41
9b	617	0.06	0.3	0.17	2.78
9c	616	0.04	0.7	0.06	1.42
9d	625	0.13	0.4	0.30	2.09
9e	623	0.02	0.3	0.06	3.15

6.2.4. DFT calculations

To further understand the experimental results, DFT calculations were performed for compounds **8x** and **9x** and their precursors in solution using the BL3YP functional, 6-31G*/LANL2DZ basis set and CPCM solvation model. In all cases, the experimental geometries are well reproduced and show that the aromatic group is nearly perpendicular to the cyclometallated moiety (*Tables 6.6* and *6.7*). The calculated values for bond lengths and angles match well those found experimentally in the crystal structure for compounds

8e and **9c**. In particular, the calculated torsion angles (80.5º for **8e** and 75.2º for **9c**) are close to the values observed experimentally (85.3º for **8e** and 83.3º for **9c**).

Upon analysis of the results, it can be observed that the change of a hydrogen for a fluorine in the central position of the cyclometallated ligand (compounds **8x** *versus* **9x**) results in a shortening of the distance between the platinum and the alkynyl ligand in *trans* position with respect to the metallated carbon while the bond length between the metal and this carbon remains constant. Finally, no significant variations in the distances and angles are observed when changing the nature of the aromatic ring attached to the alkynyl bond.

Table 6.6. Key geometrical parameters optimized at the DFT level in solution for compounds **8** and **8x**. C(1): metallated carbon of the pincer ligand. C(2): Alkyne carbon bonded to platinum. C(3): Alkyne carbon bonded to the aromatic moiety. C(4): aromatic carbon bonded to the alkyne moiety. Torsion: Angle between the aromatic moiety and the pincer ligand.

Parameter	8	8a	8b	8c	8d	8e
Pt-Cl	2.521	--	--	--	--	--
Pt-C(1)	1.930	1.962	1.961	1.962	1.963	1.963
Pt-N	2.076	2.080	2.080	2.080	2.081	2.082
Pt-C(2)	--	2.077	2.076	2.078	2.073	2.074
C(2)-C(3)	--	1.232	1.231	1.231	1.232	1.232
C(3)-C(4)	--	1.429	1.429	1.426	1.428	1.427
C(1)-Pt-N	80.4	79.5	79.5	79.5	79.5	79.5
C(1)-Pt-Cl	179.9	--	--	--	--	--
C(1)-Pt-C(2)	--	179.2	179.9	179.3	179.9	180.0
N-Pt-N	160.8	159.0	159.1	159.0	159.0	159.0
N-Pt-Cl	99.6	--	--	--	--	--
N-Pt-C(2)	--	100.5	100.5	100.5	100.5	100.5
Torsion	--	90.6	91.1	73.9	80.8	80.5

Table 6.7. Key geometrical parameters optimized at the DFT level in solution for compounds **9** and **9x**. C(1): metallated carbon of the pincer ligand. C(2): Alkyne carbon bonded to platinum. C(3): Alkyne carbon bonded to the aromatic moiety. C(4): aromatic carbon bonded to the alkyne moiety. Torsion: Angle between the aromatic moiety and the pincer ligand

Parameter	9	9a	9b	9c	9d	9e
Pt-Cl	2.516	--	--	--	--	--
Pt-C(1)	1.930	1.961	1.962	1.962	1.963	1.963
Pt-N	2.075	2.079	2.080	2.081	2.081	2.082
Pt-C(2)	--	2.073	2.077	2.076	2.071	2.072
C(2)-C(3)	--	1.231	1.232	1.231	1.232	1.232
C(3)-C(4)	--	1.430	1.429	1.426	1.428	1.428
C(1)-Pt-N	80.4	79.5	79.5	79.4	79.5	79.4
C(1)-Pt-Cl	180.0	--	--	--	--	--
C(1)-Pt-C(2)	--	179.9	179.2	179.5	179.9	180.0
N-Pt-N	160.7	159.0	159.0	158.9	158.9	158.9
N-Pt-Cl	99.6	--	--	--	--	--
N-Pt-C(2)	--	100.5	100.5	100.6	100.6	100.6
Torsion	--	90.9	90.6	74.4	80.8	80.4

The rotation of the phenanthrene moiety was also studied for compound **8e** to determine the possibility of the existence of rotational conformers using the same level of theory. The calculated barrier of 3.3 kJ/mol is not high enough to allow free rotation around the triple bond, therefore confirming that only the almost perpendicular conformation can be present in solution.

TD-DFT calculations were performed for compounds **8x** and **9x** and their precursors in solution, using the geometries previously optimized, to calculate the UV absorption spectra using dichloromethane as solvent. *Figures 6.12* and *6.13* show the energy and the nature of the orbitals involved in these transitions for all compounds, which are in all cases of the π-π* type.

HOMO → LUMO transitions are only observable in compounds **8** and **9**. The HOMO orbital is centered mainly in the central ring of the cyclometallated moiety, with smaller contributions from the platinum atom and the chlorido ligand, while the LUMO has the greatest contribution from the N-substituted rings of the same pincer ligand, also with a small contribution of the platinum atom. This transition is ILCT/LLCT in character.

For compounds **8x**, the lowest energy absorption band around 390 nm corresponds mainly to a HOMO-1 → LUMO+1 transition. The former is based mainly in the alkyne moiety and the central ring of the cyclometallated ligand, with a very small contribution of Pt, while the latter is based mainly on the three rings of the same ligand. Thus, this transition is ILCT/LLCT in character.

In this same energy region, compounds **9x** show an absorption band at this region in addition to HOMO-1 → LUMO+1 transition the that can be assigned it to a HOMO-1 → LUMO transition. As previously stated, HOMO-1 has a contribution of the alkyne moiety and the central ring of the cyclometallated ligand, while LUMO is centered on the N-substituted rings of the pincer ligand, thus this transition is also ILCT/LLCT in character. As an exception, compound **9e** only displays the latter transition.

Compounds with napthalene (**8d, 9d**) and phenanthrene (**8e**, **9e**) moieties also feature a band in the 309-319 nm interval. There are several transitions that can contribute to this band, but the one that is always present is HOMO-3 → LUMO+1 (HOMO-3 → LUMO for **9e**). Both orbitals are centered in the pincer ligand and so this transition can be regarded as ILCT.

Finally, complexes **8e** and **9e** feature a supplementary absorption band at 333-334 nm, that can be ascribed to the HOMO → LUMO+2 transition. Both orbitals are centered mainly in the phenanthrene moiety so the transition can be assigned to an ILCT.

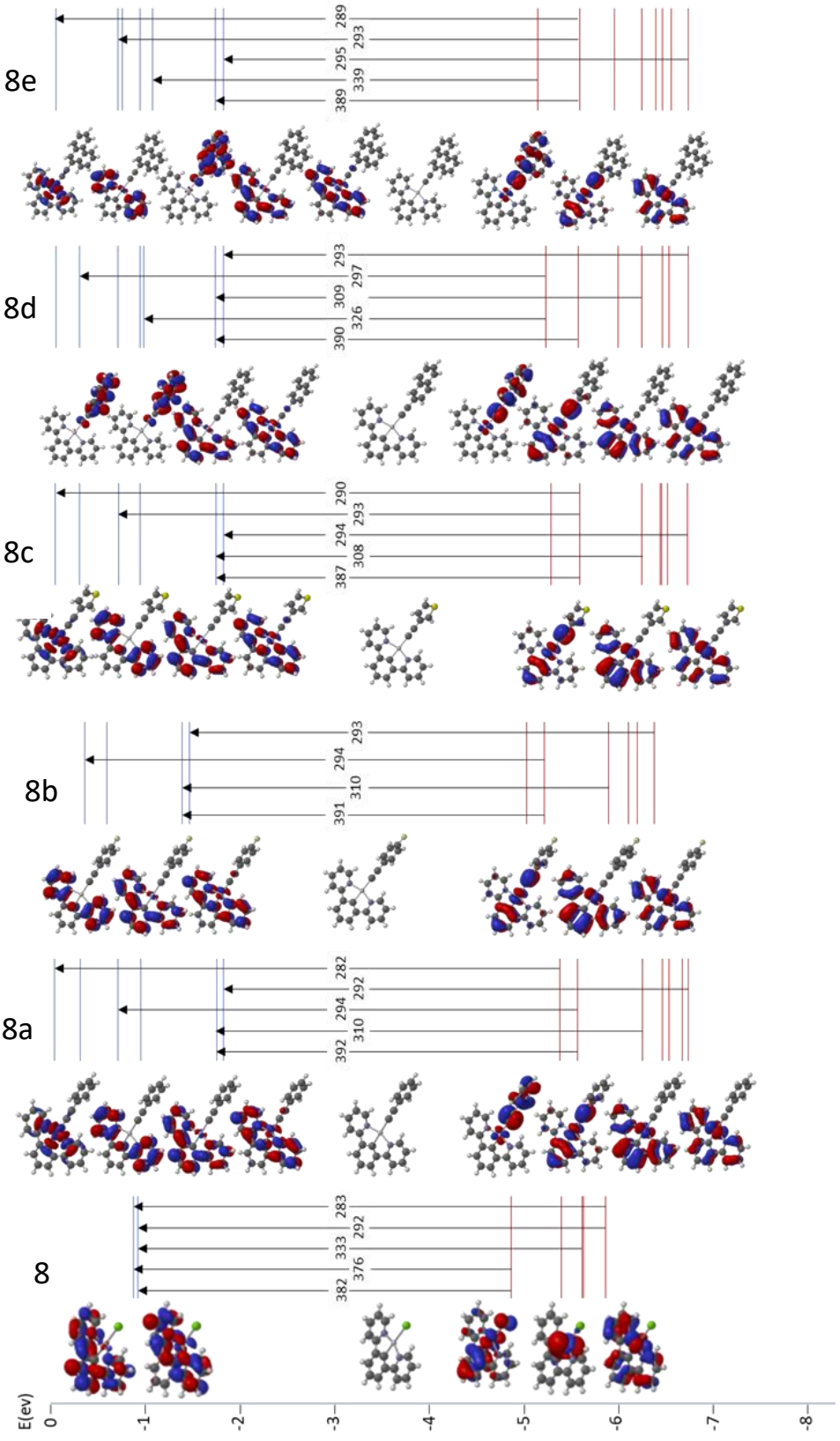

Figure 6.12. Orbitals that participate in the UV-vis transitions discussed in the text for compounds **8** and **8x**. Red lines, occupied orbitals; blue lines, empty orbitals. The numbers in the arrows show the energy of the transition in nm. The y-axis indicates the energy of the orbitals.

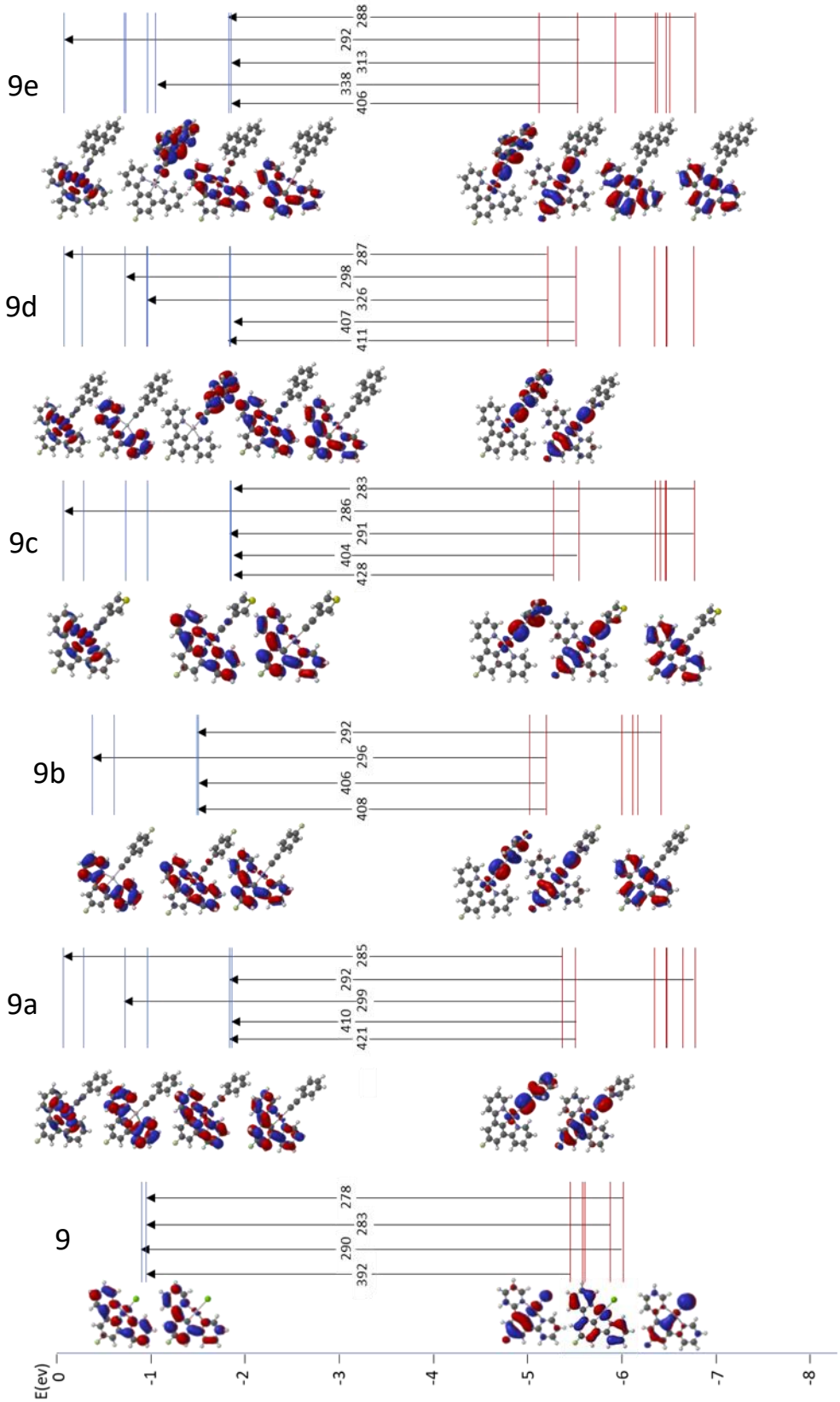

Figure 6.13. Orbitals that participate in the UV-vis transitions discussed in the text for compounds **9** and **9x**. Red lines, occupied orbitals; blue lines, empty orbitals. The numbers in the arrows show the energy of the transition in nm. The y-axis indicates the energy of the orbitals.

The triplet state for compounds **8x** and **9x** and their precursors were optimized in solution to study their emission spectra and the triplet-singlet transitions were calculated using dichloromethane as a solvent and are listed in *Table 6.8*. The geometries differ from the ground state in the orientation of the aromatic ring attached to the alkynyl bond. In the ground state this ring was found to be nearly perpendicular to the cyclometallated moiety whereas in the triplet state is nearly coplanar.

Table 6.8. Experimental and calculated emission energies.

Compound	λ_{em} (exp, nm)	λ_{em} (calc, nm)	Assignment
8	490	440.1	LUMO → HOMO-1
9	505	521.6	LUMO+1 → HOMO
8a	497	485.6	LUMO+1 → HOMO
8b	495	486.8	LUMO+1 → HOMO
8c	501	494.9	LUMO+1 → HOMO
8d	490	485.3	LUMO+1 → HOMO
8e	547	514.4	LUMO → HOMO (43%) LUMO+2 → HOMO (38%)
9a	507	503.6	LUMO+1 → HOMO
9b	511	505.6	LUMO+1 → HOMO
9c	513	512.9	LUMO+1 → HOMO
9d	520	518.0	LUMO+1 → HOMO
9e	547	527.9	LUMO+1 → HOMO

The main emission band corresponds, in most cases, to a LUMO +1 → HOMO transition, being the first one centred in the alkynyl aromatic moiety and the latter in the cyclometallated ligand with some contribution of the metal. Therefore, this transition can be assigned to present a mixed intra-ligand, ligand-to-ligand, and metal-to ligand charge transfer (ILCT/LLCT/MLCT) character in nature, confirming the previous assignment. As an example, *Figure 6.14* shows the orbitals that take part in this transition for compound **8a**.

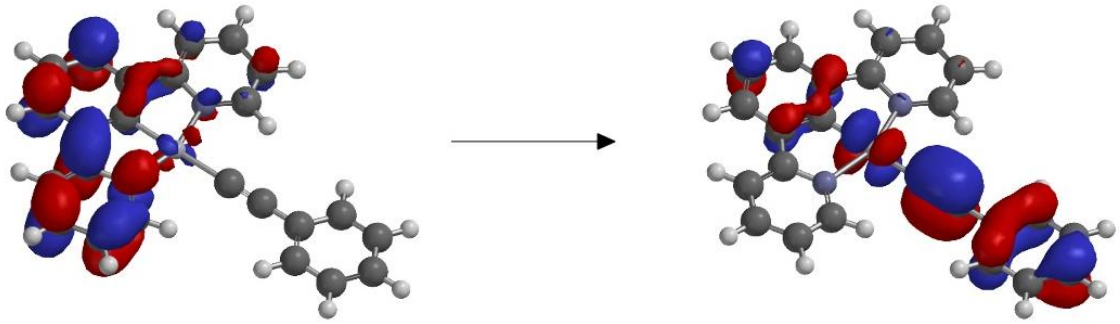

Figure 6.14. LUMO+1 and HOMO orbitals for complex **8a**.

As an exception, compound **8e** has a contribution from LUMO → HOMO and LUMO-2 → HOMO transitions. In this case, the HOMO orbital is again based mainly in the alkynyl aromatic moiety and the LUMO in the cyclometallated ligand, thus corresponding to the LUMO+1 of the remaining systems. In contrast, the LUMO+2 orbital is centred mainly in the phenanthrene group.

6.2.5. Aggregation induced emission experiments (AIE)

To try to induce the red-shifted emission in air-equilibrated samples, water was tested as a bad solvent to induce aggregation by preparing several acetonitrile/water mixtures. The resulting behavior is observed to be strongly dependent on the alkynyl aromatic group. In general, the formation of a new band around 650 nm due to the formation of emissive aggregates can be observed (*Figure 6.15*).

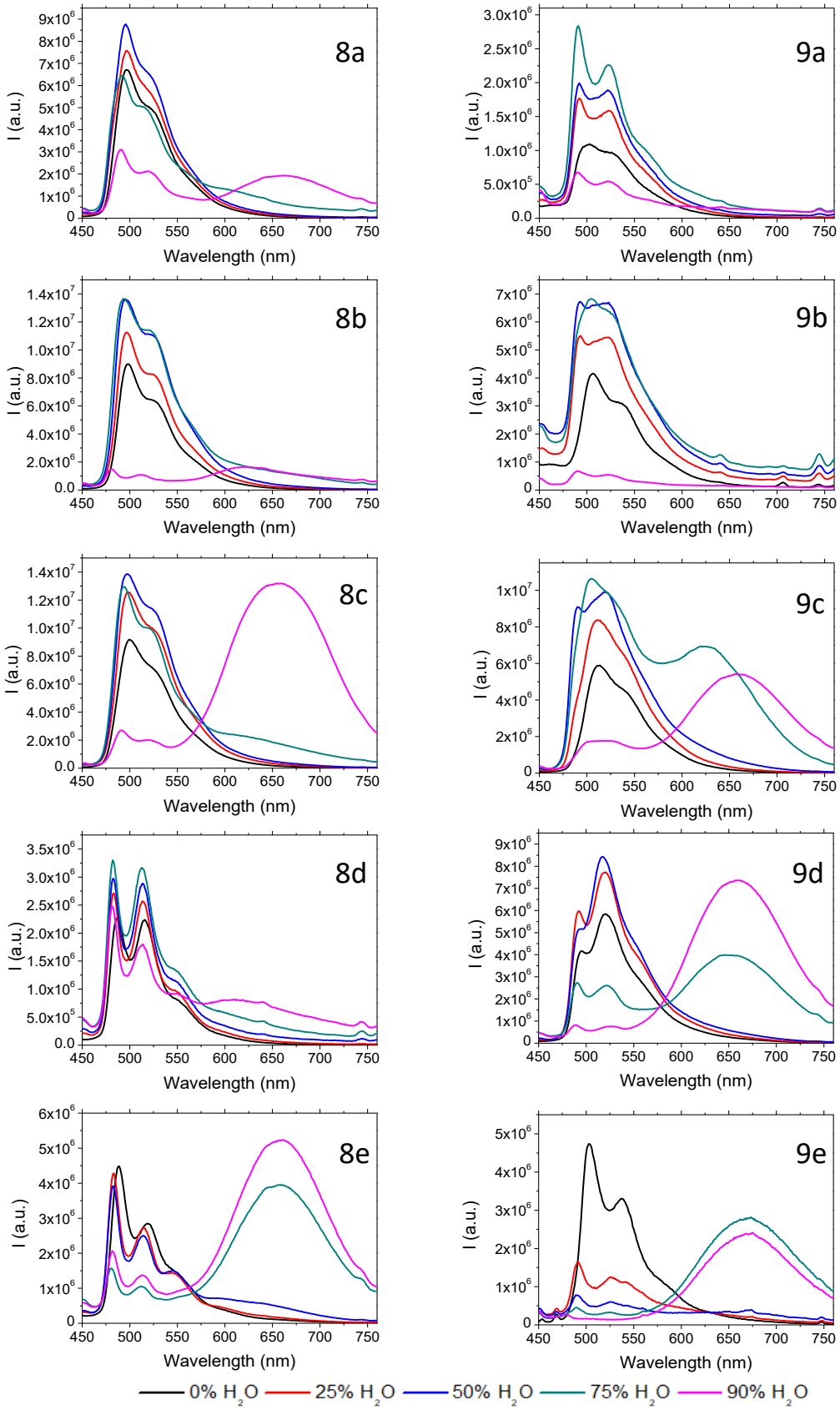

Figure 6.15. Emission spectra for acetonitrile/water mixtures of compounds **8x** (left) and **9x** (right) at 298 K (λ_{exc} = 390 nm).

The assignment of this emission band to the excimer in acetonitrile is discarded, since the latter appears at larger wavelengths, as evidenced upon deoxygenation of the acetonitrile samples (*Figure 6.16*). Excitation spectra also supports this assignment since it displays a different profile from the recorded for the monomer, with a significant red-shift upon excitation at the aggregates emission band (*Figure 6.16*).

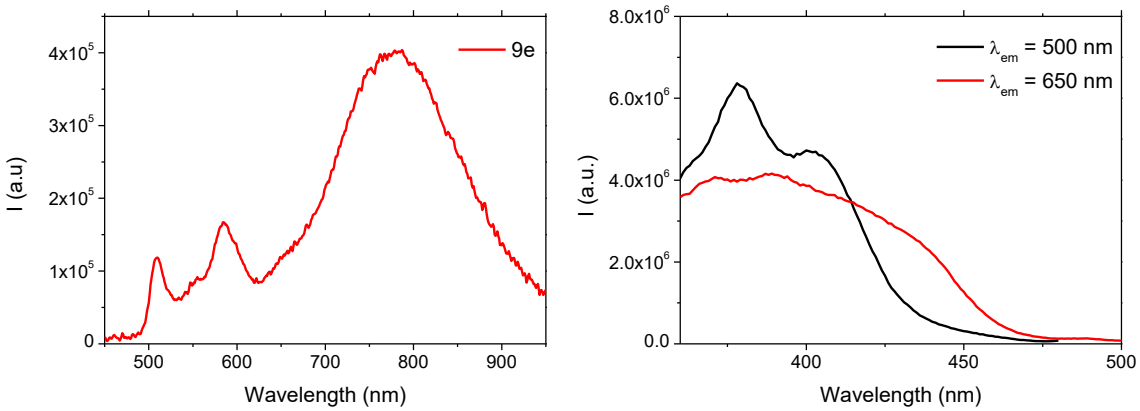

Figure 6.16. Emission spectra for a N_2-saturated acetonitrile solution of compound **9e** at 298 K (λ_{exc} = 390 nm) (left) and excitation spectra of compound **9e** in a 90% water/10% acetonitrile at the two different emission maxima at 298 K (right).

The aggregation induced emission (AIE) band is enhanced when the percentage of water is higher than 75%. At 90% water contents, this emission reaches the maximum intensity, and, in some cases, it is predominant to the monomer, even becoming the sole emission in compound **9e** affording a completely red-shifted emission. In fact, AIE seems to be more favored in compounds **9x** (*Figure 6.17*), probably due to the presence of the fluoro substituent that can establish additional intermolecular contacts favoring the aggregation process.

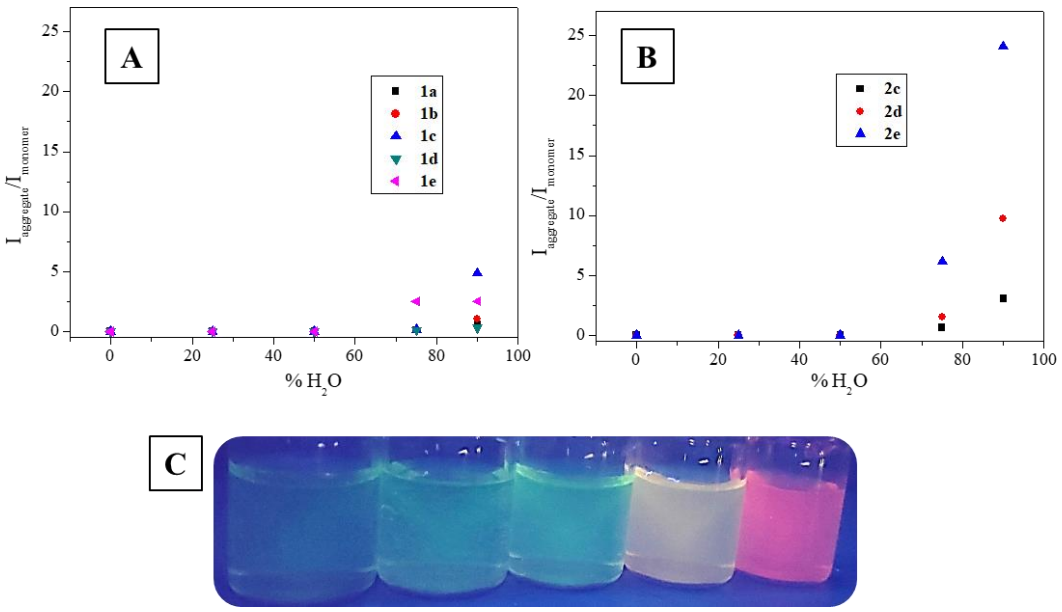

Figure 6.17. A) Plot of the $I_{aggregates}/I_{monomer}$ of compounds **8x** at different water contents (only compounds that aggregate are included in the plot); **B)** Plot of the $I_{aggregates}/I_{monomer}$ of compounds **9x** at different water contents (only compounds that aggregate are included in the plot); **C)** Acetonitrile/water mixtures under the UV lamp for compound **9e** (increasing water content from left to right: 0, 25, 50, 75 and 90%).

The total phosphorescence quantum yield increases when increasing the water percentage, as expected for an AIE behavior. This is also supported by the increasing contribution of the aggregates' quantum yield when it is present by splitting the global QY value in the corresponding contribution of the monomer and the aggregated forms. The phosphorescence lifetime values of both monomer and aggregates become larger with increasing water contents in all compounds with, in all cases, a larger lifetime for the monomeric species (*Tables 6.9* and *6.10*).

Table 6.9. Phosphorescence quantum yields and lifetimes recorded in aerated acetonitrile/water mixtures for compounds **8x**.

Compound	% H_2O	ϕ_{Ph}	ϕ_{Ph} monomer	ϕ_{Ph} aggregates	τ (μs) monomer	τ (μs) aggregates
	0	0.01	0.01	-	0.19	0.06
	25	0.02	0.02	-	0.37	0.09
8a	50	0.02	0.02	-	0.48	0.01
	75	0.03	0.01	0.02	0.85	0.27
	90	0.04	0.01	0.03	1.34	0.13
	0	0.01	0.01	-	0.25	0.08
	25	0.01	0.01	-	0.37	0.10
8b	50	0.02	0.02	-	0.47	0.15
	75	0.03	0.02	0.02	0.87	0.23
	90	0.04	0.01	0.03	1.25	0.10
	0	0.01	0.01	-	0.23	0.05
	25	0.01	0.01	-	0.35	0.07
8c	50	0.02	0.02	-	0.52	0.01
	75	0.04	0.01	0.02	0.86	0.25
	90	0.12	0.01	0.12	1.25	0.23
	0	0.01	0.01	-	0.26	0.11
	25	0.01	0.01	-	0.37	0.02
8d	50	0.02	0.02	-	0.50	0.10
	75	0.02	0.01	0.01	0.95	0.19
	90	0.03	0.01	0.02	1.17	0.09
	0	0.01	0.01	-	0.22	0.08
	25	0.01	0.01	-	0.36	0.16
8e	50	0.02	0.02	-	0.44	0.21
	75	0.07	0.01	0.06	0.74	0.20
	90	0.08	0.01	0.07	0.79	0.18

Table 6.10. Phosphorescence quantum yields and lifetimes recorded in aerated acetonitrile/water mixtures for compounds **9x**.

Compound	% H_2O	ϕ_{Ph}	ϕ_{Ph} monomer	ϕ_{Ph} aggregates	τ (μs) monomer	τ (μs) aggregates
	0	0.01	0.01	-	0.26	0.12
	25	0.01	0.01	-	0.36	0.18
9a	50	0.02	0.02	-	0.48	0.24
	75	0.03	0.03	-	0.76	0.11
	90	0.01	0.01	-	0.91	0.17
	0	0.01	0.01	-	0.24	0.10
	25	0.02	0.02	-	0.36	0.09
9b	50	0.02	0.02	-	0.47	0.13
	75	0.03	0.03	-	0.78	0.23
	90	0.01	0.01	-	0.77	0.09
	0	0.01	0.01	-	0.21	0.08
	25	0.01	0.01	-	0.22	0.08
9c	50	0.02	0.02	-	0.43	0.11
	75	0.04	0.02	0.02	0.81	0.14
	90	0.06	0.01	0.05	1.18	0.24
	0	0.01	0.01	-	0.22	0.08
	25	0.01	0.01	-	0.34	0.07
9d	50	0.01	0.01	-	0.44	0.03
	75	0.02	0.01	0.02	0.78	0.26
	90	0.07	0.01	0.07	0.78	0.11
	0	0.01	0.01	-	0.27	0.12
	25	0.01	0.01	-	0.35	0.20
9e	50	0.02	0.02	-	0.46	0.25
	75	0.06	0.01	0.05	0.77	0.18
	90	0.11	-	0.11	0.73	0.14

Radiative (k_r) and non-radiative (k_{nr}) constants were calculated for the monomer and the aggregated species where it is observable. It can be observed that the non-radiative deactivation processes are more favored in both the monomer and the aggregates, as expected for air-equilibrated conditions. Additionally, the more efficient AIE effect is directly related to the k_r rate constant. A significant increase of k_r is detected (up to one order of magnitude for compound **9d** from 0.07 s^{-1} with a 75% of H_2O to 0.66 s^{-1} with a 90% of H_2O) in the emission of the aggregates, while the contribution of k_{nr} is much less important. That is, the aggregation processes induced by the addition of water in the acetonitrile solutions are favoring the intermolecular contacts and the close distance between the molecules making the environment more rigid and favoring the efficiency of the radiative emission process.[36]

6.3. Conclusions

In this chapter, two families of [N,C,N] cyclometallated compounds has been synthesised and a thorough photophysical study has revealed their phosphorescent properties with different emission origins.

The presence of the alkynyl moiety as an ancillary ligand allows not only the phosphorescence of the monomeric species, such as what is observed in the chlorido precursors, but also the appearance of a red-shifted emission band at 700 nm in degassed solutions assigned to the formation of an excimer. The emission from the monomer has been assigned to a $^{3}\pi$-π^* transition from the [N,C,N] cyclometallated ligand that can be mixed with ^{3}MLCT or ^{3}ILCT, which is supported by DFT calculations.

Additionally, the red shift of the emission has been induced in air equilibrated conditions by using a mixture of good and bad solvents, which results in the formation of emissive aggregates that present aggregation induced emission (AIE) displaying a broad band centred around 650 nm.

For both emission origins, the behaviour is dependent on the aromatic group attached to the alkynyl moiety. Specifically, compounds **8e** and **9e** that contain a phenanthrene group, are the ones which present a larger excimer formation and a higher ability to form aggregates, being the sole emission in compound **9e** in the mixture with the highest percentage of water and therefore achieving a completely red-shifted emission. This agrees with their ability to establish π-π stacking interactions between two cyclometallated moieties that has been observed in the X-ray crystal structure.

6.4. Experimental Section

6.4.1. General procedures

Commercial reagents 1,3-dibromobenzene (Fluorochem, 99%), 2-(tributylstannyl)pyridine (Fluorochem, 95%), copper oxide (CuO, Probus, >99%), 1,3-dibromo-5-fluorobenzene (Fluorochem, 98%), sodium sulphate (Na_2SO_4, Panreac, 99%), potassium tetrachloroplatinate (K_2PtCl_4, Johnson Mattheys, 98%), phenylacetylene (Sigma Aldrich, 98%), sodium hydroxide (NaOH, Panreac, 98%) 1-ethynyl-4-fluorobenzene (Sigma Aldrich, 99%), 3-ethynyltiophene (Sigma Aldrich, 96%), 2-ethynylnaphthalene (Sigma Aldrich, 97%) and 9-ethynylphenanthrene (Sigma Aldrich, 97%); and solvents N,N-dimethylformamide (DMF, Panreac, 99%), ethyl acetate (Panreac, 99.5%), acetic acid (Panreac, >99%), methanol (Sigma Aldrich, >99%), ethanol (Fischer, >99%), diethyl ether (Carlo Erba, >99%), and hexane (Sigma Aldrich, >98%) were used as received.

6.4.2. Physical measurements

NMR spectra were recorded in $CDCl_3$ at the Unitat de RMN of the Universitat de Barcelona with a Mercury 400 spectrometer (^1H, 400 MHz; ^{19}F, 376.5 MHz). Chemical shifts are given in δ values (ppm) relative to TMS (^1H) or $CFCl_3$ (^{19}F) and coupling constants J are given in Hz.

Infrared spectra were recorded in a Thermo Scientific FT-IR Nicolet iS5 spectrometer with an iD7 ATR accessory. IR frequencies ν are given in cm^{-1}.

Electrospray mass spectra were performed at the *Unitat d'Espectrometria de Masses (Universitat de Barcelona)* in a LC/MSD-TOF spectrometer using H_2O-CH_3CN 1:1 to introduce the sample.

UV/Vis spectra were recorded in CH_2Cl_2 with a Cary 100 scan 388 Varian UV spectrometer. Emission and excitation spectra were recorded in a Horiba Jobin-Yvon SPEX Nanolog-TM spectrofluorimeter at 298 K using $5 \cdot 10^{-5}$M solutions and in solid state.

Emission quantum yields were determined with a Hamamatsu Quantaurus QY absolute photoluminescence quantum yield spectrometer C11347.

Luminescence lifetimes were measured on a JYF-DELTAPRO-NL equipment upon excitation of the samples with a 390 nm NanoLED and collecting the decays through a cut-off filter of 450 nm.

6.4.3. Synthesis and characterisation

Synthesis of 1,3-di(2-pyridinyl)benzene (L3)

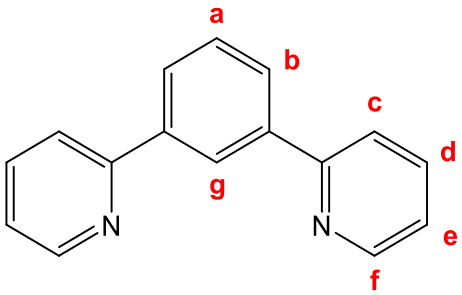

Ligand 1,3-di(2-pyridinyl)benzene (**L3**)[22] was obtained by slight modification of the method described in the literature from 0.121 ml (1 mmol) of 1,3-dibromobenzene, 0.971 ml (3 mmol) of 2-(tributylstannyl)pyridine, 0.240 g (3 mmol) of CuO and 0.007 g (0.1 mmol) of $[PdCl_2(PPh_3)_2]$ in 4 ml of dimethylformamide under a nitrogen atmosphere. The mixture was heated in a microwave reactor for 1 hour at 160 ºC. After cooling, the mixture was poured into 50 ml of ethyl acetate and was filtered. The filtrate was washed with water and dried over sodium sulphate. The resulting solution was evaporated to dryness and the crude mixture was purified by column chromatography using a mixture of hexane/diethyl ether (1:1) to give a white solid. Yield: 0.154 g (66%)

^{1}H NMR ($CDCl_3$, 400 MHz): δ 8.74 [d, 2H, ^{3}J(H-H) = 4.6, H^f], 8.66 [s, 1H, H^g], 8.09 [dd, 2H, ^{3}J(H-H) = 7.8, ^{4}J(H-H) = 1.6, H^b], 7.89 [d, 2H, ^{3}J(H-H) = 7.9, H^c], 7.82 [td, 2H, ^{3}J(H-H) = 7.8, ^{4}J(H-H) = 1.6, H^d], 7.61 [t, 1H, ^{3}J(H-H) = 7.8 Hz, H^a], 7.27-7.32 [m, 2H, H^e].

Synthesis of 2,2'-(5-fluoro-1,3-phenylene)dipyridine (L4)

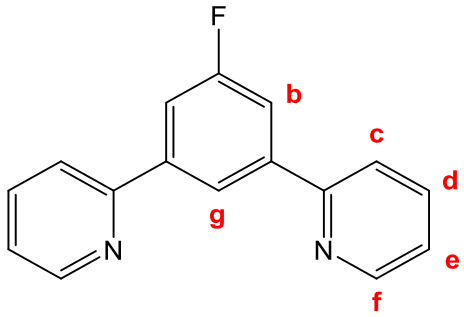

Ligand 2,2'-(5-fluoro-1,3-phenylene)dipyridine (**L4**)[22] was prepared as a white solid by following the same method from 0.126 ml (1 mmol) of 1,3-dibromo-5-fluorobenzene, 0.971 ml (3 mmol) of 2-(tributylstannyl)pyridine, 0.240 g (3 mmol) of CuO and 0.007 g (0.1 mmol) of $[PdCl_2(PPh_3)_2$. Yield: 0.178 g (71%)

^{1}H NMR ($CDCl_3$, 400 MHz): δ 8.74 [dd, 2H, ^{3}J(H-H) = 7.5, ^{4}J(H-H) = 5, , H^f], 8.43 [t, 1H, ^{4}J(H-H) = 1.5 Hz, H^g], 7.76-7.81 [m, 6H, $H^{b,c,d}$], 7.25-7.31 [m, 2H, H^e].

Synthesis of [PtCl{2,6-(2-$C_5H_4N)_2$-C_6H_3}] (8)

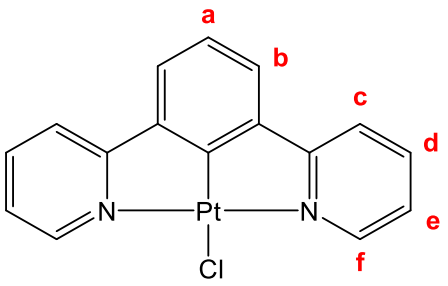

Compound [PtCl{2,6-(2-$C_5H_4N)_2$-C_6H_3}] (**8**)[22] was obtained by following the method reported in the literature from 0.138 g (0.332 mmol) of potassium tetrachloroplatinate and 0.077 g (0.332 mmol) of 1,3-di(2-pyridyl)benzene (**L3**) in 4 ml of acetic acid/water (9:1). The mixture was heated in a microwave reactor for 30 min at 160 ºC. After cooling, the mixture was filtered and the yellow solid was washed with methanol, water, ethanol and diethyl ether and dried under vacuum. Yield: 0.116 g (76%)

^{1}H NMR ($CDCl_3$, 400 MHz): δ 9.37 [d, 2H, ^{3}J(H-H) = 5.7, ^{3}J(Pt-H) = 44.2, H^f], 7.95 [td, 2H, ^{3}J(H-H) = 7.8, ^{4}J(H-H) = 1.5, H^d], 7.70 [d, 2H, ^{3}J(H-H) = 7.4, H^c], 7.47 [d, 2H, ^{3}J(H-H) = 7.7, H^b], 7.28-7.31 [m, 2H, H^e], 7.24 [t, 1H, ^{3}J(H-H) = 7.7 Hz, H^a].

Synthesis of [PtCl{2,6-(2-C_5H_4N)$_2$-4-FC_6H_2}] (9)

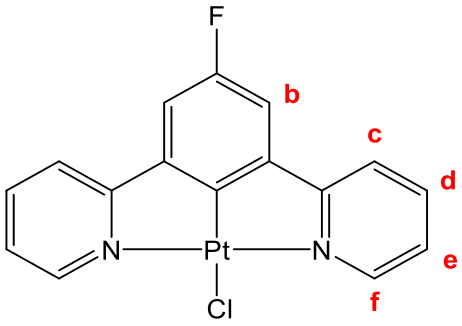

Compound [PtCl{2,6-(2-C_5H_4N)$_2$-4-FC_6H_2}] (**9**)[22] was prepared as a yellow solid by following the same method from 0.060 g (0.200 mmol) of potassium tetrachloroplatinate and 0.040 g (0.200 mmol) of 2,2'-(5-fluoro-1,3-phenylene)dipyridine (**L4**). Yield: 0.070 g (74%)

^{1}H NMR ($CDCl_3$, 400 MHz): δ 9.38 [d, 2H, ^{3}J(H-H) = 5.6, ^{3}J(Pt-H) = 41.6, H^f], 7.99 [td, 2H, ^{3}J(H-H) = 7.8, ^{4}J(H-H) = 1.6, H^d], 7.66 [d, 2H, ^{3}J(H-H) = 7.4, H^c], 7.30-7.38 [m, 2H, H^e], 7.24 [d, 2H, ^{3}J(F-H) = 10.0, H^b].

General Procedure for the synthesis of complexes 8x and 9x[24]

A mixture of arylacetylene and sodium hydroxide were stirred at room temperature under an atmosphere of nitrogen for 30 min. The corresponding precursor **8** or **9** was added and the mixture was further stirred for 24 hours. The obtained solid was filtered, washed with water, methanol and hexane and dried under vacuum.

Synthesis of [Pt(C≡CPh){2,6-(2-C_5H_4N)$_2$-C_6H_3}] (8a)

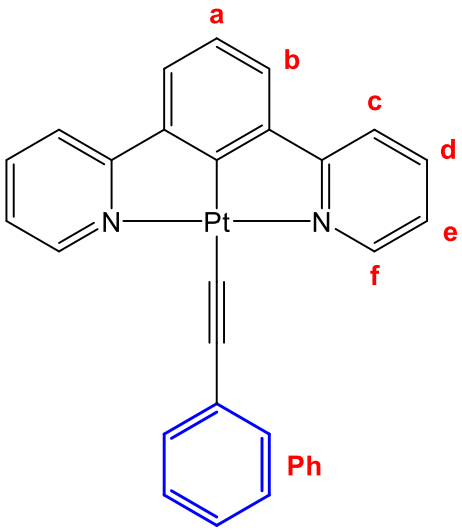

Compound [Pt(C≡CPh){2,6-(2-C_5H_4N)$_2$-C_6H_3}] (**8a**) was obtained as an orange solid from 0.025 g (0.054 mmols) of compound [PtCl{2,6-(2-C_5H_4N)$_2$-4-FC_6H_3}] (**8**), 0.011 g (0.108 mmols) of phenylacetylene and 0.004 g (0.108 mmols) of sodium hydroxide. Yield: 0.017 g (61%).

^{1}H NMR ($CDCl_3$, 400 MHz): δ 9.51 [d, 2H, ^{3}J(Pt-H) = 48.0, ^{3}J(H-H) = 5.6, H^f]; 7.93 [td, 2H, ^{3}J(H-H) = 7.8, ^{4}J(H-H) = 1.6, H^d]; 7.68 [d, 2H, ^{3}J(H-H) = 7.8, H^c]; 7.59 [d, 2H, ^{3}J(H-H) = 8.4; H^{Ph}]; 7.52 [d, 2H, ^{3}J(H-H) = 7.8; H^b]; 7.18-7.31 [m, 6H, $H^{a,e,Ph}$]. **MS-ESI$^+$**: *m/z* 951.06 [2M-C_8H_5]$^+$, 527.10 [M+H]$^+$, 426.06 [M-C_8H_5]$^+$. **IR**: υ 2082 (C≡C).

Synthesis of [Pt(C≡CPh){2,6-(2-C_5H_4N)$_2$-4-FC_6H_2}] (9a)

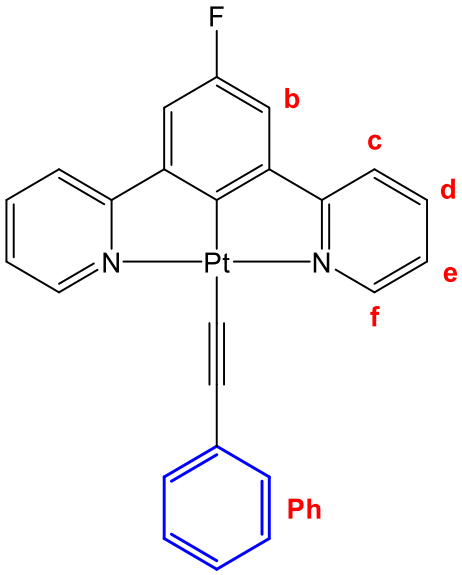

Compound [Pt(C≡CPh){2,6-(2-C_5H_4N)$_2$-4-FC_6H_2}] (**9a**) was obtained as an orange solid from 0.025 g (0.052 mmols) of compound [PtCl{2,6-(2-C_5H_4N)$_2$-4-FC_6H_2}] (**9**), 0.011 g (0.104 mmols) of phenylacetylene and 0.004 g (0.104 mmols) of sodium hydroxide. Yield: 0.017 g (61%).

^{1}H NMR ($CDCl_3$, 400 MHz): δ 9.52 [dd, 2H, ^{3}J(Pt-H) = 47.6, ^{3}J(H-H) = 5.6, ^{4}J(H-H) = 1.6, H^f]; 7.96 [td, 2H, ^{3}J(H-H) = 8.0, ^{4}J(H-H) = 1.6, H^d]; 7.64 [d, 2H, ^{3}J(H-H) = 7.6, H^{Ph}]; 7.58 [dd, 2H, ^{3}J(H-H) = 8.0, ^{4}J(H-H) = 1.1, H^c]; 7.27 [d, 2H, ^{3}J(F-H) = 10.8, H^b]; 7.23-7.26 [m, 4H, $H^{e,Ph}$]; 7.19 [t, 1H, ^{3}J(H-H) = 7.6, H^{Ph}]. **^{19}F NMR** ($CDCl_3$, 376.5 MHz): δ -118.62 [t, 1H, ^{3}J(H-F) = 9.9]. **MS-ESI$^+$**: *m/z* 989.13 $[2M-C_8H_5]^+$, 546.09 $[M+H]^+$, 444.05 $[M-C_8H_5]^+$. **IR**: ν 2085 (C≡C).

Synthesis of [Pt(C≡CPh-F){2,6-(2-C_5H_4N)$_2$-C_6H_3}] (8b)

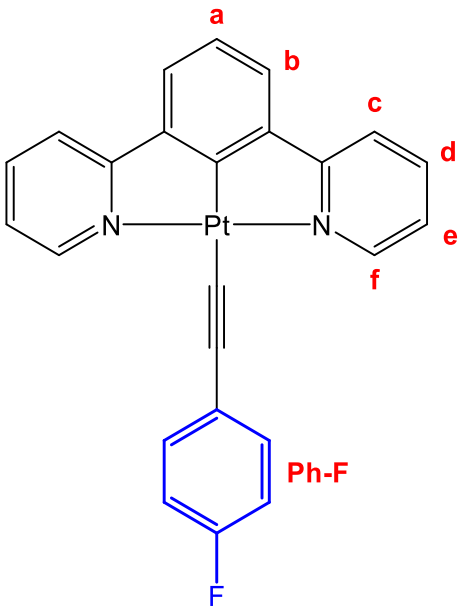

Compound [Pt(C≡CPh-F){2,6-(2-C_5H_4N)$_2$-C_6H_3}] (**8b**) was obtained as an orange solid from 0.020 g (0.043 mmols) of compound [PtCl{2,6-(2-C_5H_4N)$_2$-4-FC_6H_3}] (**8**), 0.010 g (0.086 mmols) of 1-ethynyl-4-fluorobenzene and 0.004 g (0.086 mmols) of sodium hydroxide. Yield: 0.017 g (71%).

^{1}H NMR ($CDCl_3$, 400 MHz): δ 9.49 [d, 2H, ^{3}J(Pt-H) = 47.6, ^{3}J(H-H) = 5.5, H^f]; 7.93 [td, 2H, ^{3}J(H-H) = 7.8, ^{4}J(H-H) = 1.4, H^d]; 7.69 [d, 2H, ^{3}J(H-H) = 7.8, H^c]; 7.51-7.56 [m, 4H, $H^{b,Ph-F}$]; 7.24-7.26 [m, 3H, $H^{a,e}$]; 6.97 [t, 1H, ^{3}J(F-H) = ^{3}J(H-H) = 8.8, H^{Ph-F}]. **^{19}F NMR** ($CDCl_3$, 376.5 MHz): δ -116.03 [m, 1F]. **MS-ESI$^+$**: *m/z* 971.14 [2M-C_8H_4F]$^+$, 546.09 [M+H]$^+$, 426.06 [M-C_8H_4F]$^+$. **IR**: ν 2081 (C≡C).

Synthesis of [Pt(C≡CPh-F){2,6-(2-C_5H_4N)$_2$-4-FC_6H_2}] (9b)

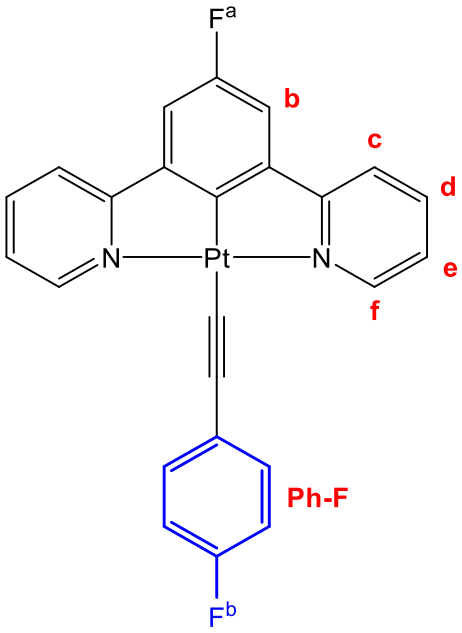

Compound [Pt(C≡CPh-F){2,6-(2-C_5H_4N)$_2$-4-FC_6H_2}] (**9b**) was obtained as an orange solid from 0.020 g (0.042 mmols) of compound [PtCl{2,6-(2-C_5H_4N)$_2$-4-FC_6H_2}] (**9**), 0.010 g (0.084 mmols) of 1-ethynyl-4-fluorobenzene and 0.003 g (0.084 mmols) of sodium hydroxide. Yield: 0.013 g (54%).

^{1}H NMR ($CDCl_3$, 400 MHz): δ 9.50 [d, 2H, ^{3}J(Pt-H) = 48.0, ^{3}J(H-H) = 5.5, H^f]; 7.97 [td, 2H, ^{3}J(H-H) = 7.9, ^{4}J(H-H) = 1.2, H^d]; 7.65 [d, 2H, ^{3}J(H-H) = 7.7, H^c]; 7.53 [dd, 2H, ^{3}J(H-H) = 8.5, ^{4}J(F-H) = 5.6, H^{Ph-F}]; 7.28 [d, 2H, ^{3}J(F-H) = 10.1, H^b]; 7.24-7.26 [m, 2H, H^e]; 6.97 [t, 1H, ^{3}J(F-H) = ^{3}J(H-H) =8.9, H^{Ph-F}]. **^{19}F NMR** ($CDCl_3$, 376.5 MHz): δ -115.88 [m, 1F, F^b], -118.14 [t, 1F, ^{3}J(H-F) = 10.0, F^a]. **MS-ESI$^+$**: *m/z* 1007.12 [2M-C_8H_4F]$^+$, 564.08 [M+H]$^+$, 444.05 [M-C_8H_4F]$^+$. **IR**: ν 2085 (C≡C).

Synthesis of [Pt(C≡CThio){2,6-(2-C_5H_4N)$_2$-C_6H_3}] (8c)

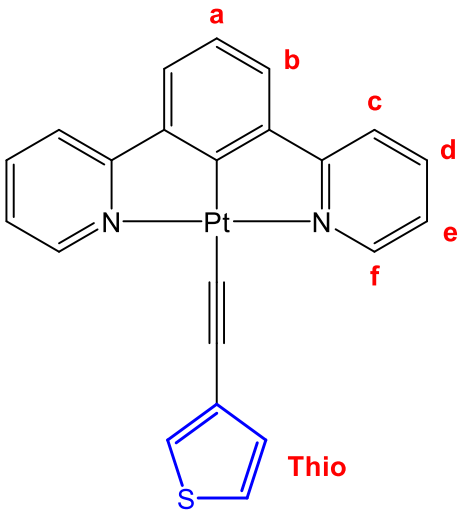

Compound [Pt(C≡CThio){2,6-(2-C_5H_4N)$_2$-C_6H_3}] (**8c**) was obtained as an orange solid from 0.020 g (0.043 mmols) of compound [PtCl{2,6-(2-C_5H_4N)$_2$-4-FC_6H_3}] (**8**), 0.009 g (0.086 mmols) of 3-ethynylthiophene and 0.004 g (0.086 mmols) of sodium hydroxide. Yield: 0.014 g (61%).

^{1}H NMR ($CDCl_3$, 400 MHz): δ 9.50 [dd, 2H, ^{3}J(Pt-H) = 47.6, ^{3}J(H-H) = 5.7, ^{4}J(H-H) = 1.6, H^f]; 7.93 [td, 2H, ^{3}J(H-H) = 7.6, ^{4}J(H-H) = 1.6, H^d]; 7.68 [d, 2H, ^{3}J(H-H) = 8.0, H^c]; 7.52 [d, 2H, ^{3}J(H-H) = 7.7, H^b]; 7.36 [dd, 1H, ^{3}J(H-H) = 2.8, ^{4}J(H-H) = 1.3, H^{Thio}]; 7.18-7.26 [m, 5H, H^{a,e,Thio}]. **MS-ESI$^+$**: *m/z* 959.11 [2M-C_6H_3S]$^+$, 534.06 [M+H]$^+$, 426.06 [M-C_6H_3S]$^+$. **IR**: ν 2076 (C≡C).

Synthesis of [Pt(C≡CThio){2,6-(2-C_5H_4N)$_2$-4-FC_6H_2}] (9c)

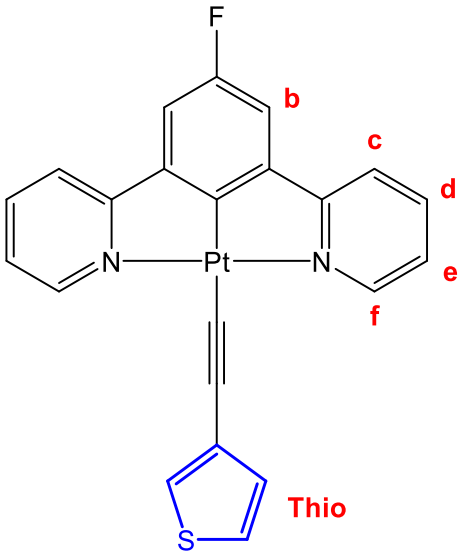

Compound [Pt(C≡CThio){2,6-(2-C_5H_4N)$_2$-4-FC_6H_2}] (**9c**) was obtained as an orange solid from 0.020 g (0.042 mmols) of compound [PtCl{2,6-(2-C_5H_4N)$_2$-4-FC_6H_2}] (**9**), 0.009 g (0.084 mmols) of 3-ethynylthiophene and 0.003 g (0.084 mmols) of sodium hydroxide. Yield: 0.015 g (65%).

^{1}H NMR ($CDCl_3$, 400 MHz): δ 9.51 [dd, 2H, ^{3}J(Pt-H) = 48.4, ^{3}J(H-H) = 5.6, ^{4}J(H-H) = 1.6, H^f]; 7.96 [td, 2H, ^{3}J(H-H) = 7.8, ^{4}J(H-H) = 1.7, H^d]; 7.64 [d, 2H, ^{3}J(H-H) = 7.9, H^c]; 7.36 [dd, 1H, ^{3}J(H-H) = 2.6, ^{4}J(H-H) = 1.5, H^{Thio}]; 7.28 [d, 2H, ^{3}J(F-H) = 10.1, H^b]; 7.21-7.25 [m, 4H, $H^{e,Thio}$]. **^{19}F NMR** ($CDCl_3$, 376.5 MHz): δ -118.47 [t, 1H, ^{3}J(H-F) = 10.0]. **MS-ESI$^+$**: *m/z* 995.09 [2M-C_6H_3S]$^+$, 552.05 [M+H]$^+$, 444.05 [M-C_6H_3S]$^+$. **IR**: ν 2081 (C≡C).

Synthesis of [Pt(C≡CNaph){2,6-(2-C_5H_4N)$_2$-C_6H_3}] (8d)

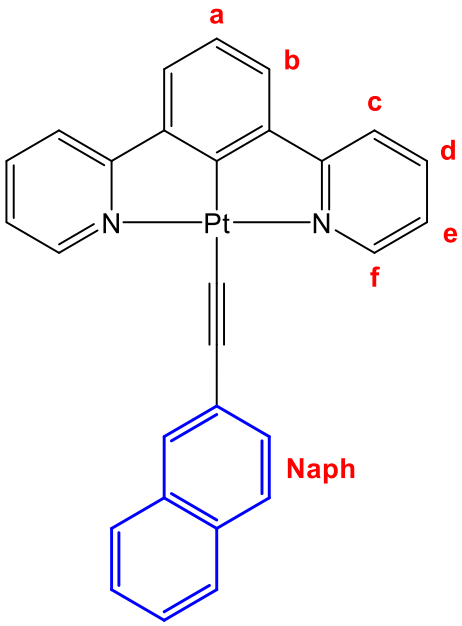

Compound [Pt(C≡CNaph){2,6-(2-C_5H_4N)$_2$-C_6H_3}] (**8d**) was obtained as an orange solid from 0.020 g (0.043 mmols) of compound [PtCl{2,6-(2-C_5H_4N)$_2$-4-FC_6H_3}] (**8**), 0.013 g (0.086 mmols) of 2-ethynylnaphthalene and 0.004 g (0.086 mmols) of sodium hydroxide. Yield: 0.020 g (80%).

^{1}H NMR ($CDCl_3$, 400 MHz): δ 9.56 [dd, 2H, ^{3}J(Pt-H) = 47.2, ^{3}J(H-H) = 5.7, ^{4}J(H-H) = 1.5, H^f]; 8.05 [s, 1H, H^{Naph}]; 7.94 [td, 2H, ^{3}J(H-H) = 7.8, ^{4}J(H-H) = 1.6, H^d], 7.73-7.81 [m, 3H, H^{Naph}]; 7.67-7.72 [m, 3H, H^{c,Naph}], 7.54 [d, 2H, ^{3}J(H-H) = 7.7, H^b]; 7.34-7.46 [m, 2H, H^{Naph}]; 7.21-7.26 [m, 3H, H^{a,e}]. **MS-ESI$^+$**: *m/z* 1003.16 [2M-$C_{12}H_7$]$^+$, 578.12 [M+H]$^+$, 426.06 [M-$C_{12}H_7$]$^+$. **IR**: ν 2085 (C≡C).

Synthesis of [Pt(C≡CNaph){2,6-(2-C_5H_4N)$_2$-4-FC_6H_2}] (9d)

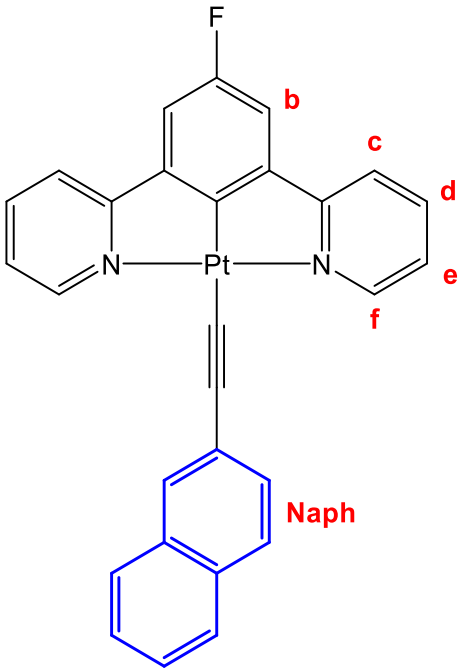

Compound [Pt(C≡CNaph){2,6-(2-C_5H_4N)$_2$-4-FC_6H_2}] (**9d**) was obtained as an orange solid from 0.015 g (0.033 mmols) of compound [PtCl{2,6-(2-C_5H_4N)$_2$-4-FC_6H_2}] (**9**), 0.010 g (0.066 mmols) of 2-ethynylnaphthalene and 0.003 g (0.066 mmols) of sodium hydroxide. Yield: 0.012 g (61%).

^{1}H NMR ($CDCl_3$, 400 MHz): δ 9.57 [dd, 2H, ^{3}J(Pt-H) = 48.0, ^{3}J(H-H) = 5.7, ^{4}J(H-H) = 1.5, H^f]; 8.05 [s, 1H, H^{Naph}]; 7.98 [td, 2H, ^{3}J(H-H) = 7.8, ^{4}J(H-H) = 1.6, H^d], 7.77-7.79 [m, 3H, H^{Naph}]; 7.66-7.68 [m, 3H, $H^{c,Naph}$]; 7.42 [m, 2H, H^{Naph}]; 7.29 [d, 2H, ^{3}J(F-H) = 10.0, H^b]; 7.26-7.29 [m, 2H, H^e]. **^{19}F NMR** ($CDCl_3$, 376.5 MHz): δ -118.62 [t, 1H, ^{3}J(H-F) = 10.0]. **MS-ESI$^+$**: *m/z* 1009.15 [2M-$C_{12}H_7$]$^+$, 596.11 [M+H]$^+$, 444.05 [M-$C_{12}H_7$]$^+$. **IR**: ν 2087 (C≡C).

Synthesis of [Pt(C≡CPhen){2,6-(2-C_5H_4N)$_2$-C_6H_3}] (8e)

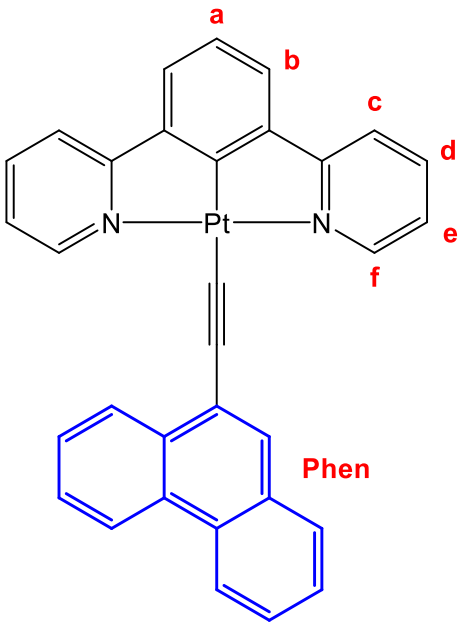

Compound [Pt(C≡CPhen){2,6-(2-C_5H_4N)$_2$-C_6H_3}] (**8e**) was obtained as an orange solid from 0.020 g (0.043 mmols) of compound [PtCl{2,6-(2-C_5H_4N)$_2$-4-FC_6H_3}] (**8**), 0.017 g (0.086 mmols) of 9-ethynylphenanthrene and 0.004 g (0.086 mmols) of sodium hydroxide. Yield: 0.017 g (63%).

^{1}H NMR ($CDCl_3$, 400 MHz): δ 9.63 [dd, 2H, ^{3}J(Pt-H) = 48.0, ^{3}J(H-H) = 5.7, ^{4}J(H-H) = 1.6, H^f]; 8.98 [m, 1H, H^{Phen}]; 8.71 [m, 1H, H^{Phen}]; 8.65 [d, 1H, ^{3}J(H-H) = 7.9, H^{Phen}]; 8.08 [s, 1H, H^{Phen}]; 7.95 [td, 2H, ^{3}J(H-H) = 7.8, ^{4}J(H-H) = 1.6, H^d], 7.84 [dd, 1H, ^{3}J(H-H) = 7.6, ^{4}J(H-H) = 1.6, H^{Phen}], 7.72 [d, 2H, ^{3}J(H-H) = 7.8, H^c]; 7.66 [m, 2H, H^{Phen}]; 7.53-7.61 [m, 3H, H^{b,Phen}]; 7.19-7.25 [m, 3H, H^{a,e}]. **MS-ESI$^+$**: *m/z* 1053.18 [2M-$C_{16}H_9$]$^+$, 628.14 [M+H]$^+$, 426.06 [M-$C_{16}H_9$]$^+$. **IR**: ν 2064 (C≡C).

Synthesis of [Pt(C≡CPhen){2,6-(2-C_5H_4N)$_2$-4-FC_6H_2}] (9e)

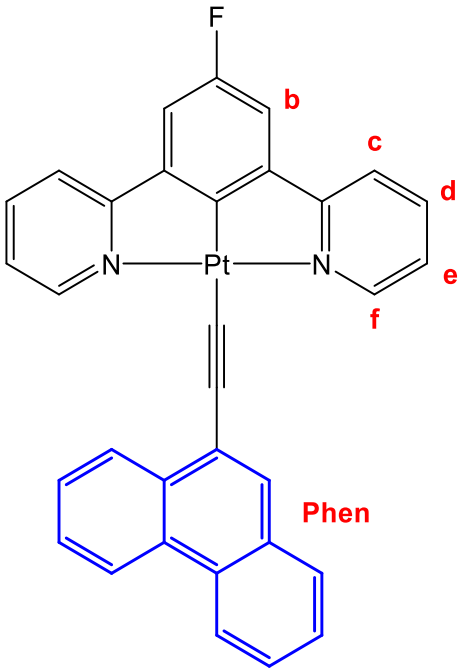

Compound [Pt(C≡CPhen){2,6-(2-C_5H_4N)$_2$-4-FC_6H_2}] (**9e**) was obtained as an orange solid from 0.020 g (0.042 mmols) of compound [PtCl{2,6-(2-C_5H_4N)$_2$-4-FC_6H_2}] (**9**), 0.017 g (0.084 mmols) of 9-ethynylphenanthrene and 0.004 g (0.084 mmols) of sodium hydroxide. Yield: 0.020 g (74%).

^{1}H NMR ($CDCl_3$, 400 MHz): δ 9.64 [dd, 2H, ^{3}J(Pt-H) = 48.4, ^{3}J(H-H) = 5.7, ^{4}J(H-H) = 1.5, H^f]; 8.97 [m, 1H, H^{Phen}]; 8.71 [m, 1H, H^{Phen}]; 8.65 [d, 1H, ^{3}J(H-H) = 7.9, H^{Phen}]; 8.08 [s, 1H, H^{Phen}]; 7.98 [td, 2H, ^{3}J(H-H) = 7.8, ^{4}J(H-H) = 1.6, H^d], 7.84 [dd, 1H, ^{3}J(H-H) = 7.3, ^{4}J(H-H) = 2.0, H^{Phen}], 7.67 [m, 4H, H^{c,Phen}]; 7.57 [m, 2H, H^{Phen}]; 7.31 [d, 2H, ^{3}J(F-H) = 10.0, H^b]; 7.24-7.28 [m, 2H, H^e]. **^{19}F NMR** ($CDCl_3$, 376.5 MHz): δ -118.35 [t, 1H, ^{3}J(H-F) = 10.0]. **MS-ESI$^+$**: *m/z* 1089.16 [2M-$C_{16}H_9$]$^+$, 646.12 [M+H]$^+$, 444.05 [M-$C_{16}H_9$]$^+$. **IR**: ν 2072 (C≡C).

6.4.4. X-ray Diffraction

Single crystals suitable for X-ray diffraction analysis were grown for compounds **8e** and **9c** by slow diffusion of methanol or hexane, respectively, in a dichloromethane solution of the compounds. Single crystal X-ray data for **8e** and **9c** were measured using a Bruker-Nonius Kappa CCD diffractometer with an APEX-II detector with graphite-monochromatized Mo-*K*α (λ = 0.71073 Å) radiation. Data collection and reduction were performed using the program *COLLECT* [37]and *HKL DENZO AND SCALEPACK*,[38]

respectively, and the intensities were corrected for absorption using *SADABS*.[39] The structures were solved with intrinsic phasing (*SHELXT*)[40] and refined by full-matrix least squares on F^2 using the *OLEX2* software,[41] which utilizes the *SHELXL* module.[42] Crystallographic details are given in Tables A6-A7.

6.4.5. Theoretical calculations

Theoretical calculations were performed at DFT level using Q-chem 5.1,[43] included in Spartan 20.[44] The functional chosen was B3LYP,[45,46] and the basis set was chosen as follows: 6-31G* for C, H, N and Cl, including polarization functions for non-hydrogen atoms,[47,48] and LANL2DZ[49] for Pt. Solvent effects were considered using the CPCM model.[50] No symmetry restrictions were imposed.

6.5. References

1. Sun, Y.; Yang, X.; Liu, B.; Guo, H.; Zhou, G.; Ma, W.; Wu, Z. *J. Mater. Chem. C* **2019**, *7*, 12552–12559.
2. Xiang, H.; Cheng, J.; Ma, X.; Zhou, X.; Chruma, J.J. *Chem. Soc. Rev.* **2013**, *42*, 6128–6185.
3. Ho, C.L.; Li, H.; Wong, W.Y. *J. Organomet. Chem.* **2014**, *751*, 261–285.
4. Sajjad, M.T.; Manousiadis, P.P.; Chun, H.; Vithanage, D.A.; Rajbhandari, S.; Kanibolotsky, A.L.; Faulkner, G.; Obrien, D.; Skabara, P.J.; Samuel, I.D.W.; Turnbull, G. A. *ACS Photonics* **2015**, *2*, 194–199.
5. Zampetti, A.; Minotto, A.; Cacialli, F. *Adv. Funct. Mater.* **2019**, *29*, 1807623.
6. Yam, V.W.W.; Law, A.S.Y. *Coord. Chem. Rev.* **2020**, *414*, 213298.
7. Fang, B.; Zhu, Y.; Hu, L.; Shen, Y.; Jiang, G.; Zhang, Q.; Tian, X.; Li, S.; Zhou, H.; Wu, J.; Tian, Y. *Inorg. Chem.* **2018**, *57*, 14134–14143.
8. Hruzd, M.; Gauthier, S.; Boixel, J.; Kahlal, S.; le Poul, N.; Saillard, J.Y.; Achelle, S.; Guen, F.R. *Dyes Pigm.* **2021**, *194*, 109622.
9. Pinter, P.; Soellner, J.; Strassner, T. *Eur. J. Inorg. Chem.* **2021**, *2021*, 3104–3107.
10. Yam, V.W.W.; Au, V.K.M.; Leung, S.Y.L. *Chem. Rev.* **2015**, *115*, 7589–7728.
11. Guo, Z.; Chan, M.C.W. *Chem. Eur. J.* **2009**, *15*, 12585–12588.
12. Mróz, W.; Botta, C.; Giovanella, U.; Rossi, E.; Colombo, A.; Dragonetti, C.; Roberto, D.; Ugo, R.; Valore, A.; Williams, J.A.G. *J. Mater. Chem.* **2011**, *21*, 8653–8661.
13. Martínez-Junquera, M.; Lara, R.; Lalinde, E.; Moreno, M.T. *J. Mater. Chem. C* **2020**, *8*, 7221–7233.
14. Zhao, Q.; Sun, J.Z. *J. Mater. Chem. C* **2016**, *4*, 10588–10609.
15. Zhao, J.; Feng, Z.; Zhong, D.; Yang, X.; Wu, Y.; Zhou, G.; Wu, Z. *Chem. Mater.* **2018**, *30*, 929–946.
16. Kalinowski, J.; Fattori, V.; Cocchi, M.; Williams, J.A.G. *Coord. Chem. Rev.* **2011**,

255, 2401–2425.

17. Lázaro, A.; Cunha, C.; Bosque, R.; Pina, J.; Ward, J.S.; Truong, K.N.; Rissanen, K.; Lima, J.C.; Crespo, M.; Seixas De Melo, J.S.; Rodríguez, L. *Inorg. Chem.* **2020**, *59*, 8220–8230.

18. Chan, A.K.W.; Ng, M.; Wong, Y.C.; Chan, M.Y.; Wong, W.T.; Yam, V.W.W. *J. Am. Chem. Soc.* **2017**, *139*, 10750–10761.

19. Kim, D.; Brédas, J.L. *J. Am. Chem. Soc.* **2009**, *131*, 11371–11380.

20. Gareth Williams, J.A.; Develay, S.; Rochester, D.L.; Murphy, L. *Coord. Chem. Rev.* **2008**, *252*, 2596–2611.

21. Dragonetti, C.; Fagnani, F.; Marinotto, D.; Di Biase, A.; Roberto, D.; Cocchi, M.; Fantacci, S.; Colombo, A. *J. Mater. Chem. C* **2020**, *8*, 7873–7881.

22. Wang, Z.; Turner, E.; Mahoney, V.; Madakuni, S.; Groy, T.; Li, J. *Inorg. Chem.* **2010**, *49*, 11276–11286.

23. Stille, J.K. *Angew. Chem. Int. Ed.* **1986**, *25*, 508–524.

24. Chen, Y.; Li, K.; Lu, W.; Chui, S.S.Y.; Ma, C.W.; Che, C.M. *Angew. Chem. Int. Ed.* **2009**, *48*, 9909-9913.

25. Lu, W.; Mi, B.X.; Chan, M.C.W.; Hui, Z.; Che, C.M.; Zhu, N.; Lee, S.T. *J. Am. Chem. Soc.* **2004**, *126*, 4958–4971.

26. Cheng, G.; Chen, Y.; Yang, C.; Lu, W.; Che, C.M. *Chem. Asian J.* **2013**, *8*, 1754–1759.

27. Baik, C.; Han, W.S.; Kang, Y.; Kang, S.O.; Ko, J. *J. Organomet. Chem.* **2006**, *691*, 5900–5910.

28. Yang, S.; Meng, F.; Wu, X.; Yin, Z.; Liu, X.; You, C.; Wang, Y.; Su, S.; Zhu, W. *J. Mater. Chem. C* **2018**, *6*, 5769–5777.

29. Nisic, F.; Colombo, A.; Dragonetti, C.; Roberto, D.; Valore, A.; Malicka, J.M.; Cocchi, M.; Freeman, G.R.; Williams, J.A.G. *J. Mater. Chem. C* **2014**, *2*, 1791–1800.

30. Zhang, H.H.; Wu, S.X.; Wang, Y.Q.; Xie, T.G.; Sun, S.S.; Liu, Y.L.; Han, L.Z.;

Zhang, X.P.; Shi, Z.F. *Dyes Pigm.* **2022**, *197*, 109857.

31. Zhao, S.; Zhu, Y.; Li, L.; Guerchais, V.; Boixel, J.; Wong, K.M.C. *Chem. Sci.* **2021**, *12*, 11056–11064.

32. Rossi, E.; Colombo, A.; Dragonetti, C.; Roberto, D.; Ugo, R.; Valore, A.; Falciola, L.; Brulatti, P.; Cocchi, M.; Williams, J.A.G. *J. Mater. Chem.* **2012**, *22*, 10650–10655.

33. Gareth Williams, J.A.; Beeby, A.; Stephen Davies, E.; Weinstein, J.A.; Wilson, C. *Inorg. Chem.* **2003**, *42*, 8609–8611.

34. Farley, S.J.; Rochester, D.L.; Thompson, A.L.; Howard, J.A.K.; Williams, J.A.G. *Inorg. Chem.* **2005**, *44*, 9690–9703.

35. Gong, Z.L.; Tang, K.; Zhong, Y.W. *Inorg. Chem.* **2021**, *60*, 6607–6615.

36. Lázaro, A.; Bosque, R.; Ward, J.S.; Rissanen, K.; Crespo, M.; Rodríguez, L. *Inorg. Chem.* **2023**, *62*, 2000-2012.

37. Hooft, R.W.W. COLLECT Nonius BV: Delft, The Netherlands, **1998**.

38. Otwinowski, Z.; Minor, W. *Methods Enzymol* **1997**, *26*, 307–326.

39. Sheldrick, G.M. SADABS, version 2008/2; University of Göttingen, Germany **1996**.

40. Sheldrick, G.M. *Acta Crystallogr., Sect. A: Found Adv.* **2015**, A*71*, 3–8.

41. Dolomanov, O. V.; Bourhis, L.J.; Gildea, R.J.; Howard, J.A.K.; Puschmann, H. *J. Appl. Cryst.* **2009**, *42*, 339–341.

42. Sheldrick, G.M. *Acta Crystallogr. Sect. C Struct. Chem.* **2015**, *C71*, 3–8.

43. Shao, Y.; Gan, Z.; Epifanovsky, E.; Gilbert, A.T.B.; Wormit, M.; Kussmann, J.; Lange, A.W.; Behn, A.; Deng, J.; Feng, X.; et al. *Mol. Phys.* **2015**, *113*, 184–215.

44. Spartan'18 v 1.4.0.; Wavefunction, Inc.: Irvine, CA, **2019**.

45. Lee, C.; Yang, eitao; Parr, R.G. *Phys. Rev. B Condens. Matter Mater Phys.* **1988**, *37*, 785–789.

46. Becke, A.D. *J. Chem. Phys.* **1993**, *98*, 5648–5652.

47. Hariharan, P.C.; Pople, J.A. *Theor. Chim. Acta* **1973**, *28*, 213–222.

48. Francl, M.M.; Pietro, W.J.; Hehre, W.J.; Binkley, J.S.; Gordon, M.S.; DeFrees, D.J.; Pople, J.A. *J. Chem. Phys.* **1982**, *77*, 3654–3665.

49. Hay, P.J.; Wadt, W.R. *J. Chem. Phys.* **1985**, *82*, 299–310.

50. Cossi, M.; Rega, N.; Scalmani, G.; Barone, V. *J. Comput. Chem.* **2003**, *24*, 669–681.

CHAPTER 7

Light-emitting electrochemical cells based on phosphorescent Ag(I)/Pt(II) compounds

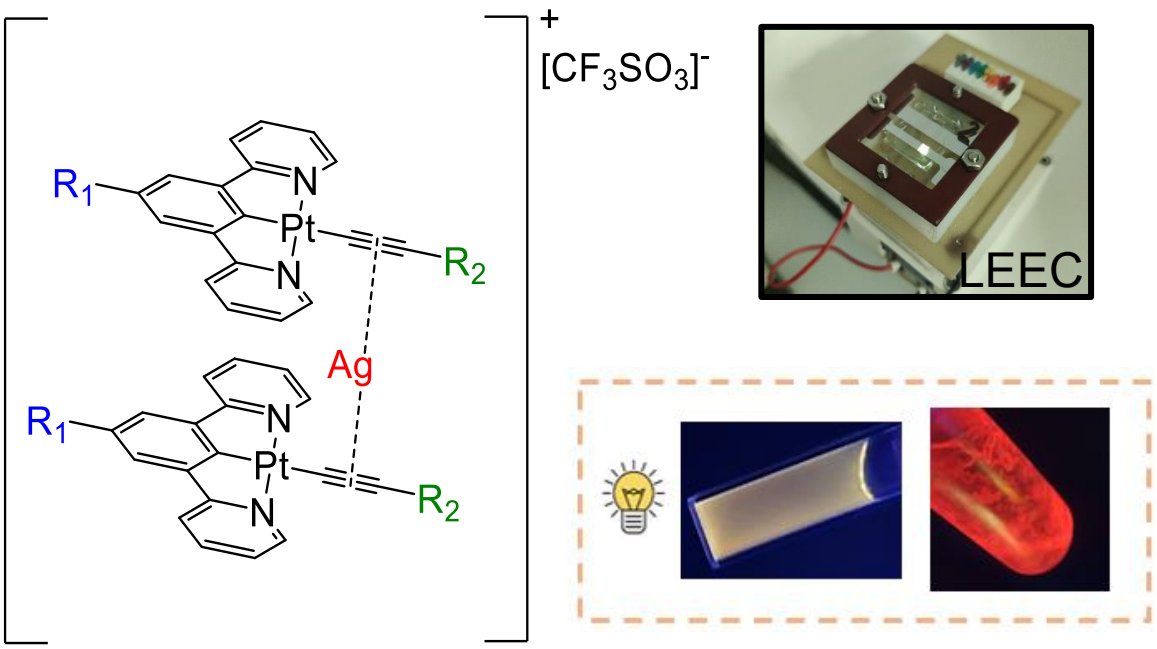

7. Light-emitting electrochemical cells based on phosphorescent Ag(I)/Pt(II) compounds

7.1. Introduction

Organometallic metal-alkynyl compounds have been widely described and their ability to form supramolecular arrays has been explored. Specifically, compounds with a σ-coordinated alkynyl bond have been an important building block thanks to their luminescent properties.[1–3]

Additionally, much attention has been attracted for compounds with a η^2-alkynyl coordination mode, especially through the coordination of d^{10} metals such as copper(I) or silver(I), which can alter the photophysical properties of these complexes (*Scheme 7.1*). Research on these complexes has mainly been dominated by structural and reactivity studies, with some reports on their luminescent properties.[4–7]

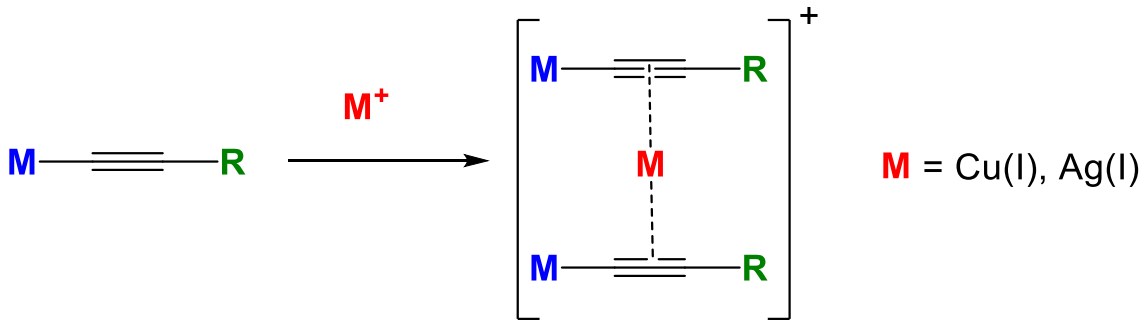

Scheme 7.1. η^2-alkynyl coordination mode for d^{10} metals.

Several platinum(II) compounds involving this bonding to copper(I) or silver(I) centres have been reported.[8–11] The d^{10} metal centres are usually found to be sandwiched between two platinum(II) alkynyl moieties and this implies a shift in their photophysical properties to lower energies compared with their monomeric unit. This is because, generally, the presence of the d^{10} metal ions would result in the narrowing of the HOMO-LUMO gap due to an increase in the acceptor ability of the alkynyl as well as the presence of new or enhanced platinophilic interactions which result in the appearance of lower energy metal-to-metal-to-ligand charge transfer (MMLCT) states.[12–14]

However, less examples are described where the platinum(II) unit is a cyclometallated compound.[15] The preparation of heterometallic derivatives of these compounds is of interest, as usually the η^2-bonded platinum(II) alkynyl compounds possess low emission quantum yields. The higher rigidity and aromaticity of these compounds results in the favouring of radiative over non-radiative emission pathways, and therefore in more efficient emissions.[16]

In summary, the use of these metals to promote the interaction between two cyclometallated platinum(II) moieties could be a good strategy to obtain compounds with an efficient red-shifted emission that would result from the aggregation between compounds and the electronic modifications that the introduction of a new metal brings. This is why, in this Chapter, a new family of heterometallic silver(I)/platinum(II) compounds was synthesised from selected compounds described in *Chapter 6* in order to evaluate the effect of the addition of silver in their photophysical properties and attempt to induce the formation of red-shifted emission as an alternative of using a mixture of good and bad solvents to obtain aggregates displaying emission bands shifted to longer wavelengths. Finally, their application for optical devices will be tested.

It has been stated that there is a need for the obtention of optical devices with an efficient red-shifted emission.[17,18] Therefore, these heterometallic compounds could be ideal for this application. Seeing that the addition of silver results in the formation of a cationic compound, Light-Emitting Electrochemical Cells (LEECs) were selected to study their application as an optical device.

LEECs are optical devices with a much simpler and cost-effective structure (*Figure 7.1*) than OLEDs, only containing two electrodes (a metal and a transparent conductive oxide) and an emissive layer, which is a host matrix containing an organic semiconductor, a supporting electrolyte and the emissive compound. These devices can produce light upon the application of an electric current through electron-hole recombination, which results in the generation of energy that can be absorbed and emitted in the form of light by the emissive dopant.[19,20] Ionic transition metal complexes have been studied as this emissive dopants in LEECs, with the best results obtained for iridium(III) compounds.[21]

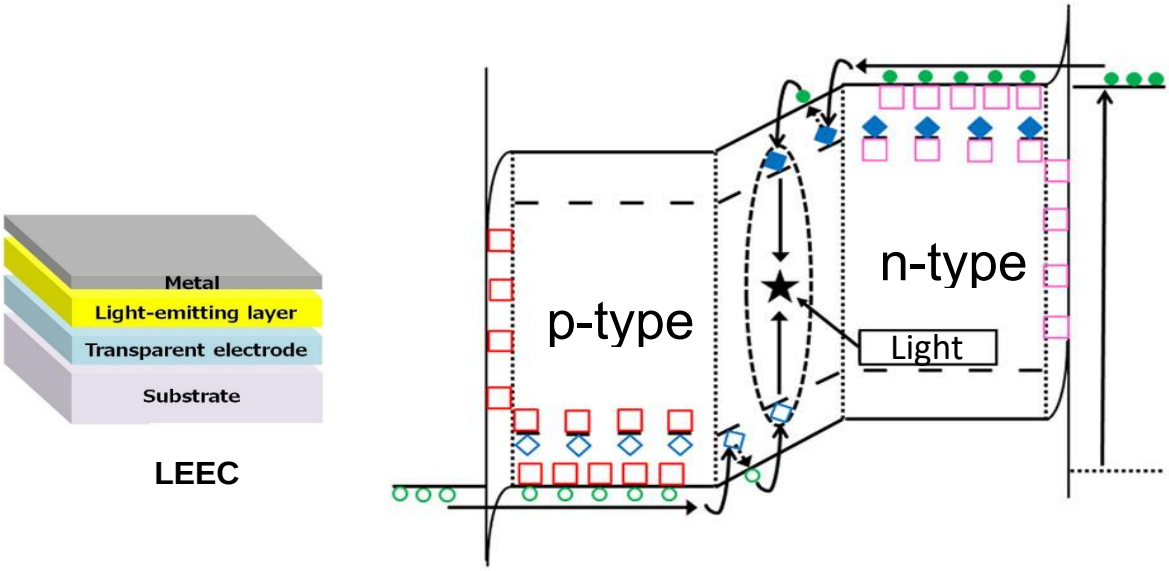

Figure 7.1. Structure of a light-emitting electrochemical cell and emission of light through electron hole recombination.[22]

7.2. Results and Discussion

7.2.1. Synthesis and characterisation

Compounds [Pt(C≡CR$_2$){2,6-(C$_5$H$_4$N)$_2$-C$_6$H$_3$}] (**8x**) and [Pt(C≡CR$_2$){2,6-(C$_5$H$_4$N)$_2$-4-FC$_6$H$_2$}] (**9x**) depicted in *Scheme 7.2* and previously described in *Chapter 6* were selected to synthesise their corresponding heterometallic compounds through the interaction of a silver(I) atom to their alkynyl bond. However, although this cation is known to present a linear coordination, it is unsure whether it would coordinate to one or two alkynyl moieties, therefore resulting in the formation of different compounds (*Scheme 7.2*) with a 2:1 or 1:1 stoichiometry.

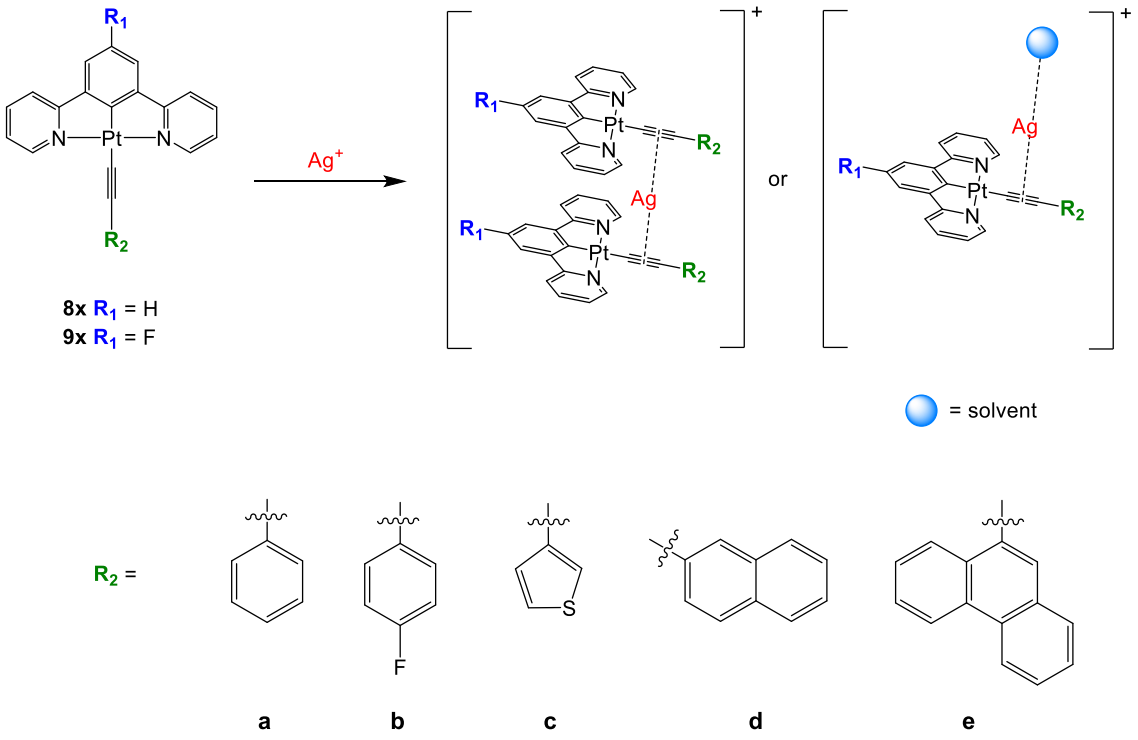

Scheme 7.2. Selected compounds and their possible silver coordination modes.

Therefore, to determine the experimental conditions that should be further used in the preparation of these compounds, titration studies followed by emission were performed by the subsequent addition of 0.1 equivalents of silver triflate to a $5 \cdot 10^{-5}$ M solution of the starting compound in acetonitrile. It was observed that upon the addition of silver(I), a new band was formed around 625 nm for all compounds, whose intensity keeps increasing up to the addition of 0.5 equivalents. This is further evidenced by plotting the intensity of this maxima versus the added silver(I) equivalents, observing the reaching of

a plateau in the curve at this point. This confirms that the formed species corresponds to the 2:1 stoichiometric compound. This is shown in *Figure 7.2* for compound **9e** as an example. Furthermore, the fact that the addition of silver results in a red-shifted broad band, supports the principle that the silver atom is approaching two [Pt(C≡CR$_2$)(N,C,N)] units, which promotes the presence of new intermolecular interactions. For this Chapter, compounds containing a phenylacetylene or a *para*-fluorobenzyl alkynyl ligand (**8a**, **9a**, **8b** and **9b**) were discarded as the new band presented a much lower intensity than the rest of compounds and thus were not of interest to study the photophysical properties of the resulting heterometallic compounds.

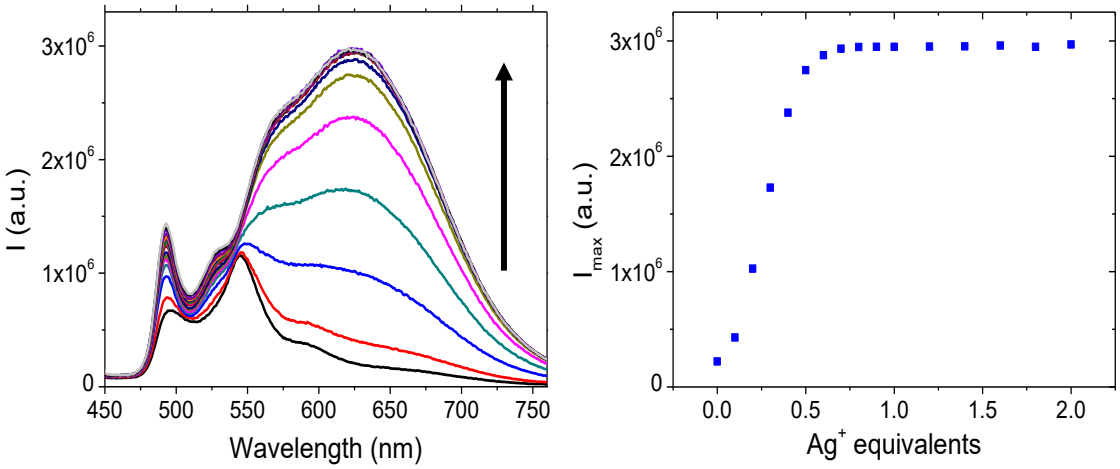

Figure 7.2. Emission titration data of compound **9f** with increasing amounts of silver triflate (λ_{exc} = 390 nm) (left) and plot of the emission maxima (λ_{em} = 640 nm) against number of equivalents of silver(I) salt (right).

Additionally, two new dinuclear cyclometallated platinum(II) compounds with 1,3-diethynylbenzene as a bridging ligand were synthesised to investigate how the presence of two alkynyl bonds affects the coordination of silver(I) and the resulting photophysical properties. For their synthesis, 2 equivalents of the chlorido precursors [PtCl{2,6-(C$_5$H$_4$N)$_2$-C$_6$H$_3$}] (**8**) and [PtCl{2,6-(C$_5$H$_4$N)$_2$-4-FC$_6$H$_2$}] (**9**) previously described in *Chapter 6* were added to solution of the previously deprotonated alkynyl ligand using sodium hydroxide as a base (*Scheme 7.3*). Final compounds [{Pt(2,6-(2-C$_5$H$_4$N)$_2$-C$_6$H$_3$)}$_2$(μ-1,3-(C≡C)$_2$-C$_6$H$_4$)] (**8f**) and [{Pt(2,6-(2-C$_5$H$_4$N)$_2$-4-FC$_6$H$_2$)}$_2$(μ-1,3-(C≡C)$_2$-C$_6$H$_4$)] (**9f**) were isolated as orange solids after precipitation and washing with water, methanol and hexane.

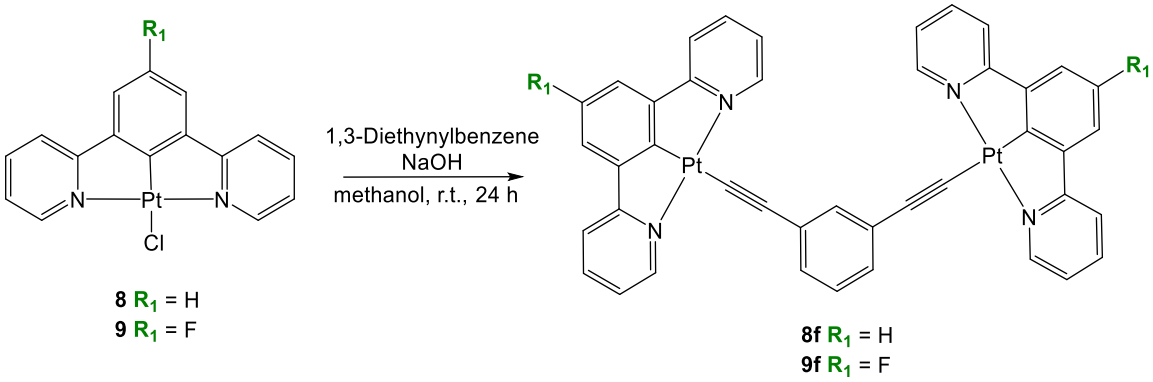

Scheme 7.3. Synthesis of compounds **8f** and **9f**.

Characterisation by ^{1}H NMR of both compounds showed the disappearance of the terminal alkynyl protons from the 1,3-diethynylbenzene as well as the presence of the aromatic protons from the [N,C,N] tridentate ligand, which are found to be equivalent for both cyclometallated units. The formation of the desired products is also supported by a significant shift of the protons that belong to the cyclometallated unit, with a downfield shift in the pyridine proton (H^{f}) of *ca.* 0.10-0.25 ppm when compared to that of the precursors. As expected, no significant changes were observed in the coupling constants of this proton with platinum between the precursors and the final compounds, as the ligand in *trans* with the nitrogen of the pyridine bond is not exchanged. Additionally, compound **9f** was also characterised by ^{19}F NMR, showing only one signal as a triplet assigned to the fluorine in the central position of the aromatic ring which is coupled with the two adjacent aromatic protons.

Infrared spectroscopy was also useful to detect the C≡C stretching vibration (around 2070 cm^{-1}) for both compounds along with the absence of the band assigned to the stretching of the terminal protons of the free alkynyl aromatic ligand (around 3300 cm^{-1}). In both cases, the protonated molecular peaks were found by mass spectrometry further confirming the successful formation of the desired products.

As well as for the previous compounds, titration curves followed by emission were performed for the dinuclear derivatives by the subsequent addition of 0.1 equivalents of silver triflate to a $5 \cdot 10^{-5}$ M solution of compounds **8f** and **9f** in acetonitrile. The results revealed that for these compounds, not only does a new broad band around 625 nm appear, but there is also a significant decrease in the emission band from the starting compounds. Upon plotting the emission intensity at the maxima of the latter versus the

added silver equivalents, it can be observed that the curve reaches a plateau from the addition of 1 equivalent. This is shown in *Figure 7.3* for compound **9f** as an example. Thus, the corresponding heterometallic compound that is formed presents a 1:1 stoichiometry, suggesting that each silver cation is interacting with two alkynyl bonds, one from each [{Pt(N,C,N)}$_2$(μ-1,3-(C≡C)$_2$-C$_6$H$_4$)] unit.

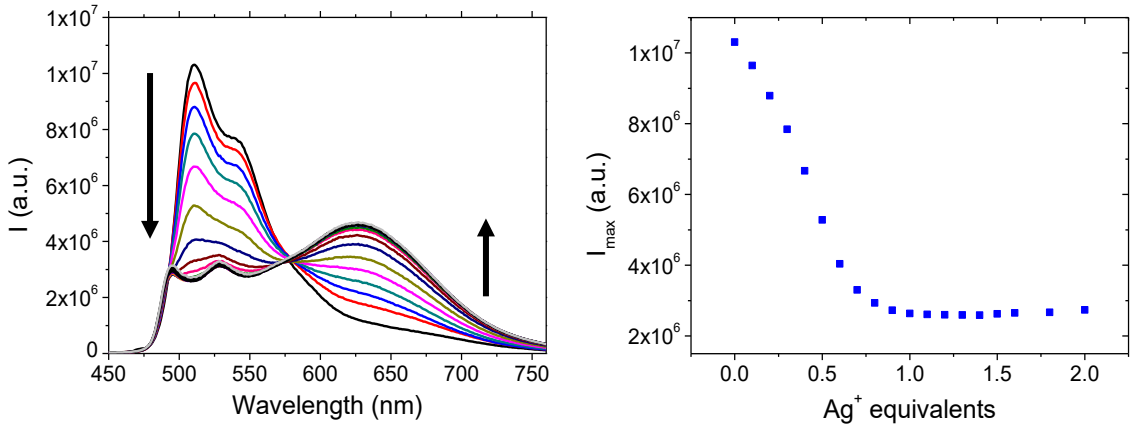

Figure 7.3. Emission titration of compound **9f** with increasing amounts of silver triflate (λ_{exc} = 390 nm) (left) and plot of the emission maxima (λ_{em} = 510 nm) against number of equivalents of silver(I) salt (right).

After having determined their final stoichiometry, the new heterometallic compounds were synthesised and isolated to characterise them and acquire further information on their structure. For the mononuclear compounds, as it was determined, 0.5 equivalents of silver triflate were added to an acetonitrile solution of the corresponding [Pt(C≡CR$_2$){2,6-(C$_5$H$_4$N)$_2$-C$_6$H$_3$}] (**8x**) or [Pt(C≡CR$_2$){2,6-(C$_5$H$_4$N)$_2$-4-FC$_6$H$_2$}] (**9x**) precursor and the mixture was further stirred for 1 hour under a nitrogen atmosphere and covered from light (*Scheme 7.4*). After removing half of the solvent, for all compounds a red solid was obtained, which was filtered and dried under vacuum.

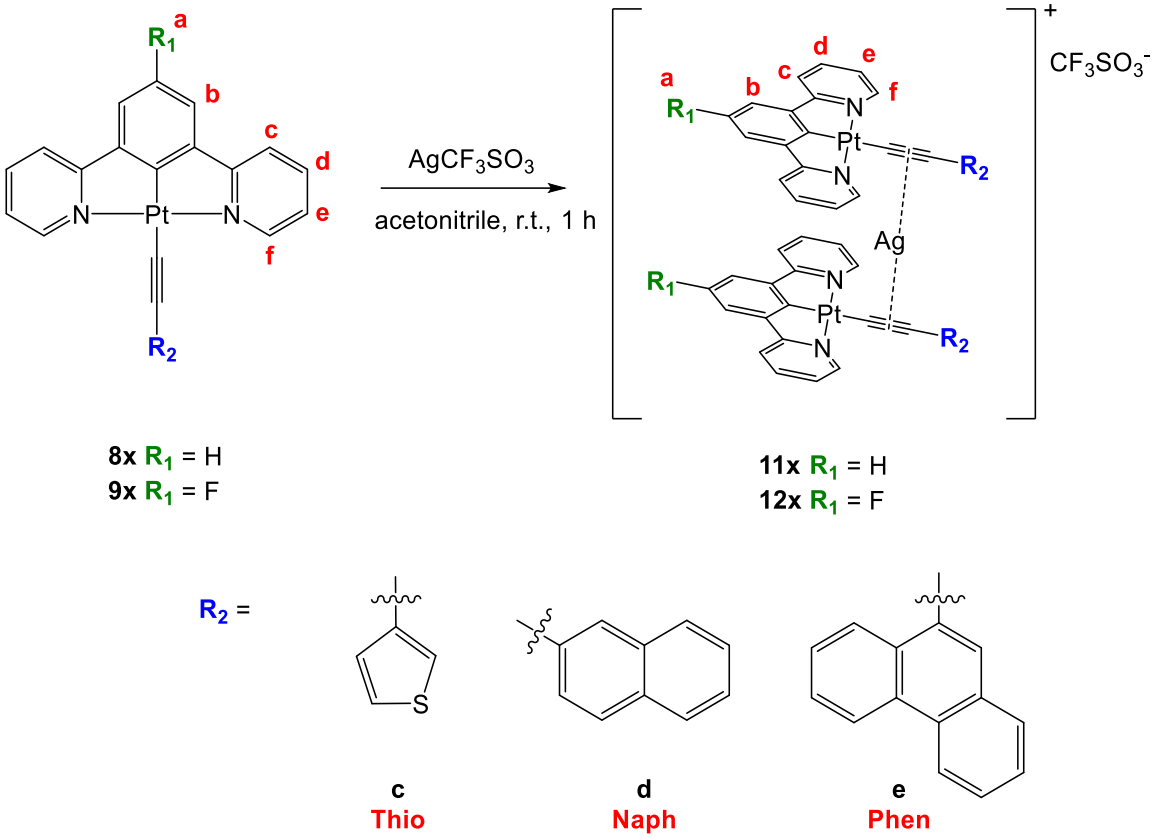

Scheme 7.4. Synthesis of compounds **11c-e** and **12c-e**.

The same procedure was performed for the obtention of compounds [Ag{Pt(2,6-(2-$C_5H_4N)_2$-C_6H_3)}$_2$(μ-1,3-(C≡C)$_2$-C_6H_4)]$_2$ [CF_3SO_3]$_2$ (**11f**) and [Ag{Pt(2,6-(2-$C_5H_4N)_2$-4-FC_6H_2)}$_2$(μ-1,3-(C≡C)$_2$-C_6H_4)]$_2$ [CF_3SO_3]$_2$ (**12f**) starting from the dinuclear precursors [{Pt(2,6-(2-$C_5H_4N)_2$-C_6H_3)}$_2$(μ-1,3-(C≡C)$_2$-C_6H_4)] (**8f**) and [{Pt(2,6-(2-$C_5H_4N)_2$-4-FC_6H_2)}$_2$(μ-1,3-(C≡C)$_2$-C_6H_4)] (**9f**), respectively (*Scheme 7.5*). As calculated in this case, 1 equivalent of silver triflate was used for their obtention as red solids, such as for the previous compounds.

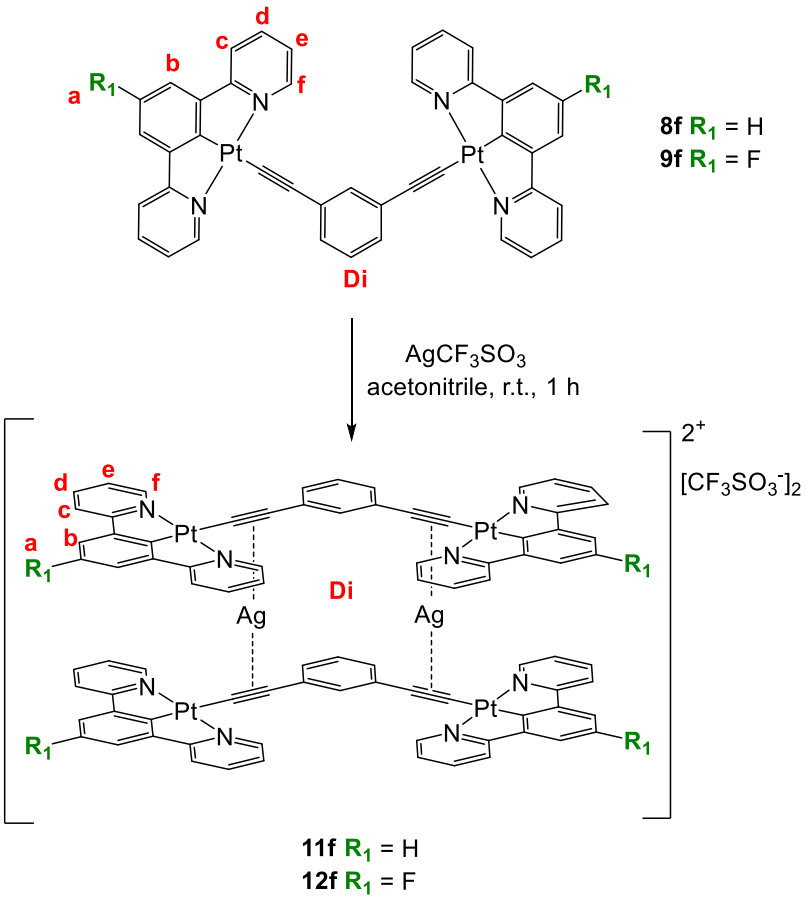

Scheme 7.5. Synthesis of compounds **11f** and **12f**.

Characterisation of all compounds by ^{1}H NMR showed the presence of all the protons from the [N,C,N] cyclometallated moiety and those from the corresponding alkynyl aromatic group, as well as the absence of the alkynyl terminal proton or any additional signals confirming that no decomposition of the compound had taken place. All the signals are shifted regarding the platinum compound prior to the addition of silver, which is shown as an example for compound **12e** compared to its precursor **9e** in *Figure 7.4*. Particularly, a larger shift is present in the protons from the cyclometallated moiety, being the largest one for the pyridine proton (H^{f}) of ca. 0.4 ppm.

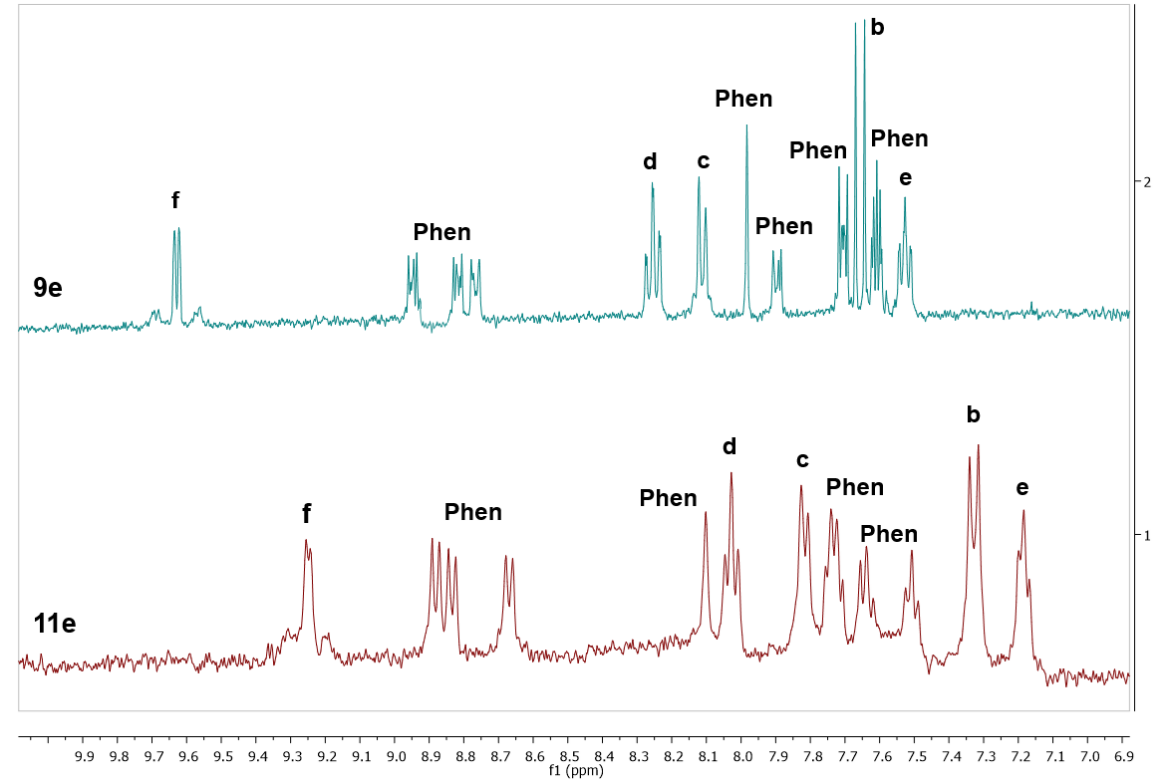

Figure 7.4. Aromatic region of the ^{1}H NMR spectra of compounds **9e** and **11e**.

All compounds were also characterised by ^{19}F NMR, which in all cases presented a singlet around -78 ppm that can be assigned to the fluorine from the triflate group, thus confirming its presence as a counterion. Compounds **12x** present an additional triplet signal around -118 ppm which corresponds to the fluorine atom in the central position of the aromatic ring in the [N,C,N] cyclometallated moiety. This signal is not significantly shifted when compared to the ^{19}F NMR of their corresponding precursors.

Furthermore, infrared spectroscopy data showed the C≡C stretching vibration shifted to lower frequencies in relation to the **8x** and **9x** precursors, with a decrease of around 30 cm^{-1}, in accordance with the complexation of the acetylenic units at d^{10} metal ions.[15] Additionally, the $[M\text{-}CF_3SO_3]^+$ or $[M\text{-}(CF_3SO_3)_2]^{2+}$ peaks were found by mass spectrometry further confirming the successful formation of the desired products which experience the loss of the corresponding counterions in the ionization process.

7.2.2. Photophysical characterisation

Absorption and emission spectra of all the compounds were recorded in 10^{-5} M acetonitrile solutions at room temperature. The results are summarized in *Table 7.1*.

Table 7.1. Spectral data for all compounds in acetonitrile solutions at 298 K.

Compound	Absorption λ_{abs}/nm (ε x 10^{-3}/ M^{-1} cm^{-1})	Emission λ_{em}/nm
11c	287 (38.6), 311 (18.3), 332 (15.5), 357 (12.2), 374 (13.8), 424 (2.0)[a]	486, 514, 653[b]
11d	287 (35.5), 307 (28.6), 383 (9.4), 427 (4.8)[a]	487, 514, 674[b]
11e	287 (34.4), 312 (28.6), 332 (18.7), 375 (10.6), 424 (3.5)[a]	486, 515, 645[b]
11f	287 (102.5), 333 (42.0), 371 (31.4), 423 (10.0)[a]	484, 514, 647[b]
12c	286 (15.9), 386 (5.3), 427 (3.5)[a]	519
12d	286 (32.8), 310 (19.0), 330 (17.5), 354 (15.0), 391 (7.1), 410 (3.8)[a]	495, 523
12e	288 (54.9), 312 (41.8), 329 (35.8), 394 (16.2), 432 (9.6)[a]	499, 540, 675[b]
12f	286 (109.0), 323 (40.6), 385 (33.0), 425 (12.8)[a]	521, 648[b]

[a] Shoulder. [b] Emission band arising from the heterometallic species.

Compounds **11x** and **12x** present several absorption bands, with a spectrum generally matching that of their precursor prior to the addition of silver but with the presence of a broader shoulder at around 425 nm, which could arise from the new heterometallic species (*Figure 7.5*). As previously reported in *Chapter 6*, the higher energy bands can be assigned to $^1\pi$-π^* transitions intrinsic of the cyclometallated (1,3-di(2-pyridyl)benzene or 2,2'-(5-fluoro-1,3-phenylene)dipyridine) ligand as they are also recorded in the absorption of the free ligands. In the lower energy region, less intense bands are observed that can correspond to mixed charge transfer and ligand centred transitions according to the literature.[17,23,24] Compounds **11f** and **12f** present molar absorptivity coefficients that are doubled regarding those of the rest of the compounds, in agreement with the fact that they present twice as many cyclometallated units.

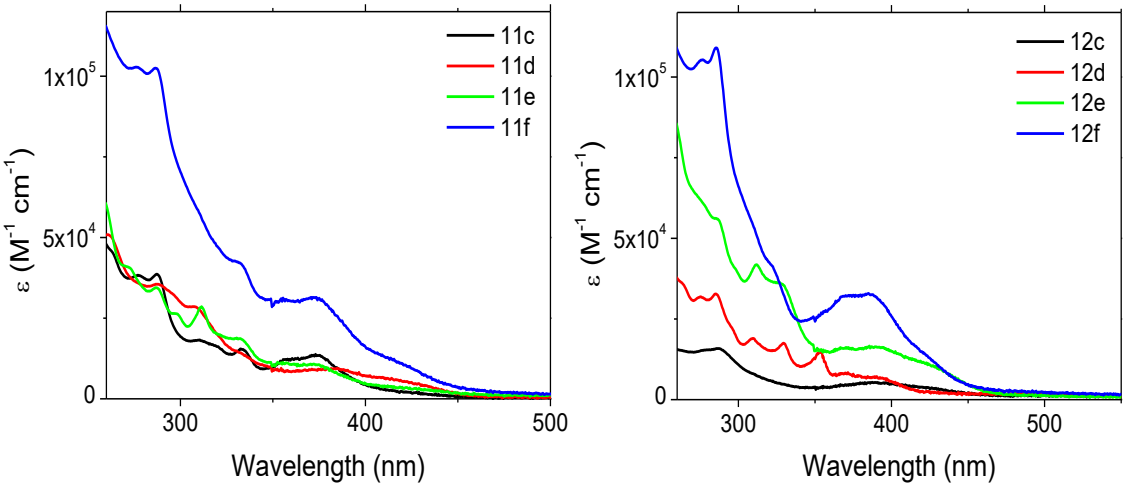

Figure 7.5. Absorption spectra for 10^{-5} M acetonitrile solutions of compounds **11x** and **12x** at room temperature.

Generally, emission spectra displayed in *Figure 7.6* show two different regions. In the higher energy region, a vibronically structured band centred around 500 nm is present for all compounds. This band matches the emission of compounds **8x** and **9x**, the precursors prior to the addition of silver, which was assigned to a mainly ligand centred $^{3}\pi$-π^{*} transition from the [N,C,N] cyclometallated ligand that can be mixed with metal-to-ligand or intraligand charge transfer transitions (^{3}MLCT or ^{3}ILCT).[17,25,26] At the lower energy region, a broad band matching the wavelength that was observed in silver titration is observed, suggesting it arises from the formation of the heterometallic compound. However, the intensity of this band is highly influenced by the nature of the cyclometallated platinum(II) precursor, being almost non-existent for some compounds. The fact that this band is not predominant as it was at the final point of the silver(I) titrations, could mean that upon the lack of silver excess in the luminescence spectra of the isolated compounds, a certain equilibrium takes place and results in a mixture of the precursor and the final compound, which is further confirmed below.

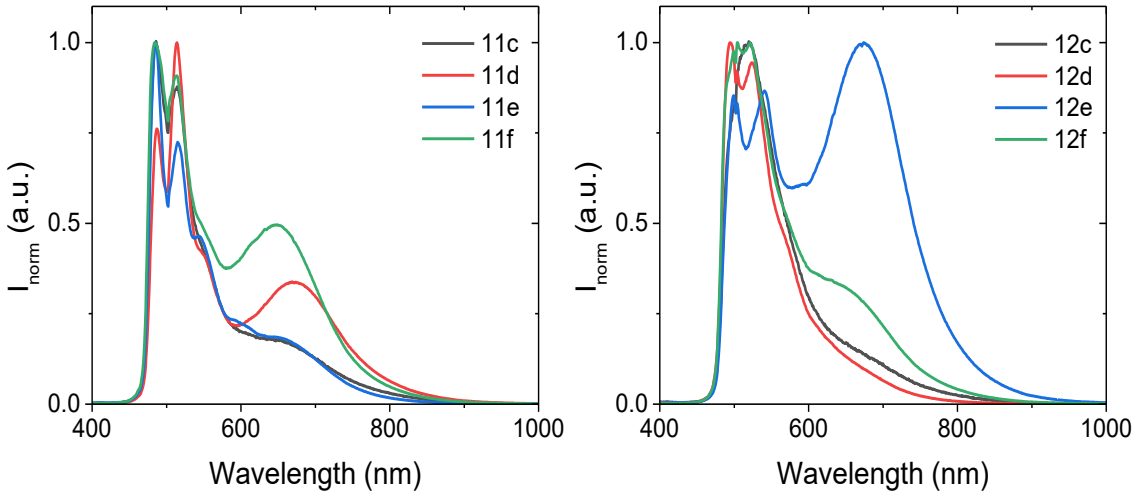

Figure 7.6. Normalised emission spectra for 10^{-5} M acetonitrile solutions of compounds **11x** and **12x** at room temperature (λ_{exc} = 365 nm).

Furthermore, excitation spectra at the higher emission wavelength revealed a red-shifted offset than spectra from the higher emission energy bands, which is shown in *Figure 7.7* for compound **12e** as an example. This band corresponds to the shoulder recorded previously in the absorption spectra and this allows to affirm that the species contributing to the emission at longer wavelengths is indeed present in the ground state and therefore, it corresponds to aggregation and not to an excimeric emission. Therefore, this is in agreement with the hypothesis of the dissociation of the heterometallic compound in solution at this concentration, to give the cyclometallated platinum(II) unit responsible for the vibrationally structured band at higher energies.

Contrary to *Chapter 6*, where the red-shift was induced through aggregation upon the addition of a bad solvent, in this case it is induced thanks to the interaction of the silver(I) atom with two cyclometallated platinum(II) compounds giving rise to a dimer. In addition to this interaction, several intermolecular contacts could be responsible of the appearance of the new emission band, such as platinophilic interactions or π-π stacking, although it is difficult to affirm in the absence of a crystalline structure or DFT calculations.

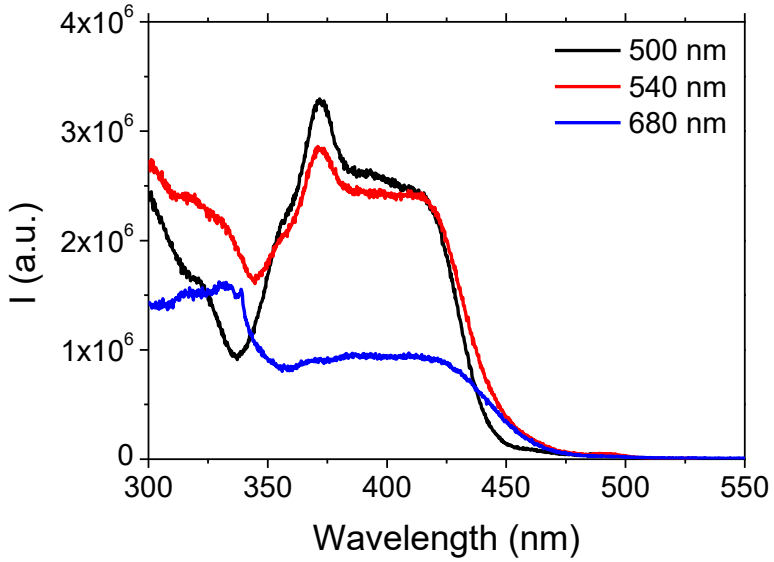

Figure 7.7. Excitation spectra for a 10^{-5} M acetonitrile solutions of compound **12e** at the different emission maxima at room temperature.

Phosphorescence quantum yields present moderate values, which are significantly lower than those of the precursors **8x** and **9x** (*Table 7.2*). This could suggest that the presence of the silver in the heterometallic compound results in a quenching of the emission. Additionally, compounds **11x** present slightly higher quantum yield values than compounds **12x**, meaning that the presence or absence of a fluorine in the central ring of the cyclometallating ligand could influence the resulting photophysical properties and efficiency of the final heterometallic compounds.

Table 7.2. Phosphorescence quantum yields and phosphorescence lifetimes recorded in degassed acetonitrile solutions at 298 K

Compound	ϕ°_{Ph}	τ^{o} (μs) λ_{em} = 500 nm	τ^{o} (μs) λ_{em} = 680 nm
11c	0.38	5.42	5.99
11d	0.36	4.81	7.12
11e	0.32	6.76	7.35
11f	0.36	4.97	8.70
12c	0.27	5.97	6.66
12d	0.21	6.73	7.33
12e	0.29	3.75	7.55
12f	0.27	3.85	5.25

Emission lifetimes are of a few microseconds, in agreement with a triplet state origin and in the order of those reported for analogous cyclometallated platinum(II) compounds (*Table 7.2*).[17] It can be noted that the emission lifetimes collected by the decay at the longer wavelength band (680 nm) are larger than those recorded at the shorter wavelength (500 nm). Additionally, the difference between them is enlarged with the presence of the band associated to the heterometallic dimer. The fact that the silver(I)/platinum(II) compounds present longer lifetimes than the emission arising from the sole platinum(II) compound, could suggest an involvement of the silver atom in the molecular orbitals present in this emission.

Emission spectra were recorded for all compounds in powder at room temperature. The results are summarised in *Table 7.3*.

Table 7.3. Spectral data for all compounds in powder.

Compound	Emission λ_{em}/nm	ϕ°_{Ph}	τ^{o} (μs)
11c	688	0.03	0.35
11d	704	0.09	0.48
11e	693	0.07	0.33
11f	721	0.06	0.38
12c	685	0.01	0.41
12d	669	0.04	0.49
12e	689	0.05	0.31
12f	703	0.03	0.44

All compounds display a broad emission band in the 685-721 nm region with significant changes in the emission wavelength between different compounds (*Figure 7.8*). Phosphorescence quantum yields have moderate values up to 9 % and the corresponding lifetimes are of hundreds of nanoseconds, in agreement with a triplet state emission origin (*Table 7.3*).

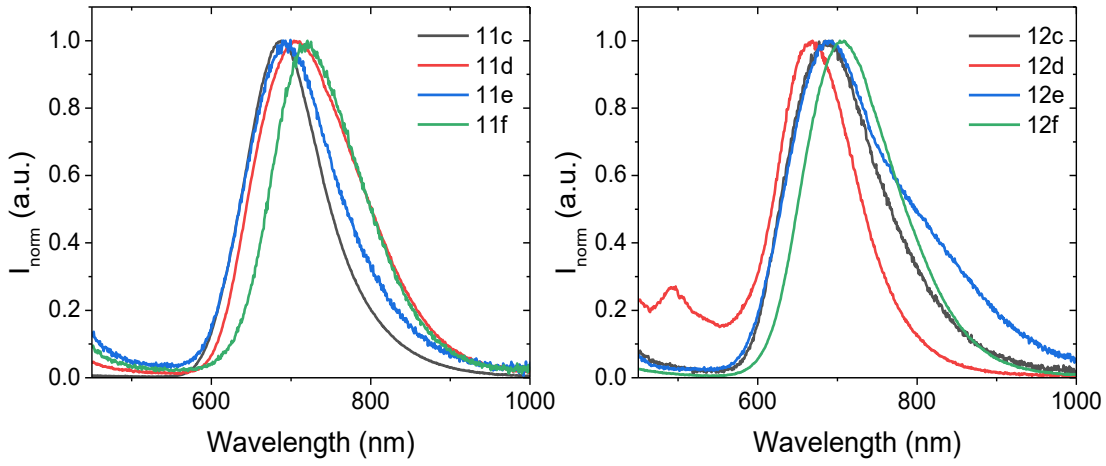

Figure 7.8. Normalised emission spectra for powder samples of compounds **11x** and **12x** at room temperature (λ_{exc} = 365 nm).

Comparing to the luminescence of the heterometallic compound present in solution, this band is further red-shifted which could suggest a different stacking in solid state. This could be due to the appearance of additional intermolecular contacts in the solid state where molecules are closer and more compact in the packing. It was observed that precursors **8x** and **9x** presented an emission band in solid state around 600 nm, due to the presence of stacking interactions as it was elucidated by single crystal X-ray diffraction in *Chapter 6*. Therefore, this could suggest that for the heterometallic compounds, additional interactions such as π···π, Pt···Pt or those related with the additional silver(I) heavy atom are responsible of the red shifting of this emission. However, the obtention of single crystal X-ray structures would be crucial to identify this new assembly.

7.2.3. Concentration studies

To further understand the aggregation processes, emission spectra for all the final compounds were recorded in acetonitrile solutions at various concentrations, higher (10^{-4} M) and lower (10^{-6} M and $2 \cdot 10^{-7}$ M) than the main studied concentration (10^{-5} M). The resulting spectra are displayed in *Figure 7.9*.

Upon increase of the concentration, all compounds show the broad band at higher wavelengths that was assigned to the presence of the heterometallic compound. When decreasing the concentration, this band decreases in intensity and, for all cases, disappears at the most diluted solution. This supports the fact that both the heterometallic dimer and the platinum(II) precursor are in an equilibrium that is highly dependent on concentration, which can justify why we only observe the silver(I)/platinum(II) final compound by characterisation in NMR where the concentration is much higher.

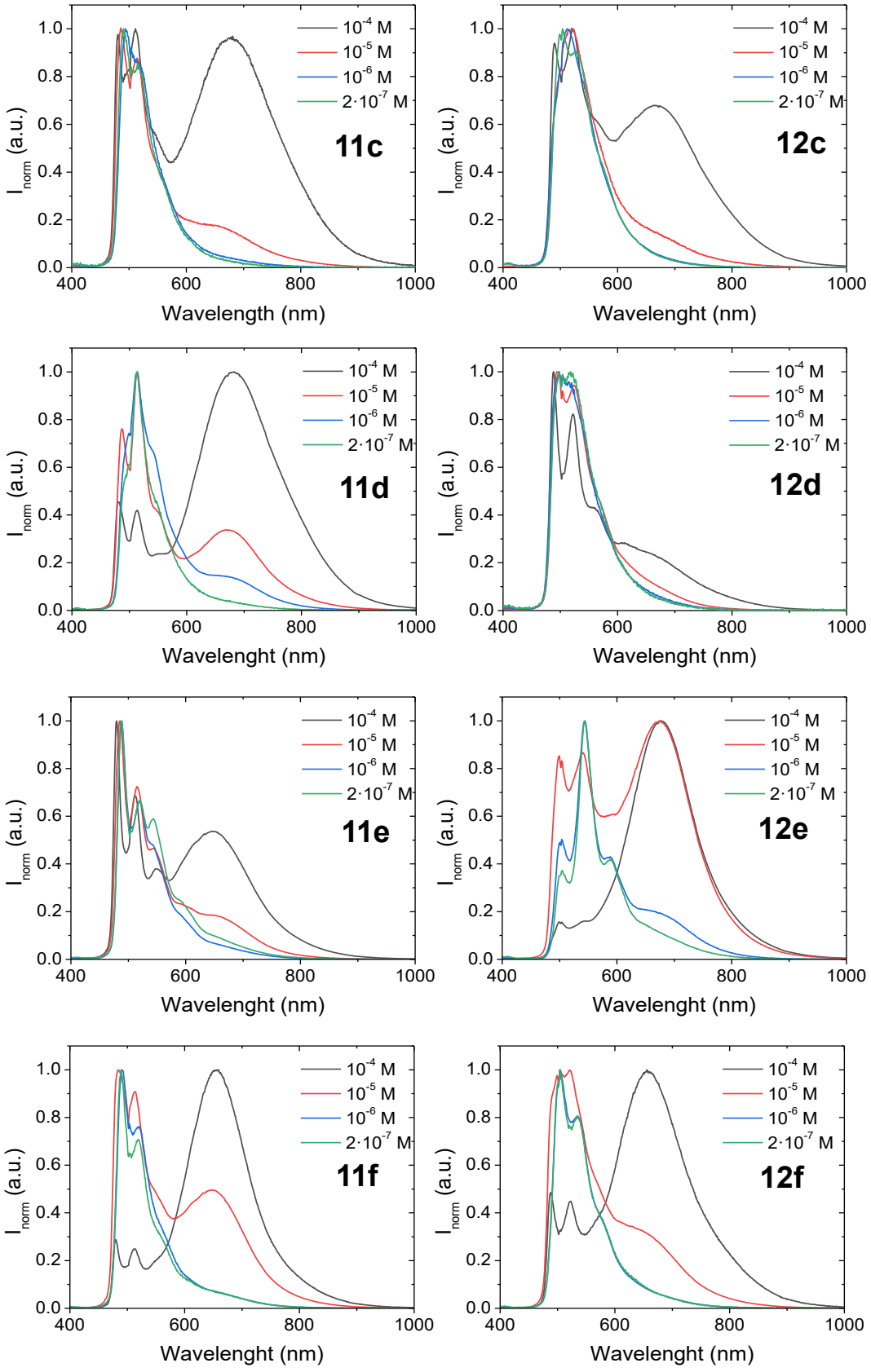

Figure 7.9. Normalised emission spectra for acetonitrile solutions at different concentrations of compounds **11x** and **12x** at room temperature (λ_{exc} = 365 nm).

The nature of the cyclometallating ligand and the ancillary ligand give rise to major differences in the dissociation of the final heterometallic compound. For example, compound **12e** already presented a significant dominance of the band at lower energy at 10^{-5} M, which becomes almost the sole emission at 10^{-4} M, is still present at 10^{-6} M as a shoulder and it becomes non-observable at $2 \cdot 10^{-7}$ M. On the other hand, other compounds such as **12d** only presents a low intensity band at higher wavelengths and it can only be observed at the highest concentration.

Recording the excitation spectra at the different emission maxima for 10^{-4} M solutions agrees with what is observed for 10^{-5} M solutions, but with the appearance of a more significant shoulder at this concentration where there is a larger number of aggregated species. This is shown in *Figure 7.10* for compound **12e**, and it is again consistent with the presence of this heterometallic dimer in the ground state.

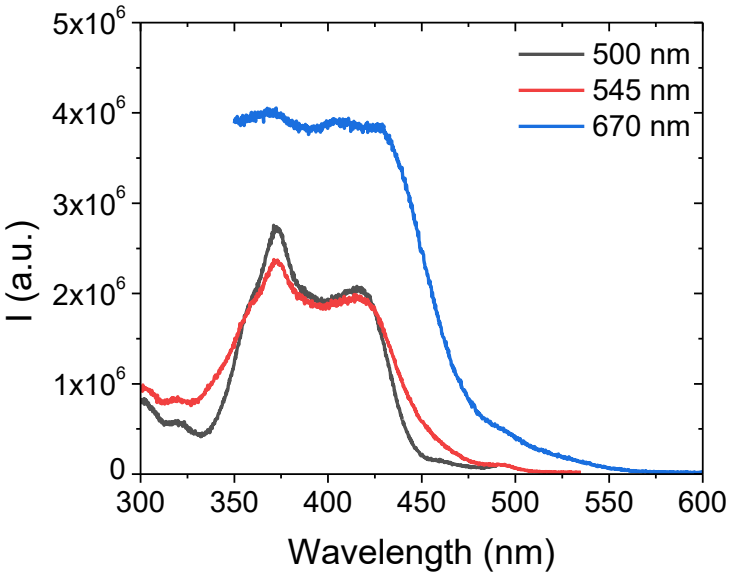

Figure 7.10. Excitation spectra for a 10^{-4} M acetonitrile solutions of compound **12e** at the different emission maxima at room temperature.

7.2.4. Light-emitting electrochemical cells (LEECs)

Compound **12e** was selected to produce proof-of-concept light-emitting electrochemical cells (LEECs). The structure of the cell follows the recently reported highly-efficient Ir(III) complex-based LEECs:[22] ITO | PEDOT:PSS (Al4083) (30 nm) | PVK:OXD7:$THABF_4$ (56:38:6) co 4% In **12e** (100 nm) | Al (100 nm). The blend of PVK {poly(9-vinylcarbazole)} and OXD7 {1,3-bis[2-(4-*tert*-butylphenyl)-1,3,4-oxadiazo-5-

yl]benzene} plays a role of a host matrix which is doped with $THABF_4$ (tetrahexylammonium tetrafluoroborate) electrolyte.

The device was driven at a constant voltage bias as previously described.[27] The LEEC demonstrated a turn-on at ~11-12 V and was driven at 12.5 V and 13 V. The electroluminescence spectrum of the LEEC (*Figure 7.11*) is representative of mainly the photoluminescence of **12e** in dilute solutions, which can be rationalised with the low emitter concentration in the emissive layer.

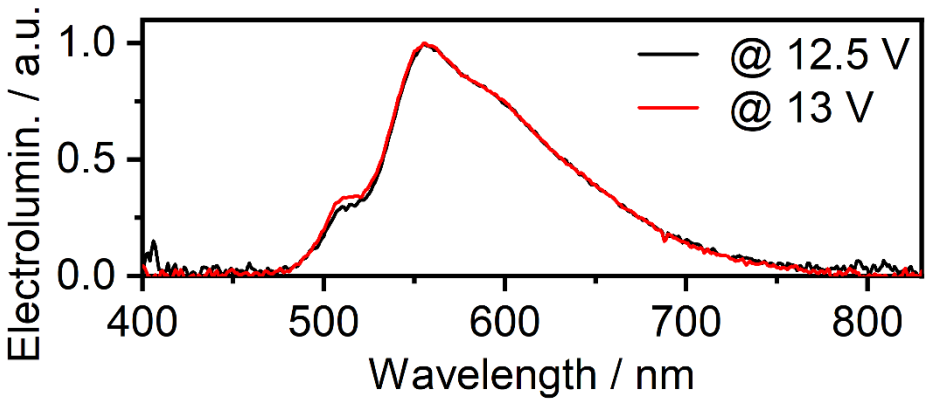

Figure 7.11. Electroluminescence spectrum of the LEEC.

The LEEC driven at 12.5 V displays a maximum luminance of 690 cd m^{-2} at t = 12.5 min and maximum EQE of 4.1 %, at t = 7.1 min. Driving the LEEC at 13 V yields a higher maximum luminance of 1970 cd m^{-2} at t = 4.6 min, but a lower maximum EQE of 2.8 %, at t = 3.1 min (*Figure 7.12*).

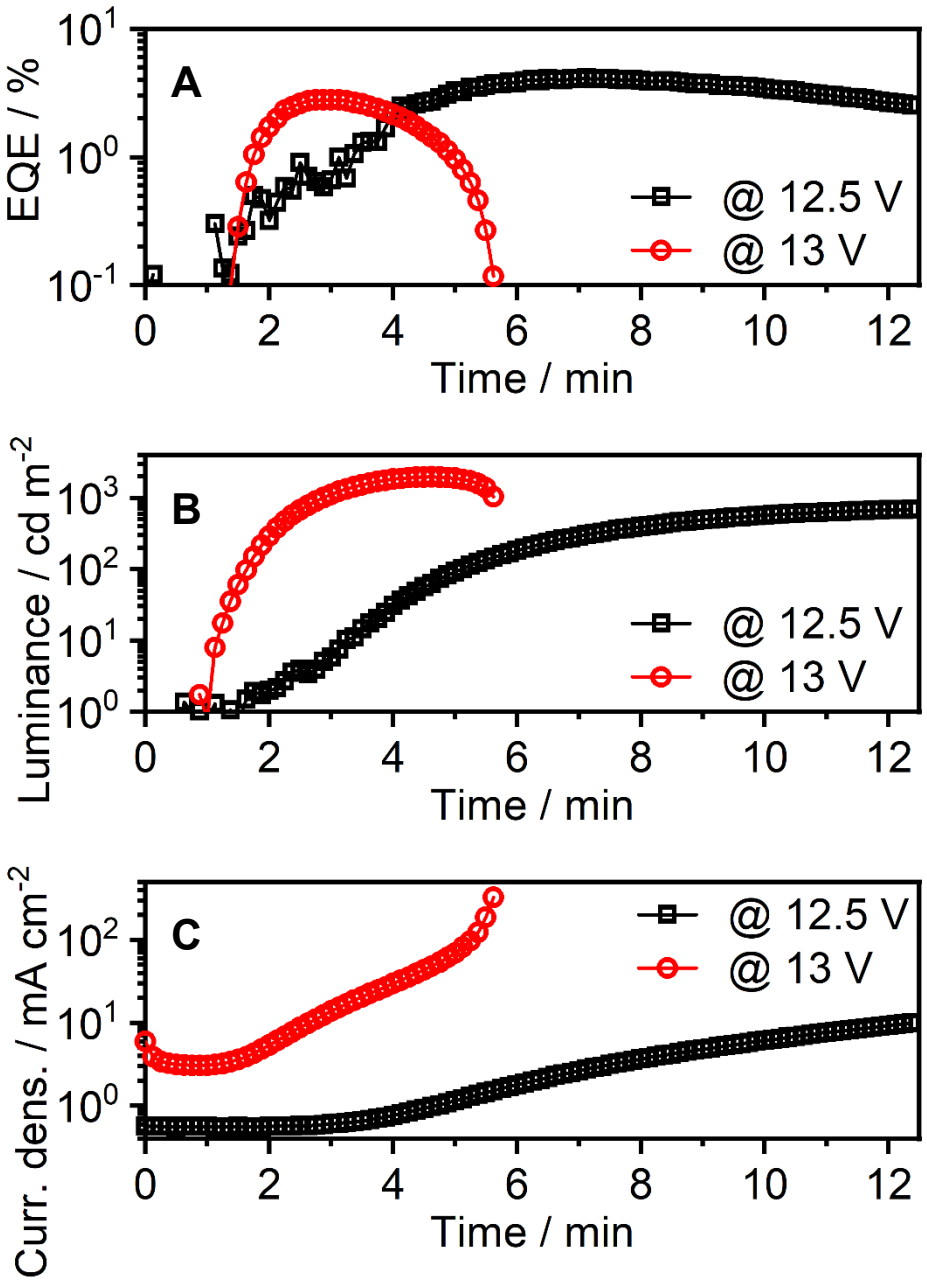

Figure 7.12. Plot of the EQE (A), luminance (B) and current density (C) of the LEEC versus time.

These characteristics are comparable with the best results reported for the most popular ionic iridium(III) complexes.[20] LEEC emitters are generally dominated by iridium(III) luminophores, likely due to their high photoluminescence efficiency and relatively simple introduction of ionic structure. A very limited number of other, mainly copper(I)[28] and silver(I),[29] complexes have been used in LEECs and a small number of metal-free

thermally activated delayed fluorescence (TADF) emitters have also been reported as LEEC emitting dopants with various results.[30–32]

Nevertheless, platinum(II) complexes have not been widely studied as LEEC luminescent dopants. To the best of our knowledge only one such work exists, but EQE and luminance have not been reported.[33] There have been however no reports of LEECs that would display appreciable luminance using a platinum(II) or a mixed silver(I)/platinum(II) complex emitter. Given that efficient and luminous LEECs are scarce and there exist very few efficient (EQE > 2-4%) and bright (luminance > 1000 cd m^{-2}) examples, these results are competitive with the best reported so far and definitely unique for platinum(II) complexes.

7.3. Conclusions

In this Chapter, the interaction of silver(I) with cyclometallated [N,C,N] platinum(II) compounds with alkynyl aromatic ancillary ligands described in *Chapter 6* was evaluated by emission titration curves, which determined that each silver atom interacts with two platinum(II) compounds.

Then, the corresponding silver(I)/platinum(II) heterometallic compounds were synthesised from mononuclear and dinuclear cyclometallated platinum(II) compounds and the coordination of silver to the alkynyl bonds was confirmed by NMR, mass spectrometry and infrared spectroscopy.

Photophysical studies revealed that in solution, the final heterometallic compounds are in equilibrium with their precursors, giving rise to two different emission bands. The presence of the silver resulted in the presence of a red-shifted broad band, with an origin in the ground state. Therefore, this confirms that use of a silver(I) atom can promote the interaction between two cyclometallated compounds therefore red-shifting the emission without the use of a bad solvent, as it was seen in *Chapter 6*.

This equilibrium was found to be highly dependent on concentration and on the nature of the cyclometallating moiety and the alkynyl aromatic ancillary ligand. Additionally, a significantly red-shifted band was observed in powder samples suggesting the presence of more complex structures in solid state, that could arise from the presence of additional intermolecular interactions.

Finally, compound **12e** was selected for the fabrication of LEECs, obtaining luminance (luminance > 1000 cd m^{-2}) and efficiency (EQE > 2-4%) values competitive with the best results reported in the literature. Specifically, to the best of our knowledge, is the first reported LEEC using a silver(I)/platinum(II) emitter.

7.4. Experimental Section

7.4.1. General procedures

Commercial reagents 1,3-diethynylbenzene (Sigma Aldrich, 97%), sodium hydroxide (NaOH, Panreac, 98%), silver triflate (CF_3SO_3Ag, Sigma Aldrich, >99%); and solvents methanol (Sigma Aldrich, >99%), hexane (Sigma Aldrich, >98%) and acetonitrile (Labkem, >99%) were used as received.

Compounds [PtCl{2,6-$(C_5H_4N)_2$-C_6H_3}] (**8**),[34] [PtCl{2,6-$(C_5H_4N)_2$-4-FC_6H_2}] (**9**),[34] [Pt(C≡Cthio){2,6-$(C_5H_4N)_2$-C_6H_3}] (**8c**),[17] [Pt(C≡Cthio){2,6-$(C_5H_4N)_2$-4-FC_6H_2}] (**9c**),[17] [Pt(C≡Cnaph){2,6-$(C_5H_4N)_2$-C_6H_3}] (**8d**),[17] [Pt(C≡Cnaph){2,6-$(C_5H_4N)_2$-4-FC_6H_2}] (**9d**),[17] [Pt(C≡Cphen){2,6-$(C_5H_4N)_2$-C_6H_3}] (**8e**)[17] and [Pt(C≡Cphen){2,6-$(C_5H_4N)_2$-4-FC_6H_2}] (**9e**)[17] were prepared as reported in the literature.

7.4.2. Physical measurements

NMR spectra were recorded in $CDCl_3$ or in acetone-d^6 at the Unitat de RMN of the Universitat de Barcelona with a Mercury 400 spectrometer (^1H, 400 MHz; ^{19}F, 376.5 MHz). Chemical shifts are given in δ values (ppm) relative to TMS (^1H) or $CFCl_3$ (^{19}F) and coupling constants J are given in Hz.

Infrared spectra were recorded in a Thermo Scientific FT-IR Nicolet iS5 spectrometer with an iD7 ATR accessory. IR frequencies ν are given in cm^{-1}.

Electrospray mass spectra were performed at the *Unitat d'Espectrometria de Masses (Universitat de Barcelona)* in a LC/MSD-TOF spectrometer using H_2O-CH_3CN 1:1 to introduce the sample.

Titration curves followed by emission were recorded in a Horiba Jobin-Yvon SPEX Nanolog-TM spectrofluorimeter at 298 K using $5 \cdot 10^{-5}$ M solutions of the starting compound.

Emission quantum yields were determined with a Hamamatsu Quantaurus QY absolute photoluminescence quantum yield spectrometer C11347.

7.4.3. Synthesis and characterisation

Synthesis of [{Pt(2,6-(2-C_5H_4N)$_2$-C_6H_3)}$_2$(μ-1,3-(C≡C)$_2$-C_6H_4)] (8f)

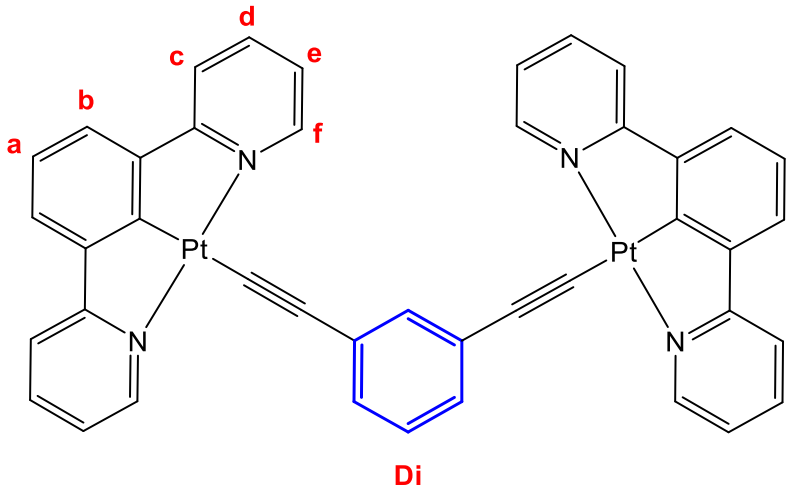

Compound [{Pt(2,6-(2-C_5H_4N)$_2$-C_6H_3)}$_2$(μ-1,3-(C≡C)$_2$-C_6H_4)] (**8f**) was obtained by stirring a mixture of 0.003 g (0.027 mmol) of 1,3-diethynylbenzene and 0.001 g (0.027 mmol) of sodium hydroxide at room temperature under an atmosphere of nitrogen for 30 min. Afterwards, 0.025 g (0.054 mmols) of compound [PtCl{2,6-(C_5H_4N)$_2$-C_6H_3}] (**8**) were added and the mixture was further stirred for 24 hours. The obtained orange solid was filtered, washed with water, methanol and hexane and dried under Yield: 0.017 g (65%).

^{1}H NMR ($CDCl_3$, 400 MHz): δ 9.47 [d, 4H, ^{3}J(Pt-H) = 47.2, ^{3}J(H-H) = 5.6, H^f]; 7.93 [td, 4H, ^{3}J(H-H) = 7.8, ^{4}J(H-H) = 1.6, H^d]; 7.72 [s, 1H, H^{Di}]; 7.68 [d, 4H, ^{3}J(H-H) = 7.8, H^c]; 7.52 [d, 2H, ^{3}J(H-H) = 8.4; H^{Di}]; 7.52 [d, 4H, ^{3}J(H-H) = 7.8; H^b]; 7.18-7.31 [m, 9H, H^{a,e,Di}]. **MS-ESI$^+$**: *m/z* 977.15 [M+H]$^+$, 552.10 [M-$C_{16}H_{11}N_2Pt$+2H]$^+$, 426.06 [M-$C_{26}H_{15}N_2Pt$]$^+$. **IR**: ν 2060 (C≡C).

Synthesis of [{Pt(2,6-(2-C_5H_4N)$_2$-4-FC_6H_2)}$_2$(μ-1,3-(C≡C)$_2$-C_6H_4)] (9f)

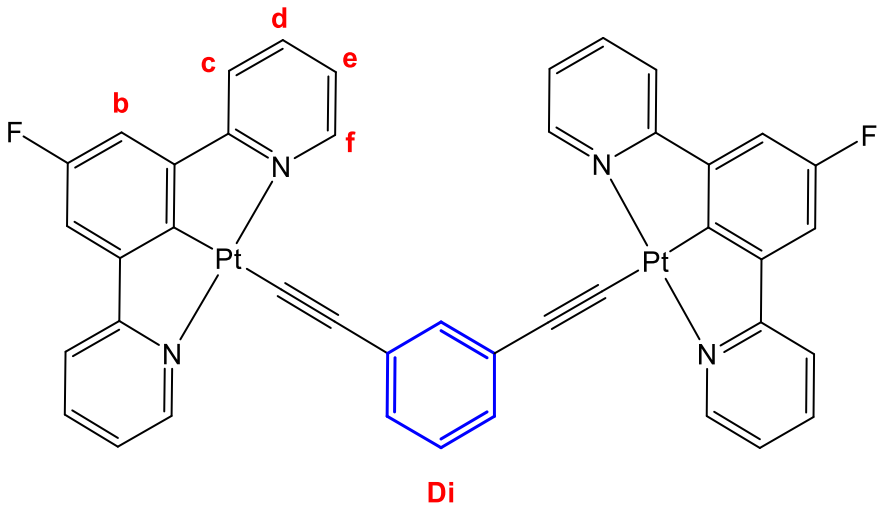

Compound [{Pt(2,6-(2-C_5H_4N)$_2$-4-FC_6H_2)}$_2$(μ-1,3-(C≡C)$_2$-C_6H_4)] (**9f**) was obtained as an orange solid by following the same method from 0.026 g (0.042 mmols) of compound [PtCl{2,6-(2-C_5H_4N)$_2$-4-FC_6H_2}] (**9**), 0.003 g (0.024 mmols) of 1,3-diethynylbenzene and 0.001 g (0.024 mmols) of sodium hydroxide. Yield: 0.013 g (54%).

^{1}H NMR ($CDCl_3$, 400 MHz): δ 9.49 [dd, 4H, ^{3}J(Pt-H) = 48.0, ^{3}J(H-H) = 5.7, ^{4}J(H-H) = 1.6, H^f]; 7.97 [td, 4H, ^{3}J(H-H) = 7.8, ^{4}J(H-H) = 1.6, H^d]; 7.71 [s, 1H, H^{Di}]; 7.65 [d, 4H, ^{3}J(H-H) = 7.8, H^c]; 7.55 [d, 2H, ^{3}J(F-H) = 7.6, H^{Di}]; 7.21-7.32 [m, 9H, $H^{b,e,Di}$]. **^{19}F NMR** ($CDCl_3$, 376.5 MHz): δ -118.34 [t, 1H, ^{3}J(H-F) = 10.0]. **MS-ESI$^+$**: *m/z* 1013.13 $[M+H]^+$, 570.09 $[M-C_{16}H_{10}FN_2Pt+2H]^+$, 426.06 $[M-C_{26}H_{14}FN_2Pt]^+$. **IR**: ν 2064 (C≡C).

General Procedure for the synthesis of complexes 11x and 12x

To a solution of the corresponding precursor **8x** or **9x** in acetonitrile under an atmosphere of nitrogen, 0.5 or 1 equivalents of silver triflate dissolved in acetonitrile were added. The mixture was stirred at room temperature covered from light for 1 hour. Half of the solvent was removed and the obtained solid was filtered and dried under vacuum.

Synthesis of [{2,6-(2-C_5H_4N)$_2$-C_6H_3}Pt(μ-C≡CThio)Ag(μ-C≡CThio)Pt{2,6-(2-C_5H_4N)$_2$-C_6H_3}] [CF_3SO_3] (11c)

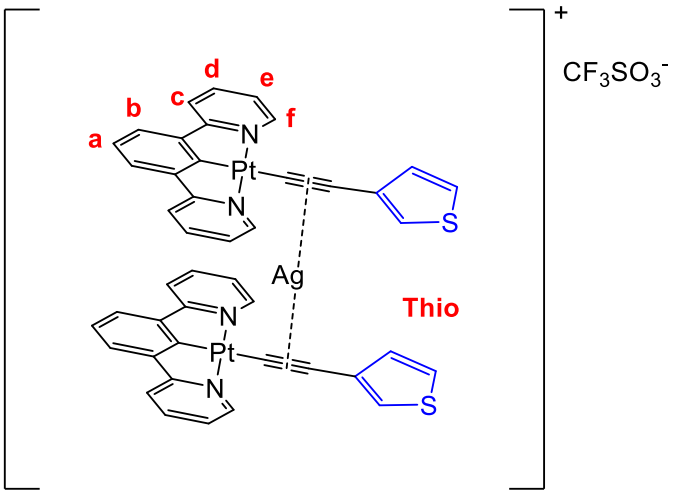

Compound [{2,6-(2-C_5H_4N)$_2$-C_6H_3}Pt(μ-C≡CThio)Ag(μ-C≡CThio)Pt{2,6-(2-C_5H_4N)$_2$-C_6H_3}] [CF_3SO_3] (**11c**) was obtained as a red solid from 0.034 g (0.064 mmols) of compound [Pt(C≡ CThio){2,6-(C_5H_4N)$_2$-C_6H_3}] (**8c**) and 0.008 g (0.032 mmols) of silver triflate. Yield: 0.033 g (73%).

^{1}H NMR (acetone-d^6, 400 MHz): δ 9.17 [d, 4H, ^{3}J(Pt-H) = 47.2, ^{3}J(H-H) = 5.7, H^f]; 8.01 [t, 4H, ^{3}J(H-H) = 7.6, H^d]; 7.68 [d, 4H, ^{3}J(H-H) = 8.0, H^c]; 7.50 [d, 4H, ^{3}J(H-H) = 7.7, H^b]; 7.39 [d, 2H, ^{3}J(H-H) = 2.8, H^{Thio}]; 7.26 [m, 4H, H^{Thio}]; 7.22 [m, 6H, $H^{a,e}$]. **MS-ESI$^+$**: *m/z* 1175.02 [M-CF_3SO_3]$^+$. **IR**: ν 2048 (C≡C).

Synthesis of [{2,6-(2-C_5H_4N)$_2$-4-FC_6H_2}Pt(μ-C≡CThio)Ag(μ-C≡CThio)Pt{2,6-(2-C_5H_4N)$_2$-4-FC_6H_2}] [CF_3SO_3] (12c)

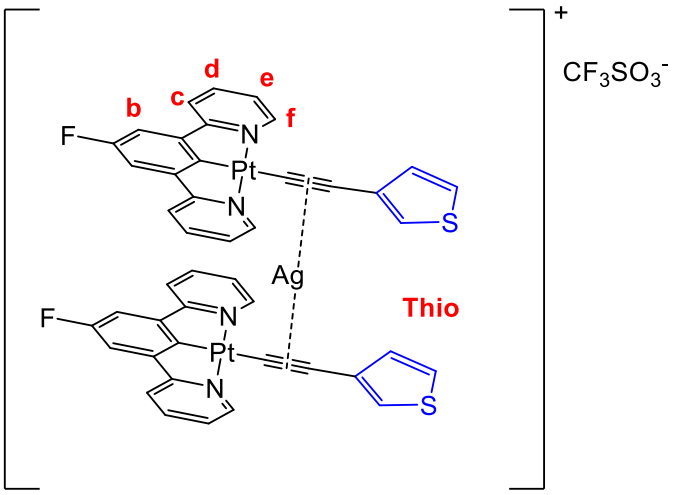

Compound [{2,6-(2-C_5H_4N)$_2$-4-FC_6H_2}Pt(μ-C≡CThio)Ag(μ-C≡CThio)Pt{2,6-(2-C_5H_4N)$_2$-4-FC_6H_2}] [CF_3SO_3] (**12c**) was obtained as a red solid from 0.032 g (0.058 mmols) of compound [Pt(C≡Cthio){2,6-(C_5H_4N)$_2$-4-FC_6H_2}] (**9c**) and 0.008 g (0.029 mmols) of silver triflate. Yield: 0.029 g (81%).

^{1}H NMR (acetone-d^6, 400 MHz): δ 9.16 [d, 4H, ^{3}J(Pt-H) = 48.1, ^{3}J(H-H) = 5.6, H^f]; 8.03 [t, 4H, ^{3}J(H-H) = 7.8, H^d]; 7.77 [d, 4H, ^{3}J(H-H) = 7.8, H^c]; 7.38 [d, 2H, ^{3}J(H-H) = 2.6, H^{Thio}]; 7.29 [d, 4H, ^{3}J(F-H) = 10.2, H^b]; 7.25 [m, 4H, H^{Thio}]; 7.21 [m, 4H, H^e]. **^{19}F NMR** ($CDCl_3$, 376.5 MHz): δ -78.04 [s,3F, $CF_3SO_3^-$]; -118.13 [t, 2H, ^{3}J(H-F) = 10.3]. **MS-ESI$^+$**: *m/z* 1210.69 [M-CF_3SO_3]$^+$ **IR**: ν 2054 (C≡C).

Synthesis of [{2,6-(2-C_5H_4N)$_2$-C_6H_3}Pt(μ-C≡CNaph)Ag(μ-C≡CNaph)Pt{2,6-(2-C_5H_4N)$_2$-C_6H_3}] [CF_3SO_3] (11d)

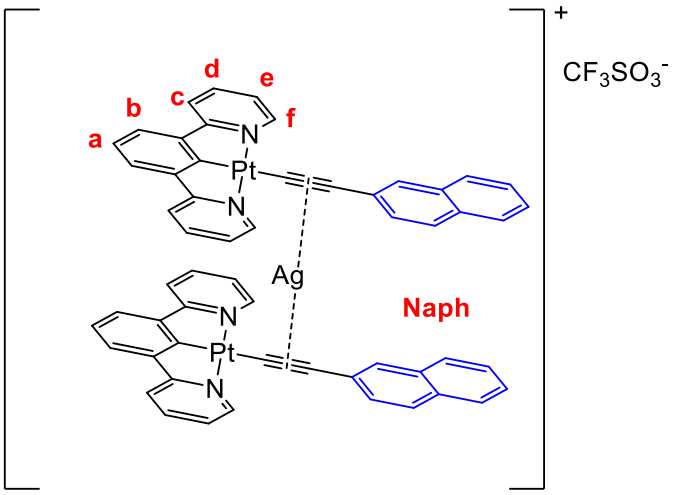

Compound [{2,6-(2-C_5H_4N)$_2$-C_6H_3}Pt(μ-C≡CNaph)Ag(μ-C≡CNaph)Pt{2,6-(2-C_5H_4N)$_2$-C_6H_3}] [CF_3SO_3] (**11d**) was obtained as a red solid from 0.048 g (0.084 mmols) of compound [Pt(C≡CNaph){2,6-(2-C_5H_4N)$_2$-C_6H_3}] (**8d**) and 0.011 g (0.042 mmols) of silver triflate. Yield: 0.042 g (69%).

^{1}H NMR (acetone-d^6, 400 MHz): δ 9.20 [d, 4H, ^{3}J(Pt-H) = 47.6, ^{3}J(H-H) = 5.6, H^f]; 8.21 [s, 2H, H^{Naph}]; 7.98 [t, 4H, ^{3}J(H-H) = 7.7, H^d], 7.79 [m, 6H, H^{Naph}]; 7.67-7.72 [m, 6H, $H^{c,Naph}$], 7.56 [d, 4H, ^{3}J(H-H) = 7.7, H^b]; 7.46 [m, 4H, H^{Naph}]; 7.23 [m, 6H, $H^{a,e}$]. **MS-ESI$^+$**: *m/z* 1263.15 [M-CF_3SO_3]$^+$. **IR**: ν 2054 (C≡C).

Synthesis of [{2,6-(2-C_5H_4N)$_2$-4-FC_6H_2}Pt(μ-C≡CNaph)Ag(μ-C≡CNaph)Pt{2,6-(2-C_5H_4N)$_2$-4-FC_6H_2}] [CF_3SO_3] (12d)

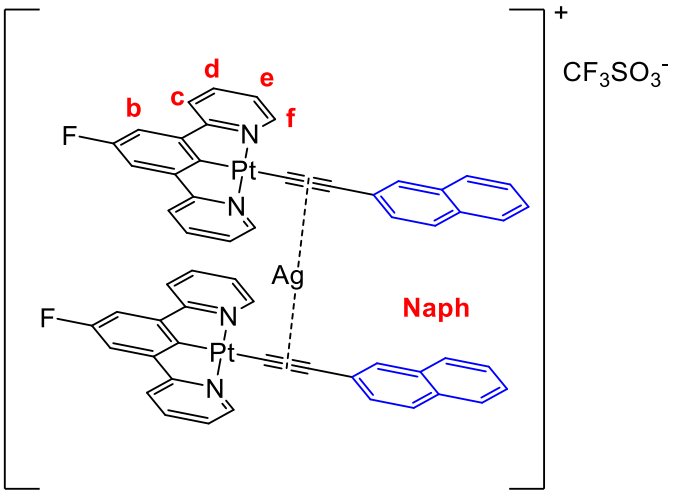

Compound [{2,6-(2-C_5H_4N)$_2$-4-FC_6H_2}Pt(μ-C≡CNaph)Ag(μ-C≡CNaph)Pt{2,6-(2-C_5H_4N)$_2$-4-FC_6H_2}] [CF_3SO_3] (**12d**) was obtained as a red solid from 0.042 g (0.070 mmols) of compound [Pt(C≡CNaph){2,6-(C_5H_4N)$_2$-4-FC_6H_2}] (**9d**) and 0.009 g (0.035 mmols) of silver triflate. Yield: 0.039 g (75%).

^{1}H NMR (acetone-d^6, 400 MHz): δ 9.23 [d, 4H, ^{3}J(Pt-H) = 47.8, ^{3}J(H-H) = 5.7, H^f]; 8.23 [s, 2H, H^{Naph}]; 8.04 [t, 4H, ^{3}J(H-H) = 7.8, H^d], 7.81 [m, 6H, H^{Naph}]; 7.72 [m, 6H, $H^{c,Naph}$]; 7.44 [m, 4H, H^{Naph}]; 7.27 [d, 4H, ^{3}J(F-H) = 10.1, H^b]; 7.24 [m, 4H, H^e]. **^{19}F NMR** ($CDCl_3$, 376.5 MHz): δ -77.97 [s,3F, $CF_3SO_3^-$]; -118.48 [t, 2H, ^{3}J(H-F) = 10.3]. **MS-ESI$^+$**: *m/z* 1299.08 [M-CF_3SO_3]$^+$. **IR**: ν 2059 (C≡C).

Synthesis of [{2,6-(2-C_5H_4N)$_2$-C_6H_3}Pt(μ-C≡CPhen)Ag(μ-C≡CPhen)Pt{2,6-(2-C_5H_4N)$_2$-C_6H_3}] [CF_3SO_3] (11e)

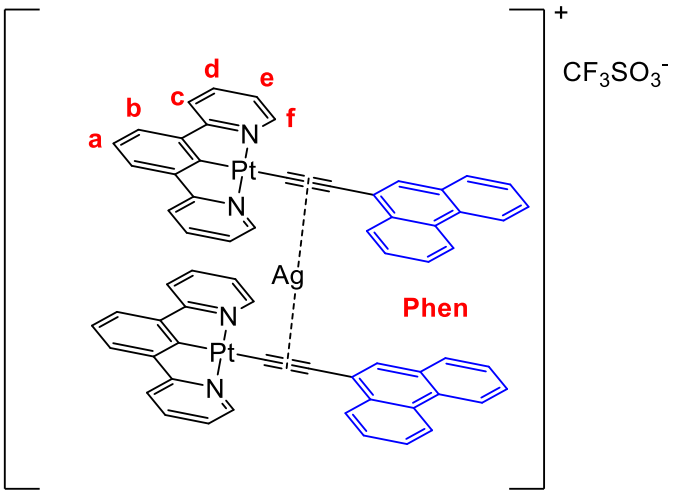

Compound [{2,6-(2-C_5H_4N)$_2$-C_6H_3}Pt(μ-C≡CPhen)Ag(μ-C≡CPhen)Pt{2,6-(2-C_5H_4N)$_2$-C_6H_3}] [CF_3SO_3] (**11e**) was obtained as a red solid from 0.043 g (0.070 mmols) of compound [Pt(C≡CPhen){2,6-(2-C_5H_4N)$_2$-C_6H_3}] (**8e**) and 0.009 g (0.034 mmols) of silver triflate. Yield: 0.041 g (78%).

^{1}H NMR (acetone-d^6, 400 MHz): δ 9.27 [d, 4H, ^{3}J(Pt-H) = 48.0, ^{3}J(H-H) = 5.7, H^f]; 8.98 [d, 2H, ^{3}J(H-H) = 7.8, H^{Phen}]; 8.81 [d, 2H, ^{3}J(H-H) = 7.8, H^{Phen}]; 8.69 [d, 2H, ^{3}J(H-H) = 7.9, H^{Phen}]; 8.08 [s, 2H, H^{Phen}]; 8.07 [t, 4H, ^{3}J(H-H) = 7.8, H^d], 7.79 [d, 4H, ^{3}J(H-H) = 7.8, H^c]; 7.75 [m, 2H, H^{Phen}], 7.66 [m, 4H, H^{Phen}]; 7.56 [m, 4H, H^{Phen}]; 7.32 [d, 4H, ^{3}J(H-H) = 7.7, H^b]; 7.19-7.22 [m, 6H, H^{a,e}]. **MS-ESI$^+$**: *m/z* 1363.24 [M-CF_3SO_3]$^+$. **IR**: ν 2045 (C≡C).

Synthesis of [{2,6-(2-C_5H_4N)$_2$-4-FC_6H_2}Pt(μ-C≡CPhen)Ag(μ-C≡CPhen)Pt{2,6-(2-C_5H_4N)$_2$-4-FC_6H_2}] [CF_3SO_3] (12e)

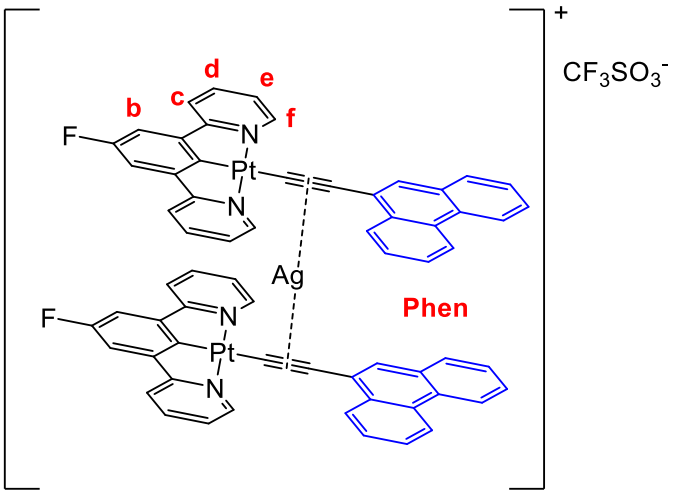

Compound [{2,6-(2-C_5H_4N)$_2$-4-FC_6H_2}Pt(μ-C≡CPhen)Ag(μ-C≡CPhen)Pt{2,6-(2-C_5H_4N)$_2$-4-FC_6H_2}] [CF_3SO_3] (**12e**) was obtained as a red solid from 0.034 g (0.052 mmols) of compound [Pt(C≡CPhen){2,6-(C_5H_4N)$_2$-4-FC_6H_2}] (**9e**) and 0.007 g (0.026 mmols) of silver triflate. Yield: 0.034 g (83%).

^{1}H NMR (acetone-d^6, 400 MHz): δ 9.25 [d, 4H, ^{3}J(Pt-H) = 48.4, ^{3}J(H-H) = 5.7, H^f]; 8.88 [d, 2H,^{3}J(H-H) = 7.8, H^{Phen}]; 8.71 [d, 2H, ^{3}J(H-H) = 7.8, H^{Phen}]; 8.67 [d, 2H, ^{3}J(H-H) = 7.7, H^{Phen}]; 8.10 [s, 2H, H^{Phen}]; 8.03 [t, 4H, ^{3}J(H-H) = 7.8, H^d], 7.81 [d, 4H, ^{3}J(H-H) = 7.8, H^c]; 7.73 [m, 2H, H^{Phen}]; 7.63 [m, 4H, H^{Phen}]; 7.51 [m, 4H, H^{Phen}]; 7.32 [d, 4H, ^{3}J(F-H) = 10.0, H^b]; 7.18 [m, 4H, H^e]. **^{19}F NMR** ($CDCl_3$, 376.5 MHz): δ -77.91 [s, 3F, $CF_3SO_3^-$]; -118.09 [t, 2H, ^{3}J(H-F) = 10.3]. **MS-ESI$^+$**: *m/z* 1399.16 [M-CF_3SO_3]$^+$. **IR**: ν 2043 (C≡C).

Synthesis of [Ag{Pt(2,6-(2-C_5H_4N)$_2$-C_6H_3)}$_2$(μ-1,3-(C≡C)$_2$-C_6H_4)]$_2$ [CF_3SO_3]$_2$ (11f)

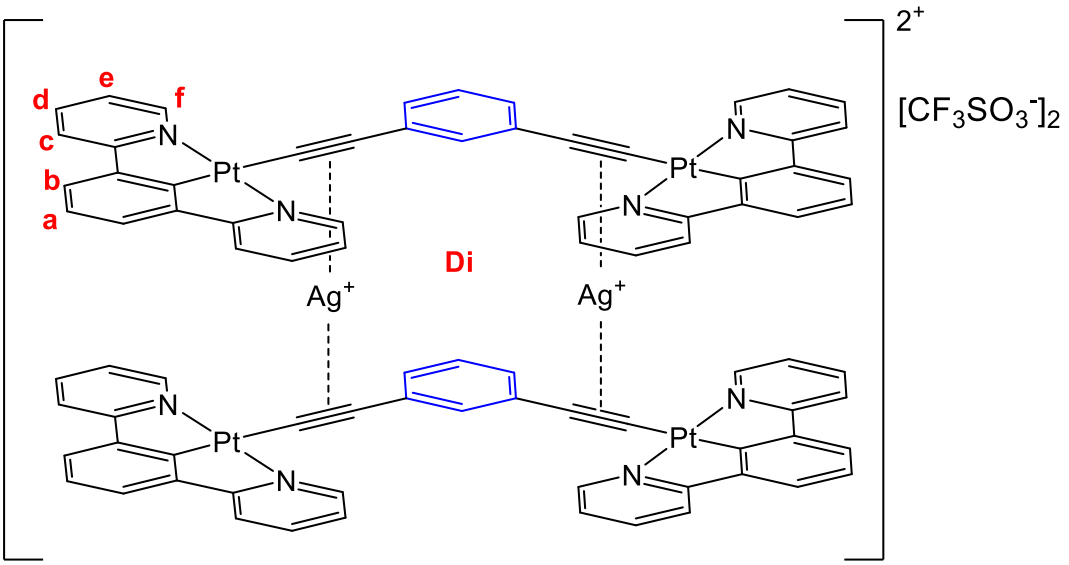

Compound [Ag{Pt(2,6-(2-C_5H_4N)$_2$-C_6H_3)}$_2$(μ-1,3-(C≡C)$_2$-C_6H_4)]$_2$ [CF_3SO_3]$_2$ (**11f**) was obtained as a red solid from 0.054 g (0.055 mmols) of compound [{Pt(2,6-(2-C_5H_4N)$_2$-C_6H_3)}$_2$(μ-1,3-(C≡C)$_2$-C_6H_4)] (**8f**) and 0.014 g (0.055 mmols) of silver triflate. Yield: 0.076 g (56%).

^{1}H NMR (acetone-d^6, 400 MHz): δ 9.11 [d, 8H, ^{3}J(Pt-H) = 47.4, ^{3}J(H-H) = 5.6, H^f]; 8.00 [t, 8H, ^{3}J(H-H) = 7.8, H^d]; 7.96 [s, 2H, H^{Di}]; 7.85 [d, 8H, ^{3}J(H-H) = 7.8, H^c]; 7.49 [d, 4H, ^{3}J(H-H) = 8.4; H^{Di}]; 7.54 [d, 8H, ^{3}J(H-H) = 7.8; H^b]; 7.28 [s, 2H, H^{Di}]; 7.22 [m, 12H, H^{a,e}]. **MS-ESI$^+$**: *m/z* 1084.75 [M-(CF_3SO_3)$_2$]$^{2+}$. **IR**: ν 2034 (C≡C).

Synthesis of [Ag-{Pt(2,6-(2-C_5H_4N)$_2$-4-FC_6H_2)}$_2$(μ-1,3-(C≡C)$_2$-C_6H_4)]$_2$ [CF_3SO_3]$_2$ (12f)

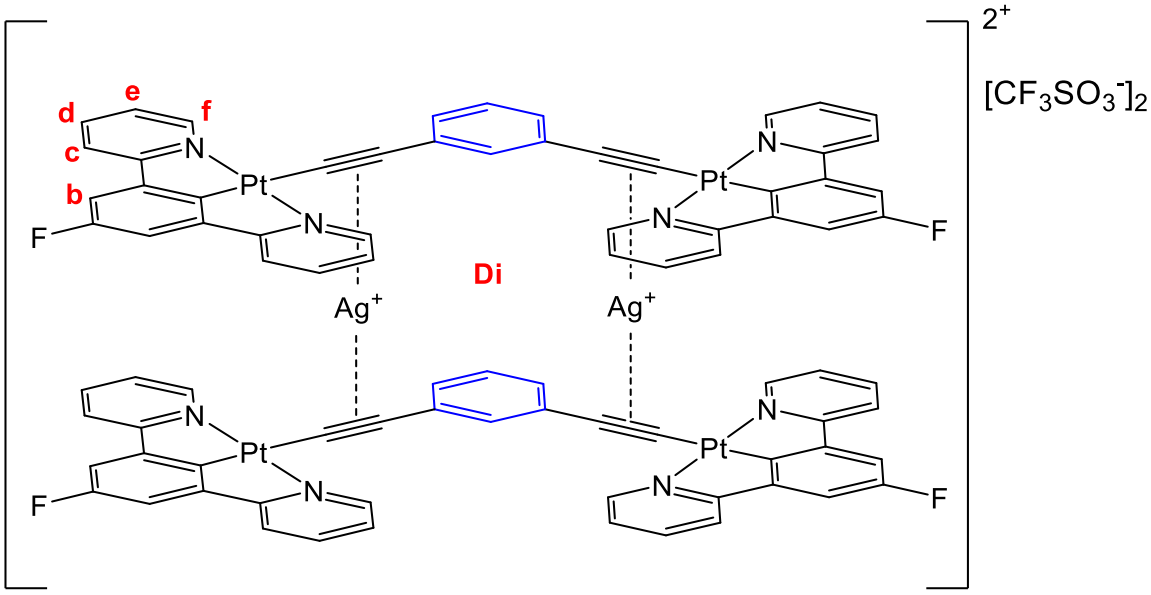

Compound [Ag{Pt(2,6-(2-C_5H_4N)$_2$-4-FC_6H_2)}$_2$(μ-1,3-(C≡C)$_2$-C_6H_4)]$_2$ [CF_3SO_3]$_2$ (**12f**) was obtained as a red solid from 0.040 g (0.040 mmols) of compound [{Pt(2,6-(2-C_5H_4N)$_2$-4-FC_6H_2)}$_2$(μ-1,3-(C≡C)$_2$-C_6H_4)] (**9f**) and 0.010 g (0.040 mmols) of silver triflate. Yield: 0.059 g (58%).

^{1}H NMR (acetone-d^6, 400 MHz): δ 9.13 [d, 8H, ^{3}J(Pt-H) = 48.2, ^{3}J(H-H) = 5.6, H^f]; 8.03 [t, 8H, ^{3}J(H-H) = 7.8, H^d]; 7.92 [s, 2H, H^{Di}]; 7.80 [d, 8H, ^{3}J(H-H) = 7.7, H^c]; 7.51 [d, 2H, ^{3}J(F-H) = 7.6, H^{Di}]; 7.31 [s, 2H, H^{Di}]; 7.27 [d, 8H, ^{3}J(F-H) = 10.1, H^b]; 7.19 [m, 8H, H^e]. **^{19}F NMR** ($CDCl_3$, 376.5 MHz): δ -77.83 [s,3F, $CF_3SO_3^-$]; -118.06 [t, 4H, ^{3}J(H-F) = 10.3]. **MS-ESI$^+$**: *m/z* 1120.87 [M-(CF_3SO_3)$_2$]$^{2+}$. **IR**: ν 2039 (C≡C).

7.4.4. Photophysical studies

Absorption spectra of 10^{-5} M acetonitrile solutions of the final compounds were recorded with a Cary 100 scan 388 Varian UV spectrometer at 298 K. Emission spectra of solutions and powders were recorded using a QePro compact spectrometer (Ocean Optics). Excitation spectra in solution were recorded with a Fluorolog fluorescence spectrometer (Jobin Yvon). Time-resolved decays in solution and powder were recorded with a Horiba DeltaFlex TCSPC system using a 330 nm SpectraLED light source. Temperature-dependent experiments were conducted using a liquid nitrogen cryostat VNF-100 (sample in flowing vapour, Janis Research) under nitrogen atmosphere, while

measurements at room temperature were recorded under vacuum in the same cryostat. Solutions were degassed using five freeze-pump-thaw cycles. Emission quantum yields were determined with a Hamamatsu Quantaurus QY absolute photoluminescence quantum yield spectrometer C11347.

7.4.5. Light-emitting electrochemical cells (LEECs) fabrication

LEECs were fabricated by vacuum thermal evaporation. Pre-cleaned indium-tin-oxide (ITO) coated glass substrates with a sheet resistance of 20 Ω cm^{-2} and ITO thickness of 100 nm was used. The substrates were first washed with acetone and then sonicated in acetone and isopropanol, for 15 min each time. Substrates were dried with compressed air and transferred into an ozone-plasma generator for 6 min at full power. Thermally deposited layers were obtained using Kurt J. Lesker Spectros II deposition system at 10^{-6} mbar base pressure. The aluminium electrode was deposited at a rate of 1 Å s^{-1}. Characterisation of LEEC devices was conducted in a 10-inch integrating sphere (Labsphere) connected to a Source Measure Unit (SMU, Keithley) and coupled with a spectrometer USB4000 (Ocean Optics). Further details are available in reference.[35] Devices of 4 × 2mm pixel size were fabricated.

The LEEC structure comprised PEDOT:PSS Al4083 (Ossila) as the hole injection layer, Al cathode, and an emissive layer composed of PVK {poly(9-vinylcarbazole), M = 90 000 Da, Sigma Aldrich}, OXD7 {1,3-bis[2-(4-tert-butylphenyl)-1,3,4-oxadiazo-5-yl]benzene, Lumtec}, and $THABF_4$ (Sigma Aldrich). The Al4083 layer was obtained by dynamic spin-coating method at 4000 RPM with the film annealed at 120 °C for 15 mins. The emissive layer was obtained with static spin-coating method at 1000 RPM from a 10 mg mL^{-1} (PVK+OXD7+THABF4+emitter) solution in CH_2Cl_2 and dried at high vacuum without annealing.

7.5. References

1. Forniés, J.; Lalinde, E.; Martín, A.; Moreno, M.T. *J. Organomet. Chem.* **1995**, *490*, 179–188.
2. Yam, V.W.-W.; Au, V.K.-M.; Leung, S.Y.L. *Chem. Rev.* **2015**, *115*, 7589–7728.
3. Li, B.; Liang, Z.; Yan, H.; Li, Y. *Mol. Syst. Des. Eng.* **2020**, *5*, 1578–1605.
4. Fresta, E.; Fernández-Cestau, J.; Gil, B.; Montaño, P.; Berenguer, J.R.; Moreno, M.T.; Coto, P.B.; Lalinde, E.; Costa, R.D. *Adv. Opt. Mater.* **2020**, *8*, 1901126.
5. Gil, B.; Forniés, J.; Gómez, J.; Lalinde, E.; Martín, A.; Moreno, M.T. *Inorg. Chem.* **2006**, *45*, 7788–7798.
6. Buschbeck, R.; Low, P.J.; Lang, H. *Coord. Chem. Rev.* **2011**, *255*, 241–272.
7. Chen, Z.N.; Zhao, N.; Fan, Y.; Ni, J. *Coord. Chem. Rev.* **2009**, *253*, 1–20.
8. Leung, S.Y.L.; Lam, W.H.; Zhu, N.; Yam, V.W.W. *Organometallics* **2010**, *29*, 5558–5569.
9. Han, L.J.; Wu, X.X.; Ma, Z.G.; Li, Y.; Wei, Q.H. *Dalton Trans.* **2020**, *49*, 8347–8353.
10. Juvenal, F.; Fortin, D.; Harvey, P.D. *Inorg. Chem.* **2020**, *59*, 7117–7134.
11. Berenguer, J.R.; Lalinde, E.; Moreno, M. T. *Coord. Chem. Rev.* **2010**, *254*, 832–875.
12. Wong, K.M.C.; Hui, C.K.; Yu, K.L.; Yam, V.W.W. *Coord. Chem. Rev.* **2002**, *229*, 123–132.
13. Zhang, Q.C.; Xiao, H.; Zhang, X.; Xu, L.J.; Chen, Z.N. *Coord. Chem. Rev.* **2019**, *378*, 121–133.
14. Quan, J.; Chen, Z.H.; Zhang, X.; Wang, J.Y.; Zhang, L.Y.; Chen, Z.N. *Inorg. Chem. Front.* **2021**, *8*, 2323–2332.
15. Lam, E.S.H.; Tam, A.Y.Y.; Lam, W.H.; Wong, K.M.C.; Zhu, N.; Yam, V.W.W. *Dalton Trans.* **2012**, *41*, 8773–8776.
16. Forniés, J.; Fuertes, S.; Martín, A.; Sicilia, V.; Lalinde, E.; Moreno, M.T. *Chem.*

Eur. J. **2006**, *12*, 8253–8266.

17. Lázaro, A.; Bosque, R.; Ward, J.S.; Rissanen, K.; Crespo, M.; Rodríguez, L. *Inorg. Chem.* **2023**, *62*, 2000-2012.

18. Chaaban, M.; Zhou, C.; Lin, H.; Chyi, B.; Ma, B. *J. Mater. Chem. C* **2019**, *7*, 5910–5924.

19. Schlingman, K.; Chen, Y.; Carmichael, R.S.; Carmichael, T.B. *Adv. Mater.* **2021**, *33*, 1–20.

20. Yang, Z.P.; Su, H.C. *Adv. Funct. Mater.* **2020**, *30*, 1906788.

21. Youssef, K.; Li, Y.; O'Keeffe, S.; Li, L.; Pei, Q. *Adv. Funct. Mater.* **2020**, *30*, 1909102.

22. Tang, S.; Sandström, A.; Lundberg, P.; Lanz, T.; Larsen, C.; Van Reenen, S.; Kemerink, M.; Edman, L. *Nat. Commun.* **2017**, *8*, 1190.

23. Hruzd, M.; Gauthier, S.; Boixel, J.; Kahlal, S.; le Poul, N.; Saillard, J.Y.; Achelle, S.; Guen, F.R. *Dyes Pigm.* **2021**, *194*, 109622.

24. Yang, S.; Meng, F.; Wu, X.; Yin, Z.; Liu, X.; You, C.; Wang, Y.; Su, S.; Zhu, W. *J. Mater. Chem. C* **2018**, *6*, 5769–5777.

25. Chan, A.K.W.; Ng, M.; Wong, Y.C.; Chan, M.Y.; Wong, W.T.; Yam, V.W.W. *J. Am. Chem. Soc.* **2017**, *139*, 10750–10761.

26. Zhang, H.H.; Wu, S.X.; Wang, Y.Q.; Xie, T.G.; Sun, S.S.; Liu, Y.L.; Han, L.Z.; Zhang, X.P.; Shi, Z.F. *Dyes Pigm.* **2022**, *197*, 109857.

27. Zhang, J.; Zhou, L.; Al-Attar, H.A.; Shao, K.; Wang, L.; Zhu, D.; Su, Z.; Bryce, M.R.; Monkman, A.P. *Adv. Funct. Mater.* **2013**, *23*, 4667–4677.

28. Weber, M.D.; Fresta, E.; Elie, M.; Miehlich, M.E.; Renaud, J.L.; Meyer, K.; Gaillard, S.; Costa, R.D. *Adv. Funct. Mater.* **2018**, *28*, 1707423.

29. Fresta, E.; Carbonell-Vilar, J.M.; Yu, J.; Armentano, D.; Cano, J.; Viciano-Chumillas, M.; Costa, R.D. *Adv. Funct. Mater.* **2019**, *29*, 1901797.

30. Lundberg, P.; Tsuchiya, Y.; Lindh, E.M.; Tang, S.; Adachi, C.; Edman, L. *Nat. Commun.* **2019**, *10*, 5307.

31. Wong, M.Y.; La-Placa, M.G.; Pertegas, A.; Bolink, H.J.; Zysman-Colman, E. *J. Mater. Chem. C* **2017**, *5*, 1699–1705.

32. Wong, M.Y.; Hedley, G.J.; Xie, G.; Kölln, L.S.; Samuel, I.D.W.; Pertegás, A.; Bolink, H.J.; Zysman-Colman, E. *Chem. Mater.* **2015**, *27*, 6535–6542.

33. Lu, W.; Chan, M.C.W.; Zhu, N.; Che, C.M.; Li, C.; Hui, Z. *J. Am. Chem. Soc.* **2004**, *126*, 7639–7651.

34. Wang, Z.; Turner, E.; Mahoney, V.; Madakuni, S.; Groy, T.; Li, J. *Inorg. Chem.* **2010**, *49*, 11276–11286.

35. de Sa Pereira, D.; Monkman, A.P.; Data, P. *J. Vis. Exp.* **2018**, *141*, e565936.

CHAPTER 8

General Conclusions

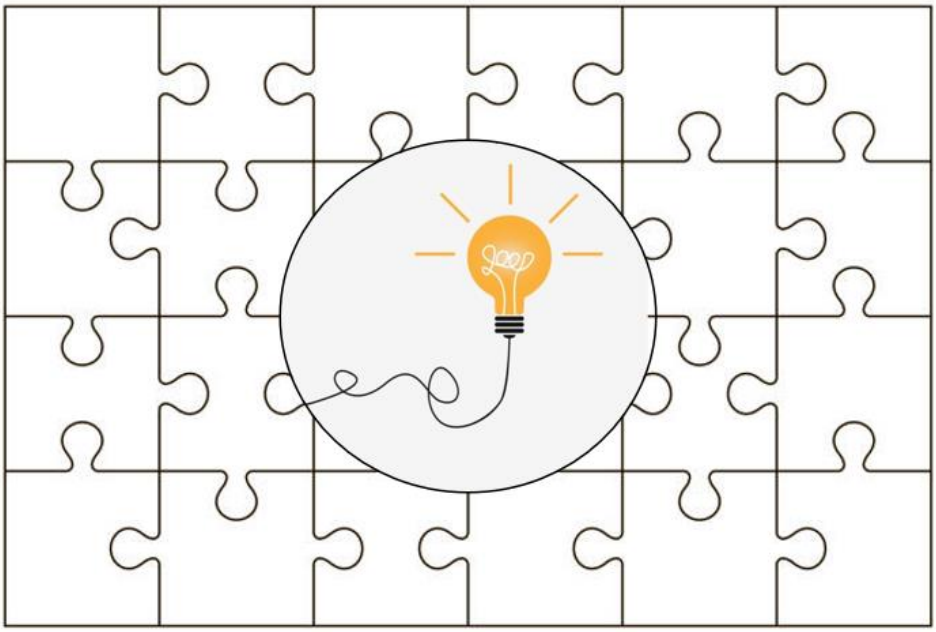

8. General Conclusions

In this Thesis, several cyclometallated platinum compounds were synthesised with a rational design targeted to their specific applications. A wide variety of synthetic approaches were performed, and several characterisation techniques allowed to successfully prove the obtention of the final compounds. In the biological area, upon tailoring the structure of the studied compounds, a very high efficacy and selectivity against a broad cancer cell panel was achieved, several techniques were used to elucidate their mechanism of action and some compounds proved to overcome platinum resistance in tumoral cells. For the optical applications, the design of the cyclometallated chromophore and the ancillary ligands lead to the obtention of highly phosphorescent compounds, which can present intermolecular interactions that lead to the red-shifting and enhancement of their emission and finally, allowed their application in the fabrication of novel and efficient optical devices.

- In *Chapter 2*, several strategies were successfully performed to obtain a large family of [C,N,N'] cyclometallated platinum compounds with different ancillary ligands (methyl or halido) and oxidation states. Upon analysis of their luminescent properties, it was determined that best results are obtained for platinum(II) compounds and that the use of iodido ligands causes a quenching in the emission. Generally, luminescence quantum yields present low values which is attributed to the low rigidity of their propylene chain which favours non-radiative pathways.

- In *Chapter 3*, a new family of [C,N,N'] cyclometallated compounds with a more rigid ethylene chain were synthesised and displayed an improvement in their luminescent properties regarding those from *Chapter 2*. Cell viability studies revealed that some selected compounds present a high efficacy and selectivity against a broad cancer cell lines panel. Specifically, platinum(IV) compounds display an enhanced effect and a complete absence of cross-resistance in multiplatinum resistant cell models, a property that was found to be intrinsic of the platinacycle. Additionally, the ability of these compounds to be reduced under cellular media was proved and was found to be a key step in their antiproliferative activity.

- In *Chapter 4*, starting from the structure that gave the best antiproliferative effect in Chapter 3, new [C,N,N'] cyclometallated platinum(IV) compounds were synthesised with hydroxido, dichloroacetato or trifluoroacetato axial ligands. The nature of these ligands resulted in differences in the reduction potentials of the platinum(IV) compounds for which the antiproliferative effect was found to be higher upon a higher tendency to be reduced, being in some cases significantly lower than cisplatin for a colorectal cancer cell line. Additionally, the new platinum(IV) compounds presented interaction with DNA prior to reduction which could suggest an alternative mechanism competing with the pro-drug behaviour.

- In *Chapter 5*, the substitution of a chlorido for different alkynyl aromatic moieties as ancillary ligands in the platinum(II) structure with the best photophysical properties from *Chapter 3*, resulted in an enhancement of the phosphorescence emission with higher quantum yields for the new derivatives. An exhaustive photophysical study revealed that the preferred deactivation pathway for these compounds is the generation of singlet oxygen, with singlet oxygen sensitisation quantum yields up to a 47%.

- In *Chapter 6*, a family of planar [N,C,N] cyclometallated platinum(II) compounds was synthesised and they were found to be able to establish intermolecular interactions between two cyclometallated moieties. This resulted in observing not only the phosphorescence of the monomeric species, but also the appearance of a red-shifted emission band attributed to an excimeric emission. Additionally, the red shift of the emission was also induced by using a mixture of good and bad solvents, which results in the formation of emissive aggregates that present aggregation induced emission (AIE). Both these phenomena were found to be extremely dependent on the aromatic group attached to the alkynyl as it modifies the resulting intramolecular interactions.

- In *Chapter 7*, the interaction of silver(I) with the compounds reported in *Chapter 6* was studied, synthesising a family of heterometallic compounds where each silver atom interacts with two cyclometallated molecules. These interaction

between the two compounds gave rise to a red-shifted emission avoiding the use of a bad solvent to promote aggregation. The presence of this emission was found to be highly dependent on the concentration and the nature of the cyclometallated platinum(II) precursor. More complex structures appeared to be present in solid state where a broad band further red shifted was observed. Finally, compound **12e** was selected for the fabrication of LEECs, obtaining luminance (luminance > 1000 cd m^{-2}) and efficiency (EQE > 2-4%) values competitive with the best results reported in the literature and, to the best of our knowledge, being the first reported example using a silver(I)/platinum(II) emitter.

APPENDIX

Table A1. Crystal data and structure refinement for compounds **1b'** and **1b**.

Compound	**1b'**	**1b**
Formula	$C_{12}H_{17}Br_2FN_2Pt$	$C_{12}H_{16}BrFN_2Pt$
Crystal size, mm	0.065 x 0.154 x 0.213	0.305 x 0.103 x 0.054
Crystal colour	yellow	yellow
Fw	563.18	482.27
Temp, K	100(2)	293(2)
Wavelength, Å	0.71073	0.71073
Crystal system	triclinic	monoclinic
Space group	$P\bar{1}$	$P2_1/c$
a, Å	10.7938(5)	15.4189(18)
b, Å	11.4007(5)	8.7061(10)
c, Å	13.4215(7)	30.311(3)
α, º	89.584(2)	90
β, º	75.569(2)	104.344(4)
γ, º	71.945(2)	90
Volume, Å^3	1516.34(13)	3942.1(8)
Z	4	12
D_{calc}, mg m^{-3}	2.467	2.438
abs. coef., mm^{-1}	14.519	13.710
F(000)	1040	2688
θ range for data coll, º	2.560 to 30.562	2.440 to 30.628
Reflns coll. / independent	88505 / 9284	95319 / 12130
Data /restraint /parameters	9284 / 0 / 329	12130 / 0 / 466
GOF on F^2	1.029	1.012
Final R index (I>2σ(I))	R1 = 0.0212 wR2 = 0.0541	R1 = 0.0604, wR2 = 0.0718
R index (all data)	R1 = 0.0242 wR2 = 0.0554	R1 = 0.1368, wR2 = 0.0858
Peak and hole, e Å^{-3}	1.832 and -2.092	3.091 and -3.050
CCDC numbers	1856035	1856038

Table A2. Crystal data and structure refinement for compounds **2b** and **3b**.

Compound	**2b**	**3b**
Formula	$C_{13}H_{19}Br_2FN_2Pt$	$C_{12}H_{16}Br_3FN_2Pt$
Crystal size, mm	0.252 x 0.127 x 0.076	0.306 x 0.174 x 0.072
Crystal colour	yellow	yellow
Fw	577.21	642.09
Temp, K	100(2)	100(2)
Wavelength, Å	0.71073	0.71073
Crystal system	monoclinic	orthorhombic
Space group	$P2_1/c$	$Pna2_1$
a, Å	8.0750(3)	15.9976(6)
b, Å	8.1606(3)	7.1424(3)
c, Å	23.9013(9)	13.7123(5)
α, º	90.0	90.0
β, º	98.3600(10)	90
γ, º	90.0	90.0
Volume, Å^3	1720.06(12)	1566.78(11)
Z	4	4
D_{calc}, mg m^{-3}	2.460	2.722
abs. coef., mm^{-1}	14.131	16.604
F(000)	1072	1176
θ range for data coll, º	2.549 to 30.539	2.546 to 30.533
Reflns coll. / independent	50.737 / 4732	20770 / 4695
Data /restraint /parameters	4732 / 2/ 175	4695/ 3/ 174
GOF on F^2	1.106	1.046
Final R index (I>2 σ(I))	R1 = 0.0197, wR2 = 0.0444	R1 = 0.0300, wR2 = 0.0673
R index (all data)	R1 = 0.0235, wR2 = 0.0458	R1 = 0.0376, wR2 = 0.0707
Peak and hole, e Å^{-3}	1.402 and -1.515	1.049 and -2.385
CCDC numbers	1856037	1856036

Table A3. Crystal data and structure refinement for compounds **4a** and **4b**.

Compound	**4a**	**4b**
Formula	$C_{11}H_{14}ClFN_2Pt$	$C_{11}H_{14}BrFN_2Pt$
Crystal size, mm	0.868 x 0.203 x 0.198	0.48 x 0.45 x 0.28
Crystal colour	orange	orange
Fw	423.78	468.24
Temp, K	293	170
Wavelength, Å	0.71073	0.71073
Crystal system	monoclinic	monoclinic
Space group	$P2_1/c$	$P2_1/c$
a, Å	9.579(4)	9.5246(3)
b, Å	10.883(4)	11.0464(4)
c, Å	12.800(5)	12.8619(5)
α, º	90	90
β, º	111.369(17)	109.564(2)
γ, º	90	90
Volume, Å^3	1242.7(8)	1275.11(8)
Z	4	4
D_{calc}, mg m^{-3}	2.265	2.439
abs. coef., mm^{-1}	11.492	14.125
F(000)	792	864
θ range for data coll, º	2.534 to 29.146	2.269 to 31.008
Reflns coll. / independent	34767 / 3331	7610 / 4017
Data /restraint /parameters	3331 / 0 / 147	4017 / 0 / 147
GOF on F^2	1.141	1.081
Final R index (I>2 σ(I))	R1 = 0.0190, wR2 = 0.0475	R1 = 0.0499, wR2 = 0.1281
R index (all data)	R1 = 0.0208, wR2 = 0.0482	R1 = 0.0578, wR2 = 0.1344
Peak and hole, e Å^{-3}	1.413 and -2.083	1.658 and -5.891
CCDC numbers	1957891	1958051

Table A4. Crystal data and structure refinement forc ompounds **5a** and **5b**.

Compound	**5a**	**5b**
Formula	$C_{11}H_{14}Cl_3FN_2Pt$	$C_{11}H_{14}Br_3FN_2Pt$
Crystal size, mm	0.5 x 0.32 x 0.16	0.44 x 0.3 x 0.05
Crystal colour	yellow	yellow
Fw	494.68	628.06
Temp, K	170	170
Wavelength, Å	0.71073	0.71073
Crystal system	orthorhombic	orthorhombic
Space group	*Pna*2$_1$	*Pna*2$_1$
a, Å	15.7680(7)	16.0684(13)
b, Å	6.7221(2)	6.9294(5)
c, Å	13.2613(6)	13.5530(7)
α, º	90.0	90.0
β, º	90.0	90
γ, º	90.0	90.0
Volume, Å^3	1405.62(10)	1509.05(18)
Z	4	4
D_{calc}, mg m^{-3}	2.338	2.764
abs. coef., mm^{-1}	10.546	17.236
F(000)	928	1144
θ range for data coll, º	2.583 to 26.372	2.535 to 31.367
Reflns coll. / independent	7042 / 2291	8347 / 4134
Data /restraint /parameters	2291 / 1/ 166	4134/ 37/ 166
GOF on F^2	1.054	1.000
Final R index (I>2 σ(I))	R1 = 0.0256, wR2 = 0.0606	R1 = 0.0567, wR2 = 0.1533
R index (all data)	R1 = 0.0276, wR2 = 0.0615	R1 = 0.0718, wR2 = 0.1636
Peak and hole, e Å^{-3}	1.112 and -1.764	2.582 and -3.194
CCDC numbers	1958052	1958053

Table A5. Crystal data and structure refinement for compounds **7b** and **7c**.

Compound	**7b**	**7c**
Formula	$C_{19}H_{18}F_2N_2Pt$	$C_{17}H_{17}FN_2PtS$
Crystal size, mm	0.42 x 0.22 x 0.18	0.22 x 0.12 x 0.10
Crystal colour	orange	orange
Fw	507.44	495.48
Temp, K	170	170
Wavelength, Å	0.71073	0.71073
Crystal system	Monoclinic	Orthorhombic
Space group	$P2_1/n$	$P2_12_12_1$
a, Å	6.3762(3)	8.8289(2)
b, Å	20.4502(10)	17.1322(3)
c, Å	12.970(6)	32.7257(6)
α, º	90	90
β, º	97.106(3)	90
γ, º	90	90
Volume, Å^3	1678.25(14)	4948.53(17)
Z	4	12
D_{calc}, mg m^{-3}	2.008	1.995
abs. coef., mm^{-1}	8.383	8.640
F(000)	968	2832
θ range for data coll, º	0.407 to 28.700	0.407 to 28.238
Reflns coll. / independent	7673 / 4297	36124 / 12181
Data /restraint /parameters	4297 / 0 / 219	12181 / 106 / 640
GOF on F^2	1.052	1.096
Final R index (I>2 σ(I))	R1 = 0.0380, wR2 = 0.0800	R1 = 0.0521, wR2 = 0.0702
R index (all data)	R1 = 0.0529, wR2 = 0.0869	R1 = 0.0529, wR2 = 0.0977
Peak and hole, e Å^{-3}	1.522 and -1.585	0.956 and -1.132
CCDC numbers	1970145	1970146

Table A6. Crystal data and structure refinement for compounds **7d** and **8e**.

Compound	**7d**	**8e**
Formula	$C_{23}H_{21}FN_2Pt$	$C_{32}H_{20}N_2Pt$
Crystal size, mm	0.18 x 0.14 x 0.04	0.24 x 0.18 x 0.04
Crystal colour	orange	yellow
Fw	539.51	627.59
Temp, K	170(2)	170
Wavelength, Å	0.71073	0.71073
Crystal system	Orthorhombic	Monoclinic
Space group	*Pna2₁*	$P2_1/c$
a, Å	10.1844(4)	16.1728(7)
b, Å	17.0874(7)	11.3593(3)
c, Å	11.2125(3)	12.6711(6)
α, º	90	90
β, º	90	99.073(2)
γ, º	90	90
Volume, Å^3	1951.25(12)	2298.70(16)
Z	4	4
D_{calc}, mg m^{-3}	1.837	1.813
abs. coef., mm^{-1}	7.209	6.129
F(000)	1040	1216
θ range for data coll, º	0.407 to 30.508	0.407 – 28.700
Reflns coll. / independent	9977 / 3880	17638 / 5083
Data /restraint /parameters	3880 / 1 / 246	5683 / 0 / 316
GOF on F^2	1.009	1.047
Final R index (I>2 σ(I))	R1 = 0.0371, wR2 = 0.0809	R1 = 0.0439, wR2 = 0.1220
R index (all data)	R1 = 0.0538, wR2 = 0.0874	R1 = 0.0597, wR2 = 0.1301
Peak and hole, e Å^{-3}	1.148 and -0.644	1.322 and -2.596
CCDC numbers	1970147	2192597

Table A7. Crystal data and structure refinement for compound **9c**.

Compound	**9c**
Formula	$C_{22}H_{13}FN_2PtS$
Crystal size, mm	0.36 x 0.18 x 0.06
Crystal colour	orange
Fw	551.49
Temp, K	170
Wavelength, Å	0.71073
Crystal system	Triclinic
Space group	$P\bar{1}$
a, Å	9.1838(3)
b, Å	9.5505(3)
c, Å	21.4829(8)
α, º	84.057(2)
β, º	85.211(2)
γ, º	73.358(2)
Volume, Å^3	1793.94(11)
Z	4
D_{calc}, mg m^{-3}	2.042
abs. coef., mm^{-1}	7.957
F(000)	1048
θ range for data coll, º	0.407 – 28.700
Reflns coll. / independent	17023 / 7859
Data /restraint /parameters	7859 / 0 /487
GOF on F^2	1.066
Final R index (I>2 σ(I))	R1 = 0.0554, wR2 = 0.0999
R index (all data)	R1 = 0.0927, wR2 = 0.1104
Peak and hole, e Å^{-3}	0.812 and -0.871
CCDC numbers	2192598